THE UNIVERSITY
of EDINBURGH

Somato-dendritic coupling in layer 5 pyramidal neurons of the mouse primary visual cortex

Valerio Francioni

Doctor of Philosophy
Centre for Discovery Brain Sciences
School of Biomedical Sciences
The University of Edinburgh
2019

Valerio Francioni

Somato-dendritic coupling in layer 5 pyramidal neurons of the mouse primary visual cortex

Doctor of Philosophy, December 2019

Supervisor:

Dr. Nathalie Rochefort

To my mother Alessia, the strongest person I know

Acknowledgements

The work presented in this thesis has been a crucial part of my life in the last four and a half years. What I learnt during this journey vastly exceeds what I could foresee when I started. I have acquired not just notions, but a method and a mindset to learn more. As such, I want to thank all the people that permitted this journey to reach this far.

First, I would like to thank my primary supervisor Dr. Nathalie Rochefort for giving me the opportunity and the resources to work in her lab. She trusted me to carry out a challenging project when I had no experience in the lab, and she nurtured me, with infinite patience, from the end of my undergraduate studies, until the completion of this Ph.D. What I owe her, is much more than I could ever pay back.

I also want to thank Professor Matthew Nolan and Professor David Willie for their invaluable insights. As my assistant supervisors, they showed great interest in my project from the beginning providing me with timely and mindful feedback every time I asked. For similar reasons, I also want to thank Professor Ian Duguid who, at a crucial time during my Ph.D., has devoted time and effort to help me shape the first draft of my first scientific manuscript.

A special thank also goes to Dr Janelle Pakan for patiently teaching me all the techniques required to perform my experiments including surgeries and imaging. Additionally, I want to thank Dr Zahid Padamsey for completing a crucial set of experiments required for the submission of a scientific manuscript that the work described in this thesis led to.

I also want to thank all the members of the Rochefort family lab, for the supportive, playful and stimulating environment that I enjoyed during these last four and a half years.

Additionally, I want to thank Alessia, my mother, to whom this thesis is dedicated, for the seemingly endless strength and support she gives me. Alessio, my stepfather for the calm and wisdom that he effortlessly infuses in anyone who comes across him. Luca, my dad, for giving me perspective when I was missing it. Pietro and Gabriele, my brothers, for unsuspectingly making me try to be a better person just to set a better example … and for the sheer joy they supply, just for being around. Paola, my partner for the countless number of little things she does for me, to make my life happier. Finally, Davide, Jacopo, Nils, Maria, Theo and Chiara, my friends, for giving me strength when I have little left.

This work belongs to the people mentioned above, more than it does to me.

Abstract

Cortical layer 5 excitatory neurons are characterized by long apical dendrites receiving inputs from multiple long-range cortical and subcortical connections. *In vitro* and *in vivo* recordings have shown that the dendrites of layer 5 pyramidal neurons support both distance-dependent filtering and local dendritic non linearities, including NMDA, calcium and sodium-mediated spikes. Additionally, the coincident occurrence of back-propagating action potentials and tuft depolarization was shown to generate widespread calcium transients in the apical tuft dendrites which leads to bursts of action potentials in the soma. In the primary visual cortex (V1), layer 5 pyramidal neurons display selective responses to physical features of visual stimuli, such as the orientation and direction of movement. In addition, layer 5 neurons activity is gain modulated by locomotion both in darkness and during visual stimulation. This gain modulation was shown to be mediated through a recurrent VIP-SST cortical circuit which was suggested to produce a net disinhibition of the apical tuft dendrites of pyramidal neurons. So far however, the dendritic activity underlying gain modulation of layer 5 pyramidal neurons during locomotion remains unexplored. Additionally, the extent to which dendritic activity is compartmentalised from the activity in other sibling branches and from the activity in the soma is a matter of debate. *In vitro* studies suggest that apical tuft branches should be highly compartmentalised, however *in vivo* studies have returned controversial results about the extent of somato-dendritic coupling.

To address these questions, I sparsely labelled layer 5 neurons of the primary visual cortex with a genetically-encoded calcium indicator (GCaMP6). I used multiplane, two-photon calcium imaging to monitor the activity in different apical tuft branches and different compartments of the neuron (soma, trunk and tuft) semi-simultaneously. I acquired data in head-fixed mice freely running on a cylindrical treadmill both in darkness and during the presentation of drifting gratings. Finally, I performed offline morphological reconstructions of the neurons imaged, in order to extract anatomical information about the neurons and dendrites I imaged.

These results showed that the apical tuft dendrites increase their activity in response to visual stimulation and locomotion. However, I found that the activity of different sibling branches belonging to one neuron had highly correlated activity. Branch-specific events were rare, small, and independent of visual stimulation and locomotion. This high correlation persisted not only between different apical tuft branches, but also between different

compartments of the neurons showing that dendritic calcium activity is systematically coincident with global events spreading throughout the entire neuron. Neither locomotion nor visual stimulation altered this high coupling between somatic and dendritic activity. However, the results showed that activity levels between soma and the apical tuft were asymmetric. While almost all dendritic events were detected in the soma, up to 40% of somatic events could not be detected in the apical tuft dendrites, suggesting that somatic signals attenuated from the soma to the apical tuft. Throughout all compartments, smaller events were more likely to decay below the detection threshold, suggesting that signals attenuated in a distance and amplitude-dependent manner from the soma to the apical tuft. These results provide important insights about the mechanisms of dendritic integration of individual layer 5 neurons in the visual cortex. They suggest that the entire neuron behaves as a single computational unit rather than many independent ones and suggest that activity in the compartments is largely driven by somatic action potentials regardless of the animal's behavioural state. Nonetheless, the extent to which these findings apply to other neuronal types, other cortical areas and different behavioural and perceptual states will have to be determined by future experiments.

Lay summary

The neocortex is the part of the mammalian brain involved in the processing of sensory and higher-order brain functions including sensory perception, attention and memory. Neurons are the building block of this part of the brain, the most abundant type of which are known as pyramidal neurons. These neurons communicate with each other by exchanging electrochemical messages which are received on cable-like structures called dendrites. These structures receive the inputs from other neurons, and they broadcast them to the main part of the neuron called the soma; depending on the strength of these inputs and their integration, the neuron will then generate electrical signals called action potentials to transfer this information to other neurons. Dendritic computation is the technical term to indicate the process by which these inputs are combined with each other within dendrites and then transferred to the soma. Electrical currents can sum, subtract, multiply and divide one another according to the spatial and temporal profile of the over 10,000 incoming inputs each neuron receives from neighbouring neurons. Understanding the mechanism behind this computation, is important to understand how the brain implements the complex tasks it is required to perform.

Extensive work performed in brain slices for the last 30 years has shown that dendrites are not just passive cables whose role is to simply deliver the information to the soma: these neuronal processes can do some computation themselves. For example, they can amplify some inputs while shutting down others. However, to what extent and in which conditions dendrites act as independent computational units in the intact brain remains unclear. To investigate this, I recorded the activity of the soma and the dendrites of pyramidal neurons in primary visual cortex during different sensory (visual stimulation and darkness) and behavioural (stationary and locomoting) conditions. Activity was recorded using a fluorescent calcium indicator. Whenever a neuron is active, calcium enters the neurons and binds to the indicator which increases its fluorescence in return. Using 2-photon microscopy, an advanced microscopy technique optimised to image the intact brain in behaving animals, I compared how the activity of soma and multiple dendrites relate to each other, and whether different perceptual or behavioural states could alter this relationship in the mouse visual cortex.

These results demonstrate that in a given pyramidal neuron, the activity of the soma and all its dendrites is highly correlated. This suggests that the entire neuron processes information as a single unit, rather than multiple independent ones. In addition, these results show that

activity in the dendrites is dominated by somatic activity. This suggests that the inputs that a neuron receives on its dendrites produce an output in the soma that is then back-propagating to the dendrites. In this process, the signals attenuate from the soma to the dendrites in a distance and amplitude-dependent manner. These results show that the information exchange between soma and dendrites is unaltered by different behavioural and perceptual states, suggesting that is a basic mechanism which is implemented independently of the specific perceptual or behavioural state of the animal. Altogether, these results suggest that signal processing in individual neurons requires a bidirectional interaction between the somatic and dendritic activity, the extent of which was previously unclear. Further studies will have to investigate the biophysical machinery that allows neurons to flow information back and forth between the soma and its dendrites and to understand what this mechanism is useful for. Insights might come from the field of machine learning. The idea is that when a machine performs a task, the difference between the target and the actual performance is calculated and utilised as an input to improve the algorithms in future trials. Is this a strategy that neurons utilise during learning? Future studies will investigate these mechanisms further.

Declaration

I declare that this thesis was composed by myself, that the work contained herein is my own except where explicitly stated otherwise in the text, and that this work has not been submitted for any other degree or professional qualification except as specified

Edinburgh, 04.12.2019

Valerio Francioni

List of Acronyms

Each acronym found in text, is defined at the time of first occurrence. However, this list has the intent to facilitate the reader.

5HT3R: Serotonin Receptor

Ach: Acetylcholine

AMPA: α-amino-3-hydroxy-5-methyl-4-isoxazolepropionic acid

AMPAR: α-amino-3-hydroxy-5-methyl-4-isoxazolepropionic acid receptor

bAP: Backpropagating action potential

BAC: backpropagation-activated Ca^{2+} spike firing

Ca^{2+}: Ionic calcium

Cpd : Cycles per degree

CT: Corticothalamic neuron

dLGN: Dorsal-lateral geniculate nucleus

DS: Direction selective

GABA: γ-aminobutyric acid

GABAA: $GABA_A$ receptor

GABAB: $GABA_B$ receptor

IT: Intratelencephalic neuron

K^+: Ionic Potassium

LP: Lateral Posterior nucleus of the thalamus

Mg^{2+}: Ionic Magnesium

MK-801: Dizocilpine

NA: Noradrenaline

Na^+: Ionic Sodium

NMDA: N-Methyl-D-aspartic acid

NMDAR: N-Methyl-D-aspartic acid receptor

OS: Orientation selective

OSI: Orientation-selectivity index

PMT: Photomultiplier tube

PT: Pyramidal tract neuron

PV: Parvalbumin

RGC: Retinal ganglion cell

ROI: Region of interest

SC: Superior Colliculus

SST: Somatostatin

TTX: Tetrodotoxin

V1: Primary visual cortex

VG: Voltage-gated

VIP: Vasointestinal peptide

Table of Contents

1. Introduction

'It's not what you look at that matters, it's what you see'

Henry David Thoreau

1.1 Studying vision

Understanding how the brain gives rise to the experience of sight is an important question that has intrigued neuroscientists for over a century. The importance of understanding visual perception stems from the fact that many mammals rely on vision to perform several behaviours fundamental for survival, such as prey hunting, predator detection, danger avoidance, navigation and partner selection. Until recently, most of the studies assessing vision were performed on animal models such as cats and macaques. These animal models are particularly appealing to study vision as they have high visual acuity and their central visual pathways, share many of the characteristics reported in humans (Briggs, 2017). Over the last decade however, the mouse has been the most common animal model used to investigate neuronal correlates of visual processing. Owing to the advent of both genetic and recording tools, the mouse has emerged as an important animal model to study vision and its underlying neuronal circuits. These tools provide the opportunity not only to record but also to manipulate the activity of individual cells of the neural circuits, allowing experimenters to causally link the anatomical organisation of these circuits to specific brain functions. The exponential increase of studies on the mouse visual system has led to an unprecedented amount of information about this system. So much so, that one could argued that we now know more about the mouse visual system than any other sensory system, in any species, including humans (Luo, Callaway and Svoboda, 2008, 2018).

1.1.1 Vision in mice

Compared to other mammalian species including humans, mice have a low visual acuity. Visual acuity is generally defined as the ability to discriminate between patterns at increasingly smaller distances, is measured in cycles per degree (how many cycles of a grating can you distinguish per one degree of visual field) and has been shown to positively correlate with the size of the eye in mammals (Veilleux and Kirk, 2014). Compared to other mammalian species, mice have rather small eyes and as such, low visual acuity. They can distinguish gratings at a maximum of 0.04 cycles per degree (cpd), cats at 0.9 and non-human primates,

such as the Haplorini primates that have the highest visual acuity in the animal kingdom can go up to 4.2 cpd (Van Hooser, 2007). Compared to humans, mice have the equivalent of 10/1000 vision, which means that they can see at 10 meters distance, what a normally sighted human can see at 1000 meters (Huberman and Niell, 2011).

Additionally, mice are mainly nocturnal. This raises questions about the validity of using this model to study vision at all, since the composition of their retina is functionally different from ours. Like humans, mice have both rods and cones but rods, which mainly operate in low-light conditions, vastly outnumber the cones (Jeon, Strettoi and Masland, 1998). Mice cones are specialised to distinguish only between green and blue light, but not between green and red (Szél and Röhlich, 1992). Interestingly, the spatial distribution of these two types of photoreceptors is not uniform across the retina. This means that the ability to distinguish colours as well as contrast sensitivity is not uniform across the visual field (Szél and Röhlich, 1992).

The mouse visual system is two orders of magnitude smaller than the one in cats or primates both in absolute and relative terms calculated as the ratio between brain and body size (Laramée and Boire, 2015). It is generally accepted as a clear trend in mammalian brain evolution that the size of the brain correlates with the number of functionally distinct cortical areas. The parcellation theory proposed by Ebbesson (1980) suggests that increasing in brain size, correlates to an increase in the number of cortical areas, leading to more specialised and less globally-connected brain areas (Ebbesson, 1980). It is suggested that evolutionarily, the specialisation of functionally distinct brain areas is advantageous to minimize connection lengths (and the metabolic cost associated with intracellular trafficking of nutrients and proteins in longer processes) and maximise connection speed (Krubitzer and Huffman, 2000). However, lesser specialisation in mice than in other mammalian species, raises concerns about the interpretation of classical lesions or inactivation studies aiming to map brain areas to specific functions. Neurons in the primary visual cortex (V1), respond selectively to visual stimuli oriented at different angles (Hubel and Wiesel, 1959) and as such, they have been referred to as orientation selective neurons (discussed in details in section 1.1.4) (Figure 1.1). One example of different specialisation in the mouse visual cortex is the salt-and-pepper organisation of orientation selective neurons in mouse V1, as opposed to a more modular arrangement of orientation selective neurons in the cats and primate's visual cortex which is arranged in orientation selective columns (Laramée and Boire (2015) but also see (Fahey *et al.*, 2019)) (Figure 1.2).

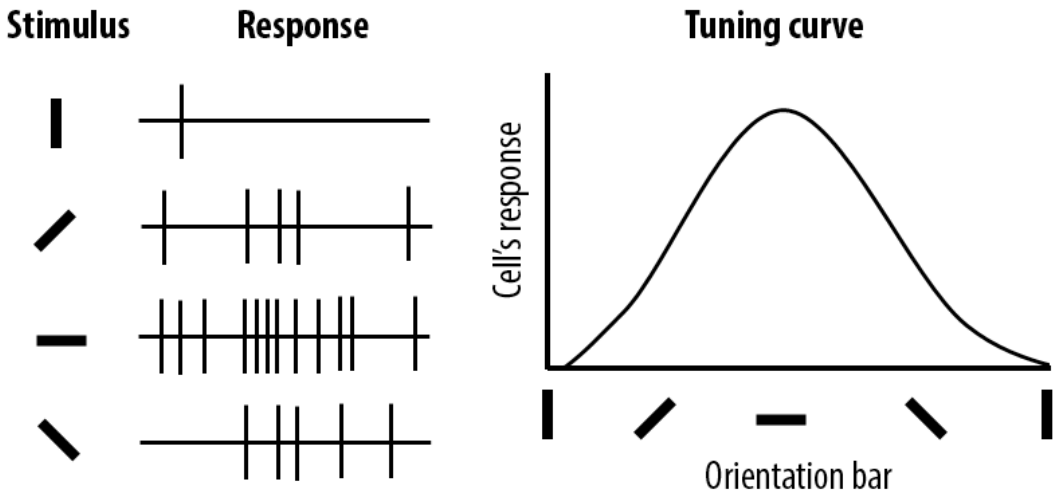

Figure 1.1: *Orientation selective neuron*.

The response of a single neuron in cat V1, to visual stimuli oriented at different angles. This neuron preferentially responded to stimuli oriented horizontally and responded with less spikes to visual stimuli oriented at different angles. The width of the tuning curve represents how selective a neuron is to a given stimulus. Figure inspired by Hubel and Wiesel (1968)

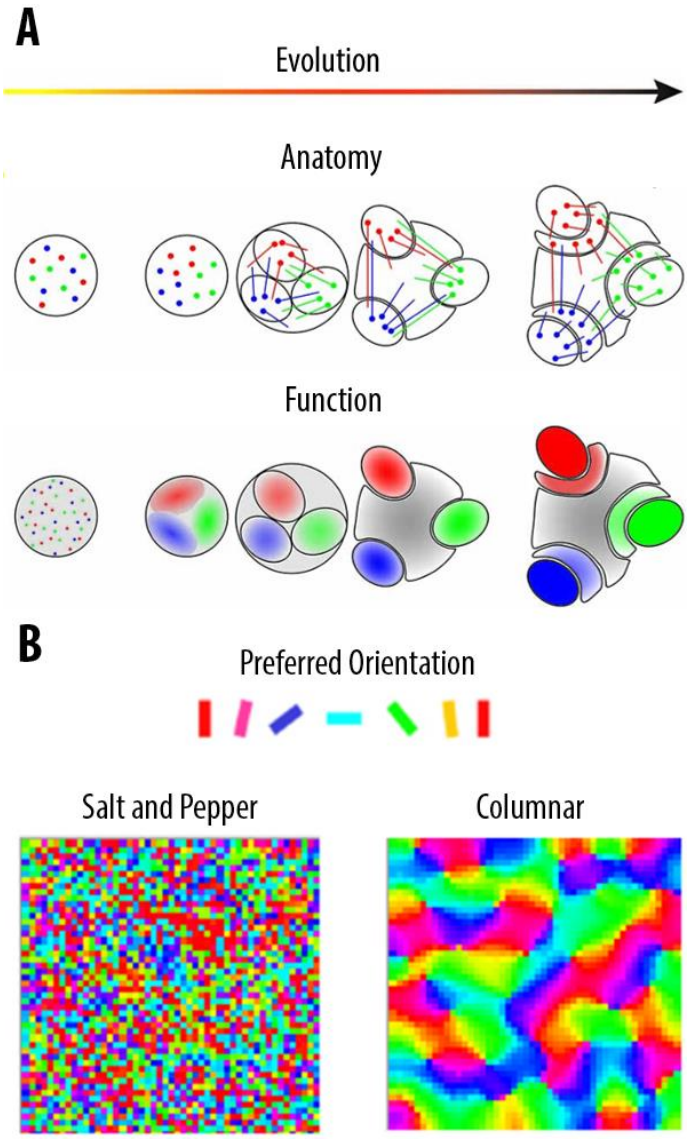

Figure 1.2: *The parcellation hypothesis and the organisation of orientation selective neurons in the primary visual cortex of mouse and cats*.

A) The parcellation hypothesis: In early evolutionary stages, neurons that process different stimuli are intermingled. With subsequent evolutionary stages and an increase in brain size, neurons that process similar features of a sensory stimulus segregate together both anatomically and functionally. Their segregation becomes increasingly clear as brain size increases resulting in functionally homogeneous areas. Intermediate areas can be regarded as hubs that connect two functionally separated areas. B) Neurons in V1, respond to visual stimuli oriented at different angles (Hubel and Wiesel, 1959). In the mouse primary visual cortex, neurons that respond to different orientations of visual stimuli are intermixed in a salt-and-pepper fashion. On the other hand, in the cat primary visual cortex, neurons that respond to different orientations are segregated into anatomically distinct areas (columnar organisation). This organisation is hypothesised to be a direct consequence of parcellation, shown in A. Figures re-adapted from (Laramée and Boire, 2015; Philips, Sur and Chakravarthy, 2017).

Despite differences between mice and humans' visual cortex, mouse models have several advantages when it comes to understand neuronal circuitry. In addition to low maintenance costs, faster gestation times and ethical advantages, the most common answer as to why mice have been used as animal models in neuroscience research is their readily modifiable genetics (Luo, Callaway and Svoboda, 2008, 2018). This is very important as genetic manipulations allows experimenters to investigate the structure and function of genetically-defined cell types and causally link neuron types to different aspects of visual perception and behaviour. An additional, and more subtle reason is that having small sizes, mice allow experimenters to gather data over larger functional areas, which is advantageous to understand how the brain integrate information from multiple sensory-motor modalities (Kim *et al.*, 2016; Hillman *et al.*, 2018). Finally, mice are simpler and safer to work with, compared to cats or monkeys. Despite these advantages, it is fundamental to understand what the mouse visual system can compute and what are the limitations of generalising these findings to other species. What do mice use vision for? Do they perform visually-driven behaviours?

Characterizing visually-driven behaviours in mice then allows the investigation of the neuronal substrate required to perform these tasks.

Mice perform at least three, ethologically relevant, visually-guided behaviours:

(1) Predator aversion. In the wild, mice are often predated by aerial species such as hawks and owls. As other senses like smell or audition can be rather ineffective at detecting these predators, mice require vision to detect their predators and avoid predation. Neuroscientists can replicate in laboratory settings the visual-stimulus associated with a looming predator, by using an expanding dark stimulus shown in a screen placed on top of an arena. In response to the stimuli, mice respond by freezing when the arena is closed, and sheltering when the arena is endowed with covers (Yilmaz and Meister, 2013). Additionally, the expanding dark stimulus triggers fear-associated behaviours when the looming stimulus is presented above, but not when it is presented below (Yilmaz and Meister, 2013). While looming, which mimics predator approaching triggers fleeing responses, sweeping, which mimics a more distal threat, triggers freezing. The interpretation of these results relies on the idea that freezing may be more advantageous to avoid detection by a distal predator, while fleeing may be a more advantageous escaping response to a looming predator (De Franceschi *et al.*, 2016).

(2) Predation. Mice also use visually-guided strategies to predate on smaller insects and smaller reptilian and amphibian species. The northern grasshopper mouse relies on hunting as its sole mean of feeding (Langley, 1989). Laboratory mice that are fed with small insects use vision for spotting long-distance preys, as well as to stalking and approaching behaviour (Hoy *et al.*, 2016).

(3) Depth perception. For most animals, falling from great heights can have hazardous consequences and as such, they must be able to perceive and estimate depths. Interestingly, depth fear is suggested to be an innate behaviour in humans and can be already observed in 6 months old infants (Gibson and Walk, 1960). The visual cliff test, originally created to test depth fear in humans, and subsequently adapted for mice, exploits a high -contrast checkboard and clear acrylic glass to create the illusion of a cliff/danger side and a swallow safer place. When mice are placed onto this platform, they tend to stay closer to the shallow side. This choice must be visually-guided as no other senses can be exploited in this behavioural paradigm. Indeed, mice that have retinal degeneracies fail to show this cautious behaviour (Fox, 1965).

Altogether, these results demonstrate how vision, despite the low visual acuity compared to other mammalian species, is ethologically relevant for survival in mice. With the advantage of genetic tools, mice are a powerful model to understand how specific circuits in the visual brain, can generate visual perception and drive adaptive behaviour.

1.1.2 Ocular dominance in the mouse visual system

In the mouse, eyes are positioned laterally and therefore, each eye largely view a portion of the visual field that is inaccessible to the other eye (referred as: The monocular visual field). However, both eyes sample the central 40 degrees of the visual field enabling the mouse to have depth perception, which crucially depends on stereopsis (Hübener, 2003) (Figure 1.2A, referred as: The binocular visual field). In carnivores and primates with frontal eyes, the eye has a well-defined line of decussation, meaning that each retinal ganglion cell (RGC) will project ipsilaterally or contralaterally according to its retinotopic location in the eye (Seabrook *et al.*, 2017). In the mouse however this wiring is rather different. First, there is no well-defined line of decussation. Additionally, the small proportion of RGCs that project ipsilaterally (less than 5%), is interspersed with contralaterally-projecting RGCs in the dorsal-lateral part of the retina (Dräger and Olsen, 1980). Differences in the arrangement of ocular maps, persist throughout the visual system (Seabrook *et al.*, 2017).

In cats and primates, RGCs project to anatomically segregated zones in the dorsolateral Geniculate Nucleus of the thalamus (dLGN). In mice this segregation of incoming RGC terminals synaptic inputs is not observed neither in in the dLGN nor in the Superior Colliculus (SC). Despite a recent study demonstrating that mouse dLGN contains an overrepresentation of neurons that respond to inputs coming from both eyes (Howarth, Walmsley and Brown, 2014), previous results demonstrate how the majority of dLGN neurons respond to inputs coming from one eye only, and not from both (Grubb and Thompson, 2003). The functional implications of this anatomical segregation in the dLGN, or lack of thereof, is yet to be clearly understood.

In the SC, ipsilateral inputs are anatomically segregated into the rostro-medial part of the deep SC layers and there is evidence that indicate that the synaptic maturation of RGCs incoming axons changes as a function of laterality (Dräger and Olsen, 1980; Godement, Salaün and Imbert, 1984). These results imply that the monocular and binocular regions of the SC process different information, and that these areas undergo different maturation processes.

In V1, ocular segregation also differs in mouse compared to primates and cats. Indeed, in both these species, inputs coming from the ipsi and contralateral eyes segregate into distinct anatomical areas. While in cats this separation is patched, in primates, the separation is striped (Hubel and Wiesel, 1963, 1969). These patterns are particularly visible in the cortical layer 4, the primary input layer for thalamic afferences in V1 (Douglas and Martin, 2004). On the other hand, mice do not show neither patched not striped arrangements of their visual cortex, but they segregate into two distinct anatomical parts of V1. The medial part of V1 receives monocular inputs that only arrive from the contralateral eye, while the more lateral part of V1, receives binocular inputs which consist in a mixture of ipsi and contralateral inputs (Dräger, 1975) (Figure 1.2A).

These results suggest that processing spatial information about the visual field in semi-parallel circuits is an evolutionary conserved strategy.

1.1.3 Retinotopic organization of mouse visual system

Visual perception relies on the processing of information about the location of a visual stimulus into the visual space and about the features of this visual stimulus (e.g. orientation, motion, direction of movement, colours). The first level where the visual field is mapped, is

the retina (Niell, 2015). In the retina, neighbouring photoreceptors detect light from neighbouring points in the visual field. This topographic mapping of the visual scene is maintained in every area of the primary visual system (retina, superior colliculus, thalamus and cortex), meaning that neighbouring neurons in these brain areas would respond to neighbouring points in the visual field (Niell, 2015; Allen *et al.*, 2016; Drager and Hubel, 2017) (Figure 1.2B, C). Indeed, the existence of a full retinotopic mapping has been adopted as a criterion to define functionally separated brain areas (Seabrook *et al.*, 2017). How a given portion of the visual field is represented in specific brain structures depends on two main factors: (1) the spatial distribution of the incoming axons (retinotopically mapped themselves), and (2) the spatial extent to which dendrites in the recipient area sample these axons. This means that despite retinotopy is maintained at every node of the visual pathway, uneven spatial arrangements of incoming axons or recipient dendrites can lead to enlargements, shrinkages and anisotropies of the visual space. With the criterion that a visual cortical area is defined by a discrete mapping of retinotopic space, as many as 11 visual cortical areas have been characterized (Wang and Burkhalter, 2007; Garrett *et al.*, 2014).

These results demonstrate how the structure of visual space is maintained at the anatomical level throughout the mouse visual system. Understanding the contingencies behind this structured organisation is key to understand how the brain extract and processes different features of the visual scene.

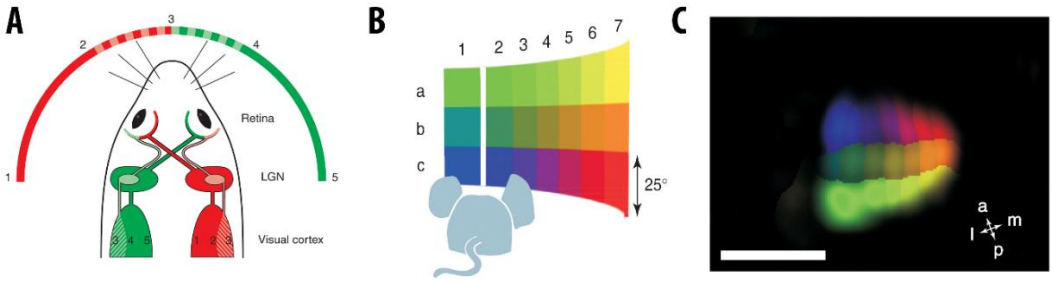

Figure 1.2: *Ocular dominance and retinotopic mapping in mouse visual system.*

A) Schemata showing the representation of the visual field in the mouse visual system. The left and right visual field of the mouse are coloured in red and green respectively. The portion of the visual field in front of the animal is the binocular part of the visual field and is seen by the temporal area of both eyes. Axons from this area project to eye-specific regions in the ipsilateral LGN while all the other axons project to the contralateral LGN crossing pathways at the optic chiasm. In the primary visual cortex, binocular vision is processed in the most lateral part. Numbers in the visual field and in the cortex show which area of V1 processes information about which area of the visual field. B,C) Schemata of the mouse visual hemi-field divided into 21 adjacent positions. Colour-coded map of the retinotopic organisation of the left primary visual cortex. The colour scheme matches the one depicted in the left panel. Abbreviations: a, anterior; p, posterior; m, medial; l, lateral. The scale bar represents 2mm. Figure is adapted from Hübener (2003)

1.1.4 On/Off receptive fields and the emergence of orientation and direction selectivity

In two articles published in 1959 and 1962, Hubel and Wiesel demonstrated for the first time that neurons in the visual cortex were responding to specific features of a visual stimulus. Three fundamental functional properties emerged from the response profile of cortical neurons in V1: (1) Selectivity for stimuli oriented at a specific angle (orientation selectivity), (2) A distinction between simple and complex responses in different neurons, and (3) for simple cells, the existence of a spatial receptive field consisting of roughly aligned ON and OFF receptive fields (Hubel and Wiesel, 1959, 1962)(Figure 1.3). Twenty years later, Drager (1975), demonstrated that many of the functional responses observed in the primary visual cortex of cats and monkeys were conserved in the primary visual cortex of mice. Using electrophysiological recordings during the presentation of visual stimuli, Drager was able to demonstrate that the receptive fields of the mouse primary visual cortex were organised in a topographic manner (Dräger, 1975). Subsequent studies demonstrated the existence of simple, complex, and orientation selective neurons in mouse V1 (Niell, 2015) (Figure 1.3).

Orientation selectivity has long been thought to be originated in the primary visual cortex. Hubel and Wiesel (1962) proposed that orientation selectivity was emerging because individual neurons in V1, would receive inputs from linearly aligned ON-centre neurons from the dLGN (Figure 1.3B). Despite this hypothesis is still widely accepted, more recent work suggests that difference in the tuning of inhibitory inputs also contributes to determine orientation selectivity (Li *et al.*, 2015). However, recent results suggest that at least in mice, this might not always be the case, and that cortical selectivity in V1 might simply be inherited from the neurons in the dLGN (Sun *et al.*, 2016). OS dLGN neurons constitute up to 40% in the mouse dLGN (Zhao *et al.*, 2013). These types of neurons are especially abundant in the dorsolateral shell of the dLGN (Marshel *et al.*, 2012; Piscopo *et al.*, 2013; Scholl *et al.*, 2013; Zhao *et al.*, 2013). On the other hand, it was noticed that projections from dLGN neurons cannot be the only mechanisms underlying the high proportion of OS neurons in V1. Indeed OS neurons in dLGN are still a minority and they tend to target V1 superficial layers only, suggesting that they may represent a parallel thalamocortical pathway in addition to the one primarily targeting layer 4 (Cruz-Martín *et al.*, 2014). Additionally, the response properties of V1 OS neurons are different from the response properties of OS dLGN neurons. Indeed, cortical neurons have elongated receptive fields and a linear response to gratings, on the other hand, OS dLGN neurons have circular and overlapping On and Off regions, and they mainly respond nonlinearly to gratings (Niell and Stryker, 2008; Bonin *et al.*, 2011). Finally, orientation selectivity in V1 is higher than orientation selectivity in the dLGN (Scholl *et al.*, 2013)

While spatially aligned ON/OFF cells give rise to orientation selective neurons, spatially aligned orientation selective neurons can give rise to complex cells and direction selective (DS) neurons (Figure 1.3C). Both complex and DS of neurons respond selectively to elongated bars moving within a 2-D area, however DS neurons are selective to movements in one direction only (Carandini, 2006). So far, two different models have been proposed to explain how direction selectivity arises in the mouse visual cortex (Hillier *et al.*, 2017; Lien and Scanziani, 2018). In the first model, direction selectivity arises from the spatial and temporal anisotropies of excitatory and inhibitory neurons, while in the second model, direction selectivity is simply inherited from direction selective retinal ganglion cells and transmitted down to the cortex (Zhao *et al.*, 2013; Hillier *et al.*, 2017; Lien and Scanziani, 2018).

Altogether these results highlight how the neural circuits involved in visual perception are wired to extract information about spatial and other features (orientation and movement direction) of visual stimuli in the animal's visual field.

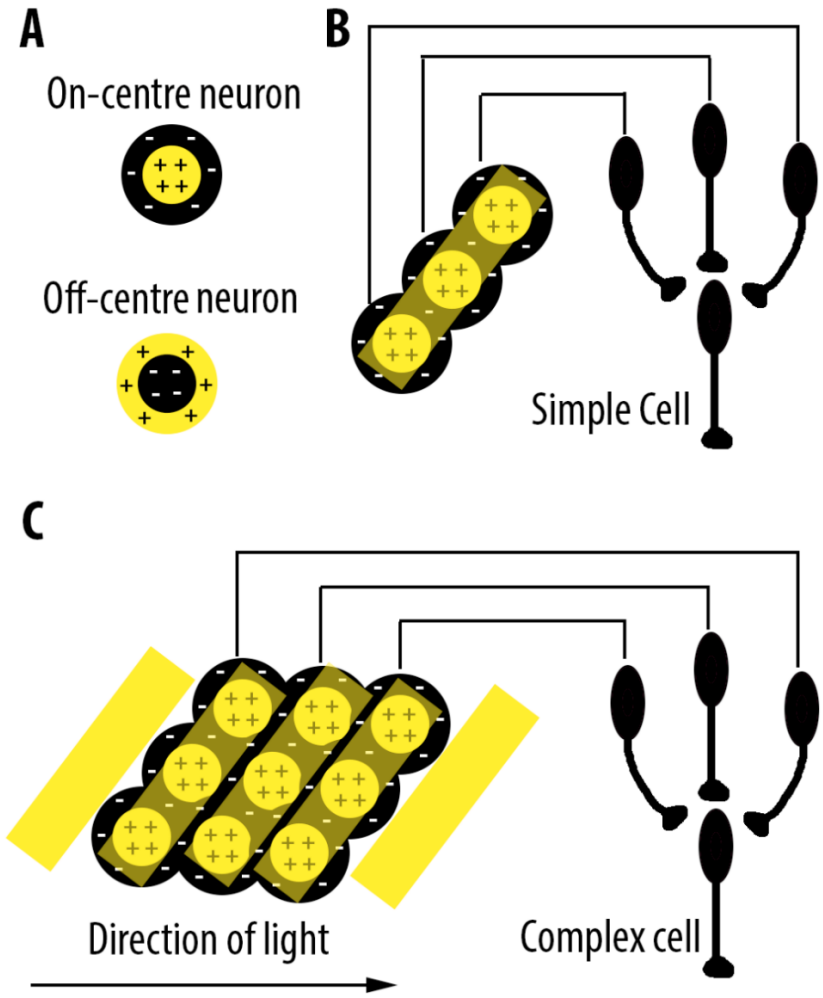

Figure 1.3: Hubel and Wiesel hierarchical model for simple and complex cells *from on-off receptive fields to complex cells.*

A) Schematic representation of ON and OFF-centre neuronal responses. ON-centre neurons are excited by a spot of light of a specific size and become hyperpolarised as the spot increases in size. OFF-centre neurons are excited by a dark spot in the middle of their receptive field and they become hyperpolarised as the dark spot increases in size. B) A simple cell is a neuron that responds to a bar of light oriented at a specific angle. Simple cells have an off surrounding that also hyperpolarizes the neuron if the spot of light expands or moves. The response of simple cells is thought to be generated by the inputs of several on-centre neurons aligned with each other at a specific angle. C) Similar to a simple cell, a complex cell also responds to oriented gratings or edges, however, differently from a simple cell, it has a degree of spatial invariance. This means that complex cells respond to angled stimuli within a larger field of view, regardless of the stimulus exact location or direction of movement. Just like the response of simple cells is generated by spatially aligned on-off centre neurons, complex cell response is thought to be generated by spatially aligned simple cells. Figure inspired from Hubel and Wiesel (1962).

1.1.5 The effects of arousal and locomotion on visual responses

Recent technological advances that allowed experimenters to study neuronal correlates of visual perception in behaving animals have revealed that cortical responses to visual stimuli are more than just feature extraction, as it was previously thought. These studies suggest that visual processing not only depends on the features of the stimulus itself, but also on several other parameters such as animal's behavioural (e.g. locomoting vs stationary) and internal state (aroused vs quiet). Additionally, the response to the same visual stimulus can be modified in an experience-dependent manner according to the contingencies associated with that stimulus in the past (e.g. aversive vs reward-associated) (Pakan, Francioni and Rochefort, 2018).

The impact of locomotion on visual processing in V1 has been studied by monitoring the speed of head-fixed mice that were free to run on cylindrical treadmill or spherical balls. Arousal has been quantified either by recording Local field potentials (LFPs) or by monitoring pupil dilation (Vinck *et al.*, 2015). Both arousal and locomotion have been associated with an increase in the activity of V1 neurons, both during darkness, and during the presentation of visual stimuli (Niell and Stryker, 2010; Polack, Friedman and Golshani, 2013; Fu *et al.*, 2014; Pakan *et al.*, 2016). Overall the effects of arousal and locomotion on neuronal responses in the primary visual cortex are rather similar, to the point that locomotion is often assumed to be a proxy of arousal (Erisken *et al.*, 2014). Despite both arousal and locomotion maintain intact the basic properties of V1 excitatory neurons, such as spatial frequency and the neuron's orientation preference, arousal but not locomotion increases the response magnitude at the preferred orientation, more than at non-preferred angles sharpening the selectivity of individual neurons. This orientation-specific gain leads to the sharpening of orientation tuning (Vinck *et al.*, 2015). On the other hand, locomotion was shown to inhibit surround suppression leading to increased spatial summation (Ayaz *et al.*, 2013; Erisken *et al.*, 2014). These effects have the net effect of increasing the reliability and robustness of neural coding in V1 (Dadarlat and Stryker, 2017). It was indeed shown that decoders used to infer the identity of the visual stimulus, based on neuronal activity perform better during locomotion compared to stationary. However, the mechanisms by which locomotion increased stimulus discriminability were layer-dependent. Indeed, while in layer 2/3 increased stimulus discriminability was due to an increase in firing rates, in layer 5 this was

mainly due to a decrease in noise correlation between different neurons (Dadarlat and Stryker, 2017).

The effects of locomotion have been demonstrated to be dependent on neuromodulatory inputs (Polack, Friedman and Golshani, 2013; Fu *et al.*, 2014). Both noradrenergic and cholinergic inputs to V1 have been involved in the gain responses of excitatory neurons in V1. Noradrenergic inputs are involved in maintaining a tonic level of membrane depolarisation of layer 2/3 neurons during locomotion, which facilitates the generation of action potentials (Polack, Friedman and Golshani, 2013). On the other hand, cholinergic inputs from the basal forebrain have been shown to increase their responsiveness during locomotion and both direct and indirect optogenetics activation of the cholinergic pathway was sufficient to recapitulate the effects of locomotion in V1 neurons, while the animal was stationary (Polack, Friedman and Golshani, 2013; Fu *et al.*, 2014).

Visual flow and locomotion are intrinsically bound to one another. Indeed, movement is intrinsically associated with changes in the visual scene we perceive. This association is learnt since birth, and it is very reliable. Indeed, very rarely the movements of our body do not correspond with a visual flow coherent with our movements. When this happens, people usually feel vertigo and loss of balance as in the notable case of the spinning tube illusion. This happens because the brain receives conflicting information from the internal sense generated by the body and from the external senses. Using virtual reality, recent studies have explored how the brain integrates information coming from body movements and visual information coming from the outside world (Harvey *et al.*, 2009; Keller, Bonhoeffer and Hübener, 2012; Saleem *et al.*, 2013). Virtual reality is particularly suitable to study these interactions as it allows the experimenter to decouple the virtual world from the animals' body movement, while recording neuronal activity (Harvey *et al.*, 2009; Saleem *et al.*, 2013; Pakan *et al.*, 2018). Using this approach, Keller's group found that a subpopulation of V1 neurons in layer 2/3 responds selectively to mismatches between the visual flow and the animal's movements (Keller, Bonhoeffer and Hübener, 2012; Zmarz and Keller, 2016). Interestingly, these neurons responded to mismatches in a specific portion of the visual field, suggesting that mismatches are topographically matched to the visual space and that neurons possess receptive fields for mismatch signals too (Zmarz and Keller, 2016). These signals have been shown to be driven by axonal boutons derived from the A24b area, a subdivision of the ACC and an adjacent part of M2, that send predictive signals to V1 in a topographically organized manner (Leinweber *et al.*, 2017). Mismatch responses are shaped

by experience during development. Indeed, mismatch responses were absent in animals that never experienced sensorimotor coupling (Attinger, Wang and Keller, 2017).

Altogether these results demonstrate how the response of individual neurons to the same visual stimulus can be altered by the behavioural and by the internal state of an animal.

1.1.6 Learning and the emergence of predictive coding in V1

In addition to study neuronal responses to visual stimuli during different behavioural states, using imaging techniques, it is now possible to track the activity of many neurons over the course of several days, while the animal learns a task. The aim is to understand whether and how, experience affects the processing of visual information (Dylda, Pakan and Rochefort, 2019).

Several studies have shown how repetitive exposure to the same visual stimulus is associated with changes in the cortical representation of that stimulus. Using LFP recordings in layer 4, it was shown that passive and repetitive exposure to a stimulus, potentiates the neuronal response to that stimulus (Frenkel *et al.*, 2006; Cooke and Bear, 2015). A second study confirmed that passive exposure to a visual stimulus could increase layer 2/3 responses to that stimulus, however, the potentiation level correlated with the amount of locomotion during the presentation of the repetitive stimulus. This effect saturated after an hour (Kaneko, Fu and Stryker, 2017). In contrast, an additional study demonstrated that the number of visually-responsive neurons in V1 decreased across days in response to repetitive, passive exposure to the same stimulus (Makino and Komiyama, 2015). The apparent discordance of these results could be attributed both to different experimental designs and to the lack of standardisation of analysis used for these studies (Pakan, Francioni and Rochefort, 2018). In addition to technical reasons, discrepancies can be explained by the results found in an additional study suggesting that cortical responses are the synthesis of activity of two distinct neuronal populations: a strongly responsive, more stable population and a weakly-responsive plastic population (Ranson, 2017). These results suggest that attenuation and potentiation are not two mutually exclusive phenomena but rather they are complementary within a circuit and population-dependent.

While it is yet not fully elucidated how passive and repetitive exposure to a visual stimulus changes the neuronal response to that stimulus over time and what mechanisms mediate these changes, there is more consensus emerging from studies using a visual task that

require an active engagement of the animal. Several independent studies demonstrate how the visual cortex enhances the representation of relevant stimuli (e.g. reward-associated) and how with time, cortical neurons become responsive to the contingencies of a specific stimulus, as opposed to the features of the stimulus itself (see reviews: Keller and Mrsic-Flogel, 2018; Pakan, Francioni and Rochefort, 2018). To motivate the animals to perform a task, the animal is generally deprived of either food or water which is then delivered during performance. Alternatively, a specific stimulus is paired to a second aversive stimulus that motivates the animal to actively avoid the aversive stimulus (Guo *et al.*, 2014). In rats V1, neurons in the deep layers of the cortex were shown to become responsive to reward timing. These neurons underwent either a sustained increase or decrease in activity which lasted according to the time interval between the presentation of a visual stimulus and the delivery of its associated reward (Shuler and Bear, 2006; Gavornik and Bear, 2014). Subsequent studies confirmed this effect and showed that the acquisition, but not the expression of this type of activity depends on cholinergic inputs arriving in V1 from the basal forebrain (Liu *et al.*, 2015). Using a stimulus discrimination task, another group has demonstrated that V1 neurons become better at discriminating a rewarded stimulus compared to a non-rewarded one. At the single cell level, neuronal responses became more reliable increasing discriminability, while at the population level, a higher proportion of neurons become selective to the rewarded task (Poort *et al.*, 2015). Similarly, using classical conditioning, it was shown that learning an orientation discrimination task, correlated with better neural discriminability, increased orientation tuning and contrast sensitivity (Jurjut *et al.*, 2017). Interestingly, neuronal changes manifested before any detectable behavioural change (Jurjut *et al.*, 2017). Using an active-avoidance task in which a specific visual stimulus was associated with a mild tail shock, it was shown that the response of layer 2/3 neurons ramps up in response to the stimulus after learning, but not in response to the same stimulus during passive viewing, before learning and during anaesthesia (Makino and Komiyama, 2015). This effect was suggested to be mediated through a predictive signal arriving from the retrosplenial cortex. In the same study, bottom up inputs, thought to represent a lower dimensional, purely sensory-driven signal coming from the thalamus and broadcasted through layer 4 neurons in the cortex, were shown to remain invariant during learning (Makino and Komiyama, 2015). An additional study demonstrated that the presentation of sustained stimuli leads to an adaptation of neuronal activity in V1 when the stimulus wasn't relevant for solving a visual task (Keller *et al.*, 2017). Finally, it was shown that responses to a given stimulus differed if this stimulus was encountered at different spatial locations.

Responses to the stimulus were modified by experience and became predictive about the expected delivery of a reward as well as to an expected reward location, even in the absence of visual stimulation (Fiser *et al.*, 2016; Pakan *et al.*, 2018) suggesting that visual responses in V1 become modulated by the animal's position (Diamanti *et al.*, 2019) (Figure 1.5).

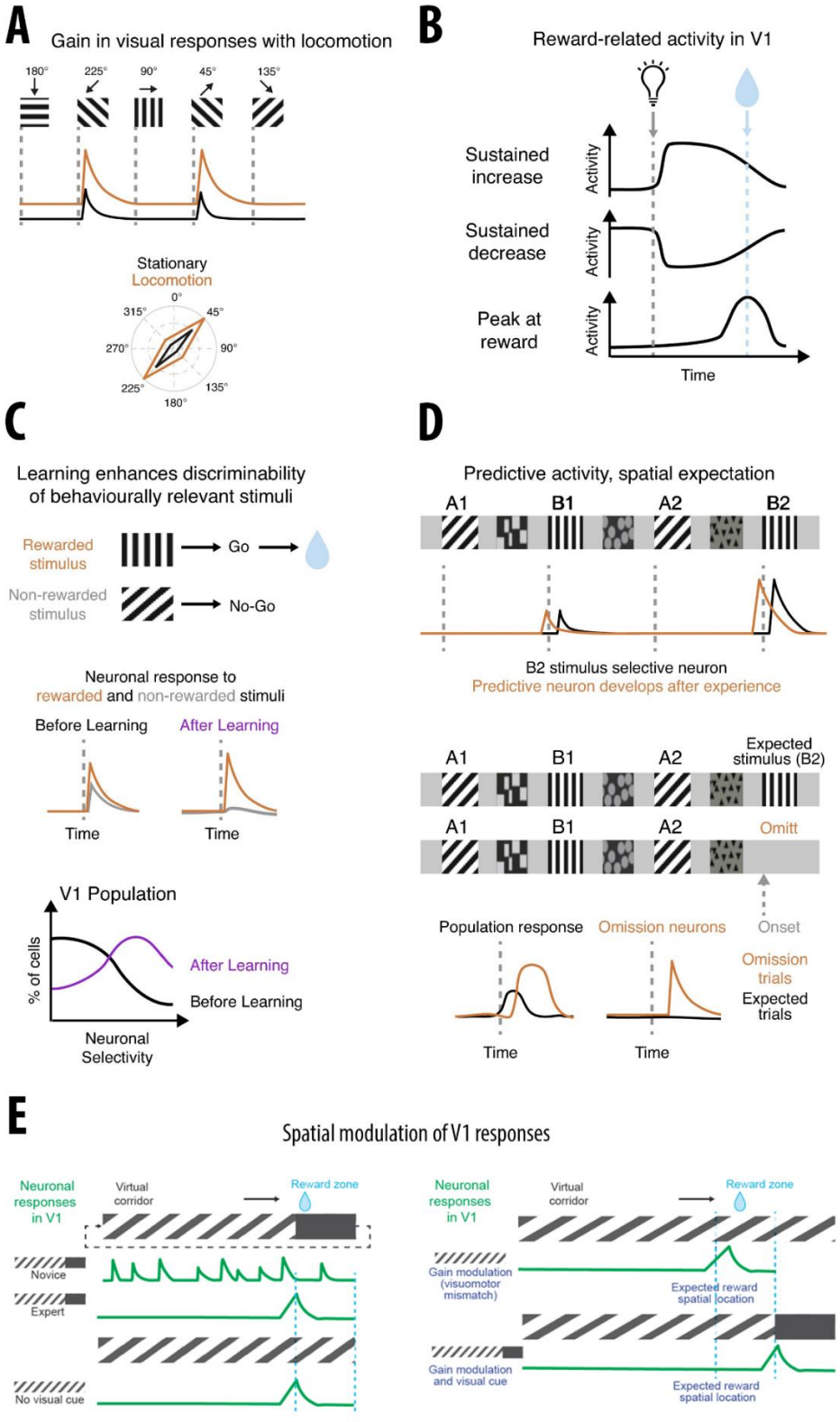

Figure 1.5: *Non-visual variables encoded by V1 neurons.*

A) Neurons in V1 are gain modulated during locomotion (orange trace). Neuronal tuning is not altered during locomotion. B) After the animal learns the association between a visual stimulus and a reward, V1 predicts the timing of reward delivery. This is mediated by either an increase or a decrease in activity after the onset of a visual stimulus associated with a reward. Some neurons peak at the expected reward time (Shuler and Bear, 2006). C) Schematic of V1 responses during the learning of a visually guided task. Example of a go/no-go task with two oriented gratings one of which is rewarded. Single neurons' response to the two presented stimuli show that neuronal discriminability between the rewarded (orange) and nonrewarded (grey) stimuli increases with task learning. On the population level (bottom panel), a higher proportion of neurons in V1 show increased selectivity to task-relevant gratings after learning (purple) (Poort *et al.*, 2015). D) *Top panel*, Traces show how neuronal responses start to be predictive of visual cues, before (black) and after (orange) repeated exposure to the same sequence. *Lower panel,* On the population level, when the stimulus is present there is an evoked response to the stimulus (black trace). When the stimulus is un-expectantly omitted (orange trace), there is a large and delayed increase in activity. A subpopulation of neurons responds selectively to these omission events, and not to the initially expected stimulus (Fiser *et al.*, 2016). E) *Left panel*, as the animal learns to associate a reward to a visual stimulus at a specific spatial location, most V1 neurons show task-related activity. If the visual stimulus is removed, V1 neurons respond to an expected reward location. In a gain-modulated corridor, in the absence of visual stimulation, neurons respond to the expected reward based on the physical distance from the reward. However, once the visual clue is re-introduced in the gain-modulated corridor, neuronal responses of layer 2/3 neurons relies on visual rather than spatial information (Pakan *et al.*, 2018). Figure is adapted from Pakan, Francioni and Rochefort (2018) and Pakan *et al.*, (2018).

1.1.7 Concluding remarks

It is now established that neurons in the visual cortex not only process information about the visual features of the world, but also integrate non-visual features including: experience, context and behavioural state-dependent variables. Since the response properties of neurons in the visual cortex emerge from the specific connectivity between neurons, understanding how functional properties emerge at the single-cell and circuit levels, requires the investigation of the wiring patterns that endow neural circuits with their complex computational properties. As such, cortical circuitry will be the focus of the next section.

1.2 Canonical circuits in the mouse cortex

Cortical processing is the result of the complex interplay between several different types of neurons. These types broadly separate into excitatory and inhibitory neurons. However,

neuronal subtypes are also distinguished based on their projection patterns, physiological, morphological, functional and molecular properties. While there is no consensus about how many types of neurons exist, or even about the features that are most relevant to characterise neurons functionally, it is clear, that there is a wide heterogeneity in cortical neuronal types (Gouwens *et al.*, 2019).

Broadly speaking, cortical excitatory neurons are referred to as principal cells, communicate through glutamatergic neurotransmitters and propagate excitatory signals within and between different brain areas. On the other hand, inhibitory neurons are often referred to as interneurons, communicate mainly locally via the inhibitory neurotransmitter GABA and are involved in gating signal flow and finely tune the responses of excitatory neurons.

Despite the diversity of neuronal types, cortical motifs seem to be maintained invariant across different cortical areas and species, suggesting that understanding the algorithms implemented by these wiring motifs, is key to understand how cortical circuits process information (Harris and Shepherd, 2015) .

1.2.1 Excitatory classes of cortical neurons

Neocortical excitatory neurons compose approximately 80% of the total of cortical neurons. These neurons have been distinguished into three subclasses based on their axonal projection patterns (Harris and Shepherd, 2015) (Figure 1.6).

(1) *Intratelencephalic neurons (IT neurons)*. IT neurons make synaptic connections with targets in the telencephalic structures including the neocortex, the striatum, the amygdala and the claustrum. Interestingly these neurons are the only type of principal neurons that send projections to the contralateral hemisphere of the brain. IT neurons are found in cortical layer 2 to 6. However, IT neurons in layer 4 constitute a functionally diverse class compared to IT neurons in all the other layers (Harris and Shepherd, 2015).

(2) *Pyramidal tract (PT) neurons*. Specifically found in layer 5B (Harris and Shepherd, 2015), PT neurons send projections to many different brain regions including the ipsilateral cortex, the striatum and the thalamus. However, they are the only subclass of excitatory neurons to target sub-cerebral areas such as the brainstem, the midbrain and the spinal cord (Harris and Shepherd, 2015; Ramaswamy and Markram, 2015). The properties of these neurons have been well characterised both *in vitro* and *in vivo* (Ramaswamy and Markram, 2015). Due to their characteristic wide apical tuft, the dendrites of PT neurons span and receive synaptic inputs from neurons in all the layers of the cortex. Interestingly, these neurons make very

few synapses locally and are mainly implicated in the broadcasting of signals to other areas. As such, they are often defined as the integrators of the cortical column: they process information from the entire cortical depth and send out the final computation without directly affecting the computation locally (Morishima, 2006; Brown and Hestrin, 2009; Kiritani *et al.*, 2012). Compared to other cell types, PT neurons have relatively depolarised resting membrane potentials, non-adapting spike trains, narrow spikes and a strong expression of hyperpolarisation-activated cation (HCN) channels (Sheets *et al.*, 2011; Shepherd, 2013; Suter, Migliore and Shepherd, 2013). Altogether, these properties endow PT neurons with the highest firing rates *in vivo* among excitatory neurons (Beloozerova *et al.*, 2003; De Kock *et al.*, 2007; De Kock and Sakmann, 2008). Dense coding expressed by these neurons may provide a computational advantage to broadcast cortical output through a relatively small number of long-projecting axons (Harris and Mrsic-Flogel, 2013). Additionally, PT neurons have distinct neuromodulatory properties suggesting that they may be particularly suitable to broadcast to other target areas, changes in the internal state of the animal (Dembrow and Johnston, 2014).

(3) *Corticothalamic (CT) neurons.* CT neurons are only found in layer 6 and they primarily project to the ipsilateral thalamus. Because of their deep cortical localisation, relatively little is known about this neuron type. CT neurons receive little excitatory inputs from thalamic and local inputs, but they are strongly innervated by high-order cortical areas (Thomson, 2010; Feldmeyer, 2012; Vélez-Fort *et al.*, 2014). Primarily, these neurons activate thalamic postsynaptic neurons through the activation of metabotropic receptors. As such, these neurons were classified as modulators rather than drivers (Swadlow, 1994; Guillery and Sherman, 2002). Intracortical CT axons, tend to target neurons in the deep layers, predominantly in layer 5 and 4. In V1, they indirectly inhibit all the other cortical layers through a disynanptic circuit mediated by Parvalbumin (PV)+ interneurons (Olsen *et al.*, 2012; Bortone, Olsen and Scanziani, 2014). While the functional role of these neurons is not well understood, some evidence suggest that by inhibiting the entire column, CT neurons may play a role in modulating gain responses to sensory inputs (Olsen *et al.*, 2012).

1.2.2 Thalamic inputs to the cortex

In addition to their projection targets IT, PT and CT neurons differ in the type of excitatory inputs they receive from different thalamic relay nuclei. The thalamus sends inputs to the

cortex in mainly two different streams (Jones, 2001; Clascá, Rubio-Garrido and Jabaudon, 2012):

(1) *The core thalamus*, composed of primary relay nuclei, sends topographically-organised information to the cortex that mainly convey sensory and motor information. Most of its connections reach all different types of cortical excitatory neurons. Core thalamus predominantly reaches the cortex on IT neurons in layer 4; however, it also targets other IT neurons in layer 3, 5 and 6, PT neurons in layer 5B and CT neurons in layer 6 (Harris and Shepherd, 2015). Interestingly, connected pairs of layer 4 neurons share a higher proportion of thalamocortical afferents compared to non-connected pairs (Morgenstern, Bourg and Petreanu, 2016). Core thalamus is considered a lower order part of the thalamus as it receives most of its afferent from the retina, even though it also receives feedback projections from the cortex (Clascá, Rubio-Garrido and Jabaudon, 2012).

(2) *The Matrix Thalamus*. It is composed of higher order thalamic areas that receive their excitatory inputs from corticothalamic axons, but it is not innervated by retinal axons. It predominantly projects onto layer 1 and layer 5 of the cortex, targeting preferentially IT neurons. Differently from the core thalamus, the matrix thalamus completely avoids layer 4. The information that the matrix thalamus conveys to the cortex is poorly understood, however matrix thalamus can be further subdivided into two different subclasses depending on whether it targets a single cortical area, or it projects more broadly (Clascá, Rubio-Garrido and Jabaudon, 2012; Harris and Shepherd, 2015).

1.2.3 Cortical connectivity

Even though each class of neurons receives strong extrinsic inputs, once it reaches the cortex, the flow of information travels mainly in a directional manner. This is because IT, PT and CT neurons in different layers are connected to each other asymmetrically. Layer 4 neurons project strongly to layer 2/3 neurons and to layer 5. However, they receive very little excitation from these neurons in return . Indeed, their main sources of excitation comes from other local layer 4 neurons and from core thalamic inputs. As such, layer 4 neurons are thought to be mainly involved in sensory processing (Feldmeyer, 2012; Makino and Komiyama, 2015). In contrast to mainly unidirectional projection pattern of layer 4 IT neurons, all the other IT neurons in different layers target each other reciprocally. Once the signal reaches layer 2/3 from layer 4, functional evidence suggests that IT neurons in layer 2/3 send projections onto each other, dense projections to both IT and PT in layer 5, weak

projections to layer 6 and avoid sending projections back to layer 4. (Douglas and Martin, 2004; Petreanu *et al.*, 2007; Thomson, 2007; Adesnik and Scanziani, 2010). Interestingly, the circuit architecture of the layer 2/3 to layer 5 motif seems to be highly conserved not only between different cortical areas, but among many different species, *suggesting* that this is a conserved cortical circuits motif (Douglas and Martin, 2004; Harris and Shepherd, 2015). In addition to excitatory inputs from layer 4, layer 2/3 neurons also receive a dense excitatory drive from layer 5. Due to their hyperpolarised membrane potential *in vivo*, layer 2/3 neurons fire sparsely (Lefort *et al.*, 2009). Under a theoretical point of view, sparse coding is instrumental to drive plastic changes and indeed, layer 2/3 neurons possess denser spine clusters compared to layer 5 neurons (Tjia *et al.*, 2017), and were shown to be the more plastic compared to other layers (Feldman and Brecht, 2005; Tjia *et al.*, 2017). Layer 5 is populated by two rather different population of neurons. IT neurons have thin dendrites that are less arborized compared to PT neurons. They are smaller than PT neurons and *in vivo*, they fire less (Chagnac-Amitai, Luhmann and Prince, 1990; Schwindt and Crill, 1999; Jacob *et al.*, 2012). PT and IT neurons wire with each other asymmetrically. While IT target both themselves and PT neurons, PT neurons almost exclusively target themselves directly, but even more strongly, they inhibit each other through a disynaptic circuit mediated by Martinotti cells (Harris and Shepherd, 2015; Ramaswamy and Markram, 2015). Interestingly, a recent study found that layer 5 neurons receive stronger cortico-cortical afferent from the same regions they project to, than the regions they do not project to (Young *et al.*, 2019).

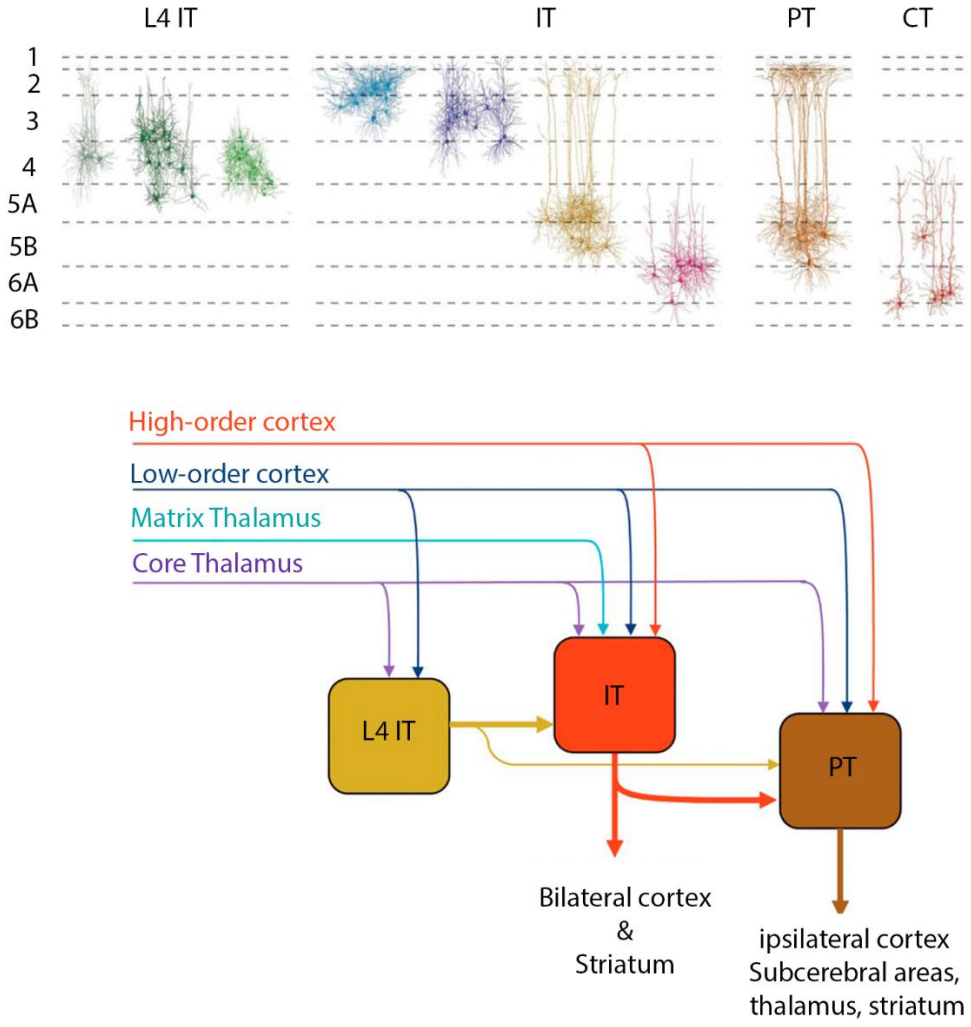

Figure 1.6: *Subtypes and connectivity of excitatory neurons in the neocortex*.

Upper panel, Neuron types defined by their layer and afferent, efferent projections. Three types of layer 4 neurons exist: pyramidal, star pyramidal and stellate. The other IT neurons are classified based on the cortical layer they occupy. PT neurons occupy layer 5B and they are characterised by a thick and widespread apical tuft, extending in layer 1. Layer 5B is defined by the presence of this neuron type. CT neuron occupy mainly layer 6. They possess an apical dendrite which spans up to the layer 4-to-layer 3 border. *Lower panel,* L4 IT neurons project mostly unidirectionally to other IT neurons in the other layers (primarily layer 2/3). Layer 4 recipient neurons project mostly unidirectionally to PT neurons in layer 5. Each class receives different and partly overlapping extrinsic inputs, but information flows in a directional manner due to the asymmetry in connectivity between different neuronal types (arrow width indicates the weight of the connection). All classes connect to other members of the same class (not shown). The relationship between CT and IT neurons is not yet clarified (CT neurons not shown). Figure re-adapted from Harris and Shepherd (2015).

1.2.4 Inhibitory circuits

Despite composing only 20% of the total number of neurons, inhibitory neurons are an extremely heterogeneous class. These neurons can be divided into several different classes based on anatomical, electrophysiological and molecular attributes; Inhibitory interneurons have been implicated in several cortical functions: gain control, feature selectivity, plasticity, temporal precision, bursts regulation, synchrony and generation of cortical rhythms, plasticity and in preventing cortical excitation runaway (Fino, Packer and Yuste, 2012). It is therefore no surprise that the dysfunction of different classes of inhibitory neurons have been implicated in several diseases including epilepsy, schizophrenia, anxiety and autism (Lewis, Hashimoto and Volk, 2005; Marín, 2012; Goldberg and Coulter, 2013).

Recent studies have highlighted that almost all cortical inhibitory neurons can be distinguished in three non-overlapping populations, based on their molecular identity. Parvalbumin (PV+), Somatostatin (SST+) and ionotropic serotonin receptor (5HT3aR+) – positive populations (Rudy *et al.*, 2011). Despite several studies aim at understanding the cortical functions of these three populations of neurons *in vivo*, it should be stressed that it is not fully clear to what extent the molecular properties of these neurons are a valid determinant to understand the functions of these neurons since these molecular markers are not necessarily involved in shaping the functional features of neurons (Tremblay, Lee and Rudy, 2016). Additionally, all these populations can be further subdivided into several subclasses (Gouwens *et al.*, 2019). The cortical functions of these neurons were studied by genetically targeting them with genetically-encoded probes to both record and manipulate their activity.

PV+ neurons. This group accounts for approximately 50% of all interneurons and includes two main subclasses of interneurons: Fast-spiking (FS) basket cells that target the soma and the perisomatic dendrites, and axo-axonic neurons that target the axon initial segment and are known as chandelier cells. They are abundant in layer 4 and (Xu, Roby and Callaway, 2010) and have a set of molecular and physiological features that allow them to spike fast, reliably and strongly (Pouille, 2001; Howard, Tamas and Soltesz, 2005; Rossignol *et al.*, 2013; Hu, Gan and Jonas, 2014; Tremblay, Lee and Rudy, 2016). Because both cell types target their postsynaptic targets close to the soma, and therefore to the site of action potential generation, they are particularly suited to effectively block somatic output (DeFelipe *et al.*, 2013).

SST+ neurons. SST+ neurons preferentially target the dendrites of their postsynaptic partner (Kawaguchi and Kubota, 1996; Kawaguchi, 1997; Wang *et al.*, 2004) suggesting that their physiological role is to influence dendritic computation. Based on their morphology, SST+ can be divided into two main subtypes: Martinotti and non-Martinotti cells (Yavorska and Wehr, 2016). Differently from non-Martinotti neurons, Martinotti cells have broad axonal arborisations in layer 1 where they target the apical tuft dendrites of pyramidal neurons. They are most abundantly found in layer 2/3 and layer 5 and they make little or no connection to other SST+ interneurons (Yavorska and Wehr, 2016).

5HT3aR neurons. This population of neurons composes approximately the 25% of all interneurons and among all other types, they are the most heterogenous class. Despite this heterogeneity all 5HT3aR neurons express 5HT3aR and nicotinic receptors (Lee *et al.*, 2010). They are the main population of layer 1 interneurons which they inhabit almost exclusively (Tremblay, Lee and Rudy, 2016). Despite their diversity, 5HT3aR interneurons can be broadly divided into VIP+ and VIP- neurons.

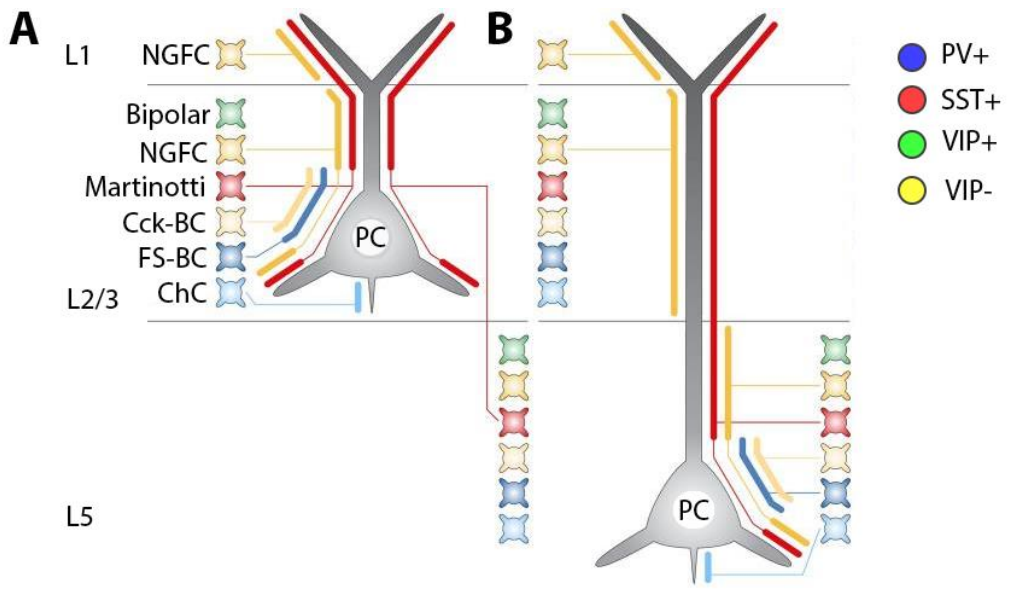

Figure 1.7: *Inhibitory neurons connectivity in the cortex*.

A) Schematic representation of inhibitory connectivity on layer 2/3 pyramidal neurons. B) Schematic of the connectivity onto layer 5 pyramidal neurons. Abbreviations: NGFC, Neurogliaform cells; Cck-BC, CCK+ Basket cells; FS-BC, Fast-spiking Basket cells; ChC, Chandelier cells. For simplicity, connections between inhibitory neurons have been omitted. Figure re-adapted from (Tremblay, Lee and Rudy, 2016)

1.3 Dendritic integration of synaptic inputs

In order to understand neural circuit function, not only do we have to determine how different types of neurons connect to each other, but we also need to characterize how the barrage of synaptic inputs that every neuron receives at any given time is integrated and transformed into an output. Does the same barrage of inputs always produce the same output, or can the neuron respond in two different ways given his previous activation history or the current network state?

Excitatory neurons receive most of their excitatory inputs onto electrically and chemically isolated structures called synaptic spines which protrude from neuronal dendrites. Spines are enriched in glutamatergic, GABAergic and neuromodulatory receptors in addition to express voltage-gated (VG) ion channels. Synaptic inputs are integrated and transmitted to the soma through the dendrites. Far from being simple passive cables however, dendrites can themselves produce all-or-none action potential-like events and are therefore capable of being an independent computational compartment themselves (Spruston, 2008). A rich

literature of *ex vivo* work on dendrites has shown the variety of active computations that dendrites have the biophysical potential to perform (for review see Stuart and Spruston (2015)). However, the occurrence and relevance of these events in the intact brain is a matter of current debate.

1.3.1 Dendritic morphology

Broadly speaking, inhibitory and excitatory neurons can be anatomically distinguished based on the presence of dendritic spines onto their dendrites, even though some exceptions exist (Kawaguchi, Karube and Kubota, 2006). Pyramidal neurons are abundantly found in the neocortex of every mammalian species that has ever been studied and therefore their typical morphology is thought to endow these neurons with integrative capabilities important for cortical computations. The distribution of these neurons, particularly abundant in high-order cognitive areas suggest that this type of neuron is associated with advanced cognitive functions (Spruston, 2008). Because of this, pyramidal neurons have been at the centre of many studies trying to elucidate the computational capabilities of single cells in the brain.

As their name suggests, pyramidal neurons have a typical pyramid-shaped soma. The dendritic tree of pyramidal neurons is divided into four different domains: basal, trunk, oblique and tuft dendrites. Basal dendrites are relatively short and originate at the base of the soma and extend in all directions in the surrounding area. The trunk is a single, thick dendrite that extends vertically until approximately 200 µm (in mice) from the cortical surface where it starts to branch into increasingly thinner dendritic branches that compose the apical tuft. Oblique dendrites are small protrusions extending in all directions that stem out from the trunk in layer 4.

1.3.2 Dendritic electrophysiological properties of cortical layer 5 pyramidal neurons

The dendrites of layer 5 pyramidal neurons express a wide variety of ion channels including: A-type and persistent K^+ channels, transient and persistent Na^+ channels, HCN channels, several different types of Ca^{2+} channels, small and large Ca^{2+}-activated potassium channels (SK and BK, respectively) that all contribute to the integration of synaptic inputs (Stafstrom *et al.*, 1985; Reuveni *et al.*, 1993; Stuart and Sakmann, 1994; Bekkers, 2000a, 2000b; Korngreen and Sakmann, 2000; Huguenard, Hamill and Prince, 2006; Kole, 2006; Almog and Korngreen, 2009; J. Kang, Huguenard and Prince, 2017). Interestingly, their distributions are

not always uniform across the dendritic tree of these neurons. A-type K^+ channels decrease in density along the somato-dendritic axis and plateau at the apical tuft (Harnett *et al.*, 2013). *In vitro*, these channels have been demonstrated to compartmentalise the apical tuft dendrites from the soma, regulate the spread of backpropagating action potentials (bAPs), and constrain the generation of dendritic spikes (Golding *et al.*, 1999; Benhassine and Berger, 2009; Harnett *et al.*, 2013); *In vivo*, during a sensory-motor behavioural task, these dendrites control the initiation and the duration of regenerative plateau potentials in the apical tuft, effectively controlling the duration and frequency of somatic bursts of action potentials (Bekkers, 2000a; Korngreen and Sakmann, 2000; Schaefer *et al.*, 2007; Harnett *et al.*, 2013; Jian Kang, Huguenard and Prince, 2017). HCN channels are activated when the membrane potential is hyperpolarised and they allow the entry of cations, providing a net depolarisation. These channels are expressed as a gradient along the somato-dendritic axis and their expression increases exponentially as a function of distance from the soma with an increase of up to more than 50-fold in the very distal part of the tuft compared to the soma (Berger, Larkum and Lüscher, 2001; Lörincz *et al.*, 2002; Berger, Senn and Lüscher, 2003; Kole, 2006; Harnett, Magee and Williams, 2015; Williams and Stuart, 2017). Whether Ca^{2+} conductance is distributed unevenly through the somato-dendritic axis, remains more controversial. To the best of my knowledge, there is no direct evidence of a non-uniform distribution of Ca^{2+} channels along the somato-dendritic axis of layer 5 pyramidal neurons, but functional evidences suggest that the trunk of neurons functions as a hotspot for the initiation of Ca^{2+} spikes (Reuveni *et al.*, 1993; Yuste *et al.*, 1994; Larkum and Zhu, 2002; Stuart and Spruston, 2015). Nonetheless, other mechanisms may favour the initiation of Ca^{2+} spikes at this spot, including a more depolarised resting potential or differences in input resistance (Ramaswamy and Markram, 2015). VG Ca^{2+} channels dominate in the dendrites of layer 5 pyramidal neurons. Both low and high-voltage activated Ca^{2+} channels are present as well as fast and slow-activating and inactivating channels (Almog and Korngreen, 2009). These channels are required for the generation of dendritic plateau potentials in the dendrites which is strongly associated with bursting of action potentials in the soma (Spruston *et al.*, 1995; Schiller *et al.*, 1997; Larkum, Kaiser and Sakmann, 1999; Larkum, Zhu and Sakmann, 1999). On the other hand, the density of Na^+, and Ca^{2+}-activated K^+ channels is uniformly distributed along the somato-dendritic axis (Schwindt and Crill, 1995; Benhassine and Berger, 2005; Astman, 2006; Książek *et al.*, 2013). Na^+ currents are required to sustain the backpropagation of somatic action potentials into the dendrites as well as for the generation of locally-generated Na^+ spikelets (Golding and Spruston, 1998; Golding, Staff and Spruston,

2002). Finally, both SK and BK channels, activated by intracellular Ca^{2+}, are required to constrain the duration and the amplitude of Ca^{2+} plateau potentials in the dendrites and as such, they regulate dendritic excitability and therefore their coupling with somatic activity (Benhassine and Berger, 2009; Książek *et al.*, 2013) (Figure 1.8).

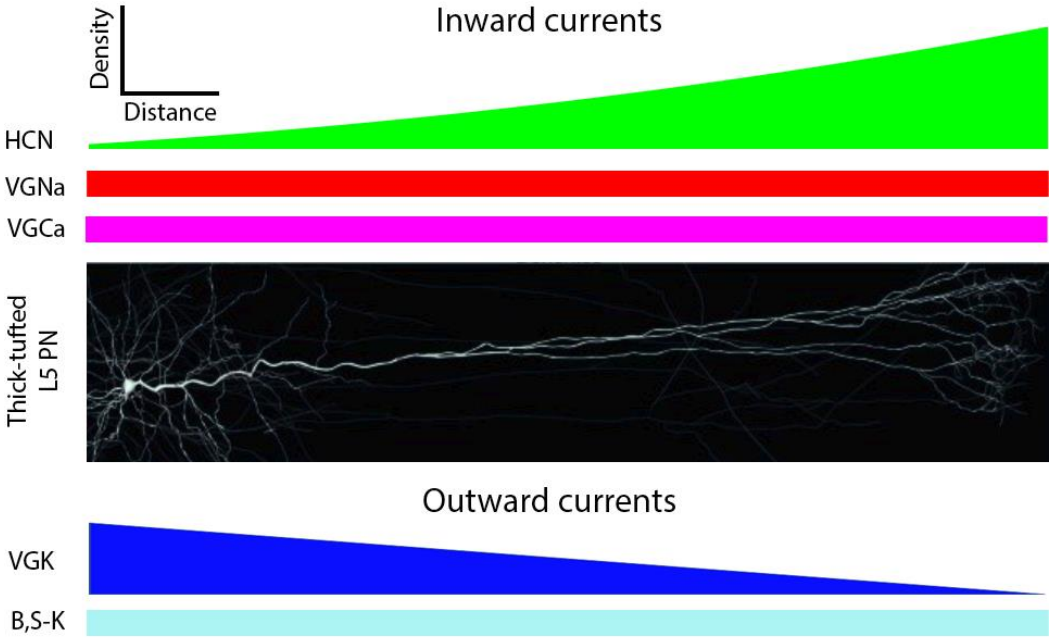

Figure 1.8: *Voltage-gated ion channels distribution in a thick-tufted layer 5 pyramidal neuron***.** Schematic of voltage-gated ion channels distribution along the somato-dendritic axis of an individual layer 5 thick tufted pyramidal neuron. Inward currents are on top, outward currents at the bottom. Each of these channels, contains several subtypes. Abbreviations: HCN, Hyperpolarisation-activated cation channel; VGNa, Voltage-gated Sodium Channel; VGCa, Voltage-gated calcium channel; VGK, Voltage-gated potassium channel; B,S-K, Big and Small calcium-activated potassium channel; L5 PN, Layer 5 pyramidal neuron. Figure re-adapted from Ramaswamy and Markram (2015)

1.3.3 Dendritic spines and synaptic plasticity

Dendritic spines are the site where most of excitatory inputs target excitatory neurons. The spine neck has a very important isolating role. Being small in diameter, the spine neck constrains the diffusion of small molecules and ions that are in the cytoplasmic fluid of the spine. For the same reason, the spine neck is a site of very high input resistance and as such,

it compartmentalises the currents generated in the spine from the main shaft of the dendrite (Beaulieu-Laroche and Harnett, 2018). In addition to compartmentalise the inputs, synaptic spines have been hypothesized to be useful to increase the surface area over which thousands of presynaptic inputs can make contact (Koch and Zador, 1993; Nimchinsky, Sabatini and Svoboda, 2002; Tsay and Yuste, 2004).

The spine head is the site where the post-synaptic density (PSD) is found. The PSD hosts several different receptors which include AMPA, NMDA, GABAA and GABAB. These receptors are attached to protein signalling machineries which have the role of triggering the molecular cascades required for both potentiation and depression of synaptic strength (Fifková and Van Harreveld, 1977; Doyle, 1978; Goldman-Rakic *et al.*, 1989; Beaulieu *et al.*, 1992; Nusser *et al.*, 1998; Nimchinsky, Sabatini and Svoboda, 2002). According to Hebbian rules of plasticity, a synapse becomes potentiated when the activation of that synapse takes part in firing the postsynaptic neuron. The mechanism through which Hebbian plasticity manifests itself, it's called Spike-timing dependent plasticity (Bliss and Collingridge, 1993; Bi and Poo, 1998). This mechanism imposes a window of approximately 20 ms, from the moment in which a synapse is activated, for the postsynaptic neuron to spike. The closer in time postsynaptic activation is to the time of synaptic activation, the stronger the potentiation at that synapse.

The mechanisms of synapse strengthening is called long-term potentiation (LTP). Similarly, it was shown that if a synapse is activated in the range of 0 to 20 ms after an action potential has already been generated, a mechanism of synaptic weakening takes place known as Long-term depression (LTD) (Bliss and Collingridge, 1993; Bear, 1996; Bi and Poo, 1998). NMDA receptors have been shown to be required to induce synaptic plasticity at synaptic spines and their antagonists block both LTP and LTD (Lüscher and Malenka, 2012). NMDA receptors are ionotropic glutamate ion channels that allows the entry of cations (especially Ca^{2+}) when opened. When glutamate binds to the NMDA receptor with the neuron at resting membrane potential, the NMDA receptor is blocked by extracellular Mg^{+} that prevents the entry of Ca^{2+}. However, when glutamate binds to the NMDA receptor and the neuron is depolarised, NMDA is unblocked by Mg^{+} and NMDA Ca^{2+} can flow in, triggering a cascade of intracellular molecular messengers that affect gene expression ultimately leading to increased AMPA insertion at the synapse during LTP and removal during LTD. Because NMDA receptors require both presynaptic glutamate release and postsynaptic activation for the release of Mg^{2+} block, these receptors act as coincidence detectors and through their activation enforce the rules of Hebbian plasticity (Yuste and Denk, 1995; Magee and Johnston, 1997; Bi and Poo, 1998; Koester and Sakmann, 1998; Golding, Staff and Spruston, 2002; Sjöström and Häusser, 2006).

The postsynaptic depolarisation can either be mediated by backpropagating action potential (Yuste and Denk, 1995; Magee and Johnston, 1997) or via the generation of dendritic spikes (Golding, Staff and Spruston, 2002; Sjöström and Häusser, 2006; Bono and Clopath, 2017).

1.3.4 Dendritic spikes' requirements

The spatial distribution of synaptic inputs matters. This is because, due to voltage attenuation with distance, inputs that arrive at different locations onto the dendritic tree are not equally effective at depolarising the soma. Indeed, the biophysical properties of the dendritic tree seem to be designed for filtering out weaker inputs (Rall, 1962; Larkum *et al.*, 1998, 2009; Williams and Stuart, 2002; Stuart and Spruston, 2015). The thickness of dendritic branches is inversely proportional to their distance from the soma. This means that inputs travelling toward the soma will have to travel toward increasingly larger dendritic diameters, and therefore lower input resistance. As a consequence, voltage attenuation of a single distal inputs arriving at the soma can be more than 40-fold (Williams and Stuart, 2002). This raises the question: how do distal inputs manage to influence the generation of somatic action potentials? What is the function of maintaining these synaptic inputs? One idea is that distal inputs can still influence somatic activity through the activation of dendritic voltage-gated channels in the dendrites to dendritic spikes.

Glutamate uncaging work *in vitro* suggests that dendritic spikes typically require the coincident activation of multiple dendritic spines at once (Williams, 2002; Polsky, Mel and Schiller, 2004; Losonczy and Magee, 2006). If activated in a relatively restricted dendritic segments, the activation of as little as four spines up to about a dozen spines is sufficient to trigger a localised dendritic spike (Stuart and Spruston, 2015). In the visual, auditory and somatosensory cortex, calcium imaging experiments reported dispersed synaptic activity across multiple branches of the dendritic tree (Jia *et al.*, 2010; Chen *et al.*, 2011; Varga *et al.*, 2011). However, two recent papers in the ferret visual cortex suggests that neurons that are more sharply tuned, also have dendrites receiving inputs with less circular dispersion compared to non-selective neurons (Wilson *et al.*, 2016) and that neighbouring spines tend to have similar response profiles (Scholl, Wilson and Fitzpatrick, 2017). Additionally, a paper from the Hofer lab, suggests that presynaptic inputs are spatially organised on the dendrites of the postsynaptic cell in a proximal to distal manner, according to the properties of their receptive fields (Iacaruso, Gasler and Hofer, 2017). However, a more recent paper from Svoboda lab highlighted the biases in the methodological approach used by these papers to

decontaminate synaptic Ca^{2+} signals from bAPs (Kerlin *et al.*, 2019). As such, the extent to which clustering occurs *in vivo*, remains controversial (Figure 1.9).

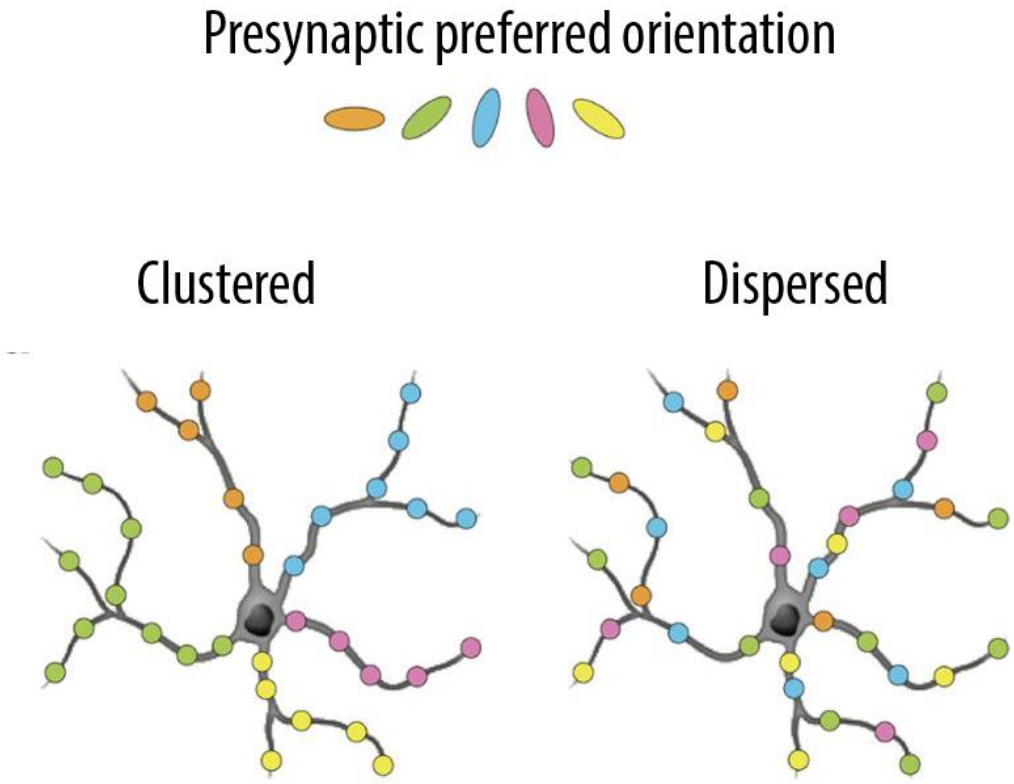

Figure 1.9: Clustered vs dispersed organisation of synaptic inputs.

In a clustered organisation, synaptic inputs with similar response profiles, arrive within the same dendritic segment. In a dispersed organisation, synaptic inputs with different response profiles are intermingled onto the same dendritic segment. Figure re-adapted from Stuart and Spruston (2015)

1.3.5 Different types of dendritic spikes

Broadly speaking there are two different types of dendritic spike: the ones originated in the dendrites and the ones originated in the soma. Dendritically-generated spikes are mainly of three kind themselves: Na^+, Ca^{2+}, and NMDA-mediated. On the other hand, backpropagating action potentials are mainly the result of Na^+-mediated currents activated in the dendrites as a consequence of somatic firing of action potentials (Stuart and Sakmann, 1994; Schiller *et al.*, 1997; Stuart, Schiller and Sakmann, 1997; Golding and Spruston, 1998; Larkum, Kaiser and Sakmann, 1999; Larkum, Zhu and Sakmann, 1999; Losonczy and Magee, 2006; Nevian *et*

al., 2007; Larkum *et al.*, 2009; Sun *et al.*, 2014), for review (Grienberger, Chen and Konnerth, 2015; Stuart and Spruston, 2015).

Na^+ spikes. Na^+ spikes are events with narrow widths, generally in the order of 5-10 ms which are generally mediated by VG Na^+ channels. Na^+ spikes can be generated in the absence of backpropagating action potentials and as such, they are dendritically-generated (Stuart and Spruston, 2015). These spikes tend to be initiated in small-diameter dendrites where electrical resistance is high. Dendritic spikes tend to attenuate as they move from high to low impedance dendrites. However, some of the voltage changes associated with these spikes can still be detected at the soma, suggesting that these spikes can influence the generation of somatic action potentials, mainly when they are generated in proximal dendrites (Stuart, Schiller and Sakmann, 1997; Golding and Spruston, 1998; Losonczy and Magee, 2006; Sun *et al.*, 2014).

NMDA spikes. Dendritic NMDA spikes are large and long-lasting events associated with the opening of NMDA receptors. Differently from Na^+ and Ca^{2+}-mediated spikes, NMDA spikes can't effectively propagate much further than the site of their generation because they require glutamate release to keep NMDA receptors active. Nevertheless, their magnitude and the long-lasting dynamics they produce onto the dendrites can affect somatic voltages substantially mainly when they manage to engage dendritic Ca^{2+} channels or Na^+ channels (Nevian *et al.*, 2007; Larkum *et al.*, 2009; Lavzin *et al.*, 2012; Hill *et al.*, 2013; Grienberger, Chen and Konnerth, 2014; Schmidt-Hieber *et al.*, 2017).

Ca^{2+} spikes. Ca^{2+} spikes are also large and long-lasting dendritic events that are mediated by the opening of VGCa channels. The generation of dendritic Ca^{2+} spikes into the dendrites is strongly correlated with the generation of bursting of action potentials and with somatic complex spikes. Complex spikes in the soma are bursts of Na^+-mediated action potentials on top of a long-lasting plateau depolarisation mediated by Ca^{2+} currents (Grienberger, Chen and Konnerth, 2014; Bittner *et al.*, 2017). Yuste *et al.* (1994) showed the existence of an apical trunk "band", near the nexus, in which calcium concentration and calcium responses were higher. Therefore, the existence of a calcium hot-zone in the apical trunk was theorized as the locus in which Ca^{2+} spikes are generated due to an increase in calcium conductance. This idea was subsequently confirmed by Larkum and Zhu (2002), who recorded from dendrites at multiple locations and showed that the threshold for the generation of dendritic Ca^{2+} spikes decreased in a distance-dependent manner from the soma and reached a minimal plateau by 600 µm of distance (mid-way through the trunk) in a layer 5 rat pyramidal neuron

(Amitai *et al.*, 1993; Yuste *et al.*, 1994; Schiller *et al.*, 1997; Golding *et al.*, 1999; Larkum, Kaiser and Sakmann, 1999; Larkum and Zhu, 2002; Grienberger, Chen and Konnerth, 2014; Bittner *et al.*, 2015).

Backpropagating action potentials (bAP). Stuart and Sakmann (1994) demonstrated for the first time that action potentials generated in the soma could retrogradely propagate into the dendrites of the neurons (Stuart and Sakmann, 1994). While backpropagation of action potentials is mediated at least partly by $VGNa^+$ channels in the dendrites, Yuste *et al.* (1994) demonstrated that somatic current injection could lead to the generation of dendritic Ca^{2+} spikes in the dendrites, even when Na^+ and K^+ channels were blocked, suggesting that somatic action potentials do not necessarily require Na^+ channels for backpropagation (Yuste *et al.*, 1994). Ca^{2+}-mediated backpropagation was shown to depend on the opening of low voltage activated Ca^{2+} channels (T-type). Interestingly, Larkum, Kaiser and Sakmann, (1999) showed that bAP-induced Ca^{2+} spikes are most efficiently triggered at critical somatic firing frequencies which varied from neuron to neuron according to the decay constant of the bAP-induced depolarisations observed in the dendrites (Larkum, Kaiser and Sakmann, 1999). BAPs are required to empower the NMDA-mediated Hebbian synaptic plasticity (Stuart and Häusser, 2001). Just like dendritic spikes which attenuate as a function of distance toward the soma, bAPs attenuate with distance too (Spruston *et al.*, 1995). The attenuation of bAP is less severe than attenuation of forward-propagating inputs due to the increase of input impedance encountered as the signal travel from thicker to thinner parts of the dendritic branch (Larkum *et al.*, 1998). However, both computational and experimental work demonstrate that that the extent of signal attenuation crucially depends on the morphology of the dendritic tree (Spruston *et al.*, 1995; Vetter, Roth and Häusser, 2001). Indeed, branching points have been shown to be a failure points for bAPs, as the sum of the cross-sectional area of the two branches originating from a parent branch is bigger than the cross-sectional area of the parent branch itself, meaning that impedance suddenly drops at these points. Due to this attenuation, synaptic plasticity in the distal apical tuft is not strictly Hebbian, as the potentiation of distal inputs required the dendritic boosting of bAPs to be implemented (Sjöström and Häusser, 2006)

Despite dendrites can generate regenerative events, it is important to remember that several lines of evidence suggest that even in the absence of proper regenerative spikes, the opening of distal Ca^{2+}, Na and NMDA channels can supralineraly sum synaptic inputs and therefore contribute significantly to action potential firing (Palmer *et al.*, 2012; Larkum, 2013; Smith *et*

al., 2013). Additionally, despite some studies suggest that these events can occur in isolation from one another (Palmer *et al.*, 2014; Cichon and Gan, 2015), dendritic recordings from the dendrites and soma of layer 5 pyramidal neurons suggest that dendritically-originated and backpropagating action potentials interact with each other creating complex superimpositions between different voltage-gated ionic currents (Svoboda *et al.*, 1997; Helmchen *et al.*, 1999; Larkum, Zhu and Sakmann, 1999; Manita *et al.*, 2015; Beaulieu-Laroche *et al.*, 2019; Gao *et al.*, 2019).

1.3.6 Functional implications of inhibitory synapses on dendrites

Inhibitory synapses onto the dendrites of pyramidal neurons play an important role in dendritic integration (Boivin and Nedivi, 2018). Due to the compartmentalisation of spines, inhibitory synapses arriving at synaptic spines or onto the dendritic shaft, can have profoundly different effects. GABA uncaging onto single spines can inhibit calcium influx into that spine without having any effect on neighbouring spines (Chiu *et al.*, 2013). In pyramidal neurons, most inhibitory synapses are located further than 125 µm away from soma, where the depolarising contribution of synaptic inputs is larger than the contribution of bAPs (DeFelipe and Fariñas, 1992; Megías *et al.*, 2001). Interestingly, GABAergic inputs onto single spines reduce but does not abolish EPSPs, meaning that inhibitory synapses onto spines are modulating, rather than shunting excitatory inputs (Chiu *et al.*, 2013). This is thought to be a mechanism to prevent saturation and effectively increase the dynamic range of the spine (Chiu *et al.*, 2013; Beaulieu-Laroche and Harnett, 2018). On the other hand, inhibitory synapses placed onto the dendritic shaft of pyramidal neurons, can attenuate both bAPs, and dendritically-generated dendritic spikes (Higley, 2014). Modelling as well as experimental evidence, show that dendritic inhibition can strongly attenuate the amplitude and duration of bAP-induced Ca^{2+} spikes (Kanemoto *et al.*, 2011; Hayama *et al.*, 2013; Stokes, Teeter and Isaacson, 2014). If located onto the apical trunk, inhibitory synapses may shunt the propagation of bAPs into the tuft, while if located onto specific tuft branches, inhibitory synapses may shunt the propagation from that specific branch to its daughter branches. As such, strategically placed inhibition can redirect bAP toward a specific subset of branches (Boivin and Nedivi, 2018). Inhibitory synapses placed onto individual branches can also block the generation of dendritic spikes onto a specific subset of branches. For example, GABA iontophoresis onto the shaft of a pyramidal dendrites can increase the threshold for the generation of a spike through glutamate uncaging (Jadi *et al.*, 2012). Interestingly, the

location of this inhibition matters. While distally placed inhibitory synapses increase the threshold for spike generation, proximally-placed inhibitory synapses are more effective at reducing the amplitude and duration of dendritic spikes (Jadi *et al.*, 2012). Therefore, inhibition plays a vital role in coupling the activity between soma and dendrites as well as in coupling the activity between different branches of the dendritic tree. Because dendritic inhibition is very efficient at blocking the generation of dendritic spikes required for somatic bursting, it has been proposed as a mechanism by which inhibitory neurons prevent runaway excitation in the network (Tremblay, Lee and Rudy, 2016). Additionally, through the activation of SST+ neurons, the most active pyramidal neurons will be the ones setting the inhibitory tone to the entire network : this mechanism can serve as a "winner takes all" mechanism in which the neurons that start bursting first, can suppress the activity of neighbouring pyramidal neurons via lateral inhibition(Coultrip, Granger and Lynch, 1992). Indeed, it was shown that as few as four Layer 5 pyramidal neurons firing was enough to drive inhibition in virtually all nearby layer 5 pyramidal neurons (Silberberg and Markram, 2007; Berger *et al.*, 2010) (Figure 1.10).

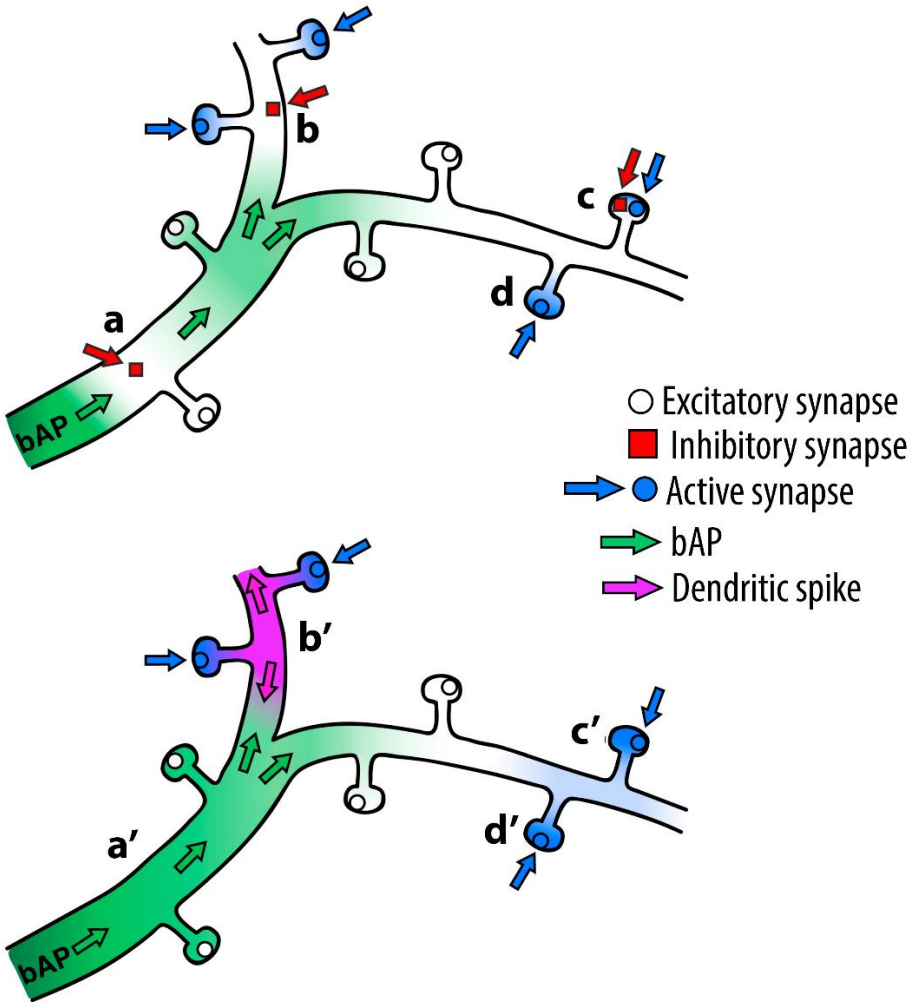

Figure 1.10: *Functional effects of inhibition on dendritic computation*.

The effects with and without inhibition are illustrated at site a-d and a'-d', respectively. a-a') Dendritic inhibition can reduce the spread of a bAP. b-b') Dendritic inhibition can prevent the coincident detection between a bAP and an incoming synaptic input therefore regulating the generation of bAP-induced Ca^{2+} spikes. c-c' and d-d') Synaptic inhibition attenuates an EPSP in the post-synaptic spine (c and c'), without affecting nearby spines (d-d'). Figure re-adapted from Boivin and Nedivi (2018)

1.3.7 Theories of local and global dendritic activity

Arguably, the most common operation that dendrites perform is filtering. Due to the passive properties of the cellular membrane, dendrites act as a high-pass filter on both somatopedal

and somatofugal inputs regardless of whether dendritic activity is globally or locally generated (Vetter, Roth and Häusser, 2001; Larkum *et al.*, 2009).

Local dendritic spikes have been proposed as a strategy to implement at least three main computational operation neurons require to perform.

(1) Logical operations: Through the generation of dendritic spikes, neurons have been suggested to be endowed with the cellular machinery to perform at least three types of logical operations: AND, OR and XOR (Stuart and Spruston, 2015). AND operations are computed when a sufficient number of synaptic inputs leads to the generation of a dendritic spike (Schmidt-Hieber *et al.*, 2017). On the other hand, OR operations are computed when different sets of presynaptic inputs, perhaps localized onto specific subsets of dendrites, are alone sufficient to generate dendritic spiking (Cichon and Gan, 2015). Finally, XOR operations are implemented when a synaptic input sufficiently strong to generate a dendritic spike, recruits feed-forward inhibition to shunt the generation of dendritic spiking elicited by a second input and vice versa (Silberberg and Markram, 2007). As a consequence, until recently, XOR operations were thought to require an intermediate inhibitory neuron to be implemented. However, a recent study demonstrated that the dendrites of human layer 2/3 neurons can perform XOR computation through the generation of dendritic Ca^{2+} spikes (Gidon *et al.*, 2020). In these dendrites, maximal dendritic activation was achieved at specific stimulations intensities and increasing dendritic stimulation beyond this point, resulted in spike attenuation (Gidon *et al.*, 2020).

Despite it should be stressed that none of these logical computations strictly requires local or branch-specific dendritic activity, the possibility of generating these operations in parallel onto non-overlapping subsets of branches, endows individual neurons with enormous algorithmic complexity. This complexity is going to be directly proportional to the number of computationally-independent dendrites a neuron possess (Stuart and Spruston, 2015).

(2) Information storage: According to the classical rules of Hebbian plasticity, synaptic inputs that do not generate action potentials should be weakened through the process of LTD. Suppose a neuron responding to the object “coffee”. In our everyday experience, the attributes of an object (e.g. brown and hot are two attributes of the object coffee) are encountered more often than the object itself. This creates a problem because the synaptic association between the object and its attributes should be weakened every time the attributes are encountered independently of the object to which a neuron responds to. In the example given above, weakening should happen every time we drink hot chocolate for hot chocolate is brown and hot but does not activate the neuron responding to the object

"coffee". Both in vivo and in vitro evidences however suggest that dendritic spikes can mediate other forms of non-Hebbian synaptic plasticity (Golding, Staff and Spruston, 2002; Remy and Spruston, 2007; Cichon and Gan, 2015). Indeed, synaptic inputs sufficiently strong to generate local Ca^{2+} or Na^{+} spikes can be potentiated even in the absence of somatic spiking through a form of local LTP (Golding, Staff and Spruston, 2002; Remy and Spruston, 2007). This form of locally-computed non-Hebbian plasticity was proposed as a mechanism to increase single neurons storage availability (Bono and Clopath, 2017). This is because the attributes of an object can strengthen their association to the object-responding neuron independently from each other and from the object itself, increasing the number of attributes that can be associated to a specific object.

In the motor cortex, neurons have been shown to segregate inputs associated with different behavioural tasks onto non-overlapping subset of branches as a mechanism to prevent catastrophic interference between different inputs streams (Cichon and Gan, 2015).

(3) Credit assignment: Credit assignment is a concept that was first formalised in the machine learning context and refers to the idea of how much credit (or blame), a specific synaptic connection should be given for a certain behavioural outcome (Richards *et al.*, 2019). In multi-layered networks this is a complex problem since the behavioural impact of synaptic weights in early layers depends on the downstream synaptic weights. In deep neural networks, credit is assigned to a specific synapse using "backpropagation" (unrelated to backpropagating action potentials (bAP) encountered previously in this thesis) which uses the chain rule to recursively calculate gradients backwards from the output (Richards *et al.*, 2019). However, backpropagation relies on biologically implausible assumptions including the symmetry of feedforward and feedback synaptic weight and the non-overlapping temporal segregation between feedforward and feedback (error calculation) inputs (Richards *et al.*, 2019). Therefore, whether biological neurons perform credit assignment in the intact brain remains unknown. Recently however, through the generation of a two-layered, biologically realistic model in which the distal tuft is compartmentalised from the soma, Guerguiev, Lillicrap and Richards (2017) demonstrated the existence of a biologically realistic model for the calculation of credit assignment. In their model, Guerguiev, Lillicrap and Richards (2017) segregated the distal tuft of a single pyramidal neuron as the place where feedback error signals and weight update are computed, from the soma where feedforward computation is computed. Importantly, it is thanks to somato-dendritic segregation that neurons in different layers of the network could coordinate synaptic weight updates.

Global spiking through the generation of bAP-activated Ca^{2+} spikes (BAC firing). For the first time, Larkum, Zhu and Sakmann (1999) showed that the coincident arrival of a dendritic input with a back-propagating action potential could generate long-lasting, high amplitude calcium plateau potentials in the apical dendrites and induce somatic bursting in the soma effectively coupling the distal tuft with the soma (Larkum, Zhu and Sakmann, 1999; Beaulieu-Laroche *et al.*, 2019). Dendritic Ca^{2+} spikes are a very powerful mechanism for the induction of somatic action potentials and indeed it turns out that they produce more action potentials than suprathreshold stimuli directly applied to the soma (Larkum, Zhu and Sakmann, 1999, 2001; Schwindt and Crill, 1999; Williams and Stuart, 1999). As such, global dendritic calcium spikes play a powerful role in the regulation of somatic firing and have been implicated in regulating three main cellular mechanisms.

(1) Coincident detection: The observation that temporally-matched inputs arriving at the basal and distal dendrites generated nonlinear somato-dendritic interactions, led to the hypothesis that global spikes are the mechanism through which single neurons implement coincident detection (i.e. feature binding) in the cortex. When initialised, dendritic Ca^{2+} spikes, generate a typical firing pattern in the soma that consists of 2-4 spikes at ~200 Hz which could be a specific signal to send to the postsynaptic neuron indicating the presence of the coincident arrival of basal (feedforward) and apical (feedback) inputs (Larkum, Zhu and Sakmann, 2001; Larkum, 2013).

(2) Gain modulation: Through the engagement of nonlinear somato-dendritic processes, BAC firing can induce gain modulation as somatic activity would effectively lower the threshold for the initiation of a spike in the apical tuft dendrites, which in turn produces burst firing in the soma. Indeed, the threshold for the generation of a Ca^{2+} spike at the nexus is halved when a single action potential is generated in the soma (Larkum, Zhu and Sakmann, 1999; Larkum, 2013). This implies that when the neuron receives basal inputs, its sensitivity to apical tuft inputs increases compared to when basal inputs are absent (Larkum, 2013). By affecting the duration of the dendritic Ca spikes, single EPSPs which would normally be attenuated with distance, can under this regime, strongly influence somatic output.

(3) Multiplexing: From an information theory perspective, neurons want to encode into their spike trains as much information as possible about the inputs that made them fire (Borst and Theunissen, 1999). In the classical view, neurons receive two streams of information: bottom-up sensory inputs onto their basal dendrites and top-down contextual signals onto their distal dendrites which are collapsed together onto a single output stream (Larkum, 2013). However, in their output, neurons have to communicate the presence of a stimulus

feature to high-order areas and they need to send a predictive signal to a low-order area (Keller and Mrsic-Flogel, 2018; Payeur, Béïque and Naud, 2019). In other words, neurons must encode both ascending and descending information, simultaneously and possibly to different target neurons. Recent computational works suggests that neurons can solve this complex task through the generation of BAC firing. Through the generation of apical-tuft-generated bursts and simple spike trains neurons can multiplex two inputs streams into a single output that can then be de-multiplexed by the downstream circuit to decode how much basal vs. apical inputs contributed to presynaptic firing (Naud and Sprekeler, 2018). This organisation allows individual neurons to process two streams of information independently (a basal/bottom-up/feedforward stream and an apical/top-down/feedback stream) and then integrate them together or separately thanks to the intrinsic biophysical properties of the neuron (Larkum, 2013; Keller and Mrsic-Flogel, 2018; Naud and Sprekeler, 2018; Kay *et al.*, 2019).

1.3.8 Studying dendritic spikes *in vivo*

When translating *in vitro* findings to dendritic physiology *in vivo*, two major points should be considered: A) the spatio-temporal sequence of synaptic activity is unknown *in vivo*, meaning that stimulation protocols *in vitro* do not necessarily apply. B) *In vivo*, most neurons receive a barrage of thousands of inputs. This happens even at rest during neuronal background activity and affect: (1) Dendritic conductance (Ulrich, 2002); (2) NMDA receptor sensitivity (Nahum-Levy *et al.*, 2001); (3) the spontaneous firing properties of layer 5 pyramidal neurons (Sakata and Harris, 2009; Hill *et al.*, 2013); (4) the effects of different neuromodulators (Lacefield *et al.*, 2019). Studying dendritic computation *in vivo* has been a major challenge because electrophysiological recordings of dendritic activity are technically demanding and so far, they have only been achieved in immobilised or anaesthetised animals (Helmchen *et al.*, 1999; Svoboda *et al.*, 1999; Smith *et al.*, 2013; Roome and Kuhn, 2018) but notably, also see Moore *et al.* (2017)). Additionally, anaesthesia has been shown to profoundly suppress the activity of dendrites-targeting SST+ neurons, suggesting that dendritic computation may be fundamentally altered during anaesthesia (Urban-Ciecko and Barth, 2016). Finally, highly associative cortical areas have been shown to be silenced during anaesthesia (Makino and Komiyama, 2015), another finding that questions the validity of the investigation of dendritic computation in anesthetized animals.

Because of the technical challenge of doing whole-cell recordings from dendrites *in vivo*, dendritic computation *in vivo* has been primarily investigated using indirect indicators of activity, predominantly calcium indicators (Varga *et al.*, 2011b; Xu *et al.*, 2012; D. N. Hill *et al.*, 2013b; Manita *et al.*, 2015; Takahashi *et al.*, 2016; Gayathri N Ranganathan *et al.*, 2018; Kerlin *et al.*, 2018; Beaulieu-Laroche *et al.*, 2019; Francioni, Padamsey and Rochefort, 2019; Park *et al.*, 2019, but also see Roome and Kuhn (2018)). Calcium imaging allows experimenters to track dendritic signal changes chronically during the acquisition or during the expression of acquired behaviours in awake behaving animals (Cichon and Gan, 2015; Peters *et al.*, 2017; Kerlin *et al.*, 2019). Additionally, developments in microscopy techniques, now allow experimenters to record simultaneously the activity of multiple dendrites together with the soma, allowing a direct comparison of the inputs and the outputs of individual neurons (Peters *et al.*, 2017; Beaulieu-Laroche *et al.*, 2019; Francioni, Padamsey and Rochefort, 2019; Kerlin *et al.*, 2019).

Despite these advantages , It is important to keep in mind about the strengths and limitations of calcium indicators (Helmchen *et al.*, 1999; Svoboda *et al.*, 1999; Xu *et al.*, 2012; Beaulieu-Laroche *et al.*, 2019; Francioni, Padamsey and Rochefort, 2019).

In 1999, Helmchen highlighted that dendrites do not always produce Ca^{2+} spikes, but that they are able to sustain putative Na^{+}-mediated spikes, derived from either bAPs or from locally-generated spikelets, that don't produce any dendritic calcium entry and therefore, are undetected by the Ca^{2+} indicator CG-1. Importantly, CG-1 could report with a high signal-to-noise ratio, calcium spikes recorded *in vivo* which were of similar amplitudes and comparable duration to the ones recorded *in vitro*. Despite the sensitivity and the dynamic range of calcium indicators markedly improved over times, all calcium indicators (dyes and genetically-encoded) seem to be well suited to detect both Ca^{2+} and NMDA spikes, but not Na^{+}-mediated currents in dendrites. This observation was then confirmed by Xu *et al.* (2012), who demonstrated, recoding from layer 5 pyramidal neurons in the somatosensory cortex that GCaMP3, was a reliable indicator for the detection of Ca^{2+}-mediated dendritic plateau potentials (largely demonstrated to be mediated by Ca^{2+} and NMDA currents), generated when dendritic activity was paired to an apical tuft inputs, but not narrow-width depolarisations generated in the absence of apical tuft stimulation (Xu *et al.*, 2012). These results were recently confirmed *in vitro* using GCaMP6f (Beaulieu-Laroche *et al.*, 2019), and indirectly supported *in vivo* by pairing voltage and calcium imaging (Roome and Kuhn, 2018).

1.3.9 *In vivo* whole-cell recordings from dendrites

The first published study about patching dendrites *in vivo*, was performed by Svoboda and Helmchen in Tank lab in 1999 from layer 2 and layer 5 neurons respectively (Helmchen *et al.*, 1999; Svoboda *et al.*, 1999). What both studies found, was that somatic action potentials could generate Ca^{2+}-mediated dendritic spikes that attenuate in a distance dependent manner (Helmchen *et al.*, 1999; Svoboda *et al.*, 1999). This distance-dependent attenuation of bAP-induced dendritic Ca^{2+}-spikes, was fully replicated by Waters *et al.* (2003) who also confirmed that the generation of dendritic Ca^{2+} signals in layer 2/3 neurons, was severely attenuated, but not completely eliminated by Tetrodotoxin (TTX) in response to single action potentials, and that attenuation is more severe for individual action potentials, compared to bursts (Waters *et al.*, 2003). In layer 5 neurons, dendritic Ca^{2+} spikes were associated with the generation of complex spike bursts at the soma (Helmchen *et al.*, 1999). In 2013, Spencer Smith from the Hausser lab, also patched the dendrites of layer 2/3 neurons, in both anaesthetised and anaesthesia-recovered animals (Smith *et al.*, 2013). Similarly to Helmchen, Smith demonstrates that dendrites could produce both fast-rising, fast-decaying (likely Na^{+}-mediated) transients and longer-lasting NMDA (and most likely Ca^{2+})-mediated plateau potentials. Smith suggested that Na^{+}-mediated currents were the result of bAPs and demonstrated that NMDA-dependent events were required for sharpening orientation-selectivity at the soma. Interestingly, Smith also observed that Na^{+} spikes could ride on top of the long-lasting NMDA-dependent depolarisation (Smith *et al.*, 2013). A similar observation was subsequently reported by Moore *et al.* (2017) in Mehta's lab. Using a tetrode coated with glial-chemoattractant, Moore developed a technique to record semi-intracellular dendritic signals, chronically in freely behaving animals. Despite the technique has not been fully validated and it does not allow experimenters to know from what type of neurons dendritic (or axonic?) recordings are obtained, Moore showed that the type of signals which could be recorded using this technique were remarkably similar to the ones obtained by Smith. Similarly, these data demonstrated that Na^{+}, spikes riding on top of long-lasting plateau depolarisations in the dendrites occur up to 10 times more frequently than somatic action potentials suggesting that these events are decoupled from somatic activity and indicating the dendritic nature of small Na^{+}-mediated spikelets (Smith *et al.*, 2013; Moore *et al.*, 2017).

1.3.10 *In vivo* findings using Ca^{2+} imaging to study dendritic integration

Global dendritic activity. Several *in vivo* studies report that the activity of different neuronal compartments is much less independent than what was predicted by *in vitro* studies. Global tuft activity (i.e. events that are detectable in multiple branches or compartments at the same time) has been shown to be common in dendrites of pyramidal neurons and it has been reported in several different cortical areas, during both passive sensory stimulation and during the performance of previously acquired behavioural tasks (Svoboda *et al.*, 1999; Varga *et al.*, 2011; Xu *et al.*, 2012; Hill *et al.*, 2013; Grienberger, Chen and Konnerth, 2014; Peters *et al.*, 2017; Sheffield, Adoff and Dombeck, 2017; Beaulieu-Laroche *et al.*, 2019; Francioni, Padamsey and Rochefort, 2019; Kerlin *et al.*, 2019; Lacefield *et al.*, 2019). In the motor cortex, during spontaneous activity, it was shown that suprathreshold activity in the soma produced activation that unreliably invaded all apical tuft branches in the tuft, suggesting that activity in the tuft was bAP-mediated (Hill *et al.*, 2013). Similarly, Xu *et al.* (2012) demonstrated that the activity of sibling branches in the apical tuft of layer 5 neurons was highly correlated during a sensory-motor task. Another study (Lacefield *et al.*, 2019) also reported global tuft activity in the somatosensory cortex which is triggered by sensory-stimulation and reward delivery when they occur together, but not independently. Despite the authors suggest that the entire apical tuft could act as a single computational unit (Xu *et al.*, 2012; Grienberger, Chen and Konnerth, 2015; Lacefield *et al.*, 2019), somatic activity was not recorded during these experiments, and therefore it is unclear whether these signals are the results of backpropagating action potentials. More recently however, (Kerlin *et al.*, 2019) demonstrated that in the anterior lateral motor cortex, the activity of the soma is highly correlated throughout the dendritic arbour in both layer 2/3 neurons and layer 5 neurons during a go-nogo licking task. The authors found that branch-specific activity is overall very rare and almost exclusively found to co-occur with global dendritic events. These branch-specific events mainly manifest as an increase in the duration of global calcium transients, rather than occurring as isolated events. In the motor cortex, another study reported highly coupled activity between the soma and the apical tuft dendrites during motor learning with coincident activity observed in over 90% of the times (Peters *et al.*, 2017). A recent paper by Beaulieu-Laroche *et al.* (2019) demonstrates how the activity of layer 5 pyramidal neurons in V1 is also strongly coupled from the soma to the nexus independently of visual stimulation and locomotion. Finally, a recent theoretical paper demonstrated that a single dendritic non-linearity could predict up to 90% of the variance observed at the somatic level and that

adding local nonlinearities onto every individual dendrite didn't increase the variance explained by the model (Ujfalussy *et al.*, 2018).

Branch-specific activity. There are three different kinds of branch-specific activity described in the literature:

(1) *Dendritic hotspots:* These events have been described as small-amplitudes dendritic calcium events. The occurrence of these hotspots is strongly reduced by the intracellular application of NMDA-receptor blockers; these hotspots appeared in a distributed (not clustered) manner throughout the dendritic tree, independently of their tuning property. These hotspots were observed in both layer 5 and layer 2/3 neurons in the somatosensory, visual and motor cortices (Jia *et al.*, 2010; Varga *et al.*, 2011; Hill *et al.*, 2013)

(2) *Dendritic Ca^{2+}-spikes:* These are large events localised in individual branches of the same amplitude as global dendritic spikes. Three articles report the observation of these spikes *in vivo* using Ca^{2+} indicators: Palmer *et al.* (2014) reports the detection of branch-specific activity in the dendrites of layer 2/3 neurons of the somatosensory cortex. Similarly, Cichon and Gan (2015), recording from multiple branches of layer 5 motor cortex neurons, reported that specific branches selectively responded to specific directions of running (forward, backward, left and right). Both these papers showed that the generation of branch-specific activity was NMDA-dependent. Cichon and Gan (2015) also showed that activity of SST+ interneurons was required for the generation of branch-specific events. Finally, Sheffield, Adoff and Dombeck (2017) found out that branch-specific Ca^{2+} events in the basal dendrites of CA1 pyramidal neurons, were instructive for the induction of somatic place fields in new virtual environments. Once the neuron acquired its place field, somatic and dendritic activity were strongly correlated, suggesting two functionally-distinct phases: an induction phase in which somatic and dendritic activity were decoupled from each other, and an implementation phase in which somato-dendritic activity was strongly correlated.

(3) *Nonuniform dendritic spread of global calcium transients:* These events have been described in the hippocampus. Sheffield and Dombeck (2015) demonstrated that coupled somato-dendritic only spread into some basal and proximal apical dendritic branches but not in others. The extent of this spread was predictive of the place field of the neuron under investigation.

1.4 Thesis aims

Layer 5 pyramidal neurons in the mouse primary visual cortex respond selectively to physical features of visual stimuli such as orientation and direction of movement (Niell and Stryker, 2008; Kim *et al.*, 2015) and their activity is modulated by locomotion (Erisken *et al.*, 2014; Dadarlat and Stryker, 2017; Pakan, Francioni and Rochefort, 2018). Several lines of evidence suggest that the stimulus selectivity is at least partly due to changes in the underlying dendritic computation of different visual stimuli (Smith *et al.*, 2013; Wilson *et al.*, 2016). Additionally, *ex vivo* experiments predict that the coupling between different dendritic compartments and the soma should be increased during period of locomotion (Hoffman and Johnston, 1999; Labarrera *et al.*, 2018). Altogether these results suggest that the computational regime of the apical dendrites of layer 5 neurons, should vary in a stimulus and condition-dependent manner. Nonetheless, the single cell computation of visual and locomotory inputs at the single cell level in V1 layer 5 pyramidal neurons, remains largely unknown. Using single plane and dual plane 2-photon calcium imaging, I imaged GCaMP6s calcium signals in the soma, trunk and distal tuft dendrites of layer 5 pyramidal neurons, both in darkness and during the presentation of drifting gratings, while head-fixed mice were either running or stationary on a cylindrical treadmill. The aim of this thesis is to understand how the apical dendrites of individual layer 5 neurons respond to different visual stimuli, during stationary and locomotion periods and how dendritic activation relates to somatic output.

2. Materials and Method

2.1 Animals

All experiments and procedures involving animals were approved by the University of Edinburgh Animal Welfare and the ethical review board (AWERB) and performed under the appropriate PIL and PPL license from the UK Home Office in accordance with the Animal (Scientific Procedures) act 1986 and the European Directive 86/609/EEC on the protection of animals used for experimental purposes.

Adult males and females aged between 8 and 10 weeks obtained from Jackson Laboratory, ME, USA (B6.Cg-*Gt(ROSA)26Sor*$^{tm14(CAG-tdTomato)Hze}$/J [RRID:IMSR_JAX:007914]) were used for experiments. Because calcium buffers can affect dendritic development, adults were chosen as it was demonstrated that the dendrites of layer 5 pyramidal neurons only reach full dendritic maturity around P60 (Romand *et al.*, 2011; Ramaswamy and Markram, 2015). Animals were group housed in groups of 2-6 animals to favour social interactions, a condition that prevents the emergence of depressive and anxious-like behaviour (Berry et al. 2012; Ieraci, Mallei, and Popoli 2016; for a full review see Kappel, Hawkins, and Mendl 2017). Mice were allowed *ad libitum* access to food and water. Each cage contained a running wheel, which was shown to have positive consequences on brain function and plasticity in the primary visual cortex (Kaneko and Stryker, 2014; Chen *et al.*, 2017). Because mice run more during the dark phase of their circadian cycle (Bains *et al.*, 2018), they were housed on a reverse 12:12 hour light/dark cycle so that they were at their peak of activity during the imaging sessions performed between 10.00 am and 5.00 pm.

2.2 Viral delivery for the sparse expression of GCaMP6

To obtain sparse labelling of excitatory neurons we used a cre-dependent approach to genetically label neurons expressing the Ca^{2+}/calmodulin-dependent protein kinase II (CaMKII). CaMKII is a protein kinase that is regulated by the Ca^{2+}/calmodulin complex and is specifically expressed in excitatory neurons (Jones, Huntley, and Benson 1994; Wang et al. 2014). AAV1.CamKII 0.4.Cre.SV40 (Penn Vector core catalogue No. 105558-AAV1, titer (GC/ml): $1.81e^{13}$) was diluted 1:10000 – 1:20000 while either AAV1.Syn.Flex.GCaMP6f.WPRE.SV40 (Penn Vector Core, catalogue No. 100833-AAV1, titer (GC/ml): $1.91e^{13}$) or AAV1.Syn.Flex.GCaMP6s.WPRE.SV40 (Penn Vector Core, catalogue No.

100845-AAV1, titer (GC/ml): 1.81e^{13}) were diluted 1:10 in the final solution. All dilutions were made in artificial cerebrospinal fluid (ACSF) sterilized using a 0.2 µm syringe filter (Cole-Parmer). This approach allowed us to obtain cre expression in a small number of excitatory neurons due to the high dilution of the CaMKII-cre virus, and yet a high concentration of intracellular GCaMP6. As a result, GCaMP6 was only expressed in neurons that were co-transfected with the CaMKII virus. Neurons transfected with either the CaMKII or the GCaMP6 virus would express either TdTomato only or express no marker at all, respectively (Figure 2.1).

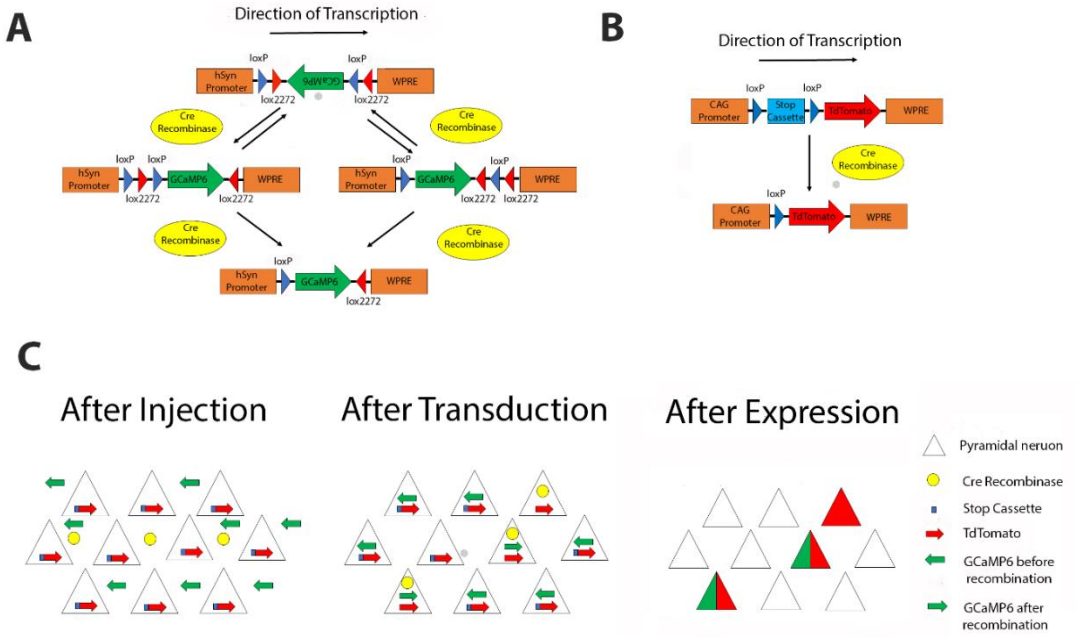

Figure 2.1: *Viral strategy for the cre-dependent, sparse expression of GCaMP6 and TdTomato in layer 5 pyramidal neurons.*

A) Schematic of the recombination process mediated by cre recombinase, to express GCaMP6. Originally, the genetic sequence coding for the GCaMP6 gene is packaged into an Adeno-Associated Virus 1 (AAV1) in a conformation preventing transcription. The GCaMP6 sequence is flanked by two recombinant Lox sites on each side: LoxP and Lox2272. These two sites recombine in a cre-dependent way. Through a double recombination process, GCaMP6 gets locked into the right direction to be transcribed (Kühn and Torres, 2002). GCaMP6 is expressed under the human synapsin promoter (hSyn) and its expression is amplified post-transcriptionally by the Woodchuck hepatitis virus Post-transcriptional Regulatory Element (WPRE) sequence. B) I used a cre-dependent TdTomato mouse line (JAX sequence: RRID:IMSR_JAX:007914). When present, cre-recombinase recombine the two loxP sites, the stop cassette gets cut off and TdTomato can be expressed. Transcription is regulated by the

CAG promoter and amplified post-transcriptionally by the WPRE sequence. C) After Injection, AAV1 transduces the neurons. Some neurons will be transduced with GCaMP6 only, some with cre-recombinase only, some with both and some will not be transduced. Because cre is expressed under the control of the CaMKII promoter (not shown), only CaMKII-positive neurons will express Cre-recombinase.

2.3 Surgical procedures

In surgical procedures, animals were anesthetized with Isoflurane: anaesthesia was induced by inhalation of 4% Isoflurane with an air flow rate of 300ml/min (Abbott Pharmaceuticals, UK) into an anaesthetic chamber and was maintained using 1-2% isoflurane for the entire duration of the procedure. During the procedure, the animal's body temperature was maintained at physiological levels using a closed-loop, adjustable heating pad which monitored the animal's temperature via a rectal probe. An opaque hydrating cream (Bepanthen, Bayer) was applied onto the eyes of the animal to prevent dryness and protect from light exposure. All surgical procedures were performed in sterile conditions.

2.3.1 Viral Injections through a bur hole

After induction of anaesthesia, mice were shaved, mounted onto a stereotaxic frame (David Kopf instruments, CA, USA) and head-fixed using ear bars. An analgesic was administered subcutaneously (Vetergesic, buprenorphine, 0.1 mg/kg of body weight) to alleviate pain. The shaved head was wiped using an antiseptic solution (Iodinated Povidone, Videne). Using a scalpel blade (Swann-Morton, No. 10 surgical blades) a small incision was made to expose bregma, the back suture and the desired injection site onto the skull of the animal. Layer 5 neurons were targeted stereotactically. Injections were performed on the left hemisphere of the brain. A three-axis stereotactic micromanipulator was used to pinpoint the desired location of the burr hole through which the viral preparation would be delivered. To target layer 5 neurons in the monocular area of V1, using an injection pipette coming with a mediolateral angle of 20 degrees and a dorsoventral angle of 70 degrees, the drilling location was calculated to be between 3 and 3.5 mm lateral from lambda and the central suture, and 2.5 mm anterior from the back suture or 1.5 mm anterior from lambda. These calculations were done using simple trigonometry and corrected empirically after the post-hoc histological characterisation of the injection site under confocal microscopy. Once the injection location was identified on the skull, a small burr hole of about 0.5 mm in diameter

was drilled using a round diamond bur (Wright-Cottrel catalogue No. KH1204005). To avoid overheating the skull, drilling was performed at low speed and avoiding drilling on the same spot for more than 5 continuous seconds. Once the bone was sufficiently thin, a single droplet of ACSF was applied for a couple of minutes to soften the skull and facilitate removal. The skull was then removed using No. 5 forceps with a bent tip which was used as a hook for lifting the bone. A glass pipette for injection (Drummond glass for Nanoject, OEM Glass Capillary) was first pulled and backfilled with mineral oil using an Hamilton syringe, then the viral preparation was sucked into the pipette using nanoject II (Drummond Scientific). Once the brain was exposed, the glass pipette, backfilled with the viral preparation was inserted, through the meninges into the brain. To prevent mechanical damage to the brain and pipette clotting, insertion was done slowly (less than 50 µm per second). Injections were made, using a nano injector (nanoject II, Drummond Scientific), at 2 different depths, 700 and 550 µm from brain surface (the deep and the superficial end of layer 5, respectively http://mouse.brain-map.org/static/atlas) to maximise spread into layer 5. A total volume of 55.2 nl was injected across the two sites (6x 4.6 nl at each location). After insertion of the pipette, 3 minutes were waited before the beginning of injection, to let the brain settle after being pushed by pipette insertion. Single 4.6 nl injections were spaced 30s from one another to allow enough time for diffusion. To avoid diffusion of the virus along the pipette tract, 3 minutes were waited after the last injection before pipette retraction or removal. The pipette was then removed slowly (less than 50 µm per second) from the brain. After the pipette was completely removed, a single drop of ACSF was applied onto the skull of the mouse and the edges of the incision were pulled together for suturing (Ethicon, Ethilon polyamide size 6) and gluing (Vetbond, 3M) the incision cut. At the end of the procedure, a single 25ml/kg dose of Ringer's solution was injected subcutaneously for rehydration. The animal was then released from head-fixation, removed from the stereotax and placed in a recovery cage heated by an underlying heating pad. A single postoperative analgesic (Vetergesic) jelly was left in the cage between 18 and 24 hours after recovery and routine checks were performed every 12 hours for the following 72 hours, and every 24 hours thereafter, to ensure the animal did not show post-operative distress symptoms.

2.3.2 Cranial window and headplate attachment

Cranial window and headplate attachment were performed one day before imaging to ensure optimal imaging conditions. This was thus performed about 2-3 weeks after viral injections to allow sufficient time for the expression of GCamP6 (Chen *et al.*, 2013).

After induction of anaesthesia, mice were shaved, mounted onto a stereotaxic frame (David Kopf instruments, CA, USA) and head fixed using ear bars. To prevent brain swelling and post-operative pain, analgesic and anti-inflammatory drugs were administered subcutaneously (Vetergesic, buprenorphine, 0.1 mg/kg of body weight; Carpaphen, Carprieve, 5mg/kg of body weight; Dexamethasone, Rapidexon, 2mg/kg of body weight). The shaved head was wiped using an antiseptic solution (Iodinated Povidone, Videne). Using a pair of surgical scissors, a circular section of skin (~1 cm large in diameter) overlaying the skull was removed. Using two cotton swabs, the skin edges were pulled apart to expose as much skull as possible. Once the skull was sufficiently exposed to work comfortably, the skin was glued in position using veterinary glue (Vetbond, 3M). To create a rough surface for subsequent adhesion of the metal headplate, the membrane attached to the skull was removed with a surgical blade (Swann-Morton, No. 10 surgical blades), by gently scraping it away.

For a cranial window over V1, a rectangular craniotomy of approximately 2x1.5 mm was drilled on top of the injection site without drilling over the back suture, to avoid bleeding. During drilling, the skull thickness was regularly monitored by applying a little pressure at different points along the perimeter of the craniotomy. Once the bone was sufficiently thinned, a drop of sterile ACSF was applied on the grove created during drilling to further soften the skull and facilitate removal. Hooked forceps were used to gently cut through the bone along the perimeter of the craniotomy and remove the skull. From this point of the surgery onward, the surface of the brain was continuously kept under sterile ACSF to avoid drying. In the case of small bleeds from the skull bone or from the dura, the surface of the brain was washed and rinsed with sterile ACSF, until blood was cleared.

For the imaging window, I used a triple glass to minimize brain movements during imaging. A triple glass window was prepared by stacking on top of each other, three cover-slip glasses (Menzel-Glaser 24x32 mm # 0), one larger and two smaller, using an optically clear UV-cured glue (Norland Optical adhesive). Overall, the summed thickness of the two glass windows inserted through the cranial window, which equal to 170-230 µm, was comparable to the thickness of the skull at the time of imaging (Smith *et al.*, 2017), suggesting that the brain did not suffer from excessive compression following the glass window implantation. The glass window was applied onto the exposed brain, still covered by the dura, which was not removed for imaging. The triple glass window was positioned so that the outer bigger glass

would sit on top of the skull on the external edges of the cranial window, while the two smaller glasses were fully fitted within the drilling perimeter of the cranial window. The triple glass window was then secured in place using Ethyl 2-cyanoacrylate glue (Locite). Once the glue dried, a metal headplate was secured on top of the bare skull of the mouse, perpendicular to the dorsoventral axis of the skull of the animal to avoid discomfort during imaging. The skull of the animal was then covered with a layer of glue (Ethyl 2-cyanoacrylate, Locite) to prevent infections and heat/water loss from the exposed skull. After that, the metal headplate was further secured in place by applying dental cement (Paladur, Heraeus Kulzer) along its edges. Once the dental cement solidified, a 25ml/kg of Ringer's solution was injected subcutaneously to rehydrate the animal after the procedure. The animal was then released from the head fixation and returned to a heated recovery cage, until full motor capacity was recovered. At that point, the animal was returned to its home cage and checked every 12 hours for post-operative symptoms.

2.4 Two-photon calcium imaging

Two-photon calcium imaging of GCamP6-labeled layer 5 pyramidal neurons was performed in 2 different set-ups. Both were equipped with a Ti:Sapphire pulsing laser and a galvo-resonant scanner. In both set-ups, mice were head-fixed, could freely run on a polystyrene cylinder (20 cm in diameter) and their running speed was recorded using an optical encoder (E7P, 250 cycles/revolution, Pewatron, Switzerland). The E7P uses a 5V supply and offers two TTL quadrature outputs, at slightly different phases from each other to estimate both speed and spinning direction. Imaging was performed using a 25x Objective (Olympus), optimized for multiphoton imaging with 2 mm working distance, NA = 1.05 in water, immersed in ultrasound gel. Ultrasound gel was preferred to water because it is more resilient to evaporation after long laser exposure. The laser was set at a wavelength of 920 nm. At this wavelength, the laser excites optimally GCaMP6 and it excites TdTomato at ~ 30% of its peak excitation (Drobizhev *et al.*, 2011). Imaging was performed using a 570 nm short-pass dichroic mirror and two single-band pass filters, a 525/50 (Scientifica) for GCaMP6 light absorption, and a 620/60 (Scientifica) for TdTomato absorption (Figure 2.2). Emitted light was collected by two GASP PMTs (~40% quantum efficiency for light at 525 nm). Layer 5 pyramidal neurons were recorded between 468 and 666 µm (528 µm median depth) from brain surface and followed up to their distal tuft dendrites along the apical trunk. Neurons which had their nucleus filled with GCaMP6 or had blobby-looking dendrites were not

selected for recording, as these signs were considered symptomatic of an unhealthy neuron. At the end of each imaging session, a z-stack was acquired to allow a more detailed, offline morphological reconstructions of the neuron imaged.

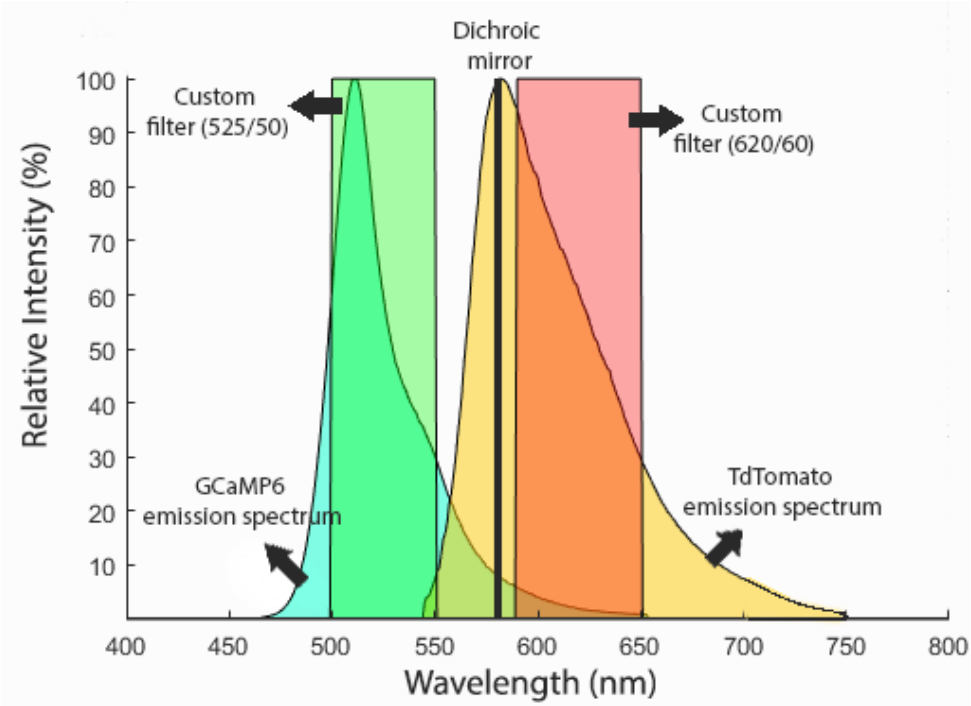

Figure 2.2: *The emission spectra of GCaMP6 and Td Tomato and setup configuration for dual fluorophore imaging.*

In cyan and in yellow the relative emission spectra of GCaMP6 and TdTomato, respectively. The green and the orange rectangular boxes represents the 525/50 nm and the 620/60 nm filters placed in front of the green and red light absorbing PMTs, respectively. The Black line at 570 nm represents the dichroic mirror for the separation of green and red light.

2.4.1 Single plane imaging with a custom-made two-photon set-up

Imaging was performed using a custom-built galvo-resonant scanning system with a Ti:Sapphire pulsing laser (Chameleon Vision-S, Coherent, CA, USA; < 70 fs pulse width, 80 MHz repetition rate) at 120 Hz, a Scientifica set-up equipped with a custom-programmed LabVIEW-based software (version 8.2; National Instruments, UK) . Three to four focal planes were acquired for each neuron. One in the soma, located between 500 and 650 µm below brain surface and 2 – 3 more fields of view in the apical tuft dendrites between 30 and 200

µm below brain surface and belonging to the same neuron. Pixel resolution varied session by session but ranged from 0.1 to 0.3 x 0.1 to 0.3 µm.

2.4.2 Multi plane data acquisition with FemtoSmart Dual two-photon set-up

Multi plane data were acquired using a FemtoSmart Dual two-photon microscope (Femtonics, Budapest, Hungary) and an ultra-fast, solid-state, single 100 fs pulse width laser (InSight DeepSee, SpectraPhysiscs, CA, USA). Images were acquired using the MESc software (Femtonics, HU). Two focal planes (512x165 pixels, pixel resolution 0.76 µm), with an average distance of 170 µm in Z, were imaged at a frequency of 96 frames/s (48 frames/s per plane) using a Piezo objective positioner kit (P725.4CA, 400 µm range, 230 Hz resonant frequency no load attached, Physic Instruments, Germany), switching between planes at 9.6 Hz (4.8 Hz per plane) (Figure 2.3).

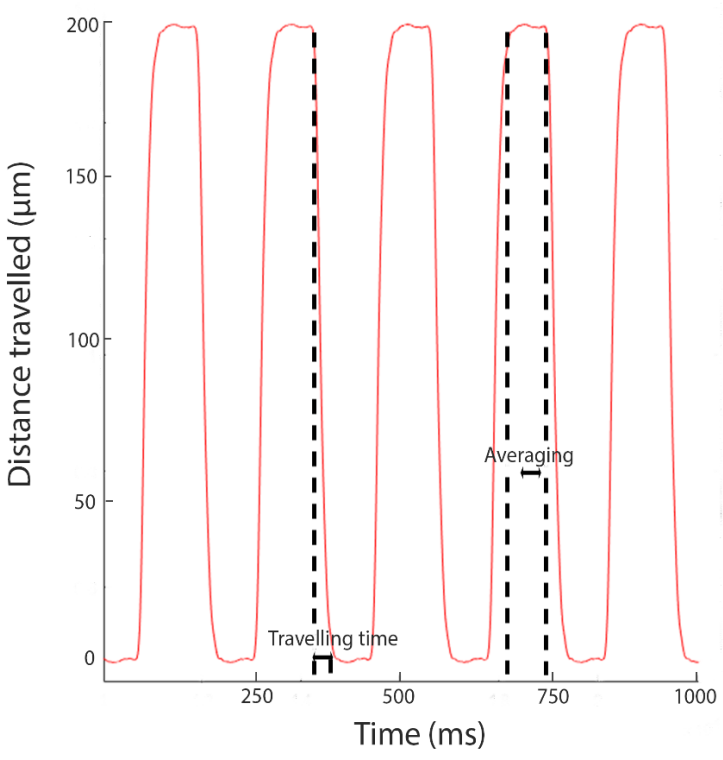

Figure 2.3: *Trace of the piezoelectric objective positioner.*

The plot shows the position of the objective compared to a reference focal plane, 0. The objective travels 200 µm in approximately 30 ms and it averages one single plane 10 times (10x frames). Travelling speed depends on distance travelled and the weight of the objective

(the heavier the slower). The averaged number of frames is set by the user. Each plane was scanned at 4.8 Hz in this example trace.

2.4.3 Habituation of mice to head-fixation

Three to four weeks after viral injections and 24 hours after the implantation of an imaging window, GCamp6-labeled neurons were imaged under 2-photon microscopy. Animals were habituated to head fixation in the setup by letting them rest in darkness, free to run, for half an hour before starting any experiment. A single experimental session never consisted of more than 3 hours and whenever the same animal was imaged more than once, it was allowed a resting period of at least 24 hours before the next imaging session. To avoid causing stress to the animals, the 2-photon imaging setup was wept with both ethanol (to disinfect) and acetic acid (to remove odours from previous animals) both at the beginning and at the end of each imaging session.

2.4.4 Visual stimulation

Visual stimuli were generated using the Psychophysics Toolbox package (Brainard, 1997) for MATLAB (Mathworks, MA) and displayed on a custom-modified backlit LED monitor (51 × 29 cm, Dell, UK) placed 20 cm from the right eye, covering 104° × 72° of the visual field. The mouse visual cortex is topographically arranged (Hübener, 2003). Because of mechanical constraints, my injections were in the anterior and medial part of monocular V1, so the screen was positioned toward the more ventral and posterior part of the mouse visual field, to maximise the proportion of neurons responding to visual stimulation. Visual stimulation trials consisted of drifting full-field square-wave gratings for 3 seconds (spatial frequency of 0.05 cycles per degree, 1.5 Hz, 8 equally spaced directions in randomized order, contrast 80%, mean luminance 37 cd/m^2). Drifting gratings were separated from one another by 4 seconds of isoluminant grey periods. Each trial started and ended with 2 seconds of dark screen. Time stamps for the onset of every stimulus were recorded and aligned to imaging frames using custom-built Matlab scripts.

Because photomultiplier tubes (PMT) are very sensitive to any source of light including ambient light, it is imperative that light coming from the stimulus-presenting screen does not contaminate the signal collected at the PMTs. To avoid photodamage, the pockel cell was off

at each turnaround points of the resonant scanner. Therefore, we synchronised the pockel cell with our stimulus-presenting screen. Both our resonant scanners in the LotosScan and Femtonics setup are 12 kHz scanners. We modified our screens to flicker at that rate so that the stimulus-presenting screen would be off during image acquisition and would light up only during turnaround points of the scanner. This allowed us to image neurons without signal contamination coming from the screen. It is important to notice that this flickering rate is well above mouse perceptual sensitivity and therefore the visual stimulus looked coherent to them (and to humans too) (Leinweber *et al.*, 2014) (Figure 2.4).

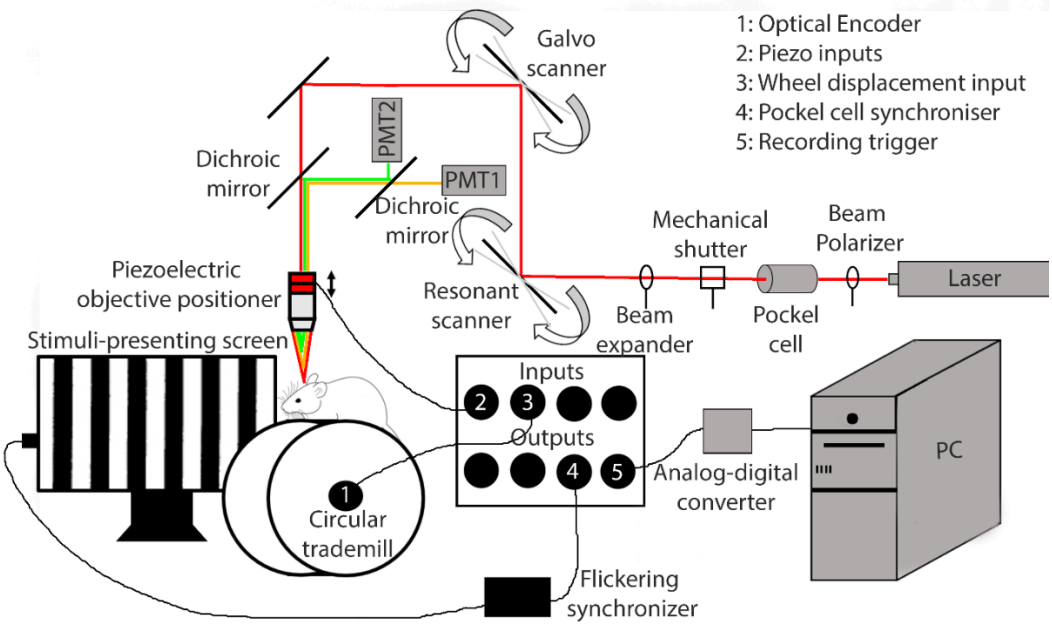

Figure 2.4: *A schematics of 2-photon imaging setup*

The laser beam originates from a tuneable laser source. It first passes through a beam polariser, a pockel cell which can be controlled using a software to regulate laser power, a mechanical shutter also controlled via an external software and finally through a beam expander. The laser beam is scanned by either a 12 (Scientifica, single plane) or a 8kHz (Femtonics, 2 planes) resonant scanner in the x axis and by a galvanometric scanner in the y axis. The laser is focussed on the z axis through a 25x magnification objective. A piezoelectric objective positioner resonates in the z axis to acquire data from multiple focal planes at the same time. Red and green light emitted by TdTomato and GCaMP6 fluorophores respectively is collected by the PMTs (see figure 2.2 for more details). Fluorescent signals are collected in darkness and during the presentation of visual stimuli as the animal can freely run on a circular treadmill. The screen flickers in antiphase with the pockel cell, being on only during turnarounds points of the scanner, when the pockel cell is off. The speed and the direction of running is acquired using an optical encoder. The recording of all external devices was synchronised using a trigger at the beginning of every recording session.

2.5 Data Analysis

2.5.1 Image processing and motion correction

Two-photon images were converted to the .tiff format and further processed using custom-made Matlab and Python scripts. Image processing required image cropping, and alignment of each frame to correct motion artefacts in x and y direction (details in section 2.5.1). Differently from movements in x and y, movement artefacts in the z dimension cannot be corrected for. By applying pressure onto the brain, the triple glass window (see section 2.3.2), minimized this kind of artefacts. Additionally, the use of TdTomato as a structural marker, allowed us to determine whether the imaging plane remained stable or moved in the z-axis. Trials with movement artefacts in the z dimension were excluded from further analysis.

Movement artefacts in the x and y dimension can be of two types: Inter-frame distortions and frame to frame displacements. Inter-frame distortions happen when movement artefacts are faster than the acquisition rate. These kinds of distortions cannot be corrected but they can be minimized to a negligible extent with a sufficiently high scanning frequency. Frame to frame displacements on the other hand can be corrected offline provided that the sample of interest (e.g. a cell soma or a dendrite) does not move out of the area covered by the scanners. 2D plane translation of single planes was performed using Sequential Image Analysis (SIMA) 1.3.2 (Kaifosh *et al.*, 2014). SIMA is a Viterbi-based algorithm that determines the probability of finding a structure of interest (defined in a pixel by pixel intensity map) in a given location, weighting the probabilities of all possible displacements from one frame to the next. TdTomato, was used as the signal for motion correction only if motion correction with GCaMP6 failed. This happened only when GCaMP6 signal was very sparse, or its baseline signal was too dark to be distinguished from background noise.

2.5.2 Image segmentation and calcium signal extraction

After motion correction, regions of interest (ROIs) were drawn manually onto averaged images of individual trials. ROIs were drawn around cell somas, which had their characteristic donut shape; the main apical trunk which looks like a dot under two-photon microscopy scanning perpendicularly to its axis of elongation; and individual branches in the distal apical

tuft which could have different shapes ranging from a single dot to a branching cable-like shape, according to their axis of elongation with respect to the scanning axis. An individual apical tuft branch was defined as the segment of a dendrite going from one branching point to the next. ROIs were always drawn manually using the polygon tool in Fiji, and they were drawn slightly larger than the averaged borders of the structure of interest. The size and shape of individual ROIs was maintained constant throughout the imaging session. ROIs were only drawn around structures which belonged to the neuron of interest as assessed during imaging and confirmed offline after cell reconstruction. ROIs which had a nearby source of signal contamination like another dendrite or a cell soma, were either re-drawn in a way that the contaminating source of signal would be excluded from the ROI, or they were excluded from analysis altogether.

After ROIs were drawn around the structure of interest, fluorescence values were calculated as a function of time. Once the raw signal was extracted, it was used to calculate $\Delta F/F_0$ defined as $(F - F_0)/F_0$. The baseline, or subtractive F_0, is the 5^{th}-percentile of the 1 Hz lowpass zero-phase, 60^{th} order FIR filtered signal of each ROI in each recording. The scale factor, or divisive F_0, is the mean of the baseline F_0 in each recording (Pakan *et al.*, 2016). Single plane data were acquired at 120 Hz, and subsequently downsampled to 5Hz for signal processing. Multi-plane data were acquired and analysed at 4.8 Hz.

2.5.3 Calcium transient analysis

Calcium transients in different cellular compartments have different dynamics. Somatic signals have a slower rising and decaying time compared to a transient of the same amplitude in the dendrites and dendrites produce much larger amplitudes of ΔF/F0 events compared to the soma, for the same amount of activity (Beaulieu-Laroche *et al.*, 2019). Because bigger events take longer to decay compared to smaller events, the difference between the mean ΔF signal in the soma and in the dendrites increases (exponentially) as the amplitudes of calcium transients increases. Additionally, to emit and come back to baseline fluorescence levels, GCaMP6 must both bind and unbind to free intracellular calcium. This process is slower for higher-amplitude or longer-lasting membrane depolarisations which generate high intracellular Ca^{2+} influx. This means that correlating ΔF/F0 on a frame-by-frame base, would bias the analysis toward larger and longer lasting calcium transients which would be statistically overrepresented. To correct for these biases, the peak amplitude of individual calcium transients was used. In this way, it was possible to (1) treat individual events as

statistically independent samples and avoid the statistical mis-representation of calcium transients of different amplitudes and (2) compensate for different rise and decay times.

To detect calcium transients, noise levels were estimated by filtering the ΔF/F0 signal using a 9th order, zero-phase, high-pass filter at 0.6 Hz (Matlab function *filter*). I then estimated the standard deviation of the filtered signal and used a threshold of 2.8 of this standard deviation using the built-in Matlab function *findpeaks.* The robustness of the results was then tested to different thresholds +/- 30% of the selected threshold.

For each peak found in any branch or compartment, an event was defined as coincident in another branch or compartment when another calcium transient could be detected in a time window of 3 seconds around the frame where the first peak was originally detected (2 seconds before, 1 after). As a consequence, peaks detected as coincident could not be further apart than 2 seconds. A large, 3 seconds window was selected for to deal with the slow dynamics of the calcium indicator can lead to long-lasting plateau calcium events, in which the peak of an event remains stably flat for prolonged periods of time and therefore making the local maximum to be detected at different points, simply due to imaging noise (Figure 2.5). The mean time interval was close to 0 ($2.19xe^{-4}$ seconds) with standard deviation of 0.28 seconds, meaning that 95% of all coincident events were found within a time interval of 0.56 seconds (Figure 2.5). To avoid the problem of assigning one peak as coincident with more than one peak, each peak could only be considered coincident with one other peak. To estimate the amplitude of a calcium transients, I took the difference between the ΔF/F0 amplitude at the frame in which a peak was detected (local maximum) and a local minimum in 2 seconds, backward sliding window. To pull data from different branches or compartments together, and to directly compare dendritic and somatic signals, the amplitudes of these peaks were normalised to the detected peak of highest amplitude for each ROI. Whenever a peak was detected in only one ROI and not in the other, the correlation was made between the peak amplitude in the ROI where the peak was detected and the difference between the maximum and minimum ΔF/F0 values in a 3 second window centred around the frame where a peak was detected in the other ROI. Correlation values were calculated as the Pearson's correlation values between event amplitudes in pairs of branches or compartments. Shuffling values were obtained by randomly shuffling the order of the events in one branch or compartment of each pair analysed. To estimate events amplification/ attenuation across compartments, residuals were extracted by calculating the robust linear regression line between normalised event amplitudes in two compartments,

and then extracting the distance, along the y-axis, of each individual point from this robust line.

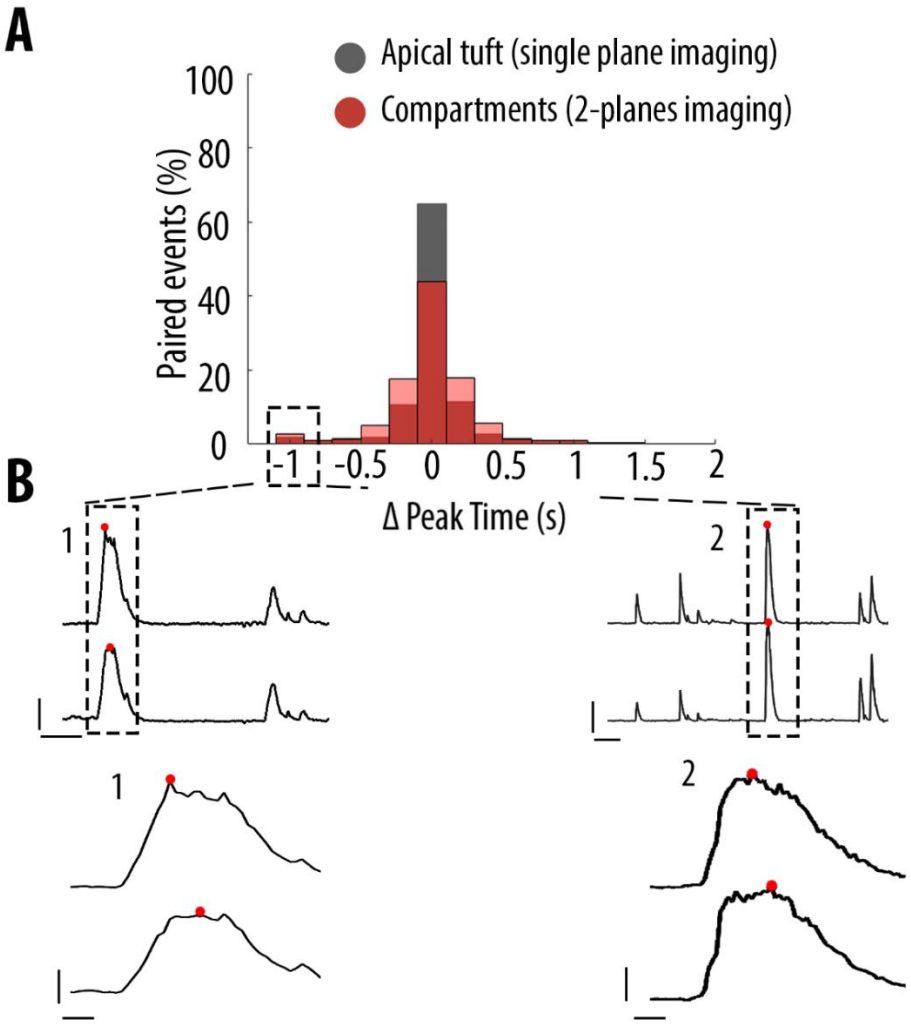

Figure 2.5: *Distribution of time intervals between peaks of calcium transients detected as coincident.*

A) Black, distribution for apical tuft events. Red, distribution for pairs of neuronal compartments (2-planes imaging). The mean time interval was close to 0 ($2.19xe^{-4}$ seconds) with standard deviation of 0.28 seconds, meaning that 95% of all coincident events were found within a time interval of 0.56 seconds. B) Examples of cases with the largest time interval between two coincident events (offset by 1 second) (dashed rectangle in A). Lower traces: zoomed view of the dashed area 1 and 2. The red dot indicates the frame at which a peak was detected for each pair of compartments. Scale bars: 0.3 ΔF/F0 (normalised to max), 10s (upper panel) and 1s (lower panel). Each bin is 200 ms.

2.5.4 Locomotion analysis

Changes in the position of the cylindrical treadmill (sampled at 12,000 Hz) were interpolated to match the rate of imaging. To define stationary and locomotion periods I used the following criteria: Stationary corresponded to periods where the instantaneous speed (as measured at the 40 Hz sampling rate) was less than 0.1 cm/s. Locomotion corresponded to periods meeting three criteria: instantaneous speed ≥ 0.1 cm/s, 0.25 Hz lowpass filtered speed ≥ 0.1 cm/s, and an average speed ≥ 0.1 cm/s over a 2 s window centered at this point in time (Pakan *et al.*, 2016). These criteria were setup to exclude times from the locomotion periods, intervals in which the animal would re-position or groom during imaging. Any inter-locomotion interval shorter than 500 ms was also labelled as locomotion. Stationary periods less than 3 s after or 0.2 s before a period of locomotion were removed from the analysis. The first one was excluded to avoid integrating as part of stationary periods, the decaying tail of the GCaMP6 signal, while the latter one was excluded from analysis because the periods preceding locomotion is a period of increased arousal where neuronal responses are distinct from the ones of quiet wakefulness. Accordingly, behavioural transitions were defined as time windows including: (1) 2 seconds before the onset of locomotion as defined above and 1 second after the onset, as well as (2) 1 second before the offset of locomotion and 20 seconds after the offset (unless another locomotion period began before the 20 seconds) (Vinck *et al.*, 2015). For this analysis, behavioural transitions were excluded from stationary and locomotion periods.

2.5.5 Orientation Selectivity

To determine the specific stimulus response parameters of each neuron to the oriented gratings, the ΔF/F0 during each presented oriented stimulus was first averaged across all trials. The preferred orientation of each neuron was the orientation that elicited the maximal response when averaged across all trials. The orientation selectivity index (OSI) was calculated as $(O_{pref}-O_{orth})/(O_{pref}+O_{orth})$ where O_{pref} represents the mean ΔF/F0 value during the presentation of the preferred orientation across trials and O_{orth} represents the mean ΔF/F0 value during the presentation of the orientation orthogonal to the preferred one. For the detailed analysis of orientation preference in chapter 4, the preferred response angle was estimated by calculating the argument of the resultant vector (V) in the complex plane, which was given by:

$$V = \frac{\sum_k R(\theta_k) e^{2i\theta_k}}{\sum_k R(\theta_k)}$$

where $R(\theta_k)$ is the mean ΔF/F0 response to angle θ_k (Mazurek, Kager and Van Hooser, 2014).

2.5.6 Morphological reconstructions

Morphological reconstructions were done using Simple Neurite Tracer, a semi-automatic ImageJ plugin for tracing the dendrites of neurons and other tube-like structures. Reconstructions were done using either the baseline fluorescence of the GCaMP6 signals, or, when GCaMP6 baseline was not distinguishable from background, TdTomato, an activity-independent marker. The distance between a branch and its soma was estimated in terms of the number of branching points that separated the soma from the recorded branch. The trunk was considered branching order 0 and sibling branches after the nexus, branching order 1 (see also Figure 3.3).

2.7 Statistics

All analysis was performed either in Matlab 2017a, or in GraphPad Prism 8. All error bars in the figures represent standard error of the mean. The details of the statistical test I used, as well the details about what I used as independent samples can be found in the relevant figure legends.

3. The apical tuft of individual layer 5 pyramidal neurons: single or multi-compartment computational unit?

3.1 Introduction

A large body of literature demonstrates that dendrites of pyramidal neurons are endowed with a wide array of voltage-gated ion channels that can supralinearly amplify synaptic inputs through the generation of dendritic spikes (Ramaswamy and Markram, 2015; Stuart and Spruston, 2015). The generation of dendritic spikes has been proposed to have three main functions: 1) To increase the efficacy of distal synaptic inputs, which would otherwise be attenuated by the filtering properties of the dendrites with distance (Rall, 1962; Spruston *et al.*, 1995; Vetter, Roth and Häusser, 2001; Larkum *et al.*, 2009); 2) To endow individual dendritic branches to perform independent computation, allowing the implementation of complex logical computations (Rall, 1962; Oswald, 2004; Branco and Häusser, 2010; Chen *et al.*, 2012; Cichon and Gan, 2015; Scholl, Wilson and Fitzpatrick, 2017; Lee *et al.*, 2019); 3) To boost the information storage capabilities of single neurons (Rall, 1962; Yang *et al.*, 2014; Cichon and Gan, 2015; Bono and Clopath, 2017).

The generation of local dendritic spikes is generally associated with a local entry of calcium, and as such, many studies have approached the investigation of dendritic integration using calcium indicators (Stuart and Sakmann, 1994; Stuart, Schiller and Sakmann, 1997; Svoboda *et al.*, 1999; Larkum, Kaiser and Sakmann, 1999; Schiller *et al.*, 2000; Vetter, Roth and Häusser, 2001; Nevian *et al.*, 2007; Larkum *et al.*, 2009; Xu *et al.*, 2012; Harnett *et al.*, 2013; Major, Larkum and Schiller, 2013; Grienberger, Chen and Konnerth, 2014; Stuart and Spruston, 2015; Harnett, Magee and Williams, 2015; Ramaswamy and Markram, 2015; Kerlin *et al.*, 2019).

Using glutamate uncaging in brain slices, it was shown that coincident synaptic inputs in few neighbouring spines could give rise to localised nonlinear dendritic responses (Williams, 2002; Polsky, Mel and Schiller, 2004; Losonczy and Magee, 2006; Stuart and Spruston, 2015), suggesting that in a high firing rate regime observed *in vivo*, dendritic branches would generate regenerative responses (Luczak *et al.*, 2007).

The tuning of layer 2/3 orientation selective neurons in V1 , was shown to be predicted by the average tuning of its presynaptic inputs (Wertz *et al.*, 2015; Wilson *et al.*, 2016). While the evidence for clustering of synaptic inputs in layer 2/3 and layer 5 of the mouse visual

cortex *in vivo* remains controversial (Jia *et al.*, 2010; Chen *et al.*, 2011; Varga *et al.*, 2011; Wilson *et al.*, 2016; Iacaruso, Gasler and Hofer, 2017; Scholl, Wilson and Fitzpatrick, 2017; Kerlin *et al.*, 2019) dendritic spikes may be generated even in the absence of clustering simply due to an increase in the overall synaptic conductance associated with a given stimulus (Ujfalussy *et al.*, 2015; Schmidt-Hieber *et al.*, 2017).

In vivo, both local (Palmer *et al.*, 2014; Cichon and Gan, 2015) and global (Xu *et al.*, 2012; Ranganathan *et al.*, 2018; Kerlin *et al.*, 2019) dendritic spikes have described in the apical tuft of layer 5 pyramidal neurons.

Using patch clamp recordings in mildly anaesthetised and anaesthesia-recovered animals, Smith *et al.* (2013) found that layer 2/3 neurons produce NMDA-dependent spikes in response to the presentation of stimuli of the preferred angle, but not in response to the presentation of stimuli at the orthogonal orientations. However, patch-clamp recordings provide no information about the spatial spread of these events. Additionally, for technical reasons these recordings were performed in immobilised animals.

Locomotion was shown to exert its gain modulation effect on V1 through both NA and Ach (Polack, Friedman and Golshani, 2013; Fu *et al.*, 2014). Both of these neuromodulators have been shown to impact dendritic excitability (Hoffman and Johnston, 1999). Recently however, Beaulieu-Laroche *et al.* (2019) reported a high correlation in the somatic and nexus activity of V1 neurons independently of visual stimulation and locomotion. Despite high coupling, they report that approximately 15% of trunk's nexus activity is independent of the soma, suggesting that these events are dendritically-generated. However, Beaulieu-Laroche *et al.* (2019) did not record data from the apical tuft where most of the independent computation should occur.

As such, it remains unknown the extent to which the apical tuft dendrites of V1 layer 5 pyramidal neurons produce local versus global dendritic spikes and whether the dendritic integrative regime is modified during locomotion or in a stimulus-specific way.

To test this, I imaged calcium signals in sibling branches of the distal apical tuft during visual stimulation and darkness, while the animal was either locomoting or stationary. To do so, I sparsely labelled layer 5 neurons with GCaMP6f and TdTomato using a cre-dependent approach. I then identified individual layer 5 neurons by following their apical trunk all the way to the superficial layer 1, where dendritic calcium signals were recorded.

The results show that the activity of the apical tuft dendrites of individual layer 5 neurons is highly correlated. Branch-specific activity was approximately 3% of the total number of events and it exclusively consisted of small-amplitude events. This high correlation persisted throughout the apical tuft independent of the distance of sibling branches from the soma. Despite both visual stimulation and locomotion increased the activity of the apical tuft dendrites of layer 5 pyramidal neurons, neither of these conditions altered the high coupling between branches.

3.2 Material and methods

Material and method used for these experiments are described in chapter 2 of this thesis.
The results described in this chapter include data from 70 apical tuft branches, recorded from 14 different neurons in 6 animals. Neurons were labelled with AAV1.CamKII 0.4.Cre.SV40 (Penn Vector core catalogue No. 105558-AAV1, titer (GC/ml): $1.81e^{13}$) diluted 1:10000 – 1:20000 and AAV1.Syn.Flex.GCaMP6f.WPRE.SV40 (Penn Vector Core, catalogue No. 100833-AAV1, titer (GC/ml): $1.91e^{13}$) diluted 1:10 in ACSF.
Data were acquired using a custom-built galvo-resonant scanning system with a Ti:Sapphire pulsing laser (Chameleon Vision-S, Coherent, CA, USA; < 70 fs pulse width, 80 MHz repetition rate) at 120 Hz, with a custom-programmed LabVIEW-based software (version 8.2; National Instruments, UK). Fluorescent traces were down-sampled to 5Hz for signal processing.

3.3 Results

3.3.1 Calcium transients are highly correlated between branches that belong to the same neuron

In order to study dendritic activity in layer 5 neurons of the mouse primary visual cortex, I imaged GCamP6f calcium signals in the apical tuft branches of individual layer 5 neurons in awake, head-fixed animals. I first investigated the correlation of calcium signals in sibling branches of individual layer 5 pyramidal neurons. I found that calcium signals in the apical tuft dendrites were highly correlated between branches that belonged to the same neuron and non-correlated for branches that belonged to different neurons (Figure 3.1). Each pair of branches had a mean Pearson's correlation value of 0.92 (Figure 3.2A). When I averaged the correlation value between branches' pairs of every field-of-view recorded in the apical

tuft of a given neuron, I obtained a very similar average Pearson's correlation value (0.92), suggesting that calcium signals are highly correlated between all tuft branches of an individual layer 5 pyramidal neuron (Figure 3.2B). To validate the results, I compared these correlation values against a shuffled dataset, in which the event size in one of the two branches was shuffled and correlated against the unshuffled branch. Shuffling the data provided the correlation value of 0, which is expected when correlating two random datasets (Figure 3.2B).

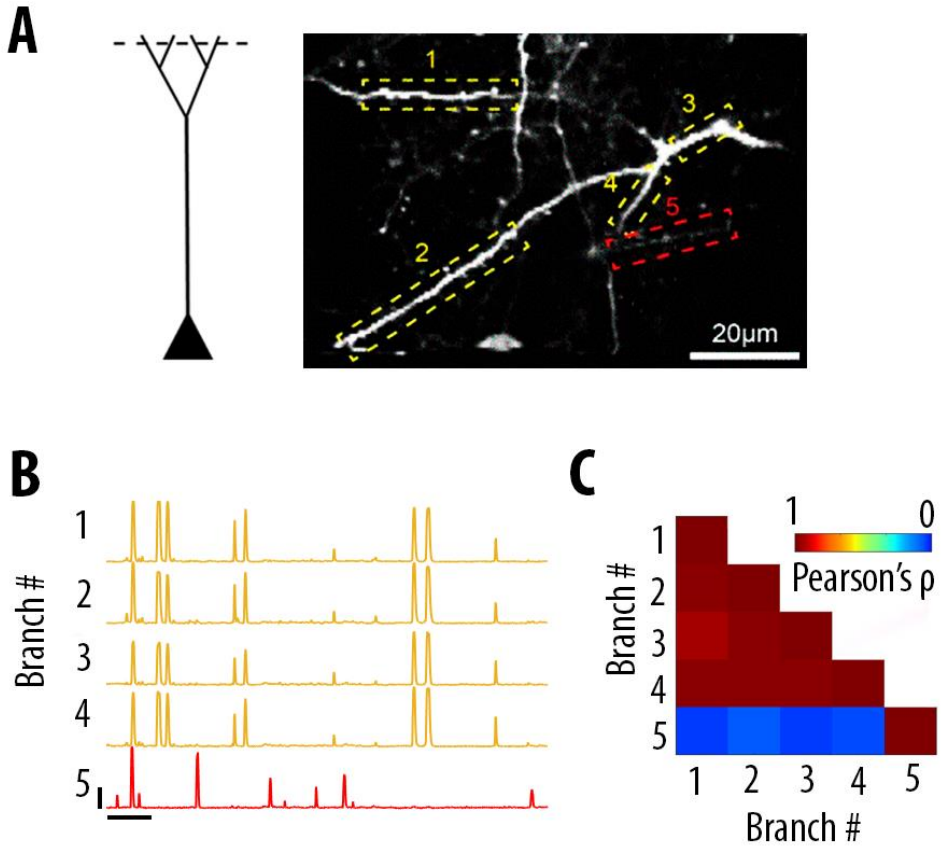

Figure 3.1: Calcium signals *in apical tuft branches were highly correlated between dendrites that belonged to the same neuron and uncorrelated between dendrites that belonged to different neurons.*

A) Single plane imaging of the apical tuft branches that belong to the same neuron (highlighted in yellow) and to a different neuron (highlighted in red). B) GCaMP6f-calcium transients of the apical tuft branches belonging to one neuron are shown in traces 1 to 4 while calcium transients of a tuft branch belonging to a different neuron is shown in trace 5. Scale bars, 0.3 ΔF/F0 (normalised to max), 20 s. **C**) Pearson's correlation matrix between the calcium transients of the branches shown in A. Branches that belong to the same neuron (branches 1 to 4, neuron 1) have a mean Pearson's correlation of 0.96, while the branch that belongs to the different neuron (branch 5, neuron 2) has a mean Pearson's correlation value of 0.13 with neuron 1's branches.

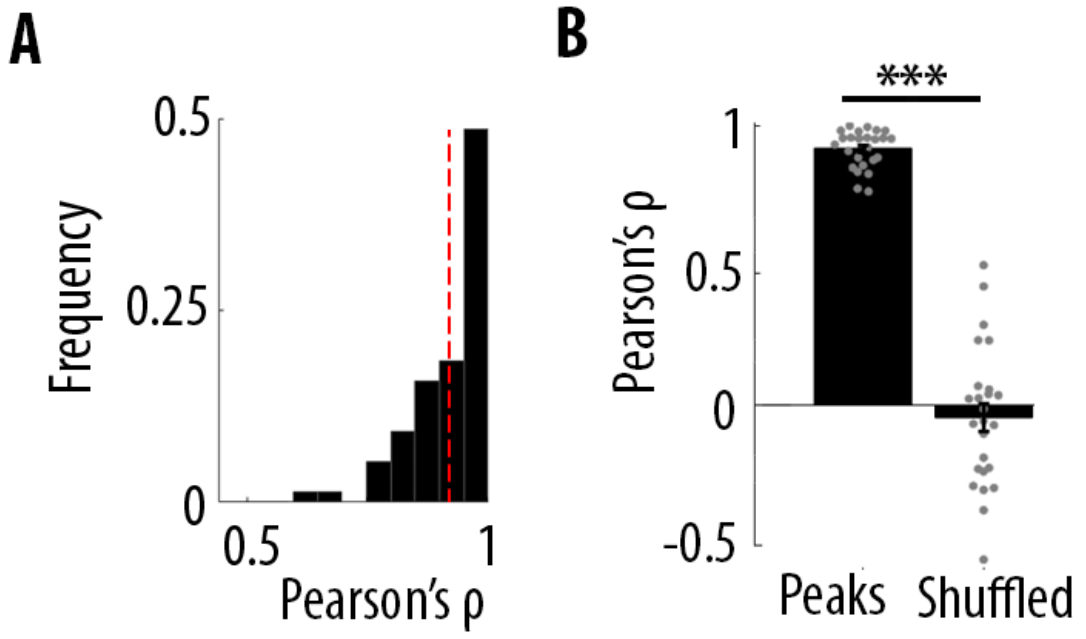

Figure 3.2: *High correlation between different apical tuft branches belonging to the same neuron*.

A) Frequency distribution of the pairwise correlation of all imaged branches (n = 76 pairwise correlations, coming from 14 neurons; 6 animals; 70 branches. Mean ρ = 0.92) B) Mean Pearson's correlation value for each imaged field of view and its corresponding shuffled data (Paired t-test, p = 3.5 e^{-15}; n = 25 fields of view, coming from 14 neurons; 6 animals; 70 branches. Mean ρ = 0.92 and -0.04; SEM = 0.01 and 0.05 for peaks and shuffled, respectively). The Pearson's value for each field of view comes from an average of the pairwise correlation between all the branches that belong to the same neuron.

3.3.2 Apical tuft dendritic calcium signals are highly correlated regardless of the branching order

The high correlation of calcium signals between dendritic branches of the same neuron may be due to the backpropagation of action potentials. However, it is known that backpropagating action potentials attenuate in a distance-dependent manner (Vetter, Roth and Häusser, 2001). Because branching points are points of sudden impedance decrease, they have been shown to be the point at which backpropagating action potentials fail to propagate with higher probability (Spruston *et al.*, 1995b; Vetter, Roth and Häusser, 2001).

In order to test whether correlation values between dendritic branches dropped as a function of distance from the soma, I have reconstructed the dendritic arborisation of the imaged neurons. To do so, I used TdTomato, an activity-independent marker and I counted

the number of branching points that separated the soma from the imaged apical tuft branches (Figure 3.3). Only sister branches (branches with the same branching order) were analysed. I was able to obtain functional data and reconstruct dendrites up to the 8th branching order. Pairs of branches which were not sisters (e.g. parent or grandparent branches) as well as branches whose branching order could not be estimated with certainty, were not included in this analysis. The results show that the amount of correlation between sister branches is high, regardless of the branching order of the imaged branches ($p = 0.34$, One-way ANOVA, Figure 3.4). For example, a pair of sister branches in the 8th branching order, had a Pearson's correlation of 0.96. These results show that the observed high correlation does not depend on the branching order of the dendrites, and that high correlation persists regardless of the distance from the soma. Altogether these results suggest that high correlation of calcium signals is a general feature of the apical tuft of layer 5 dendrites.

Finally, in order to determine whether this high correlation was due to the branch lineage, I calculated the Pearson's correlation values for branches that were either directly related to each other (sister, parents and grandparent branches), or from indirect lineages (Figure 3.5, panel A). The results show that correlation values do not change between branches that are directly and indirectly related to each other ($p = 0.72$, One-way ANOVA, Figure 3.5), suggesting that high correlation values persist across different branches' familiar lineages.

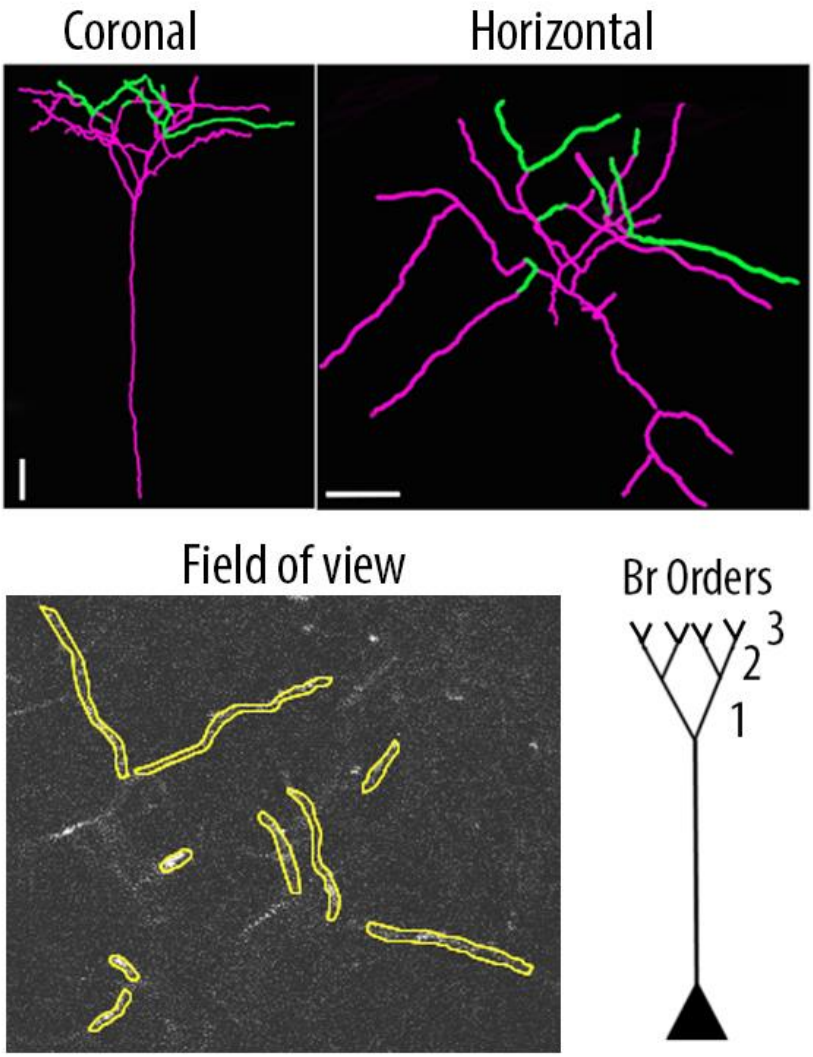

Figure 3.3: *Morphological reconstruction of the apical dendritic tuft of an individual layer 5 pyramidal neuron imaged in vivo*.

The neuron was reconstructed by taking a z-stack at the end of the imaging session (red channel, TdTomato). *Upper panels*, a coronal and a horizontal view of the reconstructed neuron. *Lower left panel*, *In vivo* two-photon image of GCaMP6f-labelled apical tuft dendrites from which calcium transients were imaged (not shown). Highlighted in yellow, the ROIs representing the same branches shown in the upper panel . *Lower right panel*, schematic of the definition of branching order.

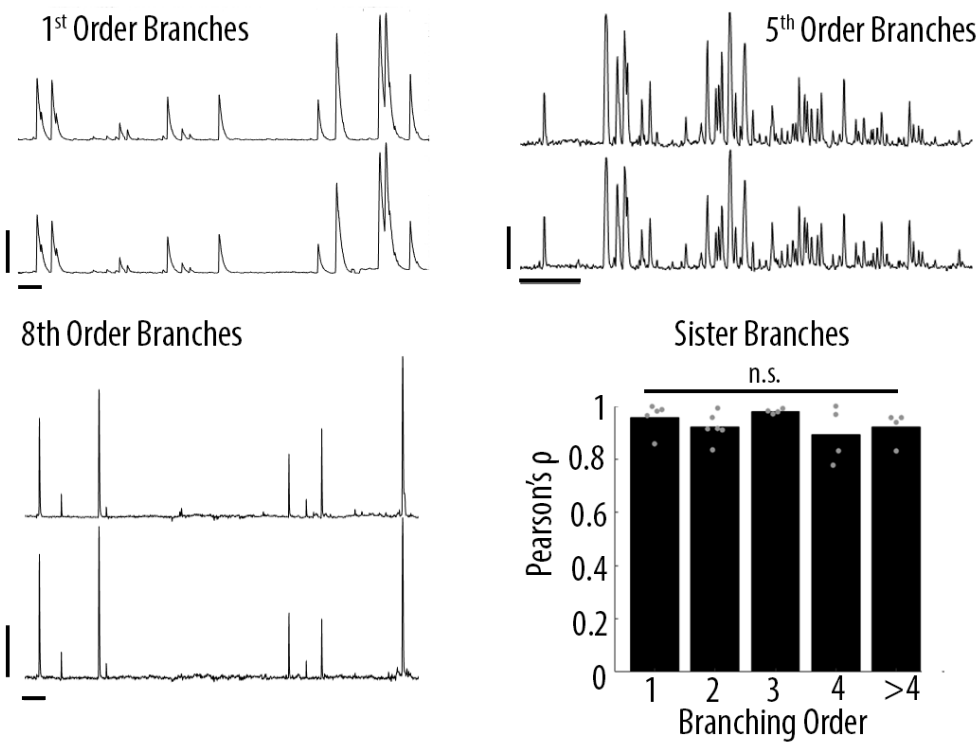

Figure 3.4: *Calcium transients in sister branches are highly correlated regardless of their branching order.*

Three representative traces of sibling branches belonging to the 1st, 5th and 8th branching order. *Bottom right panel*, quantification of the Pearson's correlation for sister branches in different branching orders. Branches with a branching order higher than 4 were pulled together (For 1st, 2nd, 3rd, 4th and more than 4th branching order, One-way ANOVA, p = 0.34; n = 5; 6; 4; 4; 4 pairs of sister branches, respectively. Scale bars, 0.3 ΔF/F0 (normalised to max), 20 s.

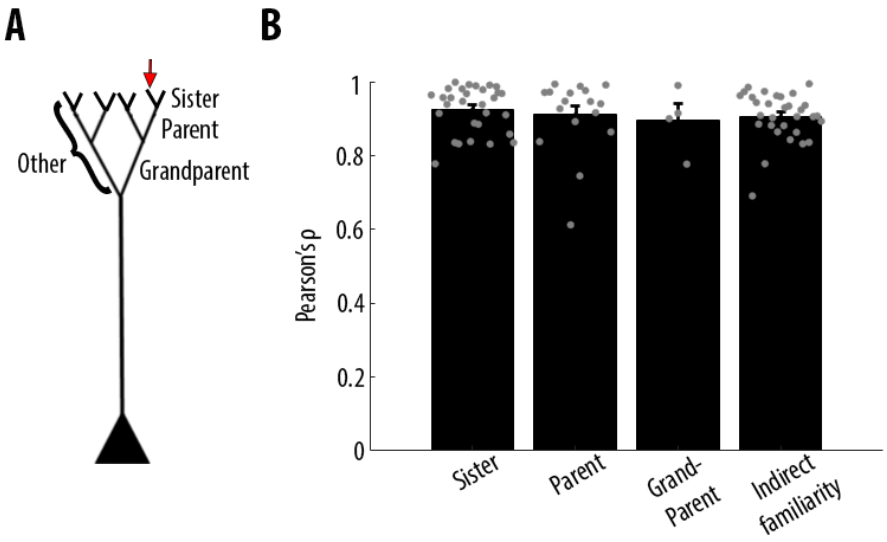

Figure 3.5: *Calcium transients in apical tuft branches are highly correlated regardless of their branching lineage.*

A) Schematic of the definition of lineage in relation to the branch indicated by the red arrow. B) Pearson's correlation for apical tuft branches that directly related to each other (sister, parent and grandparent) or from indirectly related branches (For sister, parent, grandparent and branches of indirect familiarity, One-way ANOVA, p = 0.72; n = 30; 17; 4; 31 pairs of apical tuft branches, respectively. Error bars are SEM.

3.3.3 Visual stimulation and locomotion increase apical tuft activity without affecting the high correlation between apical tuft branches

To test whether calcium signals in the apical tuft dendrites changed during visual stimulation and locomotion, I calculated the mean ΔF/F0 value for each of the four conditions (visual stimulation and darkness during stationary and locomotion) for all branches of each neuron. For each neuron, I calculated the correlation value of its branches during these conditions. These results show that while both visual stimulation and locomotion increase the mean amplitude of calcium transients in apical tuft dendrites (p = 0.0053, 0.0026 and 0.99 for visual stimulation, locomotion and interaction effect respectively, RM Two-way ANOVA on log-transformed data), neither of these conditions altered the correlation between different branches (p = 0.43, 0.62 and 0.97 for visual stimulation, locomotion and interaction effect respectively, Two-way ANOVA) (Figure 3.6).

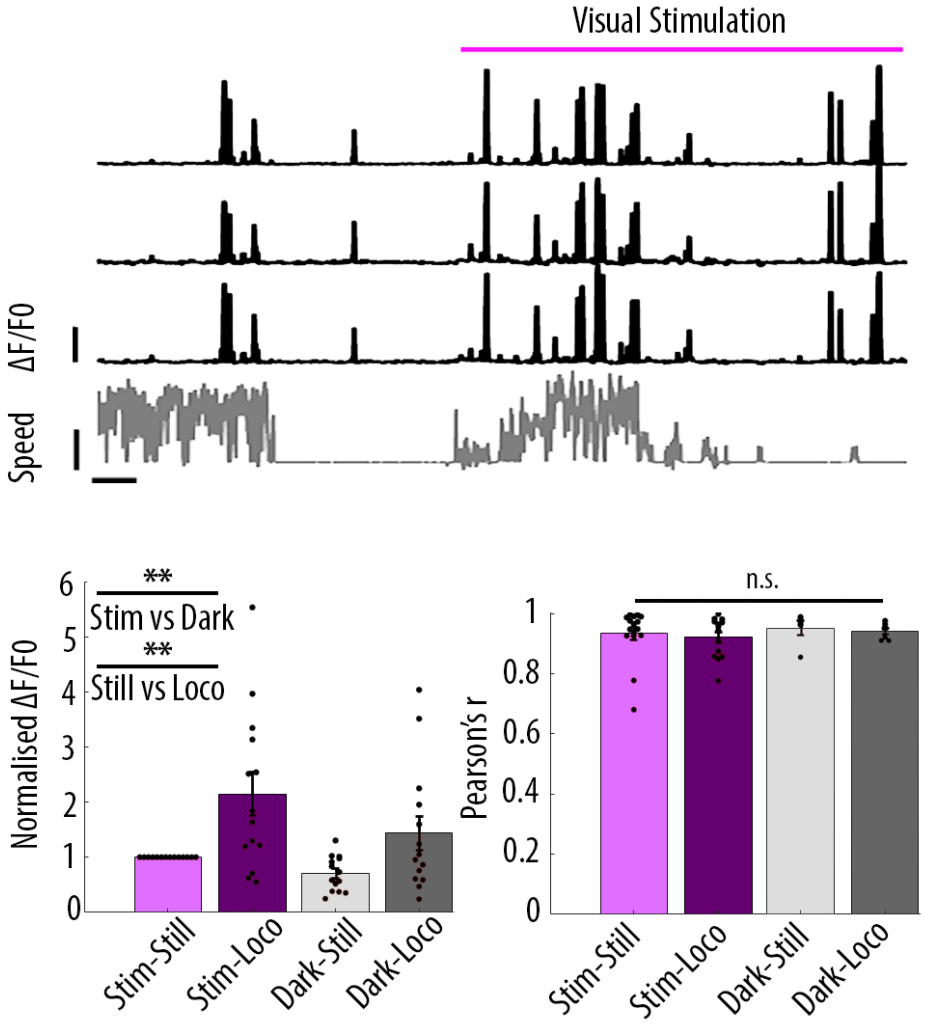

Figure 3.6: *Locomotion and visual stimulation increase the calcium signals of the apical tuft without affecting the correlation between its branches.*

A) Representative traces of 3 apical tuft branches belonging to the same neuron while the animal was either stationary or locomoting (lower panel) during either darkness or the presentation of drifting gratings (purple segment). Scale bars, 12 cm/s, 0.3 ΔF/F0 (normalised to max), 20 s. B) Mean ΔF/F0 for apical tuft dendrites during darkness (dark) and visual stimulation (stim) while the animal was either stationary (still) of locomoting (loco). Bar graph is normalised to the condition of visual stimulation during stationary period. Both visual stimulation and locomotion significantly increase the mean ΔF/F0 of tuft branches without any interaction effect (Repeated Measures Two-way ANOVA on log-transformed data, p = 0.0053, 0.0026 and 0.99 for the visual stimulation, locomotion and interaction effects respectively, n = 14 neurons). C) Pearson's correlation coefficients ρ for the apical tuft branches of individual neurons during the four conditions (stim and still, stim and loco, dark and still, dark and loco). (Two-way ANOVA, p = 0.43, 0.62 and 0.97 for visual stimulation, locomotion and interaction effects; n =16; 14; 5 and 7 field of views respectively). Error bars: SEM. Individual dots represent individual neurons

3.3.4 Branch-specific calcium signals are rare, dominated by low-amplitude events, and independent of visual stimulation and locomotion

The high overall correlation of calcium signals between apical dendritic branches does not exclude the possibility of rare branch-specific events. For example, in case these events were dominated by low amplitude transients, they would have little impact onto the overall correlation between two branches. To investigate the proportion of branch-specific events, for each pair of branches I have calculated the proportion of calcium transients that were detected in only one of the two branches of the pair (see Method section 2.5.3). The results show that branch-specific calcium transients in the apical tuft of layer 5 neurons was rare. I quantified branch-specific events in all pairs of branches (76 pairwise comparisons) as the proportion of calcium transients present in one branch and absent in the other pair's branch. Among 76 pairwise comparisons coming from 14 neurons, branch-specific calcium transients represented less than 3% of the total number of transients (Figure 3.7). These local signals were exclusively composed of transients of the smallest amplitudes (Figure 3.7A-C). In addition, neither visual stimulation with drifting gratings nor locomotion significantly affected this small proportion of branch-specific calcium signals (Three-way ANOVA, $p < 10^{-15}$ for event amplitude and $p = 0.29$; 0.8 and 0.94, for visual stimulation, locomotion and interaction between both conditions, respectively. No other interaction effect was statistically significant) (Figure 3.7D). Finally, I tested that these results were robust to changes in the time window used to define coincidence (Figure 3.8).

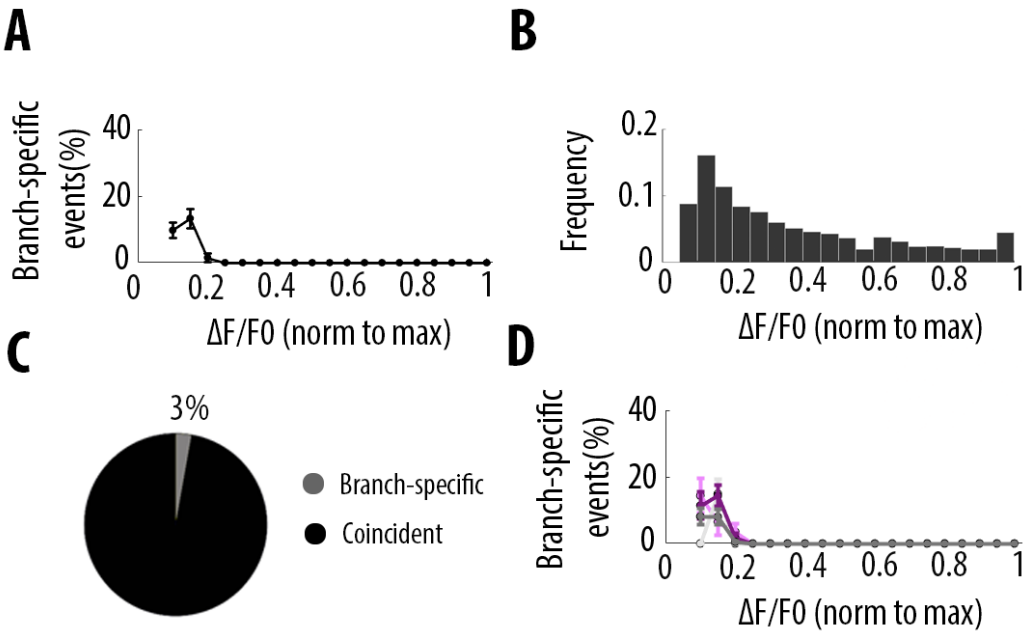

Figure 3.7: *Branch-specific activity is rare, dominated by small-amplitude events and independent of visual stimulation and locomotion*.

A) Proportion of branch-specific events as a function of event's amplitude. Each point corresponds to the weighted average of the number of events each neuron had for each bin (0.05 size). Branch specific events represent a small proportion (10-15%) of the smallest amplitude events (15% of the largest event). B) The frequency of events of different amplitudes. C) Pie chart showing the proportion of branch specific activity compared to the total number of events. Branch-specific events comprise about 3% of the total number of events. D) Weighted mean of the proportion of branch-specific events as a function of event's amplitude for the four different conditions. For all conditions, branch-specific events represent a small proportion of the smallest amplitude events as shown in A. Neither visual stimulation nor locomotion nor an interaction effect increased significantly the number of branch specific events (Three-way ANOVA, $p = 0.29$; 0.8 and 0.94, respectively; $p < 10^{-15}$ for event amplitude, n = 14 neurons).

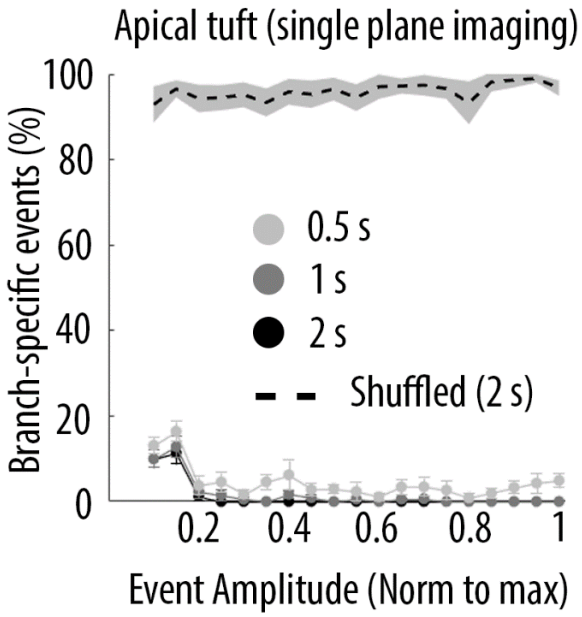

Figure 3.8: The *proportion of branch-specific events is robust to changes in the time window used to define coincidence of calcium events between apical dendrites.*

Proportion of compartment-specific events as a function of calcium transients' amplitude using different time windows (0.5s, 1s and 2s) to define coincidence of events in sibling branches. The dashed line represents the proportion of compartment-specific events obtained from shuffled ΔF/F0 signals, with the selected time window (2 s). Because the 3 seconds window is asymmetric (2 seconds backward and one second forward), two events could not be further apart than 2 seconds.

Because these events were of small amplitude, they were also the ones whose detection is more likely to be sensitive to small variations in signal amplitude, signal-to-noise ratio and detection threshold, leading to an increased proportion of false positive and false negative findings. Signal amplitude and signal-to-noise ratio depend on the expression of calcium indicator and imaging conditions. During the experiments, adjustable parameters (e.g. laser power, PMT levels) were optimised to maximise both and were kept constant throughout the recording session. Detection thresholds in the analysis of calcium transients on the other hand, were defined in the analysis of the imaging data, and therefore, I tested how the selection of different thresholds affected the results.

To do this, branch-specific calcium signals were defined using a threshold of 2.8 standard deviations in one branch, and changing the detection threshold in the second branch by up to +/- 30%. Heightening and lowering the threshold in the second branch revealed events just around detection threshold (Figure 3.9). The results show that the amount of branch

specific activity goes up to 3.8% when I use a threshold which is 30% more stringent in the second branch, compared to the first. Notably, the proportion of branch-specific events went down to 0.8% when I used a threshold which was 30% more permissive in the second branch compared to the first. This suggests that the detection of approximately 75% of all branch-specific events, was highly sensitive to variations in the detection thresholds and highlight the small amplitude of these branch-specific events. Altogether, these results indicate that branch-specific events are rare, and mostly composed of low-amplitude events (Figure 3.10). It cannot be excluded that some of the branch-specific events were of too small amplitude to be detected, in these experimental conditions. However, signals in individual synaptic spines were reliably detected (Figure 3.11) suggesting that I had the spatial resolution necessary to detect independent calcium signals on the dendrites, and that not all the detectable dendritic activity was always correlated

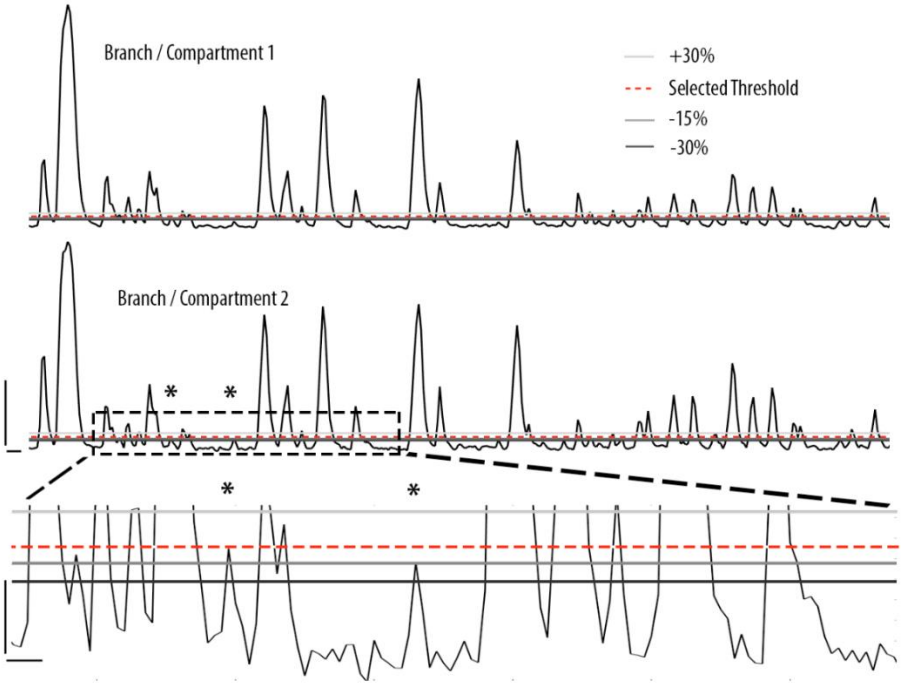

Figure 3.9: *Methodological approach to assess results robustness to variations in detection thresholds of calcium events*.

To assess the proportion of branch specific calcium events, for every calcium transient detected in one branch, I assessed whether there was another corresponding event in the second branch (see Methods). *Upper and middle panel*, ΔF/F0 traces of two sibling branches in the apical tuft branches of a single layer 5 pyramidal neurons. Asterisks indicate two events which were not detected using the selected threshold but were detected lowering the threshold by 30%. *Lower panel*, zoomed trace of the dotted area in the upper panel. To assess the resilience of the results to different thresholds, I assessed the amount of branch specific events, keeping the selected threshold in one branch (red-dotted line) and varying the threshold in the second branch from +30% to -30% (light, medium and dark grey lines, respectively). Scale bars: upper panel, 0.3 ΔF/F0 (normalised to max), 5 s; lower panel: 0.03 ΔF/F0, 1s.

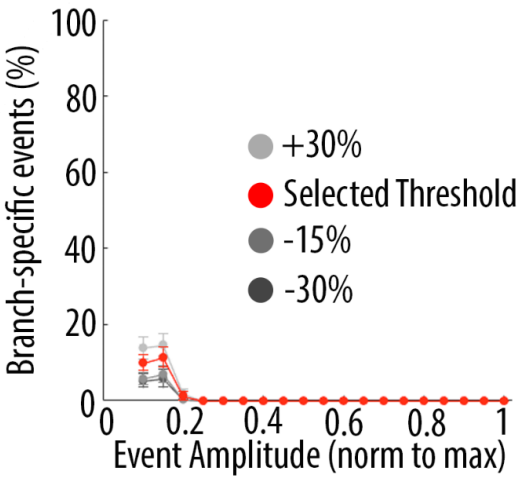

Figure 3.10: *Branch-specific activity using different detection thresholds.*

Proportion and amplitude of branch-specific events detected as a function of the amplitude and threshold selected.

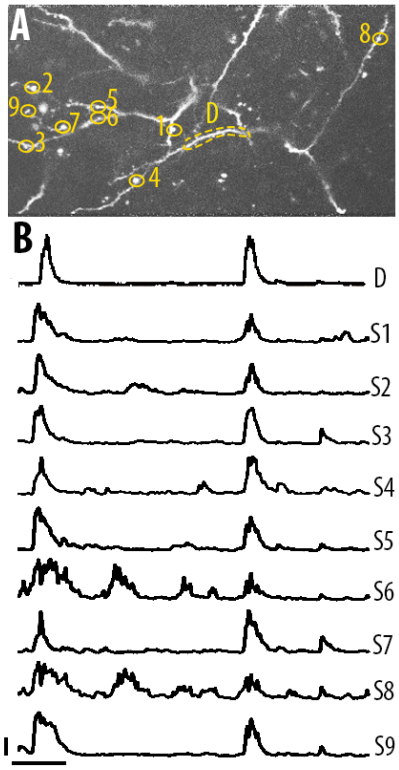

Figure 3.11: *Single spine calcium signals in the apical tuft dendrites of layer 5 neurons.*

A) Two-photon image of an example field of view showing the apical tuft branches of an individual GCaMP6-labelled layer 5 neuron. B) Example ΔF/F0 traces for the individual spines shown in panel A. Error bars indicate 0.3 ΔF/F0 (normalised to max), 10 s.

3.4 Discussion

Altogether, these results provide evidence that calcium signals in the apical tuft dendrites of individual layer 5 pyramidal neurons are highly correlated throughout the apical tuft. Increased distance from the soma did not impact correlation. Despite the apical tuft increases its activity during both visual stimulation and locomotion, neither of these conditions affected the correlation of single neurons' branches, suggesting that high correlation persists through different behavioural states and through a wide range of activity levels. In line with these results, I showed that branch-specific calcium signals were rare (3%) and that the proportion of branch-specific events did not change during visual stimulation or locomotion. Branch-specific events were exclusively composed of small amplitude calcium transients (< 20% of the largest event), and as such, were susceptible to false positive and false negative findings. In line with these results, the proportion of branch-specific activity drops by 75%, when the detection threshold is reduced in one branch only, suggesting that the detection of branch-specific events is highly sensitive to fluctuations around the detection threshold.

3.4.2 Widespread vs local dendritic activity

The generation of dendritic spikes has been proposed to serve as a compensatory mechanism for the distance-dependent attenuation imposed by the filtering properties of the dendrites. Individual EPSPs produced by synaptic inputs arriving on the distal branches of the apical tuft of layer 5 pyramidal neurons provide negligible contribution to the somatic depolarisation and therefore to its firing (Williams, 2002). Therefore, the generation of local-dendritic spikes was proposed as a mechanism to overcome these constraints and supra-linearly amplify the relevant inputs (Branco and Häusser, 2010; Schmidt-Hieber *et al.*, 2017). These results demonstrate that indeed the apical tuft generates regenerative events. However, the high correlation between branches suggests that it does so in a global, rather than branch-specific manner.

Several groups have demonstrated *ex vivo*, that few spatially arranged synaptic inputs are sufficient to induce dendritic nonlinearities (Williams, 2002; Polsky, Mel and Schiller, 2004; Losonczy and Magee, 2006; Stuart and Spruston, 2015). These results strongly predict that under *in vivo* conditions, when neurons are bombarded by thousands of inputs even at background levels of activity, the recruitment of dendritic spikes should be a predominant

feature of input integration (Stuart and Spruston, 2015). Using whole-cell patch clamp electrophysiology, Smith *et al*. (2013) showed that the apical tuft branches of individual layer 2/3 neurons in the primary visual cortex produce NMDAR-dependent spikes *in vivo* clearly distinguishable from backpropagating action potentials. Provided that similar types of computations are implemented by the dendrites of layer 2/3 and layer 5 neurons, my results suggest that the long-lasting dendritic events reported by Smith *et al*. (2013) might be global in the whole dendritic tree. On the other hand, it is possible that branch-specific activity is systematically coincident with global activity and therefore undetectable under the slow temporal dynamics of the calcium indicator GCaMP6f.

The generation of branch-specific spikes has been suggested to be instrumental for the implementation of dendritic LTP: a form of non-Hebbian plasticity suggested to increase memory storage availability and prevent catastrophic memory interference (Golding, Staff and Spruston, 2002; Cichon and Gan, 2015; Bono and Clopath, 2017). My results suggest that a low proportion of calcium events are branch-specific, and therefore dendritic LTP could be implemented in those instances of local activity. However, given the low rate of these events, their effect is likely to be overpowered by much more commonly-occurring global calcium events (Kampa, Letzkus and Stuart, 2006; Gambino *et al.*, 2014; Bittner *et al.*, 2017).

The fact that high correlation persists regardless of the distance of individual dendritic branches from the soma, as well as during visual stimulation and locomotion, suggests that global calcium signals in the apical tuft is a fundamental feature of dendritic computation of layer 5 pyramidal neurons in V1.

3.4.3 The possible origins of global apical tuft calcium signals

Global correlated calcium signals in the apical tuft dendrites would be consistent with at least three non-mutually exclusive mechanisms:

(1) Backpropagating action potentials generated in the soma may spread similarly between all sibling branches of the apical tuft. Backpropagating action potentials however, were shown to decrease in amplitude in a distance dependent manner and were shown to fail at dendritic branching points (Spruston *et al.*, 1995; Vetter, Roth and Häusser, 2001). Previous experimental and theoretical findings suggested that bAPs wouldn't reach distal location in the apical tuft of layer 5 neurons (Spruston *et al.*, 1995; Vetter, Roth and Häusser, 2001). However, Larkum, Kaiser and Sakmann (1999), demonstrated that somatic action potentials elicited beyond a critical frequency (10-20 Hz) can elicit Ca^{2+} electrogenesis in the apical tuft,

suggesting that the events observed in this study may results from bAP-activated dendritic electrogenesis.

(2) Global tuft activity resulting from the interaction between backpropagating action potentials and incoming synaptic inputs onto the apical tuft (Larkum, Zhu and Sakmann, 1999; Manita *et al.*, 2015). It was shown that when a bAP is temporally matched to an incoming input onto the apical tuft of a layer 5 pyramidal neuron, the threshold for the generation of dendritic spikes is halved and the coupling between somatic and dendritic firing is strengthened (Larkum, 2013). As a consequence of this somato-dendritic interaction, the soma produces bursts of action potentials while the apical tuft dendrites produce long-lasting Ca^{2+} plateau potentials, readily detectable by calcium indicators (Waters *et al.*, 2003; Beaulieu-Laroche *et al.*, 2019).

(3) Apical tuft inputs sum up at the Ca^{2+} initiation zone in the distal part of the apical trunk where a dendritic spike is generated. If the depolarisation is sufficiently large, the trunk will generate a large dendritic calcium spike which would then backpropagate into the apical tuft (Larkum and Zhu, 2002). Differently from point 1 and 2, the origin of the backpropagated signal would be dendritic rather than somatic and therefore would not require somatic activation to be initiated.

The results presented in this chapter leave unanswered the question as to which of the three mechanisms described above dominates in V1 layer 5 neurons of awake mice. It is possible that different mechanisms would prevail during different behavioural conditions: for example, neuromodulators may differently modify the coupling between somatic and dendritic activity depending on the behavioural state of the animal (Hoffman and Johnston, 1999; Shah, Hammond and Hoffman, 2010; Harnett *et al.*, 2013; Harnett, Magee and Williams, 2015).

The next chapters of this thesis will address the question of the coupling of these global events with somatic calcium signals.

4. High and asymmetric somato-dendritic coupling of V1 layer 5 neurons independent of visual stimulation and locomotion

4.1 Introduction

Creating a nonlinearity in the apical tuft is a powerful way to amplify the impact that specific inputs have on somatic firing. In the visual cortex, this has been proposed as a functional mechanism to sharpen the orientation selectivity of the excitatory neurons (Smith *et al.*, 2013). The preferred orientation of an orientation selective neuron can be predicted by averaging the synaptic inputs it receives (Wertz *et al.*, 2015; Wilson *et al.*, 2016). On the other hand, the overrepresentation of excitatory inputs tuned to the same orientation of the soma, doesn't seem to be compensated by an equivalent increase in tuned inhibition (Kerlin *et al.*, 2010; Liu *et al.*, 2011; Grienberger *et al.*, 2017). As a consequence, the net excitatory drive a neuron receive at the preferred orientation is larger compared to the orthogonal one. These observation are consistent with the findings of Smith *et al.* (2013), who showed that the dendrites of layer 2/3 neurons produce NMDA-dependent dendritic spikes in response to the preferred orientation of the neuron only.

In addition to respond to visual stimuli, layer 5 pyramidal neurons also increase their firing rate in response to locomotion (Erisken *et al.*, 2014; Dadarlat and Stryker, 2017). Compared to stationary periods, locomotion increases the firing rate of layer 2/3 neurons (Niell and Stryker, 2010), the primary excitatory drive to layer 5 (Harris and Shepherd, 2015). However, SST+ neurons, a class of dendrite targeting interneurons also increases their response during locomotion and visual stimulation, but not during darkness (Pakan *et al.*, 2016). As consequence, it is unclear whether the dendritic mechanisms that lead to gain modulation during locomotion in darkness and during visual stimulation, are the same as the ones that lead to orientation selectivity. Indeed, it was shown that at least part of the effects of locomotion are mediated by the neuromodulators Ach and NA (Polack, Friedman and Golshani, 2013; Fu *et al.*, 2014). Both these neuromodulators were shown to strengthen somato-dendritic coupling via their action onto dendritic K^+ channels that favours both the generation of dendritic Ca^{2+} spikes and the backpropagation of action potentials (Hoffman and Johnston, 1999; Harnett *et al.*, 2013; Labarrera *et al.*, 2018).

In vivo, several studies have looked at the activity in the apical tuft of layer 5 neurons. However, apical tuft activity was recorded either in isolation, without a simultaneous somatic

readout (Xu *et al.*, 2012; Manita *et al.*, 2015; Takahashi *et al.*, 2016; Lacefield *et al.*, 2019), or in anaesthetised animals (Hill *et al.*, 2013) which affects dendritic integration by suppressing both top-down inputs to V1 and the activity of dendrite-targeting, SST+ interneurons (Makino and Komiyama, 2015; Leinweber *et al.*, 2017). Simultaneous imaging of somatic and dendritic activity in awake and behaving animals emerged only recently, with the development of volumetric recording techniques including spatial light modulators and piezoelectric objective positioners (Peters *et al.*, 2017; Beaulieu-Laroche *et al.*, 2019; Kerlin *et al.*, 2019).

By using semi-simultaneous imaging of apical trunk and somatic GCaMP6f Beaulieu-Laroche *et al.*, (2019) found that calcium signals in layer 5 neurons, were highly correlated and that neither visual stimulation nor locomotion altered this correlation.
However, high correlation of somato-dendritic activity could result from multiple, non-mutually exclusive mechanisms including (1) a strong somatic activation leading to the generation of dendritic Ca^{2+} electrogenesis (Larkum, Kaiser and Sakmann, 1999) (2) the generation of somatic firing through a strong dendritic spike generated at the nexus (Grienberger, Chen and Konnerth, 2015) (3) the coincident occurrence of bAPs with apical tuft inputs (Larkum, Zhu and Sakmann, 1999; Larkum, 2013). As a consequence, which of these computational regimes dominates *in vivo*, and whether the computational regime dominating during visual stimulation differ from the one used during locomotion, remains poorly understood.

To address this question, I used GCaMP6s to semi-simultaneously image calcium signals in the soma, trunk and distal tuft dendrites of layer 5 pyramidal neurons, both in darkness and during the presentation of drifting gratings, while head-fixed mice were either running or stationary. In agreement with Beaulieu-Laroche *et al.* (2019), I found that dendritic calcium signals were highly correlated with somatic signals throughout the apical somato-dendritic axis (Soma, Trunk and Tuft). However, I extended these results by showing that somato-dendritic coupling was asymmetric; while almost all events observed in the tuft were also visible in the soma, around 40% of somatic events attenuated in an amplitude and distance-dependent manner from the soma to the apical tuft. This attenuation was likely due to low frequency action potentials, that were not associated with dendritic Ca^{2+} spike. Finally, the results show that neither visual stimulation nor locomotion affected the coupling of somatic and apical tuft calcium signals.

4.2 Method

Material and methods utilised for these experiments are described in chapter 2 of this thesis. For simultaneous recordings, neurons were labelled with AAV1.CamKII 0.4.Cre.SV40 (Penn Vector core catalogue No. 105558-AAV1, titer (GC/ml): $1.81e^{13}$) diluted 1:10000 – 1:20000 and AAV1.Syn.Flex.GCaMP6s.WPRE.SV40 (Penn Vector Core, catalogue No. 105558-AAV1, titer (GC/ml): $1.91e^{13}$) diluted 1:10 in ACSF. Multi-plane data were acquired using an ultra-fast, solid-state, single 100 fs pulse width laser (InSight DeepSee, SpectraPhysiscs, CA, USA) and a FemtoSmart Dual two-photon microscope (Femtonics, Budapest, Hungary). Two focal planes (512x165 pixels), with an average distance of 170 µm in Z, were imaged at a frequency of 96 frames/s (48 frames/s per plane) using a Piezo objective positioner kit (P725.4CA, Physic Instruments, Germany), switching between planes at 9.6 Hz (4.8 Hz per plane) (See figure 2.3). Fluorescent signals were analysed at 4.8 Hz. The median vertical distance between 2 planes was 170 µm. The results described in this chapter include data from 31 pairs of neuronal compartments (11 Soma-Trunk; 5 proximal trunk (pTrunk)-distal trunk(dTrunk); 9 Trunk – Tuft; 6 proximal Tuft (pTuft) -distal Tuft (dTuft)) coming from 19 neurons in 6 animals. For figure 4.6 and 4.17 to 4.21, data from this chapter and chapter 3 of this thesis were pooled together and therefore, I included in the analysis, neurons labelled with the virus GCaMP6f as described in section 3.2 of this thesis. For figure 4.6, one neuron was excluded as the peak analysis was not considered reliable due to a poor signal-to-noise.

4.2.1 Supplementary videos

Supplementary video 1 can be found at the following link:

https://drive.google.com/file/d/1U3_D9yI26NWMGx5c5au1fH-LBCKx0vPS/view?usp=sharing

Two-photon imaging movie showing calcium signals detected in the soma and not detected in the corresponding trunk of an individual layer 5 pyramidal neuron in V1.

Left panel, two-photon calcium imaging (raw data) for a pair of neuronal compartments (Soma-Trunk) imaged semi-simultaneously. Both the soma (*lower quadrant*, circled in red) and the corresponding trunk (*upper quadrant*, circled in blue) of an individual layer 5 pyramidal neuron are shown. *Right panel,* GCaMP6s calcium traces of the two compartments (red for Soma, blue for Trunk) aligned to the video shown on the left panel. Data were acquired at 4.8 Hz per plane. The two fields of view were 170 µm apart in the vertical plane. Scale bars: 10 s and 0.2 ΔF/F0 (normalised to max).

Supplementary video 2 can be found at the following link:

https://drive.google.com/file/d/1WQaC-0yBvCkJdG0V-leYG5rzkIxaH29p/view?usp=sharing

Two-photon imaging movie showing calcium signals detected in the trunk and not detected in the corresponding tuft of an individual layer 5 pyramidal neuron in V1.

Left panel, two-photon calcium imaging (raw data) for a pair of neuronal compartments (Trunk-Tuft) imaged semi-simultaneously. Both the trunk (*lower quadrant*, circled in red) and the corresponding tuft (*upper quadrant*, circled in blue, 3 branches) of an individual layer 5 pyramidal neuron are shown. *Right panel,* calcium traces of the two compartments (red for Trunk, blue for Tuft (upper right branch)) aligned to the video shown on the left panel. Data were acquired at 4.8 Hz per plane. The two fields of view were 170 µm apart in the vertical plane. Scale bars: 5 s and 0.2 ΔF/F0 (normalised to max).

4.3 Results

4.3.1 *Ex vivo* calibration of GCaMP6s and GCaMP6f signals in layer 5 soma and apical tuft dendrites

Previous studies that simultaneously imaged somatic and dendritic calcium signals *in vivo* to investigate dendritic computation, have used GCaMP6f (Peters *et al.*, 2017; Beaulieu-Laroche *et al.*, 2019; Kerlin *et al.*, 2019; Voigts and Harnett, 2019). However, I used GCaMP6s which has a better amplitude and signal-to-noise ratio compared to GCaMP6f (Chen *et al.*, 2013; Huang *et al.*, 2019). In order to understand how sensitivity differences would influence the quantification of the somato-dendritic coupling of calcium signals, Dr Zahid Padamsey in the lab, performed *ex vivo* experiments to calibrate GCaMP6s and GCaMP6f signals in V1 layer 5 soma and apical tuft dendrites. I contributed to these experiments by optimising and performing the viral injections for simultaneous 2-photon calcium imaging and whole-cell somatic recordings in slices.

The details of the method and the results of the *ex vivo* recordings are presented in the appendix 1 (Figure4) of this thesis.

The results showed that compared to GCaMP6f, low frequency events were better detected with GCamP6s, specifically in the soma, with equal sensitivity in the apical dendrites. For somatic stimulation, we could robustly detect somatic calcium signals with firing frequencies as low as 5 Hz with GCaMP6s (appendix 1, Figure 4E, 4G), and as low as 25 Hz with GCaMP6f (appendix 1, Figure 4F, 4H); we could not reliably detect calcium events associated with single action potentials with either indicator. Somatic signal amplitude increased monotonically with stimulation frequency for both indicators, with a plateau at 100-200 Hz. By contrast, in the distal dendrites, reliable signals for both indicators were only detected

when somatically-driven spiking exceeded 50Hz (appendix 1, Figure 4E-4H). For dendritic stimulation, calcium signals were reliably detected in both the soma and distal dendrites. With GCaMP6s, this was true for all frequencies tested (appendix 1, Figure 4C, 4E, 4G). With GCaMP6f, somatic signals could not be observed at lower stimulation frequencies (5 Hz) (appendix 1, Figure 4D, 4F, 4H).

Consequently, as compared to GCaMP6s, attenuation of events from soma to dendrite was underestimated whereas attenuation of events from dendrite to soma was overestimated with GCaMP6f (Francioni, Padamsey and Rochefort, 2019))

4.3.2 Calcium signals are highly correlated across different compartments of individual layer 5 neurons

Using a piezo objective, I semi-simultaneously imaged calcium transients in pairs of neuronal compartments, from the soma to the apical tuft of single layer 5 pyramidal neurons. Pairs of compartments imaged semi-simultaneously include: Soma-proximal Trunk (pTrunk); proximal Trunk (pTrunk)- distal Trunk (dTrunk); dTrunk- proximal Tuft (pTuft) and pTuft-distal Tuft (dTuft) (Figure 4.1). I found a high correlation between calcium signals in each pair of compartments imaged semi-simultaneously. The average Pearson's correlation value between the peak amplitude of individual transients was 0.74 between the soma and the proximal trunk (Figure 4.2 iv), 0.85 between the proximal and distal trunk (Figure 4.2 iii), 0.92 between the trunk and the apical tuft (Figure 4.2 ii) and 0.88 between the proximal and distal parts of the apical tuft (Figure 4.2 i. See also Figure 4.3 to visualize all compartments together). These results also confirmed the high correlation of calcium transients throughout the apical tuft that was found using GcamP6f and whose correlation is described in chapter 3 of this thesis (Figure 3.2).

These results show a consistently high linear correlation between the amplitudes of calcium transients detected across different neuronal compartments from the soma to the distal part of the apical tuft.

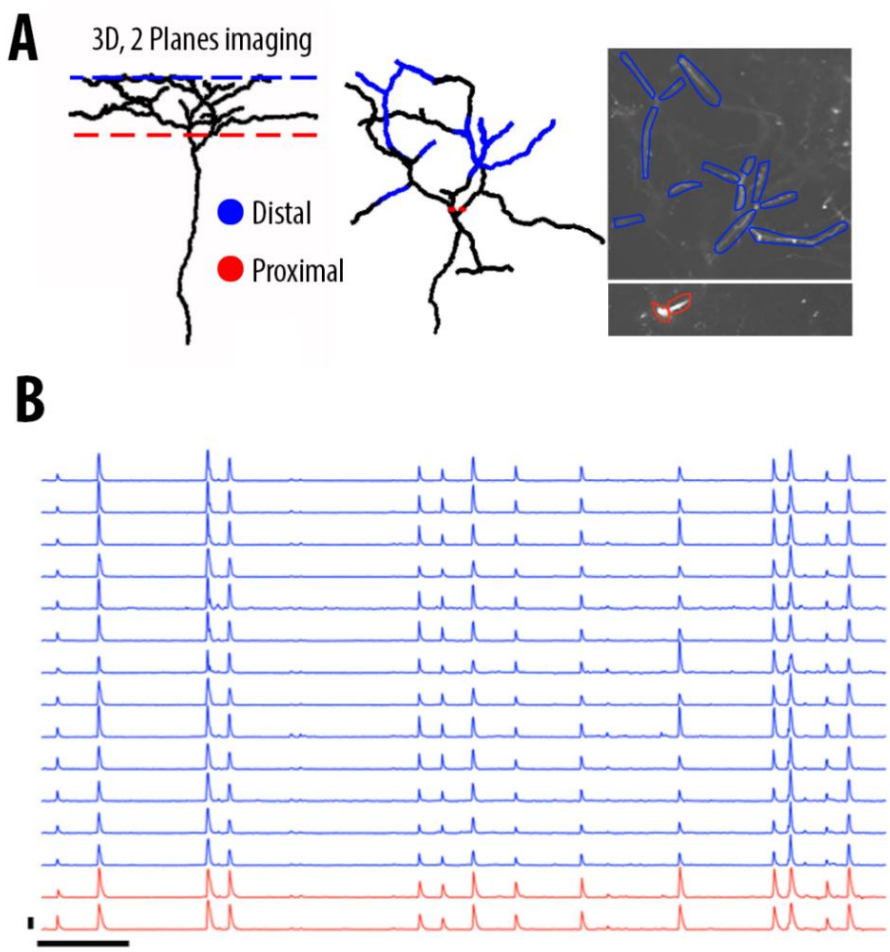

Figure 4.1: *Two-planes imaging of the apical tuft of an individual layer 5 pyramidal neuron*

A) The neuron was reconstructed by taking a z-stack at the end of the imaging session on the TdTomato static marker. *Upper left and middle panels*, a coronal and a horizontal impression of the reconstructed neuron. *Right panel*, a 2-photon imaging field of view with GCaMP6s-labelled apical tuft dendrites, from which activity was recorded (shown in B). In red the apical tuft branches belonging to the proximal part of the pair of compartments imaged together. In blue, the apical tuft branches belonging to the distal part of the pair of compartments imaged together. B) ΔF/F0 trace of calcium activity for each of the branches reconstructed and highlighted in panel A. Scale bars: 0.3 ΔF/F0 (normalised to max) and 60 seconds.

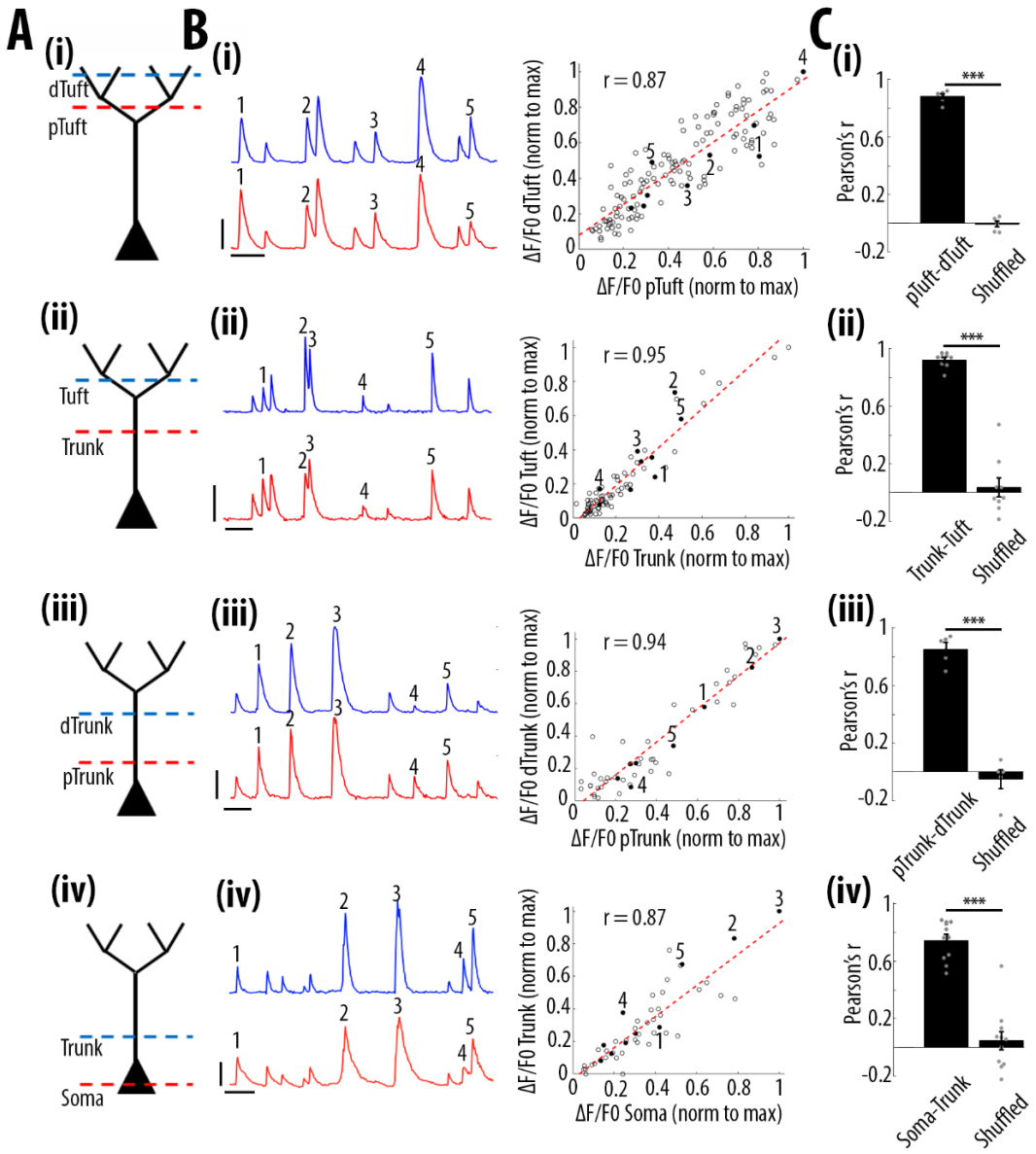

Figure 4.2. *High correlation of calcium transients between neuronal compartments (soma, trunk, apical tuft) of individual layer 5 neurons.*

A) Schemata of the compartments imaged semi-simultaneously, (i) proximal tuft-distal tuft, (ii) trunk-tuft, (iii), trunk-trunk, (iv) soma-trunk. pTrunk, dTrunk and pTuft, dTuft indicate proximal and distal portions of the trunk and the apical tuft, respectively. B) *Left panel*, representative GCaMP6s-calcium transients imaged in two neuronal compartments semi-simultaneously as shown in B. *Right panel*, scatter plot of peak amplitudes of individual calcium transients in proximal and distal compartments imaged semi-simultaneously, in one example individual neuron. Each dot represents a calcium transient. Peak amplitudes were normalized to the maximum amplitude in each compartment. Filled dots correspond to the transients indicated by numbers in the left panel. Numbers 1 to 5 in the left panel are matched to the ones in the right panel. Red dotted line indicates the best fit (least square). Pearson's correlation values (r) are indicated for each example pair of neuronal compartment. Scale bars 0.3 ΔF/F0 (normalised to max), 10 s. C) Pearson's correlation values

for each pair of compartments imaged semi-simultaneously and corresponding shuffled data (Paired t-test, pTuft-dTuft(i), $p = 1.6e^{-6}$, mean = 0.88; -0.01, sem = 0.02; 0.02, n = 6 pairs; Trunk-Tuft(ii), $p = 8e^{-7}$, mean = 0.92; 0.04, sem = 0.02; 0.07, n = 9; pTrunk-dTrunk(iii), $p = 4.4e^{-4}$, mean = 0.85; -0.05, sem = 0.05; 0.07, n = 5; Soma-Trunk(iv), $p = 4.4e^{-6}$, mean = 0.74; 0.05, sem = 0.04; 0.06, n = 11).

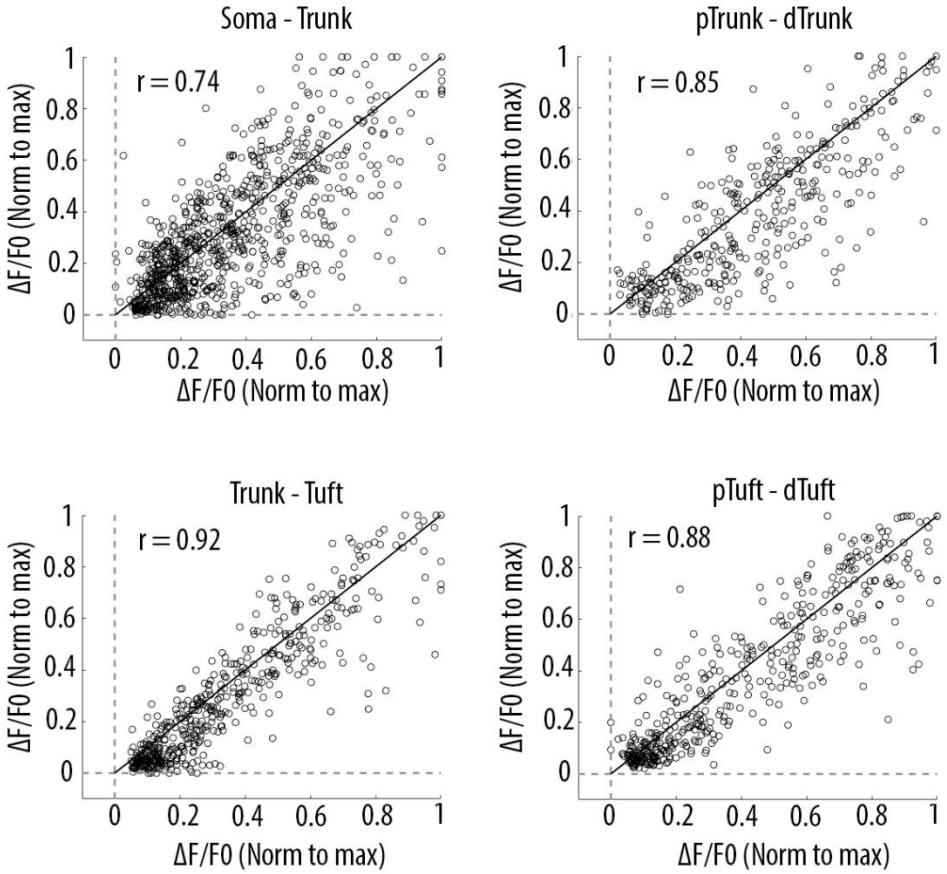

Figure 4.3: *Scatter plots of individual calcium transients' amplitudes in all proximal and distal compartments imaged semi-simultaneously.*

Each dot represents a calcium transient. All transients are normalised to the largest transient for each compartment. x-axis: proximal compartment; y-axis: distal compartment. Black line indicates the identity line. The mean Pearson's correlation values (r) calculated per neuron, as reported in figure 4.2, are indicated for each pair of compartments. Soma-Trunk, n = 858 transients from 11 neurons; pTrunk-dTrunk, n = 360 transients from 5 neurons; Trunk-Tuft, n = 479 transients from 9 neurons; pTuft-dTuft, n = 447 transients from 6 neurons; For visualization purposes, for Trunk-Tuft and pTuft-dTuft, only transients from one pair of imaged compartments are shown per neuron.

4.3.3 The frequency of calcium transients decreases in a distance and amplitude-dependent manner from the soma to the apical tuft

Next, I quantified the frequency of calcium events in each pair of proximal and distal compartments imaged semi-simultaneously (Figure 4.4 A-C). I found that the frequency of calcium transients decreased from proximal to distal compartments (Paired t-test, $p = 1.1e^{-6}$, n = 31 pairs of compartments from 19 neurons) by an average of 14% from soma to proximal trunk, 8% from proximal to distal trunk, 24% from distal trunk to apical tuft and 22% from proximal tuft to distal tuft (Figure 4.4B). From these proportions, I estimated a decrease of about 40% of calcium transients from soma to the distal part of the apical tuft (Figure 4.6). This result was confirmed by a second data set, in which somatic and apical tuft calcium transients were imaged independently in individual layer 5 neurons. I found that the mean frequency of calcium transients in the apical tuft corresponded to 62% of the frequency of events in the corresponding soma (n= 13 neurons) (Figure 4.6 B-C). The decrease in frequency of events from soma to the apical tuft was independent of neuron depth (Figure 4.6 A-D).

Next, I tested whether this decrease in frequency depended on the amplitude of the calcium transients. I predicted that if the decrease in frequency of events was due to a distance-dependent attenuation imposed by dendritic filtering, smaller events would have a higher probability of attenuating below detection threshold, compared to larger events. To assess this, I calculated the proportion of compartment-specific calcium transients as a function of their amplitude. The results show that smaller amplitude calcium transients in the proximal compartment were more likely to attenuate below detection level in the distal compartment compared to larger amplitudes events (Figure 4.4C. Also see Figure 4.5). This amplitude-dependent attenuation was consistently present through all the pairs of compartments I analysed from the soma to the distal part of the apical tuft (Figure 4.4C (i-iv)).

Interestingly, the vast majority of compartment-specific events (events that attenuated from one compartment to the next) were dominated by calcium transients in proximal compartments that were not detected in distal ones (red trace in Figure 4.5), while only 1.4% of calcium transients were found in distal compartments and not in the corresponding proximal compartment (blue trace in Figure 4.5) (see also Supplementary video 1 and 2, section 4.2.1 of this thesis). As a result, compartment-specific events were dominated by small amplitude calcium transients that attenuated from proximal to distal compartments (Two-way ANOVA, $p<10^{-15}$, $p<10^{-15}$, $p<10^{-15}$, for compartment (proximal vs distal), amplitude, and interaction effect, respectively; Figure 4.5).

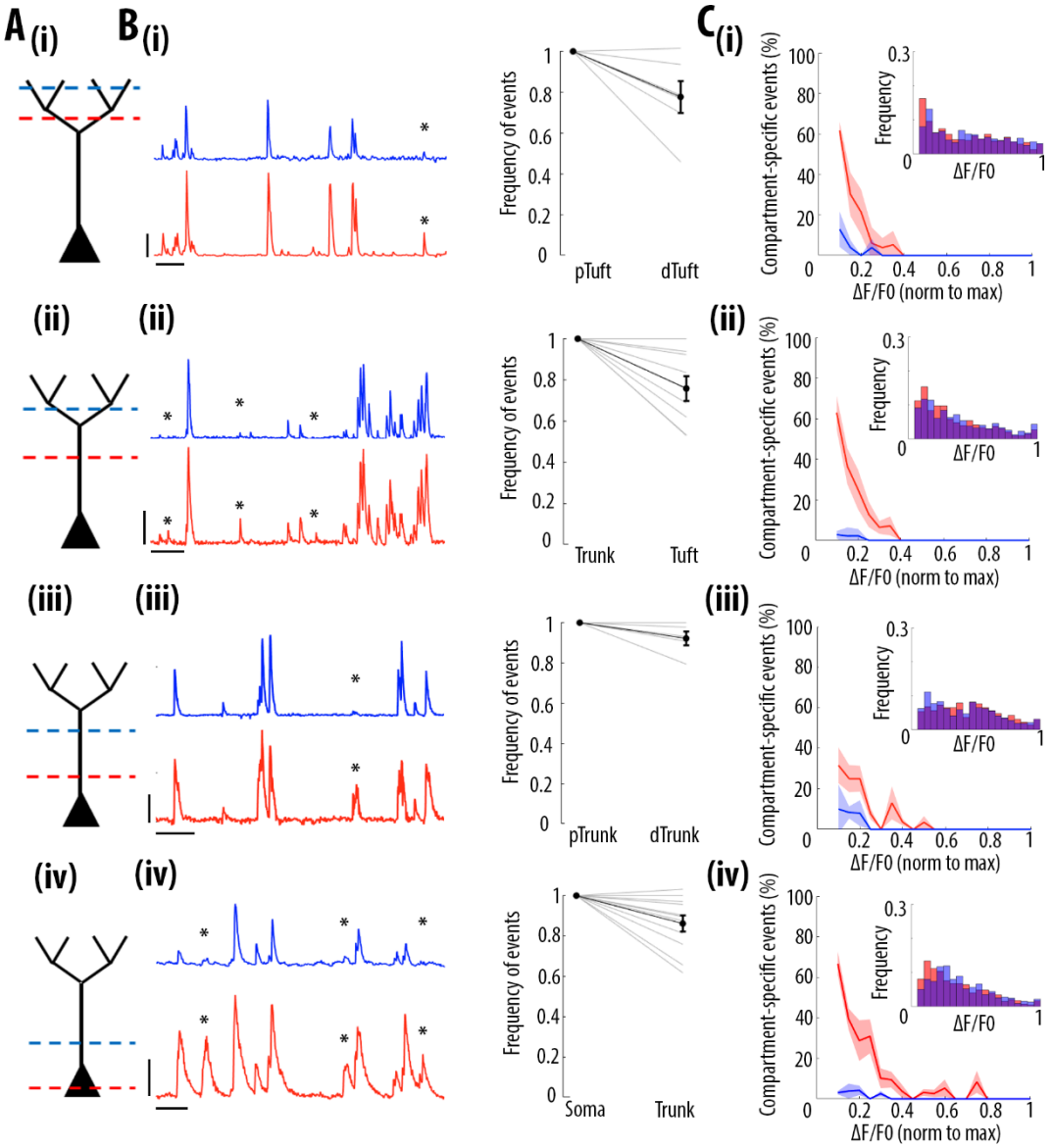

Figure 4.4: *Frequency of calcium transients decreases in a distance and amplitude-dependent dependent manner from the soma to the apical tuft.*

A) Schemata of the neuronal compartments imaged simultaneously in individual layer 5 neurons. B) *Left panel*, representative ΔF/F0 traces of GCaMP6s calcium transients imaged semi-simultaneously in two different compartments as indicated in panel A. Asterisks indicate calcium transients detected in the proximal compartment (red trace) and not detected in the distal one (blue trace). Scale bars 0.25 ΔF/F0 (normalised to max), 20 s. *Right panel*, frequency of detected calcium transients, normalised to the proximal compartment. Individual lines represent individual neurons. Error bar: SEM. C) Proportion of compartment-specific events as a function of calcium transients' amplitude. In red, proportion of events only detected in the proximal compartment. In blue, proportion of events only detected in the distal compartment. Thick line represents the weighted mean proportion. Shaded area represents the weighted sem for each bin (0.05). *Upper right panel*, frequency histogram of calcium transient peak amplitudes detected in the proximal (red) and distal (blue)

compartments. Peak amplitudes were normalized to the maximum amplitude in each compartment. For all compartments, event amplitude, compartment (proximal vs distal) and an interaction between these two factors significantly affected the proportion of compartment-specific events (Two-way ANOVA, pTuft-dTuft (i), $p < 10^{-15}$, $p = 7.8x10^{-5}$, $p = 6.2x10^{-8}$, for event amplitude, proximal versus distal compartment and interaction between amplitude and compartment, respectively, n = 6 pairs; Trunk-Tuft(ii), $p < 10^{-15}$, $p = 3.4x10^{-9}$, $p < 10^{-15}$, n = 9; pTrunk-dTrunk(iii), $p = 1.3x10^{-13}$, $p = 2.4x10^{-4}$, $p = 7x10^{-3}$, n = 5; Soma-Trunk(iv), $p < 10^{-15}$, $p < 10^{-15}$ and $p < 10^{-15}$, n = 11).

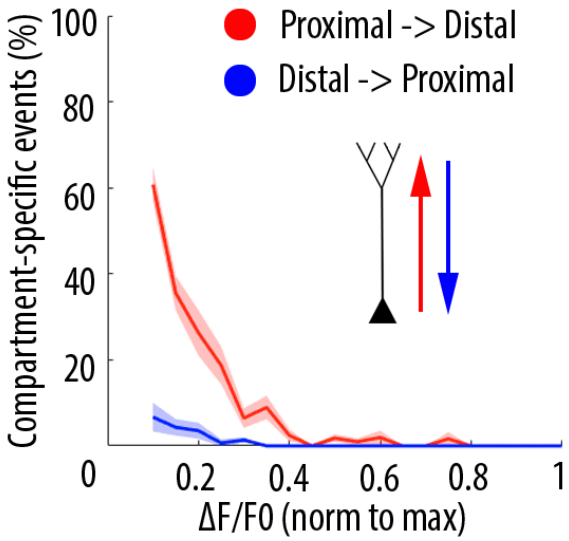

Figure 4.5: *The frequency of calcium transients decreases in a distance and amplitude-dependent manner in the proximal-to-distal direction.*

Mean proportion of compartment-specific calcium transients as a function of calcium transient amplitude (average of data points from figure 4.4 C). In red, the proportion of events only detected in the proximal compartment. In blue, proportion of events only detected in the distal compartment. Thick line and shaded area: weighted mean and sem for each bin (0.05), respectively. Event amplitude, compartment (proximal vs distal) and an interaction between these two factors significantly affected the proportion of compartment-specific events (Two-way ANOVA, $p < 10^{-15}$, $p < 10^{-15}$, $p < 10^{-15}$, n = 31 pairs of compartments from 19 neurons)

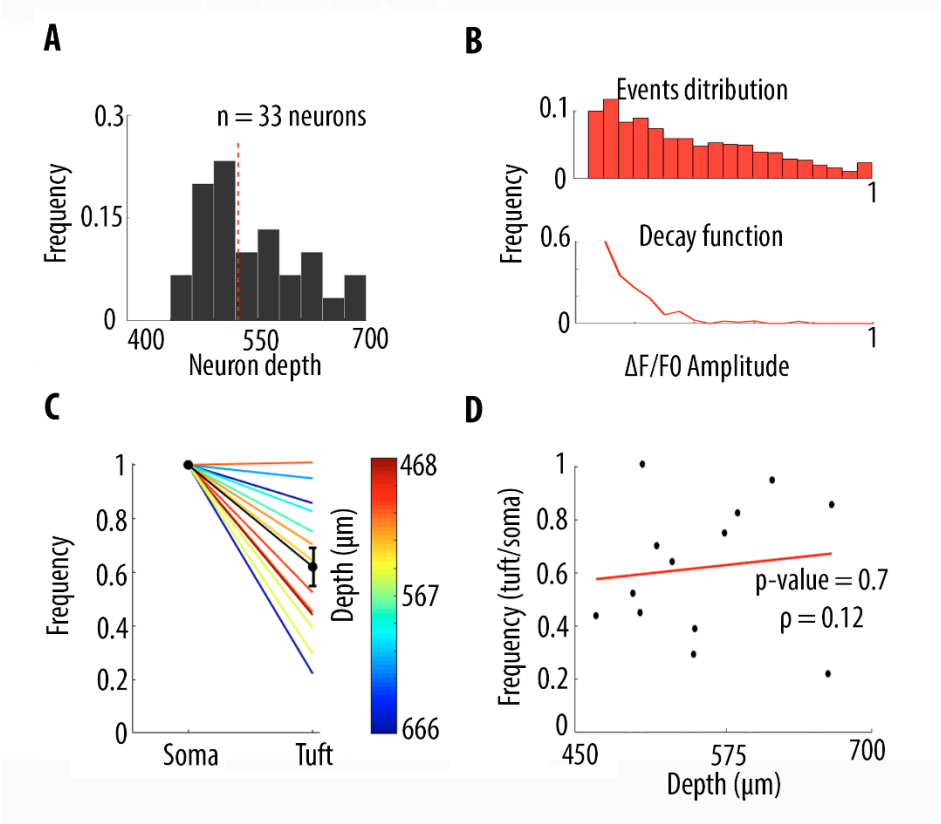

Figure 4.6: *Frequency decrease of calcium transients from soma to apical tuft*

A) Histogram distribution of the depths at which somata from neurons included in this study have been imaged. The red dotted line indicates the median (528 µm from the pia). B) *Upper panel*, the amplitude-dependent attenuation curve (same as in figure 4.5) calculated as the proportion of calcium events which were detected in the proximal compartment and not in the simultaneously imaged distal compartment, as a function of events' amplitude. This curve was calculated for pairs of compartments which were separated by 170 µm in the vertical (z) axis (see Methods). *Lower panel*, frequency histogram of calcium events' amplitude detected in the proximal compartment. Using the proportion of attenuated events and the frequency histogram of events' amplitude, I estimated the proportion of somatic events that fully attenuate as they reach the distal part of the apical tuft as follows: Pairs of compartments were imaged at 170 µm of distance (see Methods). Therefore, the proportion of compartment-specific events (upper panel, same as figure 4.5) represents the attenuation between two planes distanced 170 µm. However, the soma of the neurons I imaged, lays on average, 528 µm below pia (panel A). As such, the attenuation from the soma, to the most distal part of the apical tuft, is going to be 3.1 times (528/170) stronger than the one calculated in the upper panel. Therefore, for each amplitude bin (lower panel), I calculated the proportion of attenuated events (upper panel) multiplied by 3.1. Using this approach, I estimated that the proportion of somatic events that were not detected in the tuft was 39%.

Mathematically, this was calculated as:

$$1 - \sum_{i=1}^{20} P(Ai) \text{ x } P(Bi) \text{ x } 3.1$$

Where *P(Ai)* is the probability of an event at bin *i* to be attenuated (upper panel B) while *P(Bi)* is the probability of having an event of amplitude bin *i* (lower panel B). There are 20 bins in total as each bin is 0.05 in size on a range between 0 and 1 (event size is normalised by the largest event). C) Frequency of detected calcium transients in the apical tuft, normalised to the frequency of transients in the corresponding soma, for neurons in which both compartments were imaged non-simultaneously. Individual lines represent individual neurons (n=13 neurons). The depth of the soma is indicated by the colour scheme indicated by the bar to the side. In black, the mean. Error bar: SEM. D) Scatter plot of the proportion of apical tuft calcium transients normalised to their corresponding soma as a function of soma's depth. In red, the best fit line (least-square method, Pearson's correlation = 0.12, p-value = 0.7)

Because compartment-specific events are of small amplitude, they are also the ones whose detection is more likely to be sensitive to variations in the detection threshold. Therefore, I tested how the selection of different thresholds affected the results.

These results were robust to changes in the threshold (+/- 30%) selected for detecting calcium transients (same as in Figure 3.8). When I used a 30% more permissive threshold for event detection in the proximal compartment, and a 30% more restrictive threshold in the distal compartment, I could still observe an asymmetry in the amplitude-dependent attenuation in the proximal to distal direction (Figure 4.7). The results were also robust to the time window that was used to detect simultaneous events in different compartments (Figure 4.8).

Altogether, these results indicate calcium transients are highly correlated throughout the different compartments of a single layer 5 pyramidal neurons and that low frequency action potentials are responsible for the somato-dendritic attenuation observed in the data. Thus, somato-dendritic coupling in layer 5 pyramidal neurons in V1 is strong, but asymmetric.

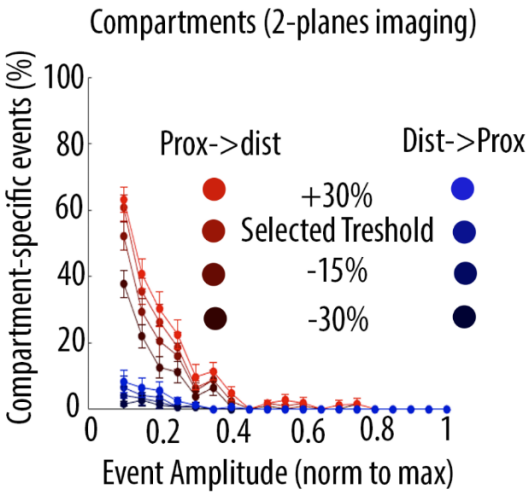

Figure 4.7: *The amplitude-dependent attenuation function is robust to variations in detection threshold.*

Proportion and amplitude of compartment-specific events detected as a function of the amplitude and threshold selected.

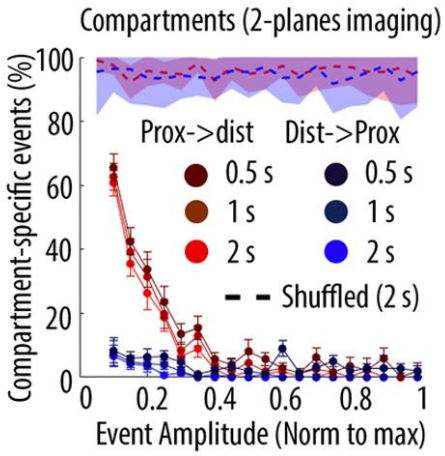

Figure 4.8: *The amplitude-dependent attenuation function is robust to changes in the coincident window size*

Proportion of compartment-specific events as a function of calcium transients' amplitude using different time windows (0.5s, 1s and 2s) to define coincidence. The dashed line represents the proportion of compartment-specific events obtained from shuffled ΔF/F0 signals, with the selected time window (2 s).

4.3.4 The majority of calcium events detected as branch-specific in the apical tuft are also detected in the trunk

Given the observation that most of the dendritic events found in the distal compartment were also found proximally, I reasoned that it was possible that branch-specific events may not necessarily be generated in the tuft, rather, they could be the result of asymmetric attenuation from back-propagating signals (Spruston *et al.*, 1995; Boivin and Nedivi, 2018). Calcium transients might be detected as branch-specific in single plane imaging, due to a lack of imaging data coming from more proximal compartments or out-of-field dendritic branches. To test this hypothesis, I first calculated the proportion of branch-specific signals, for each pair of branches, then, for all detected branch-specific event, I calculated the proportion of these events which were also detected in the trunk. On average, I found that 60% of the events detected as branch-specific were also found in the trunk (Figure 4.9).

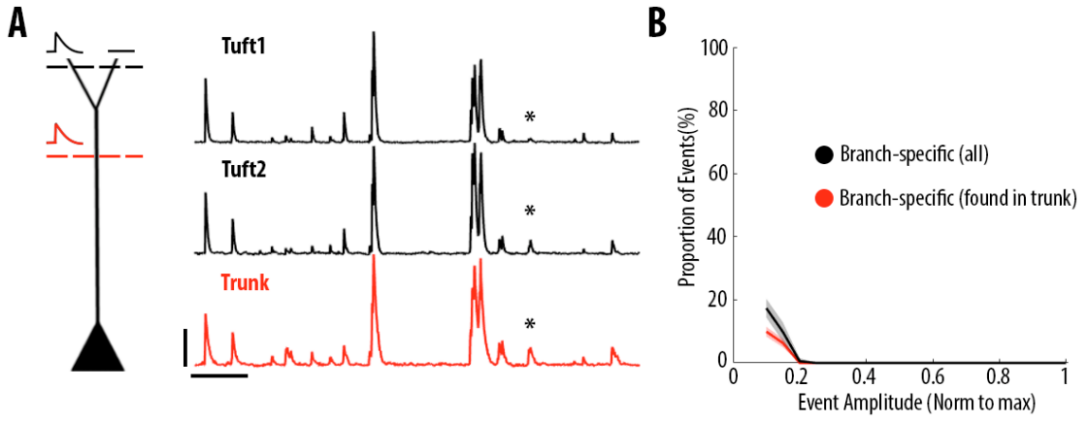

Figure 4.9: *The majority of dendritic calcium events detected as branch-specific in the apical tuft are also detected in the trunk.*

A) Example ΔF/F0 traces of GCaMP6s calcium transients imaged semi-simultaneously in the trunk (red) and in two sibling apical tuft branches (black) of an individual layer 5 neuron. The asterisks indicate a calcium transient that was detected only in one of the two apical tuft branches (tuft 2) and thus classified as a branch-specific event. This transient was also detected in the trunk of the same neuron. Scale bars 0.25 ΔF/F0 (normalised to max), 20 s. B) Proportion of apical tuft dendritic branch-specific events, as a function of GCaMP6s

calcium transient amplitude. Black, all apical tuft dendrites events detected as branch-specific. Red, proportion of branch-specific events which were also simultaneously detected in the corresponding trunk. On average, 60% of branch-specific events were also found in the trunk (n = 9 Trunk-Tuft pairs).

4.3.5 Locomotion and visual stimulation do not alter the relationship between somatic and dendritic calcium transients in layer 5 pyramidal neurons

Next, I tested whether visual stimulation, locomotion or behavioural state transitions (Vinck *et al.*, 2015) altered the coupling between the different compartments of individual layer 5 neurons. For each condition, I plotted the percentage of compartment-specific calcium transients as a function of their amplitude (Same as in Figure 4.5). I found that in all four conditions, compartment-specific events were dominated by small amplitude calcium transients in proximal compartments and that there was no significant difference between darkness and visual stimulation periods, both during stationary and locomotion periods (Figure 4.10; Three-way ANOVA, $p = 0.69$, $p = 0.21$ and $p = 0.64$ for visual stimulation, locomotion, and interaction respectively; $p < 10^{-15}$ for event amplitude; no other interaction was found to be statistically significant). Similarly, I found no significant difference between behavioural states defined by stationary, locomotion and transition periods from still to running activity (see methods), during both visual stimulation and darkness (Figure 4.11). These results indicate that the attenuation of events in an amplitude-dependent manner remained unchanged during visual stimulation and behavioural-state transitions.

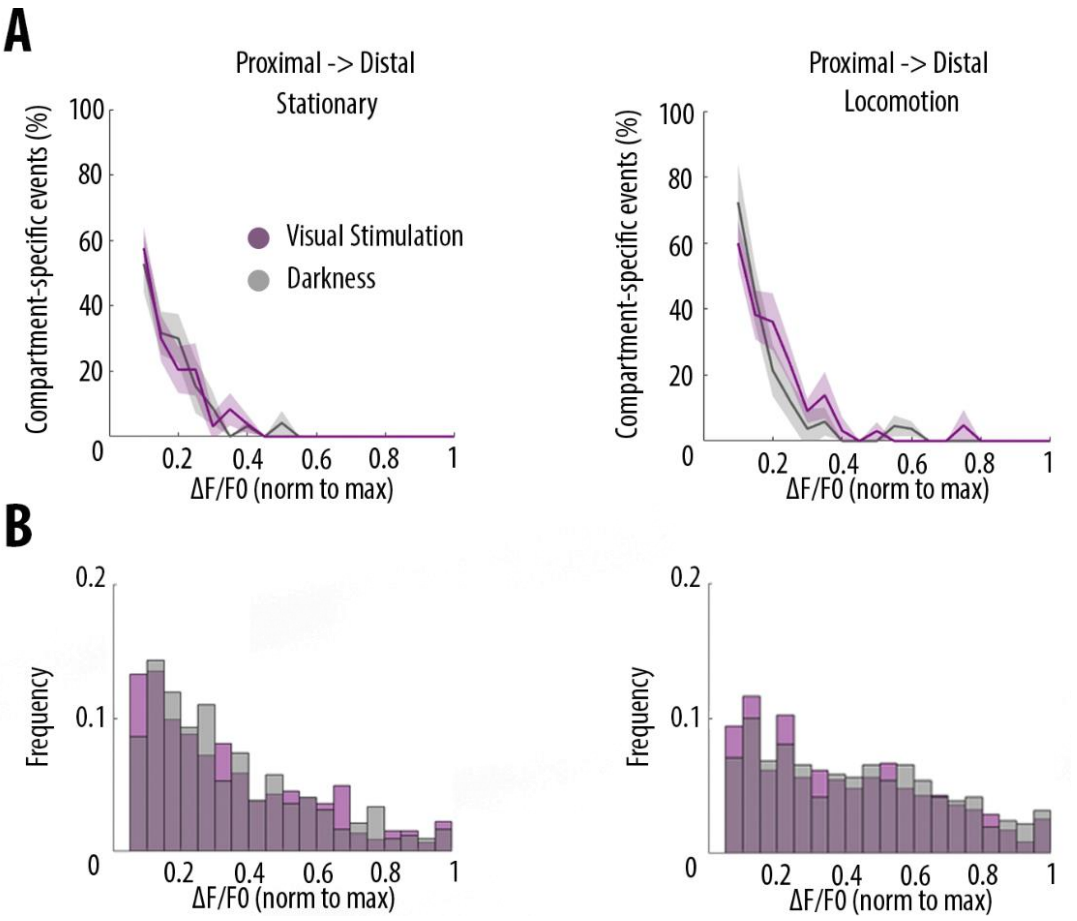

Figure 4.10: *Locomotion and visual stimulation do not alter the distance and amplitude-dependent attenuation function of calcium events from soma to apical tuft*

A) Proportion of compartment-specific events detected in the proximal compartment and not in the distal one, as a function of calcium transient amplitude, during periods of darkness (grey) and visual stimulation with drifting gratings (purple), while the animals were either stationary (left panel) or running (right panel). Neither visual stimulation nor locomotion altered the function relating calcium transients' amplitude with the proportion of compartment-specific events (Three-way ANOVA, $p = 0.69$, $p = 0.21$ and $p = 0.64$ for visual stimulation, locomotion, and interaction respectively. $p < 10^{-15}$ for event amplitude. No other interaction was found to be statistically significant). B) Frequency histogram of calcium transient peak amplitudes detected in proximal compartments during darkness (grey) and visual stimulation (purple). All transients are normalised to the largest transient for each compartment.

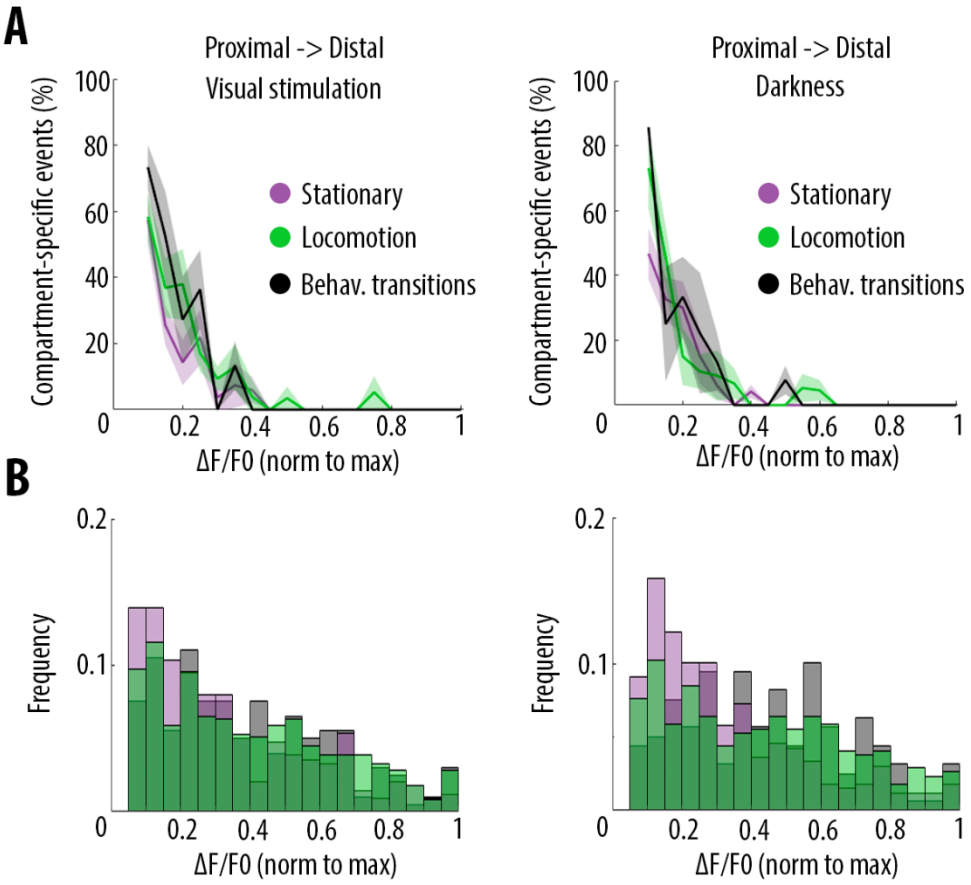

Figure 4.11: *Behavioural-state transitions do not alter the distance and amplitude-dependent attenuation function of calcium events from soma to apical tuft*

A) Proportion of compartment-specific events detected in the proximal compartment and not in the distal one, as a function of calcium transient amplitude, during periods of visual stimulation (left panel) and darkness (right panel), while the animals were either stationary (pink), running (green) or in transition between stationary and running (black). Periods of transition were excluded from stationary and locomotion periods. No significant difference was found between any condition (Three-way ANOVA, $p = 0.32$, $p = 0.42$ and $p = 0.64$ for visual stimulation, behavioural state, and interaction respectively; $p < 10\text{-}15$ for event amplitude; no other interaction was found to be statistically significant, $n = 31$ pairs of compartments from 19 neurons). B) Frequency histogram of calcium transient peak amplitudes detected in proximal compartments during stationary (purple), locomotion (green) and behavioural transitions (black) during either visual stimulation or darkness. All transients are normalised to the largest transient for each compartment.

Because smaller events are more likely to be attenuated from one compartment to the next (Figure 4.5), it is predicted that neurons with the largest amplitude somatic events will be the ones with highest somato-dendritic coupling. Indeed, the results confirmed that neurons with larger amplitude events in the proximal compartments, were the ones with higher proportion of coincident events between different compartments (Figure 4.12A, Pearson's ρ = 0.49, p-value = 0.03. n = 19 neurons). On the other hand, there was no correlation between the amount of paired somato-dendritic events and the frequency of events (Figure 4.12B, Pearson's ρ = -0.02, p-value = 0.94. n = 19 neurons).

Therefore, I quantified whether the proportion of coincident events between the proximal and distal compartments was altered during visual stimulation or locomotion. As it was shown in Figure 4.10 and 4.11, locomotion and visual stimulation tend to increase the amplitude of calcium transients. Despite a trend consistent with the distribution of events' amplitude shown in Figure 4.10 and 4.11, the results show that the proportion of coincident events was not significantly affected by visual stimulation and locomotion (Figure 4.13A, Repeated Measures Two-way ANOVA on log-transformed data, p = 0.43, p = 0.29 and p = 0.35 for visual stimulation, locomotion and interaction effects, respectively). Similarly, the number of paired events was not affected by behavioural transitions (Figure 4.13B, Two-way ANOVA on log-transformed data, p = 0.93, p = 0.87 and p = 0.51 for visual stimulation, behavioural state and interaction effects, respectively). Altogether these results show that the coupling between somatic and dendritic activity remain unchanged during visual stimulation, locomotion and behavioural transitions.

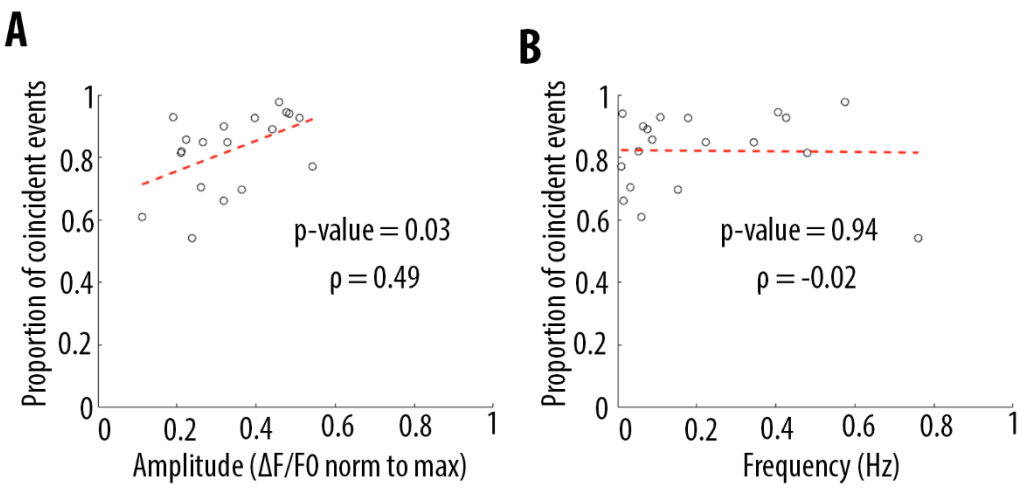

Figure 4.12: *The proportion of coincident events between proximal and distal neuronal compartments correlates with events' amplitude but not frequency*

A) Proportion of coincident events found between pairs of neuronal compartments as a function of event amplitude (ΔF/F0, normalised to max) (n = 19 neurons). There is a statistically significant correlation between the proportion of paired events and the mean amplitude of these events (p = 0.03, r^2 = 0.49, n = 19 neurons) B) Mean proportion of coincident events found between pairs of neuronal compartments as a function of event frequency (Hz). No correlation is found between event frequency (Hz) and the proportion of coincident events found between pairs of neuronal compartments (p-value = 0.94, ρ = -0.02, n = 19 neurons). Red dotted lines in A and B indicates the best fit line (least-square method).

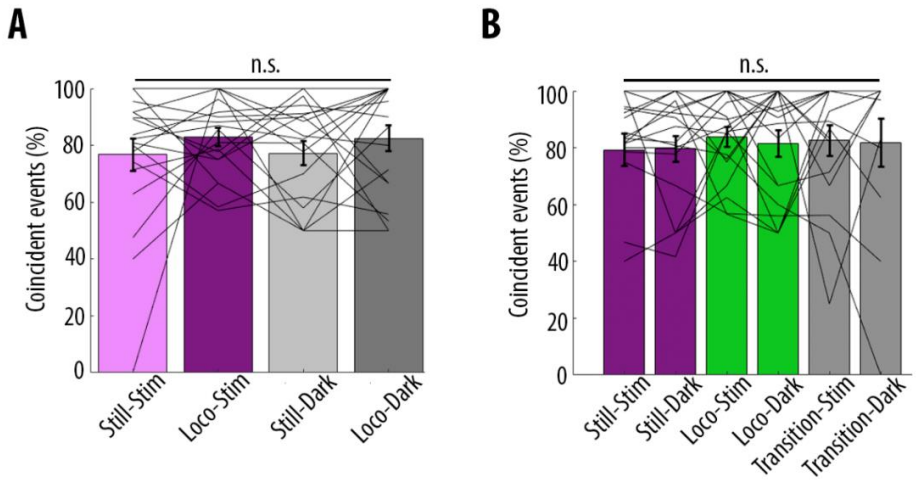

Figure 4.13: *Visual stimulation and locomotion do not alter the proportion of paired calcium events between pairs of compartments from soma to the apical tuft*

A) The proportion of coincident events across the four different conditions: visual stimulation (stim), darkness (dark), stationary (still), locomotion (loco). Locomotion shows a non-significant tendency to increase the proportion of coincident events between different neuronal compartments (Repeated Measures Two-way ANOVA on log-transformed data, p = 0.43, p = 0.29 and p = 0.35 for visual stimulation, locomotion and interaction effects, respectively, n = 19 neurons). B) Proportion of coincident calcium transients in proximal and distal compartments imaged semi-simultaneously including transitions between stationary and locomotion (transition) periods. No significant difference was found across conditions (Two-way ANOVA on log-transformed data, p = 0.93, p = 0.87 and p = 0.51 for visual stimulation, behavioural state and interaction effects, respectively, n= 19 neurons)

Investigating the probability with which calcium events attenuate from one compartment to the next, quantifies whether an event was detected in the nearby compartment. However, this type of analysis is not informative about the relationship between the amplitudes of calcium transients across compartments. Indeed, even though smaller events are attenuated with similar probabilities across the four conditions, propagating calcium transients may be actively amplified or attenuated in a condition-dependent manner as suggested by the existence of large calcium transients that were not detected in the distal compartments (see example traces and the quantification of compartment-specific events in for ΔF/F0>0.3 in Figure 4.4)

To capture these nonlinearities, I estimated the amplitude of each detected transient in each compartment and calculated a residual value as the distance from the linear robust regression fit (Figure 4.14). If events were amplified in a condition-specific manner, these events will be above the robust regression fit, and therefore have higher residual values

compared to the condition that propagated less efficiently. I then plotted the cumulative distribution of the residual value for every calcium transient in all 4 pairs of imaged compartments from soma to apical tuft (Figure 4.15). I found that, on average, the non-linear changes in calcium transient amplitude across neuronal compartments were neither significantly affected by locomotion nor by visual stimulation nor in a compartment-specific way (Figure 4.15, Three-way ANOVA, p = 0.96, p = 0.23 and p = 0.91 for visual stimulation, locomotion and interaction effect, respectively; p = 0.86 for different compartments; no other interaction effect was found to be significant; n = 11 Soma–Trunk pairs; n = 5 pTrunk–dTrunk; n = 9 Trunk–Tuft; n = 6 pTuft-dTuft from 19 neurons).The same held true when I tested behavioural transitions (Figure 4.16, Three-way ANOVA, p = 0.66, p = 0.16 and p = 0.91 for visual stimulation, behavioural state and interaction effect, respectively. p = 0.44 for different compartments. No other interaction effect was found to be significant. n = 31 compartments (n = 11 Soma–Trunk; n = 5 pTrunk–dTrunk; n = 9 Trunk–Tuft; n = 6 pTuft-dTuft) from 19 neurons). These results indicate that the relationship between the amplitude of calcium transients across compartments remains unchanged and that events of similar amplitudes are propagated with similar efficiency, independently of visual stimulation, locomotion behavioural transitions and compartments.

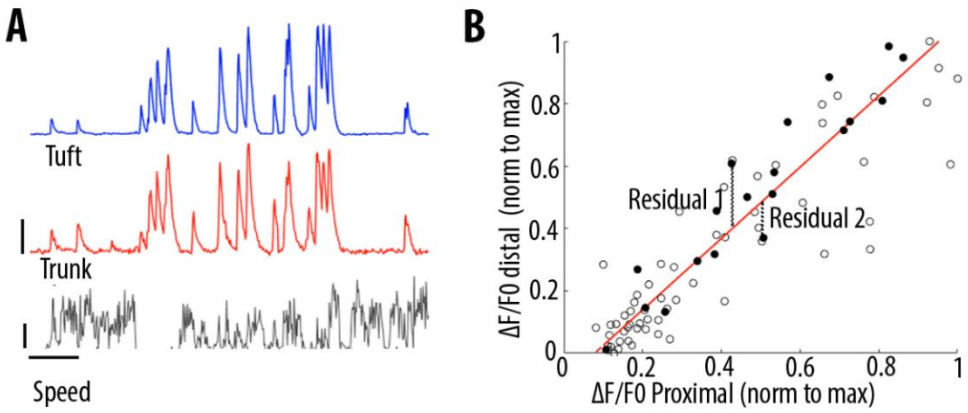

Figure 4.14: *Estimating nonlinearities between calcium transients' amplitude across neuronal compartments.*

A) Example traces of a proximal (trunk, red) and distal (tuft, blue) compartment imaged semi-simultaneously, during stationary and locomotion periods (black trace, speed). Scale bars, 0.25 ΔF/F0 (normalised to max), 12 cm/s, 20 s. B) Example of scatter plot of calcium transients' peak amplitudes imaged in a pair of neuronal compartments (trunk-tuft). Each dot represents an individual calcium transient. Filled dots correspond to the transients shown in the upper panel. The red line represents the robust linear regression fit. For each transient in each condition (visual stimulation, darkness, stationary and locomotion) a residual from the robust linear regression was calculated.

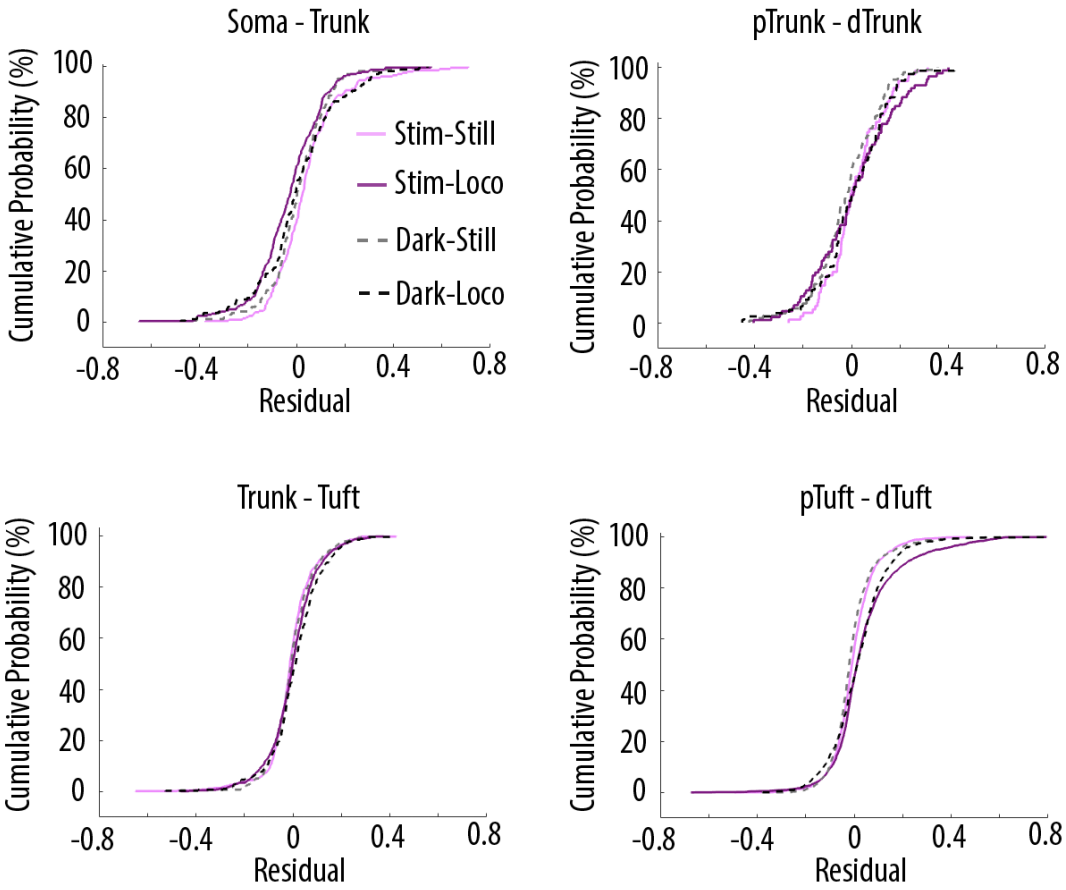

Figure 4.15: *Changes in amplitude of calcium transients across neuronal compartments does not depend on either visual stimulation or locomotion*

Cumulative distributions of the residuals calculated for each pair of compartments and for each condition: visual stimulation (pink, stim), darkness (grey, dark), stationary (still) and locomotion (loco) periods. No significant difference was found between any condition: Three-way ANOVA, p = 0.96, p = 0.23 and p = 0.91 for visual stimulation, locomotion and interaction effect, respectively; p = 0.86 for different neuronal compartments No other interaction effect was found to be significant. n = 31 compartments (n = 11 Soma-Trunk; n = 5 pTrunk–dTrunk; n = 9 Trunk– Tuft; n = 6 pTuft-dTuft from 19 neurons).

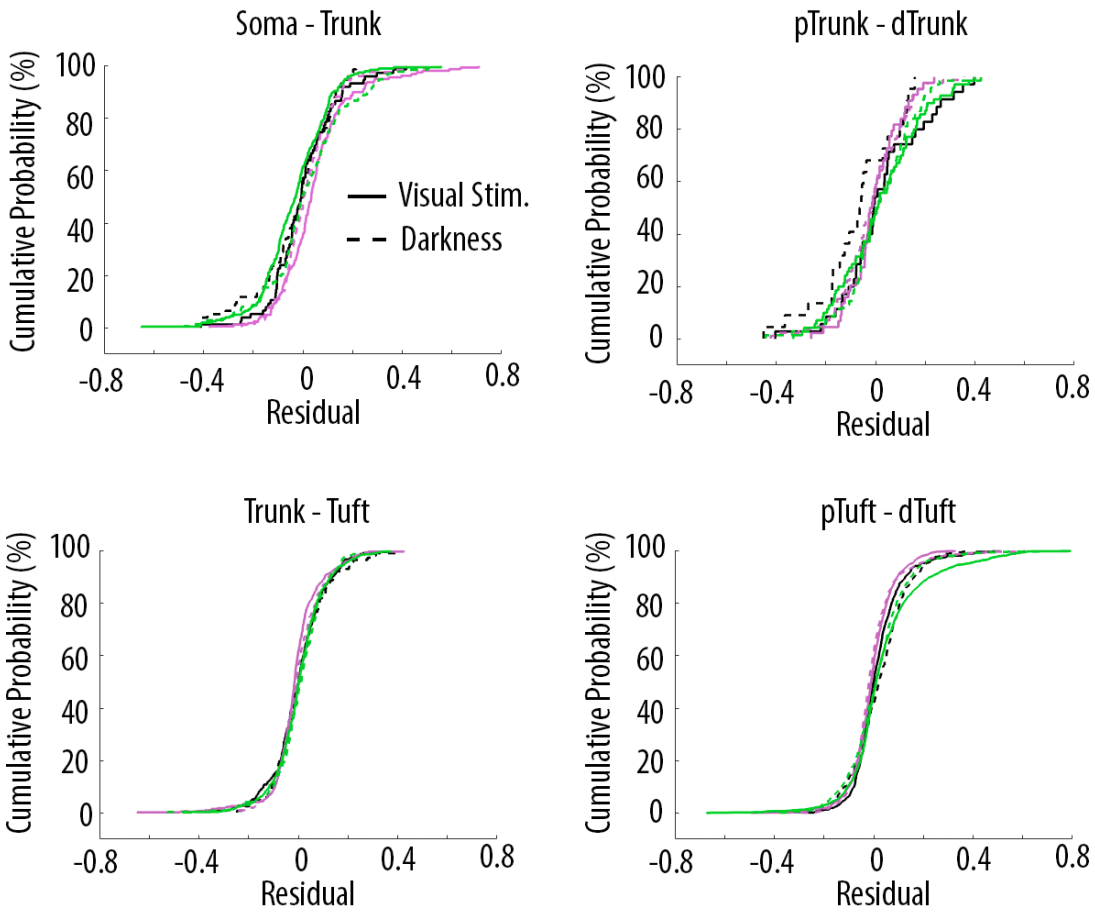

Figure 4.16: *Changes in amplitude of calcium transients across neuronal compartments does not depend on behavioural state transitions.*

Cumulative distributions of the residuals calculated for each pair of compartments and for each condition: stationary (purple), locomotion (green) and behavioural state transitions (black). No significant difference was found between any condition: Three-way ANOVA, p = 0.66, p = 0.16 and p = 0.91 for visual stimulation, behavioural state and interaction effect, respectively. p = 0.44 for different compartments. No other interaction effect was found to be significant. n = 31 compartments (n = 11 Soma–Trunk; n = 5 pTrunk–dTrunk; n = 9 Trunk–Tuft; n = 6 pTuft-dTuft) from 19 neurons

4.3.6 Orientation selectivity does not alter the relationship between somatic and dendritic calcium transients in layer 5 pyramidal neurons

Local dendritic spikes have been shown to increase orientation selectivity in the soma (Smith *et al.*, 2013). As a consequence, it is expected that neurons with the higher OSI, would also be the ones with lower correlations in their tuft dendrites. Therefore, I tested whether there is a correlation between orientation selectivity at the soma and the coupling of calcium events between soma and apical tuft dendrites. The results show that there was no statistically significant correlation between somatic orientation selectivity index (OSI, see methods) and the apical tuft correlation of calcium signals ($r^2 = 0.09$, $p = 0.67$, Figure 4.17D). I then wanted to test whether the orientation selectivity in the soma differed from that in the dendrites. To do so, I compared orientation selective responses during stationary and locomotion periods both in the apical tuft branches and in their corresponding soma (n=15 neurons) (Figure 4.18). I found that locomotion similarly increased calcium transient amplitudes both in apical tuft and soma, without a significant difference between compartments (Figure 4.19A, Paired t-test, $p = 0.38$), both during the presentation of preferred and non-preferred orientations (Figure 4.19B, Repeated measures Two-way ANOVA on log-transformed data, $p = 0.07$, 0.71 and 0.28 for stimulus-type, compartment and interaction effects respectively). As a consequence, the OSI of somatic and apical tuft responses remained unchanged during both stationary and locomotion periods (Figure 4.19C, Repeated measures Two-way ANOVA, $p = 0.49$, $p = 0.42$ and $p = 0.45$, for the effects of locomotion, neuronal compartment and interaction, respectively). Altogether, these results suggest that the response properties to oriented gratings are similar in the soma and in the apical tuft, during stationary and locomotion periods.

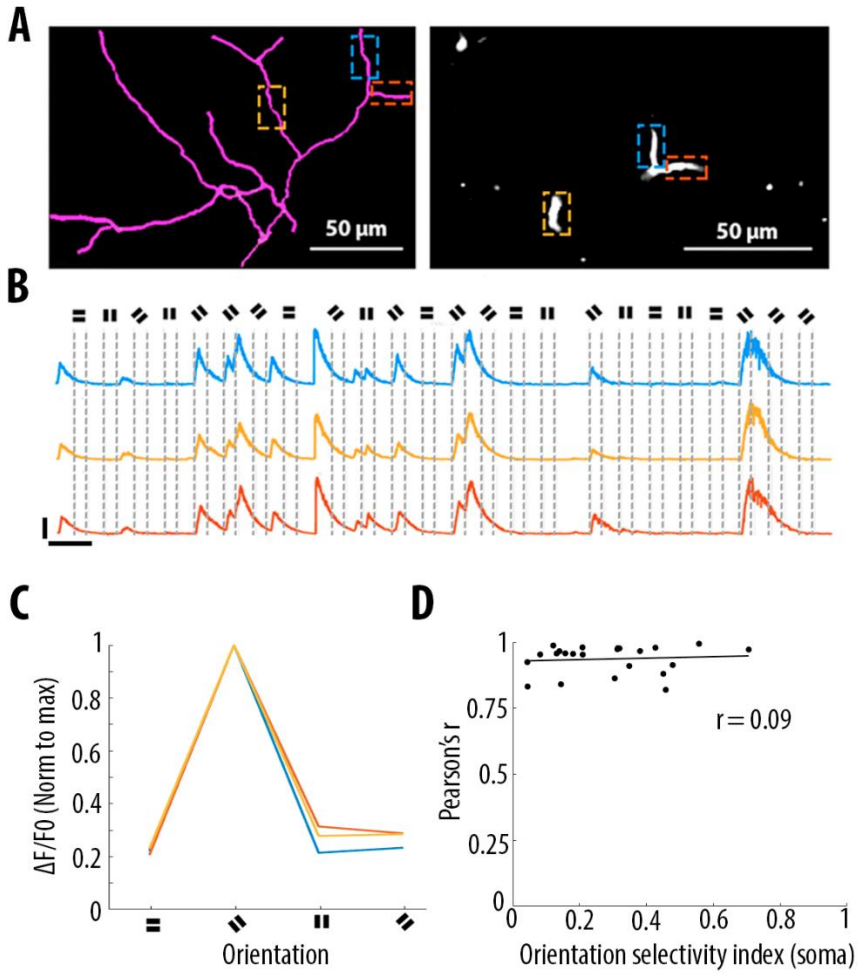

Figure 4.17: *High correlation of calcium transients in apical tuft dendrites, independent of somatic orientation selectivity.*

A) Morphological reconstruction (left) and two-photon image (right) of apical tuft branches that were imaged during the presentation of drifting gratings. B) Example calcium transients from the dendritic branches indicated by coloured dashed lines in panel A, during the presentation of drifting gratings of four different orientations. Scale bars 0.3 ΔF/F0 (normalised to max), 10 s. C) Tuning curve showing calcium transients amplitudes in response to the 4 grating orientations (average of 24 presentations of each grating, normalised to max), from the 3 branches indicated by coloured dashed lines in panel A. D) Mean Pearson's correlation value of all imaged tuft dendritic branches per neuron, as a function of the orientation selectivity of the corresponding soma (each dot corresponds to one neuron; $r^2 = 0.09$, $p = 0.67$, $n = 23$ neurons). The straight black line represents the best fit line (least square).

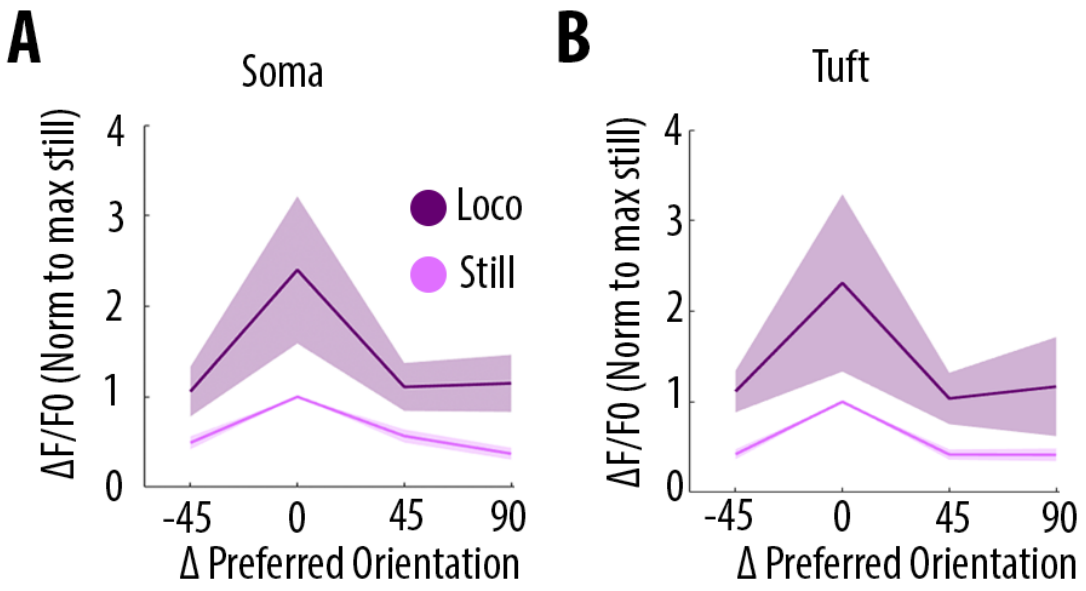

Figure 4.18*: Locomotion increases somatic and apical tuft responses to drifting gratings without altering their preferred orientation*

A) Tuning curve of somatic calcium signals from orientation selective neurons (somatic OSI > 0.3; n= 15 neurons) during stationary (still, pink) and locomotion (loco, purple) periods. Responses are normalised to the preferred orientation during stationary periods. Thick line and shaded area represent the mean and SEM, respectively. B) Same as E, for the corresponding apical tuft branches of the same neurons. For each neuron, responses from all imaged apical tuft branches were averaged (n = 15 neurons from 68 apical tuft branches from 15 neurons)

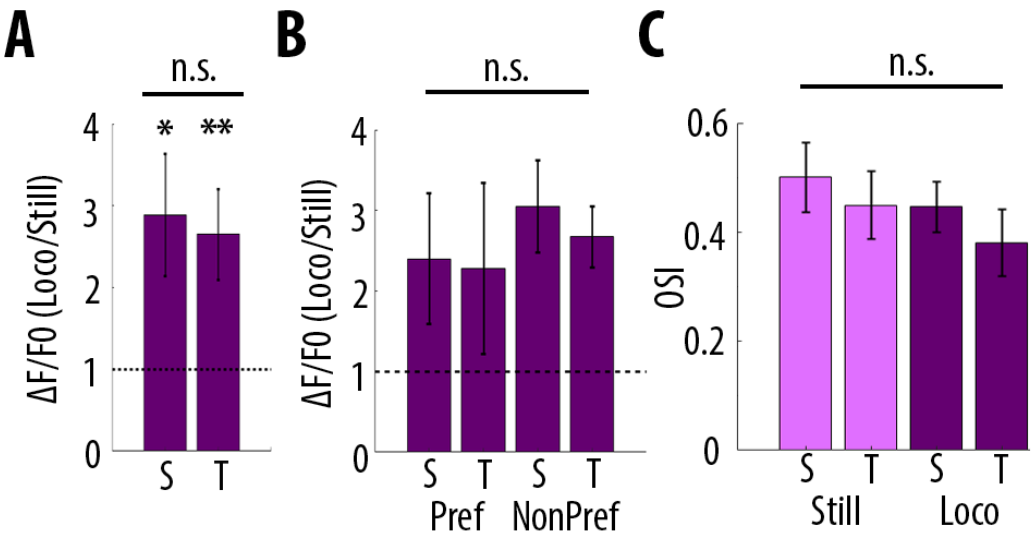

Figure 4.19*: Orientation selectivity remains unchanged between the soma and the apical tuft during both stationary and locomotion periods.*

A) Relative increase in calcium transient amplitudes during locomotion compared to stationary periods both in soma (S) and in corresponding apical tuft dendrites (T), during drifting grating presentations. Locomotion significantly increases the responses to drifting gratings both in soma and corresponding apical tuft dendrites (Repeated Measures Two-way ANOVA on log transformed data, p = 0.02 and p = 0.008 for the effect of locomotion on soma and tuft responses, respectively, n = 15 neurons) without a significant difference between compartments (Paired t-test, p = 0.38; mean (normalised to stationary) = 2.89 and 2.65, sem = 0.74 and 0.56; n = 15 soma and 15 apical tufts including 68 branches). B) Same as G for responses to the preferred (Pref) and non-preferred (NonPref) orientations (Repeated measures Two-way ANOVA on log-transformed data, p = 0.07, 0.71 and 0.28 for orientation, compartment and interaction effects respectively; mean = 2.4 and 2.28, sem = 0.81 and 1.06 for soma and apical tuft at the preferred orientation; mean = 3.05 and 2.67, sem = 0.57 and 0.38 for soma and apical tuft at the non-preferred orientation; n = 15 soma and 15 apical tufts). C) Orientation selectivity index was not significantly different between somatic and corresponding tuft dendrites responses, both during stationary (still) and locomotion (loco) periods (Repeated measures Two-way ANOVA, p = 0.49, p = 0.42 and p = 0.45, for the effects of locomotion, neuronal compartment (soma vs tuft) and interaction, respectively; mean = 0.5; 0.45, sem = 0.06, 0.06 for soma and apical tuft during stationary and mean = 0.45; 0.38, sem = 0.05, 0.06 for soma and apical tuft during locomotion, respectively; n = 15 soma and 15 apical tuft including 68 branches)

In line with these results, I found that the preferred orientation was similar throughout tuft dendritic branches and neuronal compartments of individual neurons, both during stationary and locomotion periods (Figure 4.20). Finally, the Pearson's correlation between apical tuft branches calcium signals and across neuronal compartments remained high and unchanged regardless of the grating's orientation (Figure 4.21).

Altogether, these results indicate that calcium signals in individual layer 5 pyramidal neurons are highly correlated throughout apical tuft branches and neuronal compartments, and that this high somato-dendritic coupling remains unchanged during the presentation of different visual stimuli.

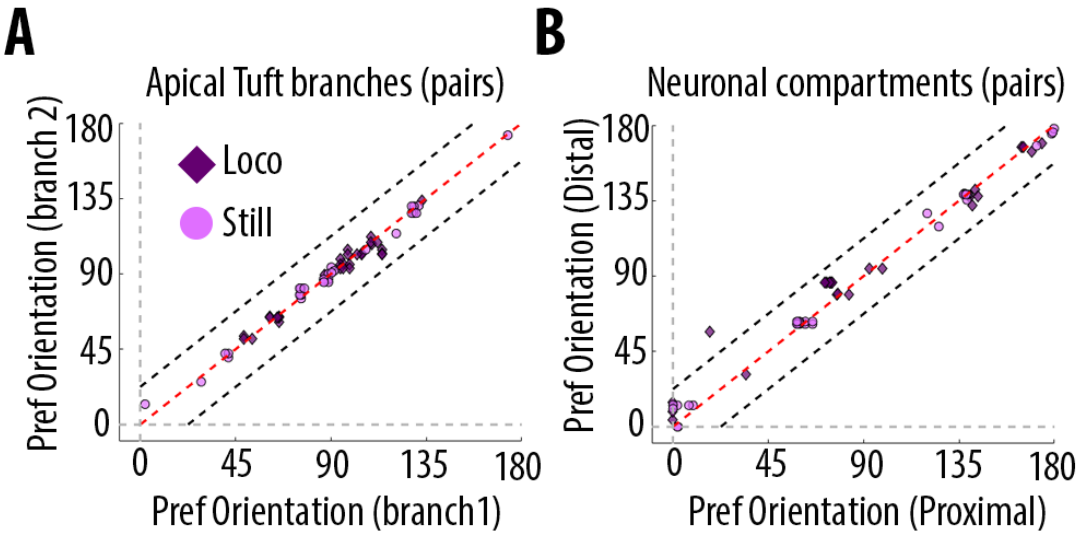

Figure 4.20: *Pairs of orientation selective branches and neuronal compartments are tuned to the same preferred orientation both during stationary and during locomotion periods*

A) Scatter plot of the preferred orientation in pairs of apical tuft branches belonging to the same neuron and imaged simultaneously, during stationary (pink circles) and locomotion (purple diamonds) periods (n = 31 pairs). Dashed red line: identity line; Dashed black lines: identity +/- 22.5 degrees in vectoral space. B) Same as J for pairs of neuronal compartments imaged simultaneously. n = 33 pairs

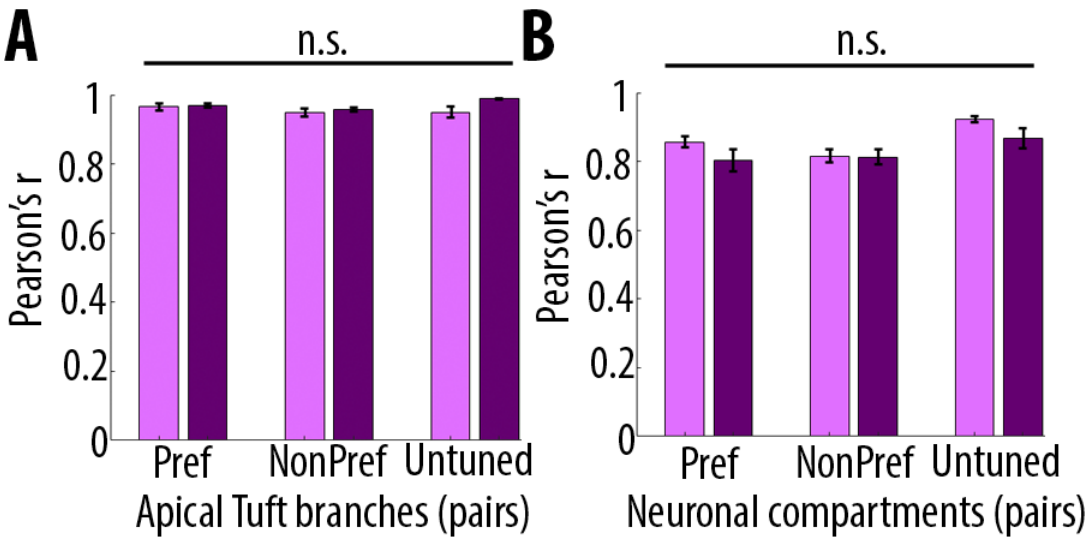

Figure 4.21: *The activity of pairs of branches and neuronal compartments are highly correlated regardless of the stimulus type and locomotion*

Pearson's correlation of calcium transients between pairs of apical tuft branches belonging to the same orientation-selective neuron, during the presentation of the preferred (Pref) and non-preferred (NonPref) grating orientations, both during stationary (pink) and locomotion (purple) periods (n = 31 pairs). Correlation values from branches belonging to non-selective neurons (OSI < 0.3, untuned), during the presentation of all oriented gratings, are shown on the right columns (n= 10 pairs). Neither gratings orientation nor locomotion significantly affected the correlation between pairs of branches (Two-way ANOVA, p = 0.20, p = 0.07 and 0.38 for orientation, locomotion and interaction effect, respectively). **M**) Same as L, for different neuronal compartments (Two-way ANOVA, p = 0.27, p = 0.09 and 0.43 for orientation, locomotion and interaction effect, respectively; n = 33 pairs for Pref, NonPref and 36 pairs for untuned). Error bars: SEM.

4.4. Discussion

4.4.1 The asymmetric coupling between somatic and dendritic calcium signals

In accordance with a recent study (Beaulieu-Laroche *et al.*, 2019), these results show that calcium signals in individual layer 5 pyramidal neurons in V1 are strongly correlated (Pearson's correlation = 0.84, on average) throughout all neuronal compartments (Soma-Trunk-Tuft). Despite this strong correlation however, the results also show that the frequency of calcium transients in the apical tuft is approximately 60% of the frequency of calcium transients in the soma, creating an asymmetry in the coupling between somatic and apical dendritic calcium signals.

Previous studies have shown that dendritic signals attenuate in a distance-dependent manner *in vivo*, suggesting that at least some of the calcium events generated in one compartment would fully attenuate as they reach the next compartment (Stuart, Schiller and Sakmann, 1997; Svoboda *et al.*, 1997; Helmchen *et al.*, 1999; Vetter, Roth and Häusser, 2001; Waters *et al.*, 2003; Larkum *et al.*, 2009). To estimate the lower bound proportion of calcium events generated in the tuft and in the soma, I investigated the proportion of attenuated events in both the somatofugal and somatopetal directions. The results show that while around 40% of somatic calcium transients decay by the time they reach the apical tuft, only 1.4% of apical tuft calcium events were not associated with somatic events (Figure 4.5). These results differ with the results of Beaulieu-Laroche *et al.* (2019) that reported that 83.9 % (median) of dendritic calcium signal (rise events) were paired with events in the soma while 73.4% of somatic events were paired with dendritic ones. This discrepancy may be explained by differences in imaging conditions including a denser labelling, which increases the amount of background signals, and the use of GCaMP6f. Compared to GCaMP6s which was used in this study, GCaMP6f has a lower signal amplitude and signal-to-noise ratio specifically in the soma leading to a lower probability of detecting low-frequency firing in layer 5 neurons (see appendix 1 of this thesis or (Francioni, Padamsey and Rochefort, 2019)). The distance-dependent attenuation is therefore most likely due to low-frequency trains of action potentials that do not trigger dendritic electrogenesis into the apical part of the of the dendritic compartments of layer 5 neurons (Larkum and Zhu, 2002). In line with these findings, my results demonstrate that the distance-dependent reduction in the frequency of calcium transients results from the attenuation of small-amplitude events, from the soma to the apical tuft, consistently throughout compartments. Notably, very rarely calcium transients were found in the distal apical tuft and attenuated toward the soma, and as a

consequence, calcium transients generated in the distal part of the dendrites were virtually always found in coincidence with somatic calcium signals. This observation is consistent with two non-mutually exclusive interpretations: (1) The generation of dendritic spikes in the apical tuft systematically leads to the generation of somatic action potentials or (2) Dendritic spikes are generated by high-frequency bAPs. Somato-dendritic coupling could in principle also be observed with lower frequency back propagating action potentials, provided they are paired with tuft inputs (Major, Larkum and Schiller, 2013; Manita *et al.*, 2015). Despite a higher sensitivity than GCaMP6f, GCaMP6s cannot detect single action potentials in layer 5 neurons (Francioni, Padamsey and Rochefort, 2019). This suggests that somatofugal attenuation might be underestimated in this study. Similarly, it is possible that in the rare instances in which I detect dendritic activity in the absence of somatic activity, low frequency somatic calcium signals were not detected in these conditions. Finally, because the attenuation of events of similar amplitudes is probabilistic (Figure 4.5), I cannot exclude that the process may also be affected by active inhibitory mechanisms along the somato-dendritic axis (Larkum, Kaiser and Sakmann, 1999; Palmer *et al.*, 2012; Pérez-Garci, Larkum and Nevian, 2013; Naka and Adesnik, 2016; Boivin and Nedivi, 2018)

4.4.2 Branch-specific activity: Dendritically-generated or asymmetric bAP invasion?

In line with the observation that most events in the distal part of the apical tuft are already detected in the proximal part of the neuron, among the rare instances in which branch-specific calcium transients were detected, 60% of them were also detected in the trunk. These results suggest that single-plane imaging may lead to the incorrect classification of events as branch-specific, due to a lack of spatial resolution required to detect the same calcium signal also in another compartment or branch. In the apical tuft of layer 5 neurons of the motor cortex, Cichon and Gan (2015) reported that apical tuft branches of a single neuron, responded selectively to either forward or backward running and that selectivity decreases in the distal-to-proximal direction with the soma being the least selective compartment (Cichon and Gan 2015). However, the authors only image one plane at the time, and as a consequence, it is not possible to determine whether branch-specific events are the result of: (1) Task-selective activity in different branches of the apical tuft which is summed up in a promiscuous fashion in the soma, or (2) Promiscuous responses in the soma that backpropagate to non-overlapping subset of apical tuft branches in a task-specific way. This kind of asymmetric attenuation could either result from stochastic processes (e.g. the opening of a sufficient number of voltage-gated ion channels to trigger a regenerative

events), or (2) the result of branch-specific inhibition to redirect the flow of bAPs to a specific subset of branches (Chen *et al.*, 2012; Boivin and Nedivi, 2018). In another study, Sheffield and Dombeck (2015) found that the majority of dendritic signals were paired to somatic signals. On the other hand, many somatic signals were not paired with dendritic calcium events. Interestingly, the fraction of dendrites co-active with the soma was predictive of the place field of CA1 neurons suggesting that dendritic and somatic co-activity can be modulated in a branch-specific manner. These results are consistent with the ones described in my experimental setting and suggest that at least part of the events described as branch-specific may result from an asymmetric invasion of bAPs.

4.4.3 Dendritic integration during locomotion and visual stimulation

These results also show that the curve describing amplitude-dependent attenuation from the proximal to the distal compartment, does not change neither during visual stimulation, nor during locomotion nor during behavioural state transitions. Despite calcium transients of similar amplitudes have the same probability to be attenuated regardless of the behavioural conditions in which the animal is in, neurons could alter the net proportion of paired somato-dendritic events in a condition-specific manner by generating a higher proportion of high frequency bursts during specific conditions. This is because larger amplitude events in the proximal compartment have a higher chance of being detected distally. Despite locomotion shows a tendency to increase the amplitude of Ca^{2+} transients, the proportion of coincident somato-dendritic events is not significantly different between different behavioural conditions. However, because the results indicate that amplitude-dependent attenuation is a continuous process that occurs throughout the length of the apical trunk and tuft, it is possible that increasing the spatial distance between the two planes recorded semi-simultaneously, would allow to detect subtler changes than the ones observed using a step size of 170 µm (as in my experimental conditions, due to technical limitations).

The electrophysiological characterisation of both GCaMP6f and GCaMP6s demonstrated that the for the same somatic response, calcium transients in the apical tuft were bigger when the tuft was stimulated and smaller when the soma was stimulated (Beaulieu-Laroche *et al.*, 2019; Francioni, Padamsey and Rochefort, 2019). This suggests that the engagement of the apical tuft during a burst of somatic action potentials can be quantified by the slope of the correlation between somatic and apical tuft activity. Importantly, changes in the slope between somatic and dendritic activity could be observed even without affecting the overall

correlation (Beaulieu-Laroche *et al.*, 2019). However, these results show that the relationship between somatic and dendritic signals remain unchanged between visual stimulation, locomotion and behavioural transitions indicating that the amplitude of somatic and dendritic events fluctuate together in a condition-independent manner.

4.4.4 Orientation selectivity under a highly correlated regime

A previous study showed that the generation of NMDA spikes in the dendrites of V1, layer 2/3 neurons is causally involved into enhancing the orientation selectivity of the neuron recorded at the soma (Smith *et al.*, 2013). In this study, dendritic signals were dominated by NMDA-dependent dendritic spikes during the presentation of the preferred orientation only, and by bAPs during the presentation of orthogonal orientations. Assuming that similar mechanisms of dendritic integration exist between layer 2/3 and layer 5 neurons, these results produce two testable predictions: (1) Neurons with the highest OSI, should be the ones with the highest proportion of NMDA spikes as also indirectly suggested by Wilson *et al.* (2016). (2) The activity of dendritic branches should be less correlated during the presentation of the preferred orientation, compared to the orthogonal one (as more branch-specific events should occur). These results indicate that this is not the case. Indeed, the level of correlation between apical tuft branches is remarkably high (>0.8), regardless of the orientation selectivity of the soma and independently of locomotion. This high correlation persists not only between different branches in the apical tuft, but throughout different compartments of the neuron, including the soma. Because the NMDA-dependent dendritic spikes characterised by Smith *et al.* (2013), are both larger and longer than the putative bAPs, the probability of detecting these events should be higher than bAP alone (Helmchen *et al.*, 1999; Xu *et al.*, 2012; Beaulieu-Laroche *et al.*, 2019; Francioni, Padamsey and Rochefort, 2019). Being NMDA-dependent, these spikes were suggested to be generated by synaptic inputs and were therefore assumed to be generated locally on the dendritic branch-recorded (Smith *et al.*, 2013). However, blocking NMDAR through the intracellular application of MK-801 was shown to strongly reduce the generation of global dendritic events (Grienberger, Chen and Konnerth, 2014) suggesting that the activation of NMDAR are required to trigger both local and global dendritic spikes (Grienberger, Chen and Konnerth, 2014; Cichon and Gan, 2015). As a consequence, my results are not incompatible with what was previously found by Smith *et al.* (2013), but they suggest that the NMDA spikes detected by Smith *et al.* (2013) might be global, rather than local. This hypothesis awaits further investigation *in vivo* through the use of voltage indicators which have the potential to overcome both the spatial

limits of whole cell dendritic recordings and the temporal limits of GCaMP6 (Roome and Kuhn, 2018; Abdelfattah *et al.*, 2019; Adam *et al.*, 2019). Indirect support to this hypothesis, comes from the work of Gao *et al.* (2019) that, using voltage imaging and computational modelling in slices, demonstrated that that bAP and NMDA-dependent dendritic spikes, could occur simultaneously creating complex dendritic waveforms, global in nature and remarkably similar to the ones recorded *in vivo* by Smith *et al.* (2013) and others (Helmchen *et al.*, 1999; Moore *et al.*, 2017).

Additionally, I found that the orientation selectivity index does not differ between the one recorded in tuft and the one recorded in the soma, neither during stationary nor during locomotion periods, despite a gain modulation -of the same magnitude in the tuft and in the soma- during locomotion compared to still (Niell and Stryker, 2010; Eriske*et al.*, 2014; Pakan *et al.*, 2016; Maria C Dadarlat and Stryker, 2017). These results are consistent with the findings in layer 2/3 that severing the apical tuft of layer 2/3 neurons does not alter somatic selectivity (Park *et al.*, 2019).

Finally, the results indicate that the preferred orientation of remains unchanged throughout the neuron and that correlation levels are not affected regardless of the orientation selectivity of the neuron (selective and non-selective), the stimulus presented (preferred and non-preferred) and the behavioural state (stationary and locomotion).

Altogether, these results suggest that high somato-dendritic coupling is a widespread feature of layer 5 neurons activity *in vivo* and that the dendritic integration of OS and non-OS neurons is the same regardless of the visual stimulus during stationary and locomotion periods.

5. Discussion

Altogether, these results show that calcium transients are highly correlated from the soma to the most distal part of individual layer 5 neurons in the primary visual cortex of awake behaving mice. Despite this high correlation, the frequency of events found in the distal apical tuft branches was 40% less than the frequency of events that I could detect in the soma. Only 1.4% of events detected in the distal part of the apical tuft could not be detected in the soma suggesting that dendritic spikes are systematically coincident with somatic action potentials. In the apical tuft, branch-specific events accounted for only 3% of the total number of events. They were exclusively composed of small-amplitude events (<0.2 ΔF/F0 normalised to max) and the majority of them (60%) were also detected in the trunk, suggesting that at least some of these events, may result from the asymmetric invasion of either trunk-generated spikes, or backpropagating action potentials.

Finally, despite visual stimulation and locomotion both increased the overall activity of V1 neurons, the somato-dendritic coupling of calcium signals remained unchanged. Similarly, orientation preference and selectivity was similar in the soma and in the tuft. Therefore, dendritic calcium signals in the distal part of the apical tuft is in essence, a filtered reflection of somatic calcium signals.

5.1 Technical challenges and limitations of the use of calcium imaging to assess dendritic activity in awake behaving mice

The analysis of my data set showed that several experimental constraints may bias results towards signals mistakenly interpreted as local dendritic calcium signals. Both the laser power, as well as the numerical aperture of the objective used to image calcium signals will impose limits on the imaging axial resolution. The axial resolution determines the amount of contamination which derives from out-of-focus neuropil. Dense labelling was already demonstrated to strongly affect correlation values between calcium signals in sibling apical tuft dendrites (Xu *et al.*, 2012). This issue can be resolved using sparse labelling. However, even if highly diluted, viral injections are unlikely to label a single neuron. Therefore, even in cases of relatively sparse labelling of individual neurons, contamination remains relevant when imaging 1-2 µm-thin structures such as dendrites. This problem could be in principle overcome using single cell loading or electroporation of synthetic dyes.

Additionally, movement artefacts may also lead to inaccurate detection of local dendrite signals due to focal plane shifts. Both signal contamination and movement artefacts are more likely to be found during specific behaviours such as locomotion. As a consequence, this may bias detection during certain conditions. To avoid this problem, I double labelled the neurons with both GCaMP6 and TdTomato, an activity-independent marker. TdTomato allowed me to exclude regions of interests that were overlapping with segments from contaminating neurons, and it allowed me to exclude recordings in which TdTomato was not detected due to z-plane shifts. Additionally, I used TdTomato to do post-hoc morphological reconstructions of the dendritic tree. This is important because assessing somato-dendritic pairs based on activity patterns, is likely to bias the results toward highly correlated somato-dendritic pairs (Peters *et al.*, 2017). In several instances, baseline fluorescence of both GCaMP6s and GCaMP6f could also be used for the same purpose.

Another parameter that may cause artefactual local dendritic signals, is the length of the imaged dendritic segments (and therefore the size of the regions of interest used to extract the changes of fluorescence over time). Small regions of interest could include spines not clearly distinguishable from the corresponding dendritic shaft, especially when the spine is located above the dendrite at the imaged focal plane. As a consequence, in small regions of interests, spine signals may be incorrectly interpreted as local dendritic signals. Differences in calcium buffering properties of individual compartments also create detection biases as they lead to different decay times of fluorescent calcium indicators between somatic and dendritic compartments (Beaulieu-Laroche *et al.*, 2019; Kerlin *et al.*, 2019). Compared to the soma, dendrites have faster decay constants. Because the decay of fluorescent signals is best described by an exponential function, the ratio between somatic and dendritic (soma: dendrites) fluorescence increases with the length of the time window during which this ratio is calculated. This can lead to biases when comparing fluorescence ratios between somatic and dendritic signals in conditions that unfold across different time-spans (e.g. stimulus sampling vs movement execution or, in my case, prolonged periods of darkness vs 3 seconds-long long visual stimuli). Several strategies have been employed to deal with this problem. Yaeger, Ringach and Trachtenberg (2019) deconvolved dendritic signals into spikes which were subsequently binned and binarized. On the other hand, Kerlin *et al.* (2018) first deconvolved and then re-convolved fluorescence signals using a "time-normalised" kernel to standardise the decay constant across somatic and dendritic calcium transients. In this study, to account for the indicator's kinetics differences, I based my analysis on the detection of individual calcium transients' amplitudes.

Local dendritic activity may be coincidently occurring within global tuft calcium events on a time scale beyond the temporal resolution of GCaMP6 signals (Kerlin *et al.*, 2019). To address this problem, Kerlin *et al.* (2018) estimated what component of the dendritic signal was locally generated, by subtracting somatic signal from it (after decay-time normalisation, described above). However, linear subtraction methods rely on the implicit assumption that the voltage-to-fluorescence relationship between soma and dendrites is linear across a range of activity levels (Chen *et al.*, 2013; Wilson *et al.*, 2016; Iacaruso, Gasler and Hofer, 2017; Kerlin *et al.*, 2019). This assumption was recently demonstrated to be incorrect by Beaulieu-Laroche *et al.* (2019) and as a consequence, a reliable method to subtract bAPs from dendritic (or spine) signals is currently lacking. In this study I therefore defined branch or compartment-specific calcium events, only the events detected in one branch or compartment, and not in the other. Because this detection depends on arbitrary thresholds, I systematically tested the impact of varying the detection threshold on all my results. This analysis demonstrates that the results were robust across a wide range of detection thresholds.

The *in vitro* electrophysiological characterisation of GCaMP6 signals demonstrated that the affinity of calcium indicators can bias the interpretation of the results. Previous studies showed that dendritic Ca^{2+} plateau potentials can reliably be detected *in vivo* using calcium indicators of lower sensitivity than GCaMP6f and GCaMP6s (Helmchen *et al.*, 1999; Xu *et al.*, 2012). At the same time, both studies identified another type of dendritic event characterised by fast-rising and fast-decaying (~30ms) currents, generating ~30 mV of depolarisation, which could not be detected using state-of-art calcium indicators neither *in vivo* (Helmchen *et al.*, 1999; Xu *et al.*, 2012) nor *ex vivo* (Beaulieu-Laroche *et al.*, 2019). The nature of these events is debatable as no pharmacological characterisation was performed; however, given the fast dynamics, it is reasonable to assume that these events may be mediated by Na^{+} currents. Two studies using direct electrophysiological dendritic recordings, demonstrated that fast dynamics dendritic events occur more frequently than somatic action potentials (on average, since simultaneous somato-dendritic recording were not acquired) as evidence of the fact that at least some of them, are dendritically generated (Smith *et al.*, 2013; Moore *et al.*, 2017). As a consequence, the detection of branch-specific events depending on Na+ currents may be underestimated using Ca^{2+} indicators. Similarly in the soma, while it was shown that GCaMP6 could detect individual action potentials in layer 2/3 neurons *in vivo* (Chen *et al.*, 2013), this is not the case for GCaMP6f in layer 5 neurons (Beaulieu-Laroche *et al.*, 2019), nor for GCaMP6s (see appendix 1 or Francioni, Padamsey

and Rochefort, 2019). Compared to GCaMP6f, GCaMP6s is superior at detecting somatic calcium events during low frequency spiking (<25 Hz) (Francioni, Padamsey and Rochefort, 2019; Huang *et al.*, 2019). However, the sensitivity of the two indicators does not change when recording dendritic signals (Francioni, Padamsey and Rochefort, 2019). These results highlight that the choice of the indicator can both quantitatively and qualitatively affect the interpretations of the results. Indeed, compared to GCaMP6s, GCaMP6f systematically underestimate the somatofugal attenuation of bAP, while overestimating the somatopedal attenuation of dendritic spikes.

Even if GCaMP6s has a better sensitivity, the detection of somatic action potentials in layer 5 neurons *in vivo* using any GCaMP sensors is biased towards larger events. Additionally, GCamP indicators report relative changes of fluorescence rather than absolute firing rates and provides little or no information about basal firing rates, suggesting that the fluorescent signals recorded *in vivo* may derive from even higher firing frequencies than the ones characterised *ex vivo*, where spontaneous activity is much lower. As a consequence, the attenuation of fluorescent signals from soma to tuft is likely to be underestimated with GCaMP signals.

5.2 High somato-dendritic coupling irrespective of visual stimulation and locomotion

In line with previous findings (Beaulieu-Laroche *et al.*, 2019) my results show that, in passive viewing conditions, changes in visual inputs (darkness versus drifting gratings) and locomotion-related inputs do not affect the relationship between somatic, trunk and apical tuft calcium signals nor the prevalence of branch-specific dendritic events in the apical tuft. The compartmentalisation between different compartments of a neurons is tightly regulated by both the dynamics and the expression levels of several ion channels including K^+ and HCN channels (Shah, Hammond and Hoffman, 2010; Ramaswamy and Markram, 2015). Both Ach and NA, two neuromodulators strongly involved in the generation of gain responses in V1, were previously demonstrated to shift the activation curves of VGK^+ channels, increasing both the efficacy of backpropagation as well as the strength and duration of dendritically-generated Ca^{2+} spikes (Hoffman and Johnston, 1999; Labarrera *et al.*, 2018). The action of these neuromodulators depends on intracellular messengers including PKA and PKC (Hoffman and Johnston, 1998, 1999; Nuñez *et al.*, 2012). One hypothesis explaining why locomotion did not affect somato-dendritic coupling, is because these intracellular

messengers affect the activation curves of K^+-channels dynamics over very long timescales (Hoffman and Johnston, 1998). It is therefore possible that somato-dendritic coupling is going to be correlated with the locomotion history of the animal, rather than the transitory behavioural changes. It is also possible that untracked behavioural states (e.g. arousal, attention) during stationary and locomotion periods may differentially shape somato-dendritic activity (Vinck *et al.*, 2015). In attempt to capture these untracked events, I tried to separate behavioural transitions as a distinct behavioural state compared to stationary and locomotion (Vinck *et al.*, 2015). However, my results demonstrated that behavioural transitions also, left somato-dendritic coupling unaltered. Some support to the idea that some hidden variable might affect coupling, is the observation that attenuation for events of the same amplitude is best described by a probabilistic exponential curve, rather than a step function (Figure 4.5). At the same time, it is likely that the same fluorescence amplitude can be given by combining the frequency and the number of action potentials in different ways. For example, 15 action potentials at 10 Hz might generate the same fluorescence change in the soma as 10 action potentials at 15 Hz. However, since frequency is critical to generate a dendritic spike, only the latter will be detected in the dendrites. Finally, it is possible that probabilistic attenuation results from the variability of GCaMP6 responses (Huang *et al.*, 2019).

In addition to the effects of neuromodulators, locomotion was hypothesised to affect the somato-dendritic relationship as much of the feedback signals arriving to V1 from locomotion-responsive areas arrives in layer 1 (Leinweber *et al.*, 2017). Nonetheless, the target of these projections is unknown. In addition to hosting the apical tuft dendrites of pyramidal neurons, layer 1 is populated by Neurogliaform cells, a population of 5HT3R+ inhibitory neurons, that through their action on GABAB receptors exert a strong control over the generation of dendritic spikes (Tamás *et al.*, 2003; Palmer *et al.*, 2012; Enrique, Larkum and Nevian, 2013; Larkum, 2013; Naka and Adesnik, 2016; Schulz and Larkum, 2019). It is therefore possible, that the excitatory drive onto the apical tuft of V1 layer 5 pyramidal neurons, might be regulated through a feedforward inhibitory circuit mediated by these neurons. Interestingly, the activity of layer 1 5HT3R+ neurons in V1 increases during locomotion (Mesik *et al.*, 2019).

It is also known that the prevalence and the dynamics of synaptic inputs received by layer 5 pyramidal neurons strongly vary between passive sensory stimulation and active learning tasks (Xu *et al.*, 2012; Hong *et al.*, 2018). It is therefore possible that during the active learning of a behavioural task, the synaptic inputs associated with this learning process would lead to

different mechanisms of dendritic integration than during passive viewing, due to an increase in the amount of top-down vs bottom up inputs (Makino and Komiyama, 2015; Manita *et al.*, 2015). Changes in synaptic integration mode can be the outcome of two distinct processes (1) by altering the activation dynamics of dendritic ion channels through post-translational modifications (Shah, Hammond and Hoffman, 2010). (2) by regulating dendritic excitability through ion channels trafficking onto the dendritic membrane (Shah, Hammond and Hoffman, 2010). LTP induction protocols has been shown to modify the activation curve of K^+ channels due to channel phosphorylation as well as increasing HCN channels insertion into the dendritic membrane (Misonou *et al.*, 2004; Fan *et al.*, 2005). Interestingly, these changes can be gradual. For example Kv2.1, a VG K^+ channel has 16 phosphorylation sites with each one of them inducing a small change in the depolarisation shift (Park *et al.*, 2006). The single cell level regulation of dendritic excitability has been proposed as a mechanism to regulate metaplasticity, suggesting that the processes governing dendritic integration can be dynamically regulated (Sjöström *et al.*, 2008). In that case, somato-dendritic coupling may change during the course of learning. Sheffield, Adoff and Dombeck (2017) for example, recently demonstrated that local dendritic spikes preceded global somato-dendritic activation during the generation of a new place field in CA1 neurons. However, the occurrence of similar processes in the cortex, remains to be tested. Interestingly, most studies that assess somato-dendritic coupling in behaviourally relevant tasks, do so once learning is complete, rather than during the acquisition of the behaviour (Xu *et al.*, 2012; Kerlin *et al.*, 2019) as a consequence, whether coupling changes during different phases of learning remain unexplored. Interestingly, somato-dendritic coupling may evolve during postnatal development when sensori-motor associations are formed (Yaeger, Ringach and Trachtenberg, 2019). Recently, it was shown in the mouse primary visual cortex, that dendrites of layer 2/3 neurons increase their coupling during adulthood, as a consequence of decreased responsiveness of dendrite-targeting interneurons to locomotion-related inputs (Yaeger, Ringach and Trachtenberg, 2019) suggesting that coupling may also change during development. Further investigations are needed to reveal these mechanisms in layer 5 visual cortical neurons. Finally, in addition to excitatory inputs, inhibitory inputs were shown to modulate electrical interactions between soma and dendrites in layer 5 neurons (Larkum, Kaiser and Sakmann, 1999; Silberberg and Markram, 2007; Labarrera *et al.*, 2018; Williams and Fletcher, 2019). Through shunting, dendritic inhibition can effectively veto, or even redirect bAP to a specific subset of branches. In my results, I detected events in the trunk that could be found in one branch, and not in its

sister branch. Despite this could just be the result of the stochastic engagement of ion channels in the tuft, branch-specific inhibition could also be involved (Boivin and Nedivi, 2018). Additionally, dendrite targeting inhibition could affect somato-dendritic coupling by blocking the generation of regenerative dendritic events (Pérez-Garci, Larkum and Nevian, 2013). Recently, it was shown that the selective hyperpolarisation of apical tuft activity, led to a reduction in the generation of dendritic Ca^{2+} spikes and had a divisive rather than subtractive effect on somatic output (Ranganathan *et al.*, 2018). These effects are likely to be similar to the ones mediated by dendrites-targeting inhibitory neurons such as Martinotti and Neurogliaform cells.

Notably, both apical tuft signals and the somato-dendritic coupling may differ between different subtypes of layer 5 pyramidal neurons. It is known that at least two main types exist: intratelencephalic neurons which connect cortical areas, and pyramidal tract neurons which project to multiple subcortical areas (Harris and Shepherd, 2015; Gerfen, Economo and Chandrashekar, 2018). These two types display different morphologies (Groh *et al.*, 2010) and receive different types of inputs (Young *et al.*, 2019). For example IT neurons in V1 were demonstrated to receive a larger fraction of feedback inputs onto the apical tuft, compared to PT neurons (Young *et al.*, 2019). The neurons included in this study had their soma located at various depths within layer 5 (range: 468-666, median 528 μm). Since I selected the imaged neurons visually based on their GCaMP6 fluorescent signal, my sample is likely biased towards layer 5 neurons with thick trunk and thick-tufted morphology. Indeed, IT layer 5 neurons rarely have apical tuft branches beyond the second order after the nexus, a characteristic displayed by PT neurons and by the majority of the neurons included in this thesis (Figure 5.1) (Young *et al.*, 2019). Recently however, it was shown that even among neurons of the same cell type, cortical thickness imposed a caudal-rostral gradient to the computational regime of layer 5B neurons where the generation of dendritic Ca^{2+} spikes was facilitated in the rostral part of rats' V1 (Fletcher and Williams, 2019).

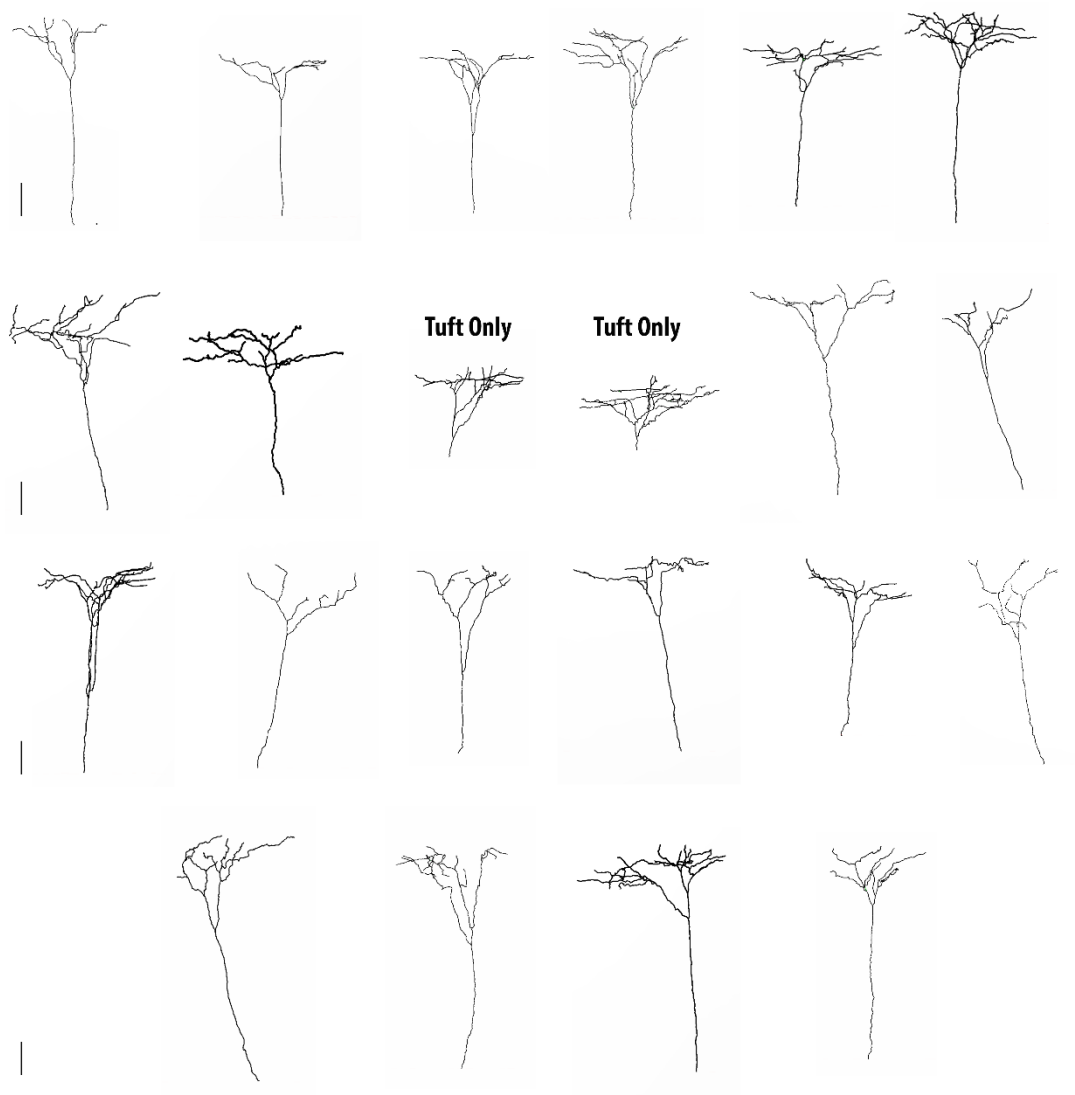

Figure 5.1: *Morphological reconstructions of the neurons included in this thesis.*

Reconstructions were obtained from structural data acquired during a z-stack recording in vivo (See method section 2.5.6). Reconstructions are limited to the portion of apical tuft dendrites present in the field of view (384x384 um) which were visible under in vivo 2-photon imaging conditions. As a result, these should be taken as the lower-bound quantification of the full apical tuft arborisation. Additionally, any branch below the nexus were not included in these reconstructions as these branches could not be reliably reconstructed due to limited imaging resolution. N = 23 neurons with a z-stack which fully included the volume between the nexus and the brain surface. Scale bars indicate 100 µm.

5.3 Global dendritic Ca^{2+} spikes: a single-cell mechanism to integrate feedforward and feedback inputs?

Dendrites are key elements of the input-output transformation in individual neurons. They receive inputs, integrate them (by adding, subtracting, multiplying or dividing) and in doing so, affect somatic output. From a computational point of view, one aim of this input-output

transformation is to preserve as much information as possible about the presynaptic inputs that generated firing, in order to transmit this information to the downstream postsynaptic neuron. Neurons encode this information into their firing rate. In 1999 Larkum discovered what he termed backpropagation-activated Ca^{2+}-spike (BAC) firing, a process through which the coincident arrival of a basal and apical inputs, generates widespread calcium transients in the apical tuft and bursts of action potentials in the soma (Larkum, Zhu and Sakmann, 1999). The occurrence of BAC firing makes a number of predictions which are consistent with the data presented in this thesis including: the generation of widespread dendritic Ca^{2+} spikes (Waters *et al.*, 2003), high-frequency bursts of somatic action potentials (Larkum, Zhu and Sakmann, 1999; Larkum, 2013; Beaulieu-Laroche *et al.*, 2019; Francioni, Padamsey and Rochefort, 2019), high somato-dendritic coupling (Helmchen *et al.*, 1999) and the failure of low-frequency action potentials to trigger Ca^{2+} spikes in the tuft (Spruston *et al.*, 1995; Larkum, Kaiser and Sakmann, 1999; Waters *et al.*, 2003). As a consequence, the coincidence of backpropagating action potentials and dendritically-generated Ca^{2+}-spikes, typical of BAC firing, is a mechanism consistent with my results, suggesting that it may be the dominating dendritic integration mode detected in these experimental conditions (Beaulieu-Laroche *et al.*, 2019; Gao *et al.*, 2019). In a recent study Ujfalussy *et al.* (2018) demonstrated that a single dendritic nonlinearity applied to the entire dendritic arbour, could explain up to 90% of somatic membrane potential variations and that adding local nonlinearities on each individual branch, did not increase model performance (Ujfalussy *et al.*, 2018). These results suggest that a global dendritic nonlinearity, consistent with the one produced during BAC firing and observed in my experimental conditions, is sufficient to describe how dendritic operations are integrated at the somatic level. Additionally, BAC firing has been proposed as a mechanism optimised for information transfer. This is because the generation, frequency and duration of a burst depends on the relative contribution of basal vs apical streams of inputs (Larkum, 2013). Experimental evidence suggests that cortical circuits are built in a way that an important component of feedback input from higher to lower cortical areas arrives at the distal apical tufts of pyramidal neurons while feedforward sensory information targets the basal dendrites (Larkum, Senn and Lüscher, 2004; Makino and Komiyama, 2015; Leinweber *et al.*, 2017; Keller and Mrsic-Flogel, 2018; Young *et al.*, 2019). It was proposed that by regulating the frequency and length of a burst, pyramidal neurons could efficiently signal the amount of congruence (or error, via the engagement of feed-forward inhibition) between a top-down contextual signal and a bottom-up sensory information (Larkum, 2013). In a recent paper it was shown how BAC firing is optimised to multiplex its output into single

spikes and bursts, maintaining intact information about feedforward information arriving on the basal dendrites and feedback information arriving on the apical tuft (Naud and Sprekeler, 2018). In the visual cortex, motor-related areas have been shown to send dense feedback axonal projections to layer 1 (Leinweber *et al.*, 2017). However, since feedback signals, arriving at the distal tuft attenuate by >40 fold when activated in the absence of a coincident backpropagating action potentials in slice, it is not clear whether apical feedback inputs have a driving or a modulatory influence onto somatic output (Williams, 2002). Despite in passive condition, top down inputs are unlikely to be fully engaged, my results show an asymmetry in the coupling between somatic and apical dendritic calcium signals: while 40% of somatic calcium transients were not triggered by apical tuft calcium events, and therefore attenuated from the soma to the apical tuft, only 1.4% of apical tuft events were not detected in the soma. These results show that only very few dendritic spikes are detected in the absence of somatic activity. This is surprising as the biophysical properties of the cellular membrane impose a stronger filter on forward than backward propagation and therefore, if dendritic spikes were generated in the tuft and propagated toward the soma, a high proportion of tuft-only events would be expected. This raises the question as to whether feedback inputs arriving on the apical tuft ever activates in isolation from the soma or whether bAPs are a requirement for their engagement. On the other hand, It is possible that tuft-driven activity may be hidden in the remaining 60% of coincident events. Indeed, these somato-dendritic coupled events could occur from either 1) high frequency back propagating action potentials or 2) strong apical tuft activity capable of driving somatic spiking. Due to the slow dynamic of the calcium indicator, in my experimental conditions I cannot provide evidence in favour of one or the other mechanism and therefore, this question remains unanswered. This is an important question to address as it determines whether top-down influence onto somatic firing requires bottom up action, or whether it can be conveyed independently. Further experiments are needed to resolve these potential mechanisms *in vivo*, for example using voltage-sensitive dyes (Chavarha *et al.*, 2018; Roome and Kuhn, 2018; Adam *et al.*, 2019) or dendritic electrophysiological recordings (Moore *et al.*, 2017), that would provide the temporal resolution to resolve the different types of dendritic events. The implications of these findings will provide important insight into the mechanisms of feature association, cellular plasticity and learning.

5.4 General conclusion and outlook

Several lines of evidence, including those described in this thesis, now suggest that calcium signals in the soma and dendrites are much more correlated than what was previously predicted by experiments in slice (Peters *et al.*, 2017; Beaulieu-Laroche *et al.*, 2019; Kerlin *et al.*, 2019). Partly, this could be due to the limits of imaging calcium signals which are slow and have limited sensitivity (Beaulieu-Laroche *et al.*, 2019; Francioni, Padamsey and Rochefort, 2019; Huang *et al.*, 2019). On the other hand, it is increasingly clear that global, widespread somato-dendritic activation is a fundamental dendritic operation computed in primary sensory (Xu *et al.*, 2012; Francioni, Padamsey and Rochefort, 2019), motor (Peters *et al.*, 2017; Kerlin *et al.*, 2019) and associative areas (Grienberger, Chen and Konnerth, 2014; Voigts and Harnett, 2019) during passive (Beaulieu-Laroche *et al.*, 2019) and reward-associated behaviours (Ranganathan *et al.*, 2018). As a consequence, understanding the functional validity of this mechanism, should be a primary goal of future research into dendritic computation. Unfortunately, this is going to be technically challenging. Dendritic whole cell recordings are hard to obtain and they have a limited spatial resolution (Helmchen *et al.*, 1999; Moore *et al.*, 2017), while voltage imaging, despite some of the recent achievements (Abdelfattah *et al.*, 2019; Adam *et al.*, 2019) and successful application (Roome and Kuhn, 2018), is not yet mature enough to be performed routinely in most labs. As a consequence, calcium imaging remains the primary technique through which dendritic computation is going to be studied until the next technical breakthrough.

Future studies should address the question as to whether the mechanisms of dendritic computation are dysfunctional in animal models of diseases such as epilepsy and autism. In both cases, dendritic channelopathies have been implicated in the pathogenesis of the conditions (Poolos and Johnston, 2012; Schmunk and Gargus, 2013). However, the mechanisms of somato-dendritic coupling *in vivo*, in animal models of these conditions are yet largely unexplored. As the functional meaning of global dendritic spikes is yet largely unknown, studying them in diseased animal models, may shed a light on their functional significance.

These results have also important implications for understanding synaptic plasticity *in vivo*. *Ex vivo* work suggested that because backpropagating action do not reach the distal tuft, the mechanisms of LTP differ at the basal and distal dendrites (Sjöström and Häusser, 2006). My results are consistent with these findings. However, the rules of synaptic potentiation in the distal tuft *in vivo*, are yet largely unexplored. Additionally, a recent paper suggests that high-

frequency action potentials triggered by long-lasting Ca spikes in CA1 neurons underly a new form of one-trial-learning, non-Hebbian plasticity designed to reinforce synaptic associations over seconds-wide temporal scales (Bittner *et al.*, 2017). My observation suggest that similar mechanisms may be implemented in the layer 5 neurons of V1. Nonetheless, whether these mechanisms are implemented, and under which conditions, is yet an open question.

In conclusion, dendritic integration in behaving animals is a young research avenue which we are just starting to explore with the potential for expansion into several distinct directions.

References

Abdelfattah, A. S. *et al.* (2019) 'Bright and photostable chemigenetic indicators for extended in vivo voltage imaging', *Science*. doi: 10.1126/science.aav6416.

Adam, Y. *et al.* (2019) 'Voltage imaging and optogenetics reveal behaviour- dependent changes in hippocampal dynamics', *Nature*. Springer US. doi: 10.1038/s41586-019-1166-7.

Adesnik, H. and Scanziani, M. (2010) 'Lateral competition for cortical space by layer-specific horizontal circuits', *Nature*. doi: 10.1038/nature08935.

Allen, A. E. *et al.* (2016) 'Visual input to the mouse lateral posterior and posterior thalamic nuclei: Photoreceptive origins and retinotopic order', *Journal of Physiology*. doi: 10.1113/JP271707.

Almog, M. and Korngreen, A. (2009) 'Characterization of voltage-gated Ca2+ conductances in layer 5 neocortical pyramidal neurons from rats', *PLoS ONE*. doi: 10.1371/journal.pone.0004841.

Amitai, Y. *et al.* (1993) 'Regenerative activity in apical dendrites of pyramidal cells in neocortex', *Cerebral Cortex*. doi: 10.1093/cercor/3.1.26.

Astman, N. (2006) 'Persistent Sodium Current in Layer 5 Neocortical Neurons Is Primarily Generated in the Proximal Axon', *Journal of Neuroscience*, 26(13), pp. 3465–3473. doi: 10.1523/JNEUROSCI.4907-05.2006.

Attinger, A., Wang, B. and Keller, G. B. (2017) 'Visuomotor Coupling Shapes the Functional Development of Mouse Visual Cortex', *Cell*. doi: 10.1016/j.cell.2017.05.023.

Ayaz, A. *et al.* (2013) 'Locomotion controls spatial integration in mouse visual cortex', *Current Biology*. doi: 10.1016/j.cub.2013.04.012.

Bains, R. S. *et al.* (2018) 'Assessing mouse behaviour throughout the light/dark cycle using automated in-cage analysis tools', *Journal of Neuroscience Methods*. Elsevier B.V., 300, pp. 37–47. doi: 10.1016/j.jneumeth.2017.04.014.

Bear, M. F. (1996) 'Long-Term Depression in Hippocampus', *Annual Review of Neuroscience*, 19(1), pp. 437–462. doi: 10.1146/annurev.neuro.19.1.437.

Beaulieu-Laroche, L. *et al.* (2019) 'Widespread and Highly Correlated Somato-dendritic Activity in Cortical Layer 5 Neurons', *Neuron*. doi: 10.1016/j.neuron.2019.05.014.

Beaulieu-Laroche, L. and Harnett, M. T. (2018) 'Dendritic Spines Prevent Synaptic Voltage Clamp', *Neuron*, 97(1), pp. 75-82.e3. doi: 10.1016/j.neuron.2017.11.016.

Beaulieu, C. *et al.* (1992) 'Quantitative Distribution of GABA-immunopositive and-immunonegative Neurons and Synapses in the Monkey Striate Cortex (Area 17)', *Cerebral Cortex*, 2(4), pp. 295–309. doi: 10.1093/cercor/2.4.295.

Bekkers, J. M. (2000a) 'Distribution and activation of voltage-gated potassium channels in cell-attached and outside-out patches from large layer 5 cortical pyramidal neurons of the rat', *Journal of Physiology*. doi: 10.1111/j.1469-7793.2000.t01-2-00611.x.

Bekkers, J. M. (2000b) 'Properties of voltage-gated potassium currents in nucleated patches from large layer 5 cortical pyramidal neurons of the rat', *Journal of Physiology*. doi: 10.1111/j.1469-7793.2000.t01-1-00593.x.

Beloozerova, I. N. *et al.* (2003) 'Activity of Different Classes of Neurons of the Motor Cortex during Postural Corrections', *The Journal of Neuroscience*, 23(21), pp. 7844–7853. doi: 10.1523/JNEUROSCI.23-21-07844.2003.

Benhassine, N. and Berger, T. (2005) 'Homogeneous distribution of large-conductance calcium-dependent potassium channels on soma and apical dendrite of rat neocortical layer 5 pyramidal neurons', *European Journal of Neuroscience*, 21(4), pp. 914–926. doi: 10.1111/j.1460-9568.2005.03934.x.

Benhassine, N. and Berger, T. (2009) 'Large-conductance calcium-dependent potassium channels prevent dendritic excitability in neocortical pyramidal neurons', *Pflügers Archiv - European Journal of Physiology*, 457(5), pp. 1133–1145. doi: 10.1007/s00424-008-0569-3.

Berger, T. K. *et al.* (2010) 'Brief Bursts Self-Inhibit and Correlate the Pyramidal Network', *PLoS Biology*. Edited by A. Bacci, 8(9), p. e1000473. doi: 10.1371/journal.pbio.1000473.

Berger, T., Larkum, M. E. and Lüscher, H.-R. (2001) 'High I h Channel Density in the Distal Apical Dendrite of Layer V Pyramidal Cells Increases Bidirectional Attenuation of EPSPs', *Journal of Neurophysiology*, 85(2), pp. 855–868. doi: 10.1152/jn.2001.85.2.855.

Berger, T., Senn, W. and Lüscher, H.-R. (2003) 'Hyperpolarization-Activated Current I h Disconnects Somatic and Dendritic Spike Initiation Zones in Layer V Pyramidal Neurons', *Journal of Neurophysiology*, 90(4), pp. 2428–2437. doi: 10.1152/jn.00377.2003.

Berry, A. *et al.* (2012) 'Social deprivation stress is a triggering factor for the emergence of anxiety- and depression-like behaviours and leads to reduced brain BDNF levels in C57BL/6J mice', *Psychoneuroendocrinology*. Elsevier Ltd, 37(6), pp. 762–772. doi: 10.1016/j.psyneuen.2011.09.007.

Bi, G. and Poo, M. (1998) 'Synaptic Modifications in Cultured Hippocampal Neurons: Dependence on Spike Timing, Synaptic Strength, and Postsynaptic Cell Type', *The Journal of Neuroscience*, 18(24), pp. 10464–10472. doi: 10.1523/JNEUROSCI.18-24-10464.1998.

Bittner, K. C. *et al.* (2015) 'Conjunctive input processing drives feature selectivity in hippocampal CA1 neurons', *Nature Neuroscience*, 18(8), pp. 1133–1142. doi: 10.1038/nn.4062.

Bittner, K. C. *et al.* (2017) 'Behavioral time scale synaptic plasticity underlies CA1 place fields', *Science*, 357(6355), pp. 1033–1036. doi: 10.1126/science.aan3846.

Bliss, T. V. P. and Collingridge, G. L. (1993) 'A synaptic model of memory: long-term potentiation in the hippocampus', *Nature*, 361(6407), pp. 31–39. doi: 10.1038/361031a0.

Boivin, J. R. and Nedivi, E. (2018) 'Functional implications of inhibitory synapse placement on signal processing in pyramidal neuron dendrites', *Current Opinion in Neurobiology*, 51, pp. 16–22. doi: 10.1016/j.conb.2018.01.013.

Bonin, V. *et al.* (2011) 'Local Diversity and Fine-Scale Organization of Receptive Fields in Mouse Visual Cortex', *Journal of Neuroscience*. doi: 10.1523/jneurosci.2974-11.2011.

Bono, J. and Clopath, C. (2017) 'Modeling somatic and dendritic spike mediated plasticity at the single neuron and network level', *Nature Communications*. Springer US, 8(1), p. 706. doi: 10.1038/s41467-017-00740-z.

Borst, A. and Theunissen, F. E. (1999) 'Information theory and neural coding', *Nature Neuroscience*. doi: 10.1038/14731.

Bortone, D. S., Olsen, S. R. and Scanziani, M. (2014) 'Translaminar Inhibitory Cells Recruited

by Layer 6 Corticothalamic Neurons Suppress Visual Cortex', *Neuron*, 82(2), pp. 474–485. doi: 10.1016/j.neuron.2014.02.021.

Branco, T. and Häusser, M. (2010) 'The single dendritic branch as a fundamental functional unit in the nervous system', *Current Opinion in Neurobiology*. doi: 10.1016/j.conb.2010.07.009.

Briggs, F. (2017) *Mammalian Visual System Organization*. doi: 10.1093/acrefore/9780190264086.013.66.

Brown, S. P. and Hestrin, S. (2009) 'Intracortical circuits of pyramidal neurons reflect their long-range axonal targets', *Nature*, 457(7233), pp. 1133–1136. doi: 10.1038/nature07658.

Carandini, M. (2006) 'What simple and complex cells compute', *Journal of Physiology*. doi: 10.1113/jphysiol.2006.118976.

Chagnac-Amitai, Y., Luhmann, H. J. and Prince, D. A. (1990) 'Burst generating and regular spiking layer 5 pyramidal neurons of rat neocortex have different morphological features', *Journal of Comparative Neurology*. doi: 10.1002/cne.902960407.

Chavarha, M. *et al.* (2018) 'Fast two-photon volumetric imaging of an improved voltage indicator reveals electrical activity in deeply located neurons in the awake brain', *BioRXiv*.

Chen, C. *et al.* (2017) 'The exercise-glucocorticoid paradox: How exercise is beneficial to cognition, mood, and the brain while increasing glucocorticoid levels', *Frontiers in Neuroendocrinology*. Elsevier Inc., 44, pp. 83–102. doi: 10.1016/j.yfrne.2016.12.001.

Chen, J. L. *et al.* (2012) 'Clustered Dynamics of Inhibitory Synapses and Dendritic Spines in the Adult Neocortex', *Neuron*. Elsevier Inc., 74(2), pp. 361–373. doi: 10.1016/j.neuron.2012.02.030.

Chen, T.-W. *et al.* (2013) 'Ultrasensitive fluorescent proteins for imaging neuronal activity', *Nature*, 499(7458), pp. 295–300. doi: 10.1038/nature12354.

Chen, X. *et al.* (2011) 'Functional mapping of single spines in cortical neurons in vivo', *Nature*, 475(7357), pp. 501–505. doi: 10.1038/nature10193.

Chiu, C. Q. *et al.* (2013) 'Compartmentalization of GABAergic Inhibition by Dendritic Spines', *Science*, 340(6133), pp. 759–762. doi: 10.1126/science.1234274.

Cichon, J. and Gan, W.-B. (2015) 'Branch-specific dendritic Ca2+ spikes cause persistent synaptic plasticity', *Nature*, 520(7546), pp. 180–185. doi: 10.1038/nature14251.

Clascá, F., Rubio-Garrido, P. and Jabaudon, D. (2012) 'Unveiling the diversity of thalamocortical neuron subtypes', *European Journal of Neuroscience*. doi: 10.1111/j.1460-9568.2012.08033.x.

Cooke, S. F. and Bear, M. F. (2015) 'Visual recognition memory: A view from V1', *Current Opinion in Neurobiology*. doi: 10.1016/j.conb.2015.06.008.

Coultrip, R., Granger, R. and Lynch, G. (1992) 'A cortical model of winner-take-all competition via lateral inhibition', *Neural Networks*. doi: 10.1016/S0893-6080(05)80006-1.

Cruz-Martín, A. *et al.* (2014) 'A dedicated circuit links direction-selective retinal ganglion cells to the primary visual cortex', *Nature*. doi: 10.1038/nature12989.

Dadarlat, M. C. and Stryker, M. P. (2017) 'Locomotion Enhances Neural Encoding of Visual Stimuli in Mouse V1', *The Journal of Neuroscience*, 37(14), pp. 3764–3775. doi:

10.1523/JNEUROSCI.2728-16.2017.

DeFelipe, J. *et al.* (2013) 'New insights into the classification and nomenclature of cortical GABAergic interneurons', *Nature Reviews Neuroscience*, 14(3), pp. 202–216. doi: 10.1038/nrn3444.

DeFelipe, J. and Fariñas, I. (1992) 'The pyramidal neuron of the cerebral cortex: Morphological and chemical characteristics of the synaptic inputs', *Progress in Neurobiology*, 39(6), pp. 563–607. doi: 10.1016/0301-0082(92)90015-7.

Dembrow, N. and Johnston, D. (2014) 'Subcircuit-specific neuromodulation in the prefrontal cortex', *Frontiers in Neural Circuits*. doi: 10.3389/fncir.2014.00054.

Diamanti, E. M. *et al.* (2019) 'Spatial encoding in the visual pathway arises in cortex and depends on active navigation', *bioRxiv*, p. 832915. doi: 10.1101/832915.

Douglas, R. J. and Martin, K. A. C. (2004) 'NEURONAL CIRCUITS OF THE NEOCORTEX', *Annual Review of Neuroscience*. doi: 10.1146/annurev.neuro.27.070203.144152.

Doyle, D. (1978) 'The Fine Structure of the Nervous System: The Neurons and Supporting Cells', *Journal of Neurology, Neurosurgery & Psychiatry*, 41(2), pp. 191–192. doi: 10.1136/jnnp.41.2.191-c.

Dräger, U. C. (1975) 'Receptive fields of single cells and topography in mouse visual cortex', *Journal of Comparative Neurology*. doi: 10.1002/cne.901600302.

Drager, U. C. and Hubel, D. H. (2017) 'Topography of visual and somatosensory projections to mouse superior colliculus', *Journal of Neurophysiology*. doi: 10.1152/jn.1976.39.1.91.

Dräger, U. C. and Olsen, J. F. (1980) 'Origins of crossed and uncrossed retinal projections in pigmented and albino mice', *Journal of Comparative Neurology*. doi: 10.1002/cne.901910306.

Drobizhev, M. *et al.* (2011) 'Two-photon absorption properties of fluorescent proteins', *Nature Methods*, 8(5), pp. 393–399. doi: 10.1038/nmeth.1596.

Dylda, E., Pakan, J. M. P. and Rochefort, N. L. (2019) 'Chronic Two-Photon Calcium Imaging in the Visual Cortex of Awake Behaving Mice', in *Handbook of Behavioral Neuroscience*. doi: 10.1016/B978-0-12-812028-6.00013-6.

Ebbesson, S. O. E. (1980) 'The parcellation theory and its relation to interspecific variability in brain organization, evolutionary and ontogenetic development, and neuronal plasticity', *Cell and Tissue Research*. doi: 10.1007/BF00234781.

Enrique, P., Larkum, M. E. and Nevian, T. (2013) 'Inhibition of dendritic Ca 2 + spikes by GABA B receptors in cortical pyramidal neurons is mediated by a direct G i / o - βγ -subunit interaction with Ca v 1 channels', 7, pp. 1599–1612. doi: 10.1113/jphysiol.2012.245464.

Erisken, S. *et al.* (2014) 'Effects of Locomotion Extend throughout the Mouse Early Visual System', *Current Biology*, 24(24), pp. 2899–2907. doi: 10.1016/j.cub.2014.10.045.

Fahey, P. G. *et al.* (2019) 'A global map of orientation tuning in mouse visual cortex', *bioRxiv*, p. 745323. doi: 10.1101/745323.

Fan, Y. *et al.* (2005) 'Activity-dependent decrease of excitability in rat hippocampal neurons through increases in Ih', *Nature Neuroscience*. doi: 10.1038/nn1568.

Feldman, D. E. and Brecht, M. (2005) 'Map plasticity in somatosensory cortex', *Science*. doi:

10.1126/science.1115807.

Feldmeyer, D. (2012) 'Excitatory neuronal connectivity in the barrel cortex', *Frontiers in Neuroanatomy*, 6. doi: 10.3389/fnana.2012.00024.

Fifková, E. and Van Harreveld, A. (1977) 'Long-lasting morphological changes in dendritic spines of dentate granular cells following stimulation of the entorhinal area', *Journal of Neurocytology*, 6(2), pp. 211–230. doi: 10.1007/BF01261506.

Fino, E., Packer, a. M. and Yuste, R. (2012) 'The Logic of Inhibitory Connectivity in the Neocortex', *The Neuroscientist*. doi: 10.1177/1073858412456743.

Fiser, A. *et al.* (2016) 'Experience-dependent spatial expectations in mouse visual cortex', *Nature Neuroscience*. doi: 10.1038/nn.4385.

Fletcher, L. N. and Williams, S. R. (2019) 'Neocortical Topology Governs the Dendritic Integrative Capacity of Layer 5 Pyramidal Neurons', *Neuron*. doi: 10.1016/j.neuron.2018.10.048.

Fox, M. W. (1965) 'The visual cliff test for the study of visual depth perception in the mouse', *Animal Behaviour*. doi: 10.1016/0003-3472(65)90040-0.

De Franceschi, G. *et al.* (2016) 'Vision Guides Selection of Freeze or Flight Defense Strategies in Mice', *Current Biology*. doi: 10.1016/j.cub.2016.06.006.

Francioni, V., Padamsey, Z. and Rochefort, N. L. (2019) 'High and asymmetric somato-dendritic coupling of v1 layer 5 neurons independent of visual stimulation and locomotion', *eLife*. doi: 10.7554/eLife.49145.

Frenkel, M. Y. *et al.* (2006) 'Instructive Effect of Visual Experience in Mouse Visual Cortex', *Neuron*. doi: 10.1016/j.neuron.2006.06.026.

Fu, Y. *et al.* (2014) 'A cortical circuit for gain control by behavioral state', *Cell*. doi: 10.1016/j.cell.2014.01.050.

Gambino, F. *et al.* (2014) 'Sensory-evoked LTP driven by dendritic plateau potentials in vivo', *Nature*. doi: 10.1038/nature13664.

Gao, P. P. *et al.* (2019) 'Local Glutamate-Mediated Dendritic Plateau Potentials Change the State of the Cortical Pyramidal Neuron', *bioRxiv*, p. 828582. doi: 10.1101/828582.

Garrett, M. E. *et al.* (2014) 'Topography and Areal Organization of Mouse Visual Cortex', *Journal of Neuroscience*. doi: 10.1523/jneurosci.1124-14.2014.

Gavornik, J. P. and Bear, M. F. (2014) 'Learned spatiotemporal sequence recognition and prediction in primary visual cortex', *Nature Neuroscience*. doi: 10.1038/nn.3683.

Gerfen, C. R., Economo, M. N. and Chandrashekar, J. (2018) 'Long distance projections of cortical pyramidal neurons', *Journal of neuroscience research*. doi: 10.1002/jnr.23978.

Gibson, E. J. and Walk, R. D. (1960) 'The "visual cliff".', *Scientific American*. doi: 10.1038/scientificamerican0460-64.

Gidon, A. *et al.* (2020) 'Dendritic action potentials and computation in human layer 2/3 cortical neurons', *Science*. doi: 10.1126/science.aax6239.

Godement, P., Salaün, J. and Imbert, M. (1984) 'Prenatal and postnatal development of retinogeniculate and retinocollicular projections in the mouse', *Journal of Comparative Neurology*. doi: 10.1002/cne.902300406.

Goldberg, E. M. and Coulter, D. A. (2013) 'Mechanisms of epileptogenesis: A convergence on neural circuit dysfunction', *Nature Reviews Neuroscience*. doi: 10.1038/nrn3482.

Golding, N. L. *et al.* (1999) 'Dendritic Calcium Spike Initiation and Repolarization Are Controlled by Distinct Potassium Channel Subtypes in CA1 Pyramidal Neurons', *The Journal of Neuroscience*, 19(20), pp. 8789–8798. doi: 10.1523/JNEUROSCI.19-20-08789.1999.

Golding, N. L. and Spruston, N. (1998) 'Dendritic Sodium Spikes Are Variable Triggers of Axonal Action Potentials in Hippocampal CA1 Pyramidal Neurons', *Neuron*, 21(5), pp. 1189–1200. doi: 10.1016/S0896-6273(00)80635-2.

Golding, N. L., Staff, N. P. and Spruston, N. (2002) 'Dendritic spikes as a mechanism for cooperative long-term potentiation', *Nature*, 418(6895), pp. 326–331. doi: 10.1038/nature00854.

Goldman-Rakic, P. S. *et al.* (1989) 'Dopamine synaptic complex with pyramidal neurons in primate cerebral cortex.', *Proceedings of the National Academy of Sciences*, 86(22), pp. 9015–9019. doi: 10.1073/pnas.86.22.9015.

Gouwens, N. W. *et al.* (2019) 'Classification of electrophysiological and morphological neuron types in the mouse visual cortex', *Nature Neuroscience*. doi: 10.1038/s41593-019-0417-0.

Grienberger, C. *et al.* (2017) 'Inhibitory suppression of heterogeneously tuned excitation enhances spatial coding in CA1 place cells', *Nature Neuroscience*, 20(3), pp. 417–426. doi: 10.1038/nn.4486.

Grienberger, C., Chen, X. and Konnerth, A. (2014) 'NMDA Receptor-Dependent Multidendrite Ca 2+ Spikes Required for Hippocampal Burst Firing In Vivo', *Neuron*. Elsevier Inc., 81(6), pp. 1274–1281. doi: 10.1016/j.neuron.2014.01.014.

Grienberger, C., Chen, X. and Konnerth, A. (2015) 'Dendritic function in vivo', *Trends in Neurosciences*. Elsevier Ltd, 38(1), pp. 45–54. doi: 10.1016/j.tins.2014.11.002.

Groh, A. *et al.* (2010) 'Cell-type specific properties of pyramidal neurons in neocortex underlying a layout that is modifiable depending on the cortical area', *Cerebral Cortex*. doi: 10.1093/cercor/bhp152.

Grubb, M. S. and Thompson, I. D. (2003) 'Quantitative Characterization of Visual Response Properties in the Mouse Dorsal Lateral Geniculate Nucleus', *Journal of Neurophysiology*. doi: 10.1152/jn.00699.2003.

Guerguiev, J., Lillicrap, T. P. and Richards, B. A. (2017) 'Towards deep learning with segregated dendrites', *eLife*, 6, pp. 1–37. doi: 10.7554/eLife.22901.

Guillery, R. W. and Sherman, S. M. (2002) 'Thalamic Relay Functions and Their Role in Corticocortical Communication', *Neuron*, 33(2), pp. 163–175. doi: 10.1016/S0896-6273(01)00582-7.

Guo, Z. V. *et al.* (2014) 'Procedures for behavioral experiments in head-fixed mice', *PLoS ONE*. doi: 10.1371/journal.pone.0088678.

Harnett, M. T. *et al.* (2013) 'Potassium channels control the interaction between active dendritic integration compartments in layer 5 cortical pyramidal neurons', *Neuron*. doi: 10.1016/j.neuron.2013.06.005.

Harnett, M. T., Magee, J. C. and Williams, S. R. (2015) 'Distribution and Function of HCN Channels in the Apical Dendritic Tuft of Neocortical Pyramidal Neurons', *Journal of*

Neuroscience. doi: 10.1523/jneurosci.2813-14.2015.

Harris, K. D. and Mrsic-Flogel, T. D. (2013) 'Cortical connectivity and sensory coding', *Nature*, 503(7474), pp. 51–58. doi: 10.1038/nature12654.

Harris, K. D. and Shepherd, G. M. G. (2015) 'The neocortical circuit: Themes and variations', *Nature Neuroscience*. doi: 10.1038/nn.3917.

Harvey, C. D. *et al.* (2009) 'Intracellular dynamics of hippocampal place cells during virtual navigation', *Nature*. doi: 10.1038/nature08499.

Hayama, T. *et al.* (2013) 'GABA promotes the competitive selection of dendritic spines by controlling local Ca2+ signaling', *Nature Neuroscience*, 16(10), pp. 1409–1416. doi: 10.1038/nn.3496.

Helmchen, F. *et al.* (1999) 'In vivo dendritic calcium dynamics in deep-layer cortical pyramidal neurons', *Nature Neuroscience*. doi: 10.1038/14788.

Higley, M. J. (2014) 'Localized GABAergic inhibition of dendritic Ca2+ signalling', *Nature Reviews Neuroscience*, 15(9), pp. 567–572. doi: 10.1038/nrn3803.

Hill, D. N. *et al.* (2013) 'Multibranch activity in basal and tuft dendrites during firing of layer 5 cortical neurons in vivo', *Proceedings of the National Academy of Sciences*, 110(33), pp. 13618–13623. doi: 10.1073/pnas.1312599110.

Hillier, D. *et al.* (2017) 'Causal evidence for retina-dependent and -independent visual motion computations in mouse cortex', *Nature Neuroscience*. doi: 10.1038/nn.4566.

Hillman, E. M. *et al.* (2018) 'High-speed 3D imaging of cellular activity in the brain using axially-extended beams and light sheets', *Current Opinion in Neurobiology*. doi: 10.1016/j.conb.2018.03.007.

Hoffman, D. A. and Johnston, D. (1998) 'Downregulation of transient K+ channels in dendrites of hippocampal CA1 pyramidal neurons by activation of PKA and PKC', *Journal of Neuroscience*. doi: 10.1523/jneurosci.18-10-03521.1998.

Hoffman, D. A. and Johnston, D. (1999) 'Neuromodulation of dendritic action potentials', *Journal of Neurophysiology*. doi: 10.1152/jn.1999.81.1.408.

Hong, Y. K. *et al.* (2018) 'Sensation, movement and learning in the absence of barrel cortex', *Nature*. Springer US, pp. 542–546. doi: 10.1038/s41586-018-0527-y.

Van Hooser, S. D. (2007) 'Similarity and diversity in visual cortex: Is there a unifying theory of cortical computation?', *Neuroscientist*. doi: 10.1177/1073858407306597.

Howard, A., Tamas, G. and Soltesz, I. (2005) 'Lighting the chandelier: New vistas for axo-axonic cells', *Trends in Neurosciences*. doi: 10.1016/j.tins.2005.04.004.

Howarth, M., Walmsley, L. and Brown, T. M. (2014) 'Binocular integration in the mouse lateral geniculate nuclei', *Current Biology*. doi: 10.1016/j.cub.2014.04.014.

Hoy, J. L. *et al.* (2016) 'Vision Drives Accurate Approach Behavior during Prey Capture in Laboratory Mice', *Current Biology*. doi: 10.1016/j.cub.2016.09.009.

Hu, H., Gan, J. and Jonas, P. (2014) 'Fast-spiking, parvalbumin+ GABAergic interneurons: From cellular design to microcircuit function', *Science*. doi: 10.1126/science.1255263.

Huang, L. *et al.* (2019) 'Relationship between spiking activity and simultaneously recorded fluorescence signals in transgenic mice expressing GCaMP6', *bioRxiv*, p. 788802. doi:

10.1101/788802.

Hubel, D. H. and Wiesel, T. N. (1959) 'Receptive fields of single neurones in the cat's striate cortex', *The Journal of Physiology*. doi: 10.1113/jphysiol.1959.sp006308.

Hubel, D. H. and Wiesel, T. N. (1962) 'Receptive fields, binocular interaction and functional architecture in the cat's visual cortex', *The Journal of Physiology*. doi: 10.1113/jphysiol.1962.sp006837.

Hubel, D. H. and Wiesel, T. N. (1963) 'Shape and arrangement of columns in cat's striate cortex', *The Journal of Physiology*. doi: 10.1113/jphysiol.1963.sp007079.

Hubel, D. H. and Wiesel, T. N. (1968) 'Receptive fields and functional architecture of monkey striate cortex', *The Journal of Physiology*. doi: 10.1113/jphysiol.1968.sp008455.

Hubel, D. H. and Wiesel, T. N. (1969) 'Anatomical demonstration of columns in the monkey striate cortex', *Nature*. doi: 10.1038/221747a0.

Hübener, M. (2003) 'Mouse visual cortex', *Current Opinion in Neurobiology*, 13(4), pp. 413–420. doi: 10.1016/S0959-4388(03)00102-8.

Huberman, A. D. and Niell, C. M. (2011) 'What can mice tell us about how vision works?', *Trends in Neurosciences*. doi: 10.1016/j.tins.2011.07.002.

Huguenard, J. R., Hamill, O. P. and Prince, D. A. (2006) 'Sodium channels in dendrites of rat cortical pyramidal neurons.', *Proceedings of the National Academy of Sciences*. doi: 10.1073/pnas.86.7.2473.

Iacaruso, M. F., Gasler, I. T. and Hofer, S. B. (2017) 'Synaptic organization of visual space in primary visual cortex', *Nature*. doi: 10.1038/nature23019.

Ieraci, A., Mallei, A. and Popoli, M. (2016) 'Social Isolation Stress Induces Anxious-Depressive-Like Behavior and Alterations of Neuroplasticity-Related Genes in Adult Male Mice', *Neural Plasticity*, 2016. doi: 10.1155/2016/6212983.

Jacob, V. *et al.* (2012) 'Regular Spiking and Intrinsic Bursting Pyramidal Cells Show Orthogonal Forms of Experience-Dependent Plasticity in Layer V of Barrel Cortex', *Neuron*. doi: 10.1016/j.neuron.2011.11.034.

Jadi, M. *et al.* (2012) 'Location-Dependent Effects of Inhibition on Local Spiking in Pyramidal Neuron Dendrites', *PLoS Computational Biology*. Edited by B. S. Gutkin, 8(6), p. e1002550. doi: 10.1371/journal.pcbi.1002550.

Jeon, C.-J., Strettoi, E. and Masland, R. H. (1998) 'The Major Cell Populations of the Mouse Retina', *The Journal of Neuroscience*. doi: 10.1523/jneurosci.18-21-08936.1998.

Jia, H. *et al.* (2010) 'Dendritic organization of sensory input to cortical neurons in vivo', *Nature*, 464(7293), pp. 1307–1312. doi: 10.1038/nature08947.

Jones, E. G. (2001) 'The thalamic matrix and thalamocortical synchrony', *Trends in Neurosciences*. doi: 10.1016/S0166-2236(00)01922-6.

Jones, E. G., Huntley, G. W. and Benson, D. L. (1994) 'Alpha calcium/calmodulin-dependent protein kinase II selectively expressed in a subpopulation of excitatory neurons in monkey sensory-motor cortex: comparison with GAD-67 expression.', *The Journal of neuroscience : the official journal of the Society for Neuroscience*, 14(2), pp. 611–629. doi: 10.1523/JNEUROSCI.14-02-00611.1994.

Jurjut, O. *et al.* (2017) 'Learning Enhances Sensory Processing in Mouse V1 before Improving Behavior', *The Journal of Neuroscience*. doi: 10.1523/jneurosci.3485-16.2017.

Kaifosh, P. *et al.* (2014) 'SIMA: Python software for analysis of dynamic fluorescence imaging data', *Frontiers in Neuroinformatics*, 8(September), pp. 1–10. doi: 10.3389/fninf.2014.00080.

Kampa, B. M., Letzkus, J. J. and Stuart, G. J. (2006) 'Requirement of dendritic calcium spikes for induction of spike-timing-dependent synaptic plasticity', *The Journal of Physiology*, 574(1), pp. 283–290. doi: 10.1113/jphysiol.2006.111062.

Kaneko, M., Fu, Y. and Stryker, M. P. (2017) 'Locomotion Induces Stimulus-Specific Response Enhancement in Adult Visual Cortex', *The Journal of Neuroscience*. doi: 10.1523/jneurosci.3760-16.2017.

Kaneko, M. and Stryker, M. P. (2014) 'Sensory experience during locomotion promotes recovery of function in adult visual cortex', pp. 1–16. doi: 10.7554/eLife.02798.

Kanemoto, Y. *et al.* (2011) 'Spatial Distributions of GABA Receptors and Local Inhibition of Ca2+ Transients Studied with GABA Uncaging in the Dendrites of CA1 Pyramidal Neurons', *PLoS ONE*. Edited by F. Tell, 6(7), p. e22652. doi: 10.1371/journal.pone.0022652.

Kang, J., Huguenard, J. R. and Prince, D. A. (2017) 'Development of BK channels in neocortical pyramidal neurons', *Journal of Neurophysiology*. doi: 10.1152/jn.1996.76.1.188.

Kang, Jian, Huguenard, J. R. and Prince, D. A. (2017) 'Voltage-Gated Potassium Channels Activated During Action Potentials in Layer V Neocortical Pyramidal Neurons', *Journal of Neurophysiology*. doi: 10.1152/jn.2000.83.1.70.

Kappel, S., Hawkins, P. and Mendl, M. T. (2017) 'To group or not to group? Good practice for housing male laboratory mice', *Animals*, 7(12), pp. 1–25. doi: 10.3390/ani7120088.

Kawaguchi, Y. (1997) 'GABAergic cell subtypes and their synaptic connections in rat frontal cortex', *Cerebral Cortex*, 7(6), pp. 476–486. doi: 10.1093/cercor/7.6.476.

Kawaguchi, Y., Karube, F. and Kubota, Y. (2006) 'Dendritic branch typing and spine expression patterns in cortical nonpyramidal cells', *Cerebral Cortex*, 16(5), pp. 696–711. doi: 10.1093/cercor/bhj015.

Kawaguchi, Y. and Kubota, Y. (1996) 'Physiological and morphological identification of somatostatin- or vasoactive intestinal polypeptide-containing cells among GABAergic cell subtypes in rat frontal cortex', *The Journal of Neuroscience*. doi: 10.1523/jneurosci.16-08-02701.1996.

Kay, J. W. *et al.* (2019) 'A Bayesian decomposition of BAC firing as a mechanism for apical amplification in neocortical pyramidal neurons', *bioRxiv*. doi: 10.1101/604066.

Keller, A. J. *et al.* (2017) 'Stimulus relevance modulates contrast adaptation in visual cortex', *eLife*. doi: 10.7554/eLife.21589.

Keller, G. B., Bonhoeffer, T. and Hübener, M. (2012) 'Sensorimotor Mismatch Signals in Primary Visual Cortex of the Behaving Mouse', *Neuron*. doi: 10.1016/j.neuron.2012.03.040.

Keller, G. B. and Mrsic-Flogel, T. D. (2018) 'Predictive Processing: A Canonical Cortical Computation', *Neuron*. doi: 10.1016/j.neuron.2018.10.003.

Kerlin, A. *et al.* (2019) 'Functional clustering of dendritic activity during decision-making', *eLife*. doi: 10.7554/eLife.46966.

Kerlin, A. M. *et al.* (2010) 'Broadly Tuned Response Properties of Diverse Inhibitory Neuron Subtypes in Mouse Visual Cortex', *Neuron*, 67(5), pp. 858–871. doi: 10.1016/j.neuron.2010.08.002.

Kim, E. J. *et al.* (2015) 'Three Types of Cortical Layer 5 Neurons That Differ in Brain-wide Connectivity and Function', *Neuron*. Elsevier Inc., 88(6), pp. 1253–1267. doi: 10.1016/j.neuron.2015.11.002.

Kim, T. H. *et al.* (2016) 'Long-Term Optical Access to an Estimated One Million Neurons in the Live Mouse Cortex', *Cell Reports*. doi: 10.1016/j.celrep.2016.12.004.

Kiritani, T. *et al.* (2012) 'Hierarchical Connectivity and Connection-Specific Dynamics in the Corticospinal-Corticostriatal Microcircuit in Mouse Motor Cortex', *Journal of Neuroscience*, 32(14), pp. 4992–5001. doi: 10.1523/JNEUROSCI.4759-11.2012.

Koch, C. and Zador, A. (1993) 'The function of dendritic spines: devices subserving biochemical rather than electrical compartmentalization', *The Journal of Neuroscience*. doi: 10.1523/jneurosci.13-02-00413.1993.

De Kock, C. P. J. *et al.* (2007) 'Layer- and cell-type-specific suprathreshold stimulus representation in rat primary somatosensory cortex', *The Journal of Physiology*, 581(1), pp. 139–154. doi: 10.1113/jphysiol.2006.124321.

De Kock, C. P. J. and Sakmann, B. (2008) 'High frequency action potential bursts (≥ 100 Hz) in L2/3 and L5B thick tufted neurons in anaesthetized and awake rat primary somatosensory cortex', *The Journal of Physiology*, 586(14), pp. 3353–3364. doi: 10.1113/jphysiol.2008.155580.

Koester, H. J. and Sakmann, B. (1998) 'Calcium dynamics in single spines during coincident pre- and postsynaptic activity depend on relative timing of back-propagating action potentials and subthreshold excitatory postsynaptic potentials', *Proceedings of the National Academy of Sciences*, 95(16), pp. 9596–9601. doi: 10.1073/pnas.95.16.9596.

Kole, M. H. P. (2006) 'Single Ih Channels in Pyramidal Neuron Dendrites: Properties, Distribution, and Impact on Action Potential Output', *Journal of Neuroscience*. doi: 10.1523/jneurosci.3664-05.2006.

Korngreen, A. and Sakmann, B. (2000) 'Voltage-gated K + channels in layer 5 neocortical pyramidal neurones from young rats: Subtypes and gradients', *Journal of Physiology*. doi: 10.1111/j.1469-7793.2000.00621.x.

Krubitzer, L. and Huffman, K. J. (2000) 'Arealization of the neocortex in mammals: Genetic and epigenetic contributions to the phenotype', in *Brain, Behavior and Evolution*. doi: 10.1159/000006667.

Książek, A. *et al.* (2013) 'Properties of BK-type Ca++-dependent K+ channel currents in medial prefrontal cortex pyramidal neurons in rats of different ages', *Frontiers in Cellular Neuroscience*. doi: 10.3389/fncel.2013.00185.

Kühn, R. and Torres, R. M. (2002) 'Cre/loxP recombination system and gene targeting.', *Methods in molecular biology (Clifton, N.J.)*. doi: 10.1385/1-59259-178-7:175.

Labarrera, C. *et al.* (2018) 'Adrenergic Modulation Regulates the Dendritic Excitability of Layer 5 Pyramidal Neurons In Vivo', *Cell Reports*, 23(4), pp. 1034–1044. doi: 10.1016/j.celrep.2018.03.103.

Lacefield, C. O. *et al.* (2019) 'Reinforcement Learning Recruits Somata and Apical Dendrites

across Layers of Primary Sensory Cortex', *Cell Reports*, 26(8), pp. 2000-2008.e2. doi: 10.1016/j.celrep.2019.01.093.

Langley, W. M. (1989) 'Grasshopper mouse's use of visual cues during a predatory attack', *Behavioural Processes*. doi: 10.1016/0376-6357(89)90035-1.

Laramée, M. and Boire, D. (2015) 'Visual cortical areas of the mouse : comparison of parcellation and network structure with primates', 8(January), pp. 1–16. doi: 10.3389/fncir.2014.00149.

Larkum, M. (2013) 'A cellular mechanism for cortical associations: An organizing principle for the cerebral cortex', *Trends in Neurosciences*. Elsevier Ltd, 36(3), pp. 141–151. doi: 10.1016/j.tins.2012.11.006.

Larkum, M. E. *et al.* (1998) 'Integration of Excitatory Postsynaptic Potentials in Dendrites of Motoneurons of Rat Spinal Cord Slice Cultures', *Journal of Neurophysiology*, 80(2), pp. 924–935. doi: 10.1152/jn.1998.80.2.924.

Larkum, M. E. *et al.* (2009) 'Synaptic integration in tuft dendrites of layer 5 pyramidal neurons: A new unifying principle', *Science*, 325(5941), pp. 756–760. doi: 10.1126/science.1171958.

Larkum, M. E., Kaiser, K. M. M. and Sakmann, B. (1999) 'Calcium electrogenesis in distal apical dendrites of layer 5 pyramidal cells at a critical frequency of back-propagating action potentials', *Proceedings of the National Academy of Sciences*, 96(25), pp. 14600–14604. doi: 10.1073/pnas.96.25.14600.

Larkum, M. E., Senn, W. and Lüscher, H. (2004) 'Top-down Dendritic Input Increases the Gain of Layer 5 Pyramidal Neurons', (October), pp. 1059–1070. doi: 10.1093/cercor/bhh065.

Larkum, M. E. and Zhu, J. J. (2002) 'Signaling of Layer 1 and Whisker-Evoked Ca 2+ and Na + Action Potentials in Distal and Terminal Dendrites of Rat Neocortical Pyramidal Neurons In Vitro and In Vivo', *The Journal of Neuroscience*, 22(16), pp. 6991–7005. doi: 10.1523/JNEUROSCI.22-16-06991.2002.

Larkum, M. E., Zhu, J. J. and Sakmann, B. (1999) 'A new cellular mechanism for coupling inputs arriving at different cortical layers', *Nature*. doi: 10.1038/18686.

Larkum, M. E., Zhu, J. J. and Sakmann, B. (2001) 'Dendritic mechanisms underlying the coupling of the dendritic with the axonal action potential initiation zone of adult rat layer 5 pyramidal neurons', *The Journal of Physiology*, 533(2), pp. 447–466. doi: 10.1111/j.1469-7793.2001.0447a.x.

Lavzin, M. *et al.* (2012) 'Nonlinear dendritic processing determines angular tuning of barrel cortex neurons in vivo', *Nature*. doi: 10.1038/nature11451.

Lee, K.-S. *et al.* (2019) 'Functional Synaptic Architecture of Callosal Inputs in Mouse Primary Visual Cortex', *Neuron*, 101(3), pp. 421-428.e5. doi: 10.1016/j.neuron.2018.12.005.

Lee, S. *et al.* (2010) 'The Largest Group of Superficial Neocortical GABAergic Interneurons Expresses Ionotropic Serotonin Receptors', *Journal of Neuroscience*, 30(50), pp. 16796–16808. doi: 10.1523/JNEUROSCI.1869-10.2010.

Lefort, S. *et al.* (2009) 'The Excitatory Neuronal Network of the C2 Barrel Column in Mouse Primary Somatosensory Cortex', *Neuron*, 61(2), pp. 301–316. doi: 10.1016/j.neuron.2008.12.020.

Leinweber, M. *et al.* (2014) 'Two-photon Calcium Imaging in Mice Navigating a Virtual Reality Environment', *Journal of Visualized Experiments*, (84), pp. 1–6. doi: 10.3791/50885.

Leinweber, M. *et al.* (2017) 'A Sensorimotor Circuit in Mouse Cortex for Visual Flow Predictions', *Neuron*. doi: 10.1016/j.neuron.2017.08.036.

Lewis, D. a, Hashimoto, T. and Volk, D. W. (2005) 'Cortical inhibitory neurons and schizophrenia.', *Nature reviews. Neuroscience*, 6(4), pp. 312–24. doi: 10.1038/nrn1648.

Li, X. Y. *et al.* (2015) 'Synaptic Basis for Differential Orientation Selectivity between Complex and Simple Cells in Mouse Visual Cortex', 35(31), pp. 11081–11093. doi: 10.1523/JNEUROSCI.5246-14.2015.

Lien, A. D. and Scanziani, M. (2018) 'Cortical direction selectivity emerges at convergence of thalamic synapses', *Nature*. doi: 10.1038/s41586-018-0148-5.

Liu, B. *et al.* (2011) 'Broad Inhibition Sharpens Orientation Selectivity by Expanding Input Dynamic Range in Mouse Simple Cells', *Neuron*, 71(3), pp. 542–554. doi: 10.1016/j.neuron.2011.06.017.

Liu, C. H. *et al.* (2015) 'Selective Activation of a Putative Reinforcement Signal Conditions Cued Interval Timing in Primary Visual Cortex', *Current Biology*. doi: 10.1016/j.cub.2015.04.028.

Lörincz, A. *et al.* (2002) 'Polarized and compartment-dependent distribution of HCN1 in pyramidal cell dendrites', *Nature Neuroscience*, 5(11), pp. 1185–1193. doi: 10.1038/nn962.

Losonczy, A. and Magee, J. C. (2006) 'Integrative Properties of Radial Oblique Dendrites in Hippocampal CA1 Pyramidal Neurons', *Neuron*, 50(2), pp. 291–307. doi: 10.1016/j.neuron.2006.03.016.

Luczak, A. *et al.* (2007) 'Sequential structure of neocortical spontaneous activity in vivo', *Proceedings of the National Academy of Sciences*, 104(1), pp. 347–352. doi: 10.1073/pnas.0605643104.

Luo, L., Callaway, E. M. and Svoboda, K. (2008) 'Genetic Dissection of Neural Circuits', *Neuron*. doi: 10.1016/j.neuron.2008.01.002.

Luo, L., Callaway, E. M. and Svoboda, K. (2018) 'Genetic Dissection of Neural Circuits: A Decade of Progress', *Neuron*. doi: 10.1016/j.neuron.2018.03.040.

Lüscher, C. and Malenka, R. C. (2012) 'NMDA receptor-dependent long-term potentiation and long-term depression (LTP/LTD)', *Cold Spring Harbor Perspectives in Biology*. doi: 10.1101/cshperspect.a005710.

Magee, J. C. and Johnston, D. (1997) 'A synaptically controlled, associative signal for Hebbian plasticity in hippocampal neurons', *Science*. doi: 10.1126/science.275.5297.209.

Major, G., Larkum, M. E. and Schiller, J. (2013) 'Active properties of neocortical pyramidal neuron dendrites.', *Annual review of neuroscience*, 36, pp. 1–24. doi: 10.1146/annurev-neuro-062111-150343.

Makino, H. and Komiyama, T. (2015) 'Learning enhances the relative impact of top-down processing in the visual cortex', *Nature Neuroscience*, 18(8), pp. 1116–1122. doi: 10.1038/nn.4061.

Manita, S. *et al.* (2015) 'A Top-Down Cortical Circuit for Accurate Sensory Perception', *Neuron*. Elsevier Inc., 86(5), pp. 1304–1316. doi: 10.1016/j.neuron.2015.05.006.

Marín, O. (2012) 'Interneuron dysfunction in psychiatric disorders', *Nature Reviews Neuroscience*. doi: 10.1038/nrn3155.

Marshel, J. H. *et al.* (2012) 'Anterior-Posterior Direction Opponency in the Superficial Mouse Lateral Geniculate Nucleus', *Neuron*. doi: 10.1016/j.neuron.2012.09.021.

Mazurek, M., Kager, M. and Van Hooser, S. D. (2014) 'Robust quantification of orientation selectivity and direction selectivity', *Frontiers in Neural Circuits*, 8. doi: 10.3389/fncir.2014.00092.

Megías, M. *et al.* (2001) 'Total number and distribution of inhibitory and excitatory synapses on hippocampal CA1 pyramidal cells', *Neuroscience*, 102(3), pp. 527–540. doi: 10.1016/S0306-4522(00)00496-6.

Mesik, L. *et al.* (2019) 'Sensory- and Motor-Related Responses of Layer 1 Neurons in the Mouse Visual Cortex', *The Journal of neuroscience : the official journal of the Society for Neuroscience*. doi: 10.1523/JNEUROSCI.1722-19.2019.

Misonou, H. *et al.* (2004) 'Regulation of ion channel localization and phosphorylation by neuronal activity', *Nature Neuroscience*. doi: 10.1038/nn1260.

Moore, J. J. *et al.* (2017) 'Dynamics of cortical dendritic membrane potential and spikes in freely behaving rats', *Science*, 355(6331), p. eaaj1497. doi: 10.1126/science.aaj1497.

Morgenstern, N. A., Bourg, J. and Petreanu, L. (2016) 'Multilaminar networks of cortical neurons integrate common inputs from sensory thalamus', *Nature Neuroscience*. doi: 10.1038/nn.4339.

Morishima, M. (2006) 'Recurrent Connection Patterns of Corticostriatal Pyramidal Cells in Frontal Cortex', *Journal of Neuroscience*, 26(16), pp. 4394–4405. doi: 10.1523/JNEUROSCI.0252-06.2006.

Nahum-Levy, R. *et al.* (2001) 'Desensitization of NMDA Receptor Channels Is Modulated by Glutamate Agonists', *Biophysical Journal*, 80(5), pp. 2152–2166. doi: 10.1016/S0006-3495(01)76188-7.

Naka, A. and Adesnik, H. (2016) 'Inhibitory Circuits in Cortical Layer 5', 10(May), pp. 1–16. doi: 10.3389/fncir.2016.00035.

Naud, R. and Sprekeler, H. (2018) 'Sparse bursts optimize information transmission in a multiplexed neural code', *Proceedings of the National Academy of Sciences of the United States of America*. doi: 10.1073/pnas.1720995115.

Nevian, T. *et al.* (2007) 'Properties of basal dendrites of layer 5 pyramidal neurons: A direct patch-clamp recording study', *Nature Neuroscience*, 10(2), pp. 206–214. doi: 10.1038/nn1826.

Niell, C. M. (2015) 'Cell Types, Circuits, and Receptive Fields in the Mouse Visual Cortex', *Annual Review of Neuroscience*, 38(1), pp. 413–431. doi: 10.1146/annurev-neuro-071714-033807.

Niell, C. M. and Stryker, M. P. (2008) 'Highly Selective Receptive Fields in Mouse Visual Cortex', *Journal of Neuroscience*. doi: 10.1523/jneurosci.0623-08.2008.

Niell, C. M. and Stryker, M. P. (2010) 'Modulation of Visual Responses by Behavioral State in Mouse Visual Cortex', *Neuron*. doi: 10.1016/j.neuron.2010.01.033.

Nimchinsky, E. A., Sabatini, B. L. and Svoboda, K. (2002) 'Structure and Function of Dendritic

Spines', *Annual Review of Physiology*, 64(1), pp. 313–353. doi: 10.1146/annurev.physiol.64.081501.160008.

Nuñez, A. *et al.* (2012) 'Cholinergic-mediated response enhancement in barrel cortex layer V pyramidal neurons', *Journal of Neurophysiology*, 108(6), pp. 1656–1668. doi: 10.1152/jn.00156.2012.

Nusser, Z. *et al.* (1998) 'Cell Type and Pathway Dependence of Synaptic AMPA Receptor Number and Variability in the Hippocampus', *Neuron*, 21(3), pp. 545–559. doi: 10.1016/S0896-6273(00)80565-6.

Olsen, S. R. *et al.* (2012) 'Gain control by layer six in cortical circuits of vision', *Nature*. doi: 10.1038/nature10835.

Oswald, A.-M. M. (2004) 'Parallel Processing of Sensory Input by Bursts and Isolated Spikes', *Journal of Neuroscience*. doi: 10.1523/jneurosci.0459-04.2004.

Pakan, J. *et al.* (2018) 'The Impact of Visual Cues, Reward, and Motor Feedback on the Representation of Behaviorally Relevant Spatial Locations in Primary Visual Cortex', *Cell Reports*, 24(10), pp. 2521–2528. doi: 10.1016/j.celrep.2018.08.010.

Pakan, J. M., Francioni, V. and Rochefort, N. L. (2018) 'Action and learning shape the activity of neuronal circuits in the visual cortex', *Current Opinion in Neurobiology*, 52, pp. 88–97. doi: 10.1016/j.conb.2018.04.020.

Pakan, J. M. P. *et al.* (2016) 'Behavioral-state modulation of inhibition is context-dependent and cell type specific in mouse visual cortex', *eLife*, 5. doi: 10.7554/eLife.14985.

Palmer, L. M. *et al.* (2012) 'The Cellular Basis of GABAB-Mediated Interhemispheric Inhibition', *Science*, 335(6071), pp. 989–993. doi: 10.1126/science.1217276.

Palmer, L. M. *et al.* (2014) 'NMDA spikes enhance action potential generation during sensory input', *Nature Neuroscience*. Nature Publishing Group, 17(3), pp. 383–390. doi: 10.1038/nn.3646.

Park, J. *et al.* (2019) 'Contribution of Apical and Basal Dendrites of L2/3 Pyramidal Neurons to Orientation Encoding in Mouse V1', *bioRxiv*, p. 566588. doi: 10.1101/566588.

Park, K. S. *et al.* (2006) 'Graded regulation of the Kv2.1 potassium channel by variable phosphorylation', *Science*. doi: 10.1126/science.1124254.

Payeur, A., Béïque, J. C. and Naud, R. (2019) 'Classes of dendritic information processing', *Current Opinion in Neurobiology*. doi: 10.1016/j.conb.2019.07.006.

Pérez-Garci, E., Larkum, M. E. and Nevian, T. (2013) 'Inhibition of dendritic Ca2+ spikes by GABAB receptors in cortical pyramidal neurons is mediated by a direct Gi/o-βγ-subunit interaction with Cav1 channels', *Journal of Physiology*. doi: 10.1113/jphysiol.2012.245464.

Peters, A. J. *et al.* (2017) 'Reorganization of corticospinal output during motor learning', *Nature Neuroscience*, 20(8), pp. 1133–1141. doi: 10.1038/nn.4596.

Petreanu, L. *et al.* (2007) 'Channelrhodopsin-2-assisted circuit mapping of long-range callosal projections', *Nature Neuroscience*. doi: 10.1038/nn1891.

Philips, R. T., Sur, M. and Chakravarthy, V. S. (2017) 'The influence of astrocytes on the width of orientation hypercolumns in visual cortex: A computational perspective', *PLoS Computational Biology*. doi: 10.1371/journal.pcbi.1005785.

Piscopo, D. M. *et al.* (2013) 'Diverse Visual Features Encoded in Mouse Lateral Geniculate Nucleus', *Journal of Neuroscience*. doi: 10.1523/jneurosci.5187-12.2013.

Polack, P. O., Friedman, J. and Golshani, P. (2013) 'Cellular mechanisms of brain state-dependent gain modulation in visual cortex', *Nature Neuroscience*. doi: 10.1038/nn.3464.

Polsky, A., Mel, B. W. and Schiller, J. (2004) 'Computational subunits in thin dendrites of pyramidal cells', *Nature Neuroscience*, 7(6), pp. 621–627. doi: 10.1038/nn1253.

Poolos, N. P. and Johnston, D. (2012) 'Dendritic ion channelopathy in acquired epilepsy', *Epilepsia*. doi: 10.1111/epi.12033.

Poort, J. *et al.* (2015) 'Learning Enhances Sensory and Multiple Non-sensory Representations in Primary Visual Cortex', *Neuron*. doi: 10.1016/j.neuron.2015.05.037.

Pouille, F. (2001) 'Enforcement of Temporal Fidelity in Pyramidal Cells by Somatic Feed-Forward Inhibition', *Science*, 293(5532), pp. 1159–1163. doi: 10.1126/science.1060342.

Rall, W. (1962) 'Theory of Physiological Properties of Dendrites', *Annals of the New York Academy of Sciences*. doi: 10.1111/j.1749-6632.1962.tb54120.x.

Ramaswamy, S. and Markram, H. (2015) 'Anatomy and physiology of the thick-tufted layer 5 pyramidal neuron', *Frontiers in Cellular Neuroscience*, 9. doi: 10.3389/fncel.2015.00233.

Ranganathan, G. N. *et al.* (2018) 'Active dendritic integration and mixed neocortical network representations during an adaptive sensing behavior', *Nature Neuroscience*. Springer US, 21(11), pp. 1583–1590. doi: 10.1038/s41593-018-0254-6.

Ranson, A. (2017) 'Stability and Plasticity of Contextual Modulation in the Mouse Visual Cortex', *Cell Reports*. doi: 10.1016/j.celrep.2016.12.080.

Remy, S. and Spruston, N. (2007) 'Dendritic spikes induce single-burst long-term potentiation', *Proceedings of the National Academy of Sciences*, 104(43), pp. 17192–17197. doi: 10.1073/pnas.0707919104.

Reuveni, I. *et al.* (1993) 'Stepwise repolarization from Ca2+ plateaus in neocortical pyramidal cells: evidence for nonhomogeneous distribution of HVA Ca2+ channels in dendrites', *The Journal of Neuroscience*, 13(11), pp. 4609–4621. doi: 10.1523/JNEUROSCI.13-11-04609.1993.

Richards, B. A. *et al.* (2019) 'A deep learning framework for neuroscience', *Nature Neuroscience*. doi: 10.1038/s41593-019-0520-2.

Romand, S. *et al.* (2011) 'Morphological Development of Thick-Tufted Layer V Pyramidal Cells in the Rat Somatosensory Cortex', *Frontiers in Neuroanatomy*, 5(February), pp. 1–27. doi: 10.3389/fnana.2011.00005.

Roome, C. J. and Kuhn, B. (2018) 'Simultaneous dendritic voltage and calcium imaging and somatic recording from Purkinje neurons in awake mice', *Nature Communications*. Springer US, 9(1), p. 3388. doi: 10.1038/s41467-018-05900-3.

Rossignol, E. *et al.* (2013) 'CaV2.1 ablation in cortical interneurons selectively impairs fast-spiking basket cells and causes generalized seizures', *Annals of Neurology*. doi: 10.1002/ana.23913.

Rudy, B. *et al.* (2011) 'Three groups of interneurons account for nearly 100% of neocortical GABAergic neurons', *Developmental Neurobiology*. doi: 10.1002/dneu.20853.

Sakata, S. and Harris, K. D. (2009) 'Laminar Structure of Spontaneous and Sensory-Evoked Population Activity in Auditory Cortex', *Neuron*, 64(3), pp. 404–418. doi: 10.1016/j.neuron.2009.09.020.

Saleem, A. B. *et al.* (2013) 'Integration of visual motion and locomotion in mouse visual cortex', *Nature Publishing Group*. Nature Publishing Group, 16(12), pp. 1864–1869. doi: 10.1038/nn.3567.

Schaefer, A. T. *et al.* (2007) 'Dendritic voltage-gated K + conductance gradient in pyramidal neurones of neocortical layer 5B from rats', *Journal of Physiology*. doi: 10.1113/jphysiol.2006.122564.

Schiller, J. *et al.* (1997) 'Calcium action potentials restricted to distal apical dendrites of rat neocortical pyramidal neurons', *The Journal of Physiology*, 505(3), pp. 605–616. doi: 10.1111/j.1469-7793.1997.605ba.x.

Schiller, J. *et al.* (2000) 'NMDA spikes in basal dendrites of cortical pyramidal neurons', *Nature*. doi: 10.1038/35005094.

Schmidt-Hieber, C. *et al.* (2017) 'Active dendritic integration as a mechanism for robust and precise grid cell firing', *Nature Neuroscience*, 20(8), pp. 1114–1121. doi: 10.1038/nn.4582.

Schmunk, G. and Gargus, J. J. (2013) 'Channelopathy pathogenesis in autism spectrum disorders', *Frontiers in Genetics*. doi: 10.3389/fgene.2013.00222.

Scholl, B. *et al.* (2013) 'Emergence of Orientation Selectivity in the Mammalian Visual Pathway', *Journal of Neuroscience*. doi: 10.1523/jneurosci.0404-13.2013.

Scholl, B., Wilson, D. E. and Fitzpatrick, D. (2017) 'Local Order within Global Disorder: Synaptic Architecture of Visual Space', *Neuron*, 96(5), pp. 1127-1138.e4. doi: 10.1016/j.neuron.2017.10.017.

Schulz, J. M. and Larkum, M. E. (2019) 'Dendritic GABAB receptors control nonlinear information transfer along the dendro-somatic axis in layer 5 pyramidal neurons', *bioRxiv*, p. 762625. doi: 10.1101/762625.

Schwindt, P. C. and Crill, W. E. (1995) 'Amplification of synaptic current by persistent sodium conductance in apical dendrite of neocortical neurons', *Journal of Neurophysiology*, 74(5), pp. 2220–2224. doi: 10.1152/jn.1995.74.5.2220.

Schwindt, P. and Crill, W. (1999) 'Mechanisms Underlying Burst and Regular Spiking Evoked by Dendritic Depolarization in Layer 5 Cortical Pyramidal Neurons', *Journal of Neurophysiology*, 81(3), pp. 1341–1354. doi: 10.1152/jn.1999.81.3.1341.

Seabrook, T. A. *et al.* (2017) 'Architecture, Function, and Assembly of the Mouse Visual System', *Annual Review of Neuroscience*. doi: 10.1146/annurev-neuro-071714-033842.

Shah, M. M., Hammond, R. S. and Hoffman, D. A. (2010) 'Dendritic ion channel trafficking and plasticity', *Trends in Neurosciences*. doi: 10.1016/j.tins.2010.03.002.

Sheets, P. L. *et al.* (2011) 'Corticospinal-specific HCN expression in mouse motor cortex: I h -dependent synaptic integration as a candidate microcircuit mechanism involved in motor control', *Journal of Neurophysiology*, 106(5), pp. 2216–2231. doi: 10.1152/jn.00232.2011.

Sheffield, M. E. J., Adoff, M. D. and Dombeck, D. A. (2017) 'Increased Prevalence of Calcium Transients across the Dendritic Arbor during Place Field Formation', *Neuron*. Elsevier Inc., 96(2), pp. 490-504.e5. doi: 10.1016/j.neuron.2017.09.029.

Sheffield, M. E. J. and Dombeck, D. A. (2015) 'Calcium transient prevalence across the dendritic arbour predicts place field properties', *Nature*, 517(7533), pp. 200–204. doi: 10.1038/nature13871.

Shepherd, G. M. G. (2013) 'Corticostriatal connectivity and its role in disease', *Nature Reviews Neuroscience*, 14(4), pp. 278–291. doi: 10.1038/nrn3469.

Shuler, M. G. and Bear, M. F. (2006) 'Reward timing in the primary visual cortex', *Science*. doi: 10.1126/science.1123513.

Silberberg, G. and Markram, H. (2007) 'Disynaptic Inhibition between Neocortical Pyramidal Cells Mediated by Martinotti Cells', *Neuron*, 53(5), pp. 735–746. doi: 10.1016/j.neuron.2007.02.012.

Sjöström, P. J. *et al.* (2008) 'Dendritic excitability and synaptic plasticity', *Physiological Reviews*. doi: 10.1152/physrev.00016.2007.

Sjöström, P. J. and Häusser, M. (2006) 'A Cooperative Switch Determines the Sign of Synaptic Plasticity in Distal Dendrites of Neocortical Pyramidal Neurons', *Neuron*, 51(2), pp. 227–238. doi: 10.1016/j.neuron.2006.06.017.

Smith, I. T. *et al.* (2017) 'Stream-dependent development of higher visual cortical areas', *Nature Neuroscience*, 20(2), pp. 200–208. doi: 10.1038/nn.4469.

Smith, S. L. *et al.* (2013) 'Dendritic spikes enhance stimulus selectivity in cortical neurons in vivo', *Nature*, 503(7474), pp. 115–120. doi: 10.1038/nature12600.

Spruston, N. *et al.* (1995) 'Activity-dependent action potential invasion and calcium influx into hippocampal CA1 dendrites', *Science*, 268(5208), pp. 297–300. doi: 10.1126/science.7716524.

Spruston, N. (2008) 'Pyramidal neurons: Dendritic structure and synaptic integration', *Nature Reviews Neuroscience*. doi: 10.1038/nrn2286.

Stafstrom, C. E. *et al.* (1985) 'Properties of persistent sodium conductance and calcium conductance of layer V neurons from cat sensorimotor cortex in vitro', *Journal of Neurophysiology*. doi: 10.1152/jn.1985.53.1.153.

Stokes, C. C. A., Teeter, C. M. and Isaacson, J. S. (2014) 'Single dendrite-targeting interneurons generate branch-specific inhibition', *Frontiers in Neural Circuits*. doi: 10.3389/fncir.2014.00139.

Stuart, G. J. and Häusser, M. (2001) 'Dendritic coincidence detection of EPSPs and action potentials', pp. 63–71.

Stuart, G. J. and Sakmann, B. (1994) 'Active propagation of somatic action potentials into neocortical pyramidal cell dendrites', *Nature*, 367(6458), pp. 69–72. doi: 10.1038/367069a0.

Stuart, G. J. and Spruston, N. (2015) 'Dendritic integration: 60 years of progress', *Nature Neuroscience*, 18(12), pp. 1713–1721. doi: 10.1038/nn.4157.

Stuart, G., Schiller, J. and Sakmann, B. (1997) 'Action potential initiation and propagation in rat neocortical pyramidal neurons', *The Journal of Physiology*, 505(3), pp. 617–632. doi: 10.1111/j.1469-7793.1997.617ba.x.

Sun, Q. *et al.* (2014) 'Dendritic Na+ spikes enable cortical input to drive action potential output from hippocampal CA2 pyramidal neurons', *eLife*, 3(November), pp. 1–24. doi:

10.7554/eLife.04551.

Sun, W. *et al.* (2016) 'Thalamus provides layer 4 of primary visual cortex with orientation- and direction-tuned inputs', 1(2). doi: 10.1038/nn.4196.

Suter, B. A., Migliore, M. and Shepherd, G. M. G. (2013) 'Intrinsic Electrophysiology of Mouse Corticospinal Neurons: a Class-Specific Triad of Spike-Related Properties', *Cerebral Cortex*, 23(8), pp. 1965–1977. doi: 10.1093/cercor/bhs184.

Svoboda, K. *et al.* (1997) 'In vivo dendritic calcium dynamics in neocortical pyramidal neurons', *Nature*, 385(6612), pp. 161–165. doi: 10.1038/385161a0.

Svoboda, K. *et al.* (1999) 'Spread of dendritic excitation in layer 2/3 pyramidal neurons in rat barrel cortex in vivo', *Nat Neurosci*, 2, pp. 65–73. doi: 10.1038/4569.

Swadlow, H. A. (1994) 'Efferent neurons and suspected interneurons in motor cortex of the awake rabbit: axonal properties, sensory receptive fields, and subthreshold synaptic inputs', *Journal of Neurophysiology*, 71(2), pp. 437–453. doi: 10.1152/jn.1994.71.2.437.

Szél, Á. and Röhlich, P. (1992) 'Two cone types of rat retina detected by anti-visual pigment antibodies', *Experimental Eye Research*. doi: 10.1016/0014-4835(92)90090-F.

Takahashi, N. *et al.* (2016) 'Active cortical dendrites modulate perception', *Science*, 354(6319), pp. 1587–1590. doi: 10.1126/science.aah6066.

Tamás, G. *et al.* (2003) 'Identified sources and targets of slow inhibition in the neocortex', *Science*. doi: 10.1126/science.1082053.

Thomson (2010) 'Neocortical layer 6, a review', *Frontiers in Neuroanatomy*. doi: 10.3389/fnana.2010.00013.

Thomson, A. M. (2007) 'Functional maps of neocortical local circuitry', *Frontiers in Neuroscience*. doi: 10.3389/neuro.01.1.1.002.2007.

Tjia, M. *et al.* (2017) 'Pyramidal Neurons in Different Cortical Layers Exhibit Distinct Dynamics and Plasticity of Apical Dendritic Spines', *Frontiers in Neural Circuits*. doi: 10.3389/fncir.2017.00043.

Tremblay, R., Lee, S. and Rudy, B. (2016) 'GABAergic Interneurons in the Neocortex: From Cellular Properties to Circuits', *Neuron*, 91(2), pp. 260–292. doi: 10.1016/j.neuron.2016.06.033.

Tsay, D. and Yuste, R. (2004) 'On the electrical function of dendritic spines', *Trends in Neurosciences*, 27(2), pp. 77–83. doi: 10.1016/j.tins.2003.11.008.

Ujfalussy, B. B. *et al.* (2015) 'Dendritic nonlinearities are tuned for efficient spike-based computations in cortical circuits.', *eLife*, 4, p. e10056. doi: 10.7554/eLife.10056.

Ujfalussy, B. B. *et al.* (2018) 'Global and Multiplexed Dendritic Computations under In Vivo-like Conditions', *Neuron*. doi: 10.1016/j.neuron.2018.08.032.

Ulrich, D. (2002) 'Dendritic Resonance in Rat Neocortical Pyramidal Cells', *Journal of Neurophysiology*, 87(6), pp. 2753–2759. doi: 10.1152/jn.2002.87.6.2753.

Urban-Ciecko, J. and Barth, A. L. (2016) 'Somatostatin-expressing neurons in cortical networks', *Nature Reviews Neuroscience*. Nature Publishing Group. doi: 10.1038/nrn.2016.53.

Varga, Z. *et al.* (2011) 'Dendritic coding of multiple sensory inputs in single cortical neurons

in vivo', *Proceedings of the National Academy of Sciences*, 108(37), pp. 15420–15425. doi: 10.1073/pnas.1112355108.

Veilleux, C. C. and Kirk, E. C. (2014) 'Visual acuity in mammals: Effects of eye size and ecology', *Brain, Behavior and Evolution*. doi: 10.1159/000357830.

Vélez-Fort, M. *et al.* (2014) 'The Stimulus Selectivity and Connectivity of Layer Six Principal Cells Reveals Cortical Microcircuits Underlying Visual Processing', *Neuron*, 83(6), pp. 1431–1443. doi: 10.1016/j.neuron.2014.08.001.

Vetter, P., Roth, A. and Häusser, M. (2001) 'Propagation of Action Potentials in Dendrites Depends on Dendritic Morphology', *Journal of Neurophysiology*, 85(2), pp. 926–937. doi: 10.1152/jn.2001.85.2.926.

Vinck, M. *et al.* (2015) 'Arousal and Locomotion Make Distinct Contributions to Cortical Activity Patterns and Visual Encoding', *Neuron*, 86(3), pp. 740–754. doi: 10.1016/j.neuron.2015.03.028.

Voigts, J. and Harnett, M. T. (2019) 'Somatic and Dendritic Encoding of Spatial Variables in Retrosplenial Cortex Differs during 2D Navigation', *Neuron*. doi: 10.1016/J.NEURON.2019.10.016.

Wang, Q. and Burkhalter, A. (2007) 'Area map of mouse visual cortex', *Journal of Comparative Neurology*. doi: 10.1002/cne.21286.

Wang, X. *et al.* (2013) 'Distribution of CaMKIIα expression in the brain in vivo, studied by CaMKIIα-GFP mice', *Brain Research*, 1518, pp. 9–25. doi: 10.1016/j.brainres.2013.04.042.

Wang, Y. *et al.* (2004) 'Anatomical, physiological and molecular properties of Martinotti cells in the somatosensory cortex of the juvenile rat', *Journal of Physiology*. doi: 10.1113/jphysiol.2004.073353.

Waters, J. *et al.* (2003) 'Supralinear Ca2+ influx into dendritic tufts of layer 2/3 neocortical pyramidal neurons in vitro and in vivo', *Journal of Neuroscience*, 23(24), pp. 8558–8567. doi: 10.1523/jneurosci.23-24-08558.2003.

Wertz, A. *et al.* (2015) 'Single-cell–initiated monosynaptic tracing reveals layer-specific cortical network modules', *Science*, 349(6243), pp. 70–74. doi: 10.1126/science.aab1687.

Williams, S. R. (2002) 'Dependence of EPSP Efficacy on Synapse Location in Neocortical Pyramidal Neurons', *Science*, 295(5561), pp. 1907–1910. doi: 10.1126/science.1067903.

Williams, S. R. and Fletcher, L. N. (2019) 'A Dendritic Substrate for the Cholinergic Control of Neocortical Output Neurons', *Neuron*. doi: 10.1016/j.neuron.2018.11.035.

Williams, S. R. and Stuart, G. J. (1999) 'Mechanisms and consequences of action potential burst firing in rat neocortical pyramidal neurons', *Journal of Physiology*. doi: 10.1111/j.1469-7793.1999.00467.x.

Williams, S. R. and Stuart, G. J. (2002) 'Dependence of EPSP efficacy on synapse location in neocortical pyramidal neurons', *Science*. doi: 10.1126/science.1067903.

Williams, S. R. and Stuart, G. J. (2017) ' Site Independence of EPSP Time Course Is Mediated by Dendritic I h in Neocortical Pyramidal Neurons ', *Journal of Neurophysiology*. doi: 10.1152/jn.2000.83.5.3177.

Wilson, D. E. *et al.* (2016) 'Orientation selectivity and the functional clustering of synaptic inputs in primary visual cortex', *Nature Neuroscience*, 19(8), pp. 1003–1009. doi:

10.1038/nn.4323.

Xu, N. *et al.* (2012) 'Nonlinear dendritic integration of sensory and motor input during an active sensing task.', *Nature*. Nature Publishing Group, 492(7428), pp. 247–51. doi: 10.1038/nature11601.

Xu, X., Roby, K. D. and Callaway, E. M. (2010) 'Immunochemical characterization of inhibitory mouse cortical neurons: Three chemically distinct classes of inhibitory cells', *Journal of Comparative Neurology*. doi: 10.1002/cne.22229.

Yaeger, C. E., Ringach, D. L. and Trachtenberg, J. T. (2019) 'Neuromodulatory control of localized dendritic spiking in critical period cortex', *Nature*. Springer US, pp. 100–104. doi: 10.1038/s41586-019-0963-3.

Yang, G. *et al.* (2014) 'Sleep promotes branch-specific formation of dendritic spines after learning.', *Science (New York, N.Y.)*, 344(6188), pp. 1173–8. doi: 10.1126/science.1249098.

Yavorska, I. and Wehr, M. (2016) 'Somatostatin-Expressing Inhibitory Interneurons in Cortical Circuits', *Frontiers in Neural Circuits*, 10. doi: 10.3389/fncir.2016.00076.

Yilmaz, M. and Meister, M. (2013) 'Rapid innate defensive responses of mice to looming visual stimuli', *Current Biology*. doi: 10.1016/j.cub.2013.08.015.

Young, H. *et al.* (2019) 'Laminar-specific cortico-cortical loops in mouse visual cortex', *bioRxiv*. doi: 10.1101/773085.

Yuste, R. *et al.* (1994) 'Ca2+ accumulations in dendrites of neocortical pyramidal neurons: An apical band and evidence for two functional compartments', *Neuron*, 13(1), pp. 23–43. doi: 10.1016/0896-6273(94)90457-X.

Yuste, R. and Denk, W. (1995) 'Dendritic spines as basic functional units of neuronal integration', *Nature*, 375(6533), pp. 682–684. doi: 10.1038/375682a0.

Zhao, X. *et al.* (2013) 'Orientation-selective Responses in the Mouse Lateral Geniculate Nucleus', *Journal of Neuroscience*. doi: 10.1523/jneurosci.0095-13.2013.

Zmarz, P. and Keller, G. B. (2016) 'Mismatch Receptive Fields in Mouse Visual Cortex', *Neuron*. Elsevier Inc., 92(4), pp. 766–772. doi: 10.1016/j.neuron.2016.09.057.

Appendix 1: Francioni V., Padamsey Z. and Rochefort, N. L. (2019)

eLIFE elifesciences.org

RESEARCH ARTICLE

High and asymmetric somato-dendritic coupling of V1 layer 5 neurons independent of visual stimulation and locomotion

Valerio Francioni[1,2], Zahid Padamsey[1], Nathalie L Rochefort[1,2]*

[1]Centre for Discovery Brain Sciences, Edinburgh Medical School, Biomedical Sciences, University of Edinburgh, Edinburgh, United Kingdom; [2]Simons Initiative for the Developing Brain, University of Edinburgh, Edinburgh, United Kingdom

Abstract Active dendrites impact sensory processing and behaviour. However, it remains unclear how active dendritic integration relates to somatic output in vivo. We imaged semi-simultaneously GCaMP6s signals in the soma, trunk and distal tuft dendrites of layer 5 pyramidal neurons in the awake mouse primary visual cortex. We found that apical tuft signals were dominated by widespread, highly correlated calcium transients throughout the tuft. While these signals were highly coupled to trunk and somatic transients, the frequency of calcium transients was found to decrease in a distance-dependent manner from soma to tuft. Ex vivo recordings suggest that low-frequency back-propagating action potentials underlie the distance-dependent loss of signals, while coupled somato-dendritic signals can be triggered by high-frequency somatic bursts or strong apical tuft depolarization. Visual stimulation and locomotion increased neuronal activity without affecting somato-dendritic coupling. High, asymmetric somato-dendritic coupling is therefore a widespread feature of layer 5 neurons activity in vivo.

***For correspondence:** n.rochefort@ed.ac.uk

Competing interests: The authors declare that no competing interests exist.

Funding: See page 22

Received: 10 July 2019
Accepted: 22 December 2019
Published: 27 December 2019

Reviewing editor: Yukiko Goda, RIKEN, Japan

Introduction

Active dendritic conductances impact the integration of synaptic inputs and the resulting somatic output (***Grienberger et al., 2015***; ***Stuart and Spruston, 2015***). Different types of active dendritic currents have been described to support local dendritic nonlinear events, primarily driven by NMDA- and voltage-gated conductances (***Schiller et al., 1997***; ***Larkum et al., 1999b***). In cortical layer 5 pyramidal neurons, nonlinear dendritic spikes have been reported in the long apical dendrite and tuft, both in vitro and in vivo (***Grienberger et al., 2015***; ***Stuart and Spruston, 2015***). These dendritic events are generally associated with calcium influx both locally and globally in the apical tuft (***Xu et al., 2012***; ***Hill et al., 2013***; ***Palmer et al., 2014***; ***Cichon and Gan, 2015***; ***Manita et al., 2015***; ***Takahashi et al., 2016***). Additionally, the coincident occurrence of back-propagating action potentials and tuft depolarization was shown to generate widespread calcium transients in the apical tuft dendrites (***Spruston et al., 1995***; ***Magee, 1997***; ***Svoboda et al., 1997***; ***Helmchen et al., 1999***; ***Larkum et al., 1999b***; ***Waters et al., 2003***; ***Manita et al., 2015***).

The frequency and dynamics of local dendritic nonlinearities in vivo have been a matter of debate. Events described as local dendritically-generated spikes were reported in layer 2/3 neurons of the visual and somatosensory cortex during sensory stimulation (***Smith et al., 2013***; ***Palmer et al., 2014***). In the visual cortex, it has been suggested that dendritic spikes triggered by visual input enhance somatic tuning to the preferred orientation (***Smith et al., 2013***). However, single dendrite recordings prevented conclusions about the spatial extent and the branch-specific nature of the detected events. Using calcium imaging in the mouse motor cortex, one study suggested that

individual branches of densely labelled layer 5 neurons selectively display local calcium transients correlated with specific motor outputs (**Cichon and Gan, 2015**). However, other studies reported prevalent global calcium signals throughout layer 5 apical tuft dendrites in the barrel and motor cortex (**Xu et al., 2012**; **Hill et al., 2013**). While layer 5 apical dendritic calcium transients were shown to correlate with behaviourally relevant features (**Xu et al., 2012**; **Takahashi et al., 2016**; **Peters et al., 2017**; **Ranganathan et al., 2018**; **Kerlin et al., 2019**), the coupling between apical tuft activity and somatic output remains poorly understood.

By using semi-simultaneous imaging of apical trunk and somatic GCaMP6f signals in layer 5 neurons, a recent study has shown that apical trunk dendritic calcium signals were highly correlated with somatic signals in the primary visual cortex (V1) of awake behaving mice (**Beaulieu-Laroche et al., 2019**). Layer 5 pyramidal neurons in V1 display selective responses to physical features of visual stimuli, such as the orientation and direction of movement (**Niell and Stryker, 2008**; **Kim et al., 2015**) and their activity is modulated by locomotion (**Erisken et al., 2014**; **Dadarlat and Stryker, 2017**; **Pakan et al., 2018a**). However, **Beaulieu-Laroche et al. (2019)** found that neither visual stimulation nor locomotion altered the high somato-dendritic coupling of calcium transients.

Here, we used a similar approach to image GCaMP6s calcium signals in the soma, trunk and distal tuft dendrites of layer 5 pyramidal neurons, both in darkness and during the presentation of drifting gratings, while head-fixed mice were either running or stationary. In agreement with **Beaulieu-Laroche et al. (2019)**, we found that the apical trunk dendritic calcium signals were highly correlated with somatic signals. We extended these results by showing that the whole apical tuft was highly correlated to trunk activity; the vast majority of dendritic calcium transients in the apical tuft were coincident with global events, with rare cases of branch-specific activity, limited to the smallest amplitude events. In addition, by imaging somatic and dendritic GCaMP6s signals, we found that somato-dendritic coupling was asymmetric; while almost all events observed in the tuft were also visible in the soma, around 40% of somatic events attenuated in an amplitude and distance-dependent manner from the soma to the apical tuft. Ex vivo recordings of GCaMP6s signals suggested that coupled somato-dendritic events likely reflected either strong apical tuft inputs or high frequency somatic activity, whereas attenuated events were likely caused by low frequency back-propagating action potentials. We compared GCaMP6s with GCaMP6f signals and showed that due to a reduced sensitivity, attenuation of events from soma to dendrite were underestimated with GCaMP6f (**Beaulieu-Laroche et al., 2019**). Finally, our results show that neither visual stimulation nor locomotion affected the in vivo coupling of somatic and apical tuft calcium signals.

Results

Highly correlated, widespread calcium signals in apical tuft dendrites of single layer 5 neurons

We imaged changes in fluorescence over time in apical dendrites of individual layer 5 pyramidal neurons sparsely labelled with either the calcium sensor GCaMP6s or GCaMP6f (**Chen et al., 2013**) in the primary visual cortex of adult mice. Using single-plane two-photon imaging (at 120 Hz), we first monitored changes of GCaMP6f signals in individual apical tuft dendrites of head-fixed, awake behaving mice that were free to run on a cylindrical treadmill (**Figure 1A**). Our results showed highly correlated calcium signals in all apical dendritic branches belonging to the same neuron and imaged in a given field of view (Pearson's correlation coefficient r = 0.92, SEM = 0.01, n = 25 fields of view recorded from 14 neurons, 6 animals) (**Figure 1B, C and D**). Given that electrical signals are known to attenuate in a distant dependent manner, we tested whether the correlation of calcium transients between apical tuft branches decreased with distance from the apical trunk (nexus). We reconstructed each individual neuron for which we imaged the apical tuft and quantified the correlation of fluorescence signals across sibling branches. We found that calcium signals in sibling branches were highly correlated (average Pearson's correlation coefficient r = 0.92) regardless of their branching order (One-way ANOVA, p=0.34) (**Figure 1E and F**). In addition to the global, widespread calcium transients, we also observed in individual spines, calcium signals that were not correlated with dendritic signals (**Figure 1—figure supplement 1**), indicating that we could resolve spine calcium signals in our experimental conditions.

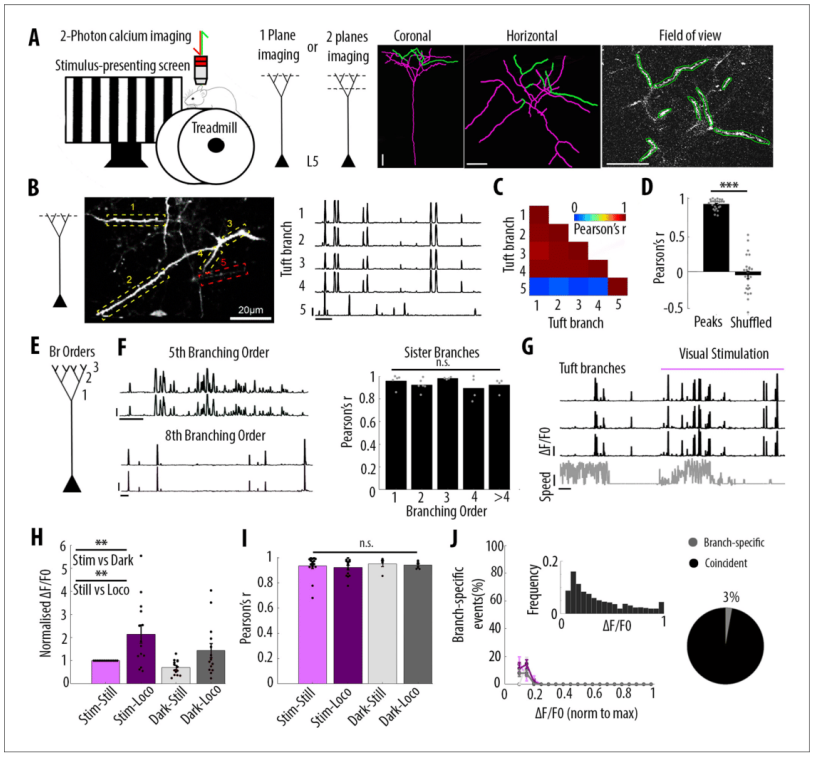

Figure 1. Highly correlated activity in the whole apical tuft of layer 5 pyramidal neurons. (**A**) Schematic of the methodological approach. Calcium transients were recorded either in multiple apical tuft dendrites in a single focal plane, or semi-simultaneously in different compartments of individual neurons (Soma, Trunk and Tuft). At the end of each imaging session, a z-stack was recorded for post-hoc reconstruction of each imaged neuron. (**B**) Single plane imaging of the apical tuft branches of an individual layer 5 neuron. GCaMP6f-calcium transients of the apical tuft branches belonging to one neuron are shown in traces 1 to 4 while calcium transients of a tuft branch belonging to a different neuron is shown in trace 5. Scale bars, 0.3 ΔF/F0 (normalised to max), 20 s. (**C**) Pearson's correlation matrix between the calcium transients of the branches shown in B. Branches that belong to the same neuron (branches 1 to 4, neuron 1) have a mean Pearson's correlation of 0.96, while the branch that belongs to the different neuron (branch 5, neuron 2) has a mean Pearson's correlation value of 0.13 with neuron 1's branches. (**D**) Mean Pearson's correlation value between tuft dendrites calcium transient peak amplitudes for each imaged field of view and corresponding shuffled data (Paired t-test, $p=3.5e^{-15}$; mean = 0.92 and −0.04, sem = 0.01 and 0.05 for branches and shuffled data, respectively; n = 25 fields of view; coming from 14 neurons; six animals; 70 branches). (**E**) Schematic of the definition of branching orders. (**F**) Two representative traces of sibling branches belonging to the 5th and 8th branching order and a quantification of the Pearson's correlation for sibling tuft branches of different branching orders (right panel). (For 1st, 2nd, 3rd, 4th and more than 4th branching order, One-way ANOVA, p=0.34; mean = 0.96; 0.92; 0.98; 0.89; 0.92, sem = 0.02; 0.02; 0.01; 0.05; 0.03, n = 5; 6; 4; 4; 4 pairs of branches, respectively). Scale bars, 0.3 ΔF/F0 (normalised to max), 20 s. (**G**) Representative traces of 3 tuft branches belonging to the same neuron while the animal was either stationary or running (grey signal, speed) during either darkness or the presentation of drifting gratings (purple segment). Scale bars, 12 cm/s, 0.3 ΔF/F0 (normalised to max), 20 s. (**H**) Mean ΔF/F0 for apical tuft dendrites during darkness (dark) and visual stimulation (stim) while the animal was either stationary (still) or running (loco). Bar graph is normalised to visual stimulation during stationary condition. Both visual stimulation and locomotion significantly increase the mean ΔF/F0 of tuft branches without any interaction effect (Repeated Measures Two-way ANOVA on log-transformed data, p=0.005, 0.003 and 0.99 for

Figure 1 continued on next page

Figure 1 continued

stim, loco and interaction effects respectively, mean (normalised to condition stim/still)=1; 2.15; 0.7; 1.4, sem = 0; 0.38; 0.08 and 0.3, n = 14 neurons). (**I**) Pearson's correlation coefficients between tuft dendrites calcium transients of individual neurons during stim-still, stim-loco, dark-still and dark-loco conditions. (Two-way ANOVA, p=0.43, 0.62 and 0.97 for stim, loco and interaction effects; mean = 0.93; 0.92; 0.95 and 0.94, sem = 0.02; 0.02; 0.02; 0.01, n = 16; 14; 5 and 7 fields of views respectively, from 14 neurons). (**J**) Proportion of branch-specific events as a function of GCaMP6f calcium transients' amplitude for the four different conditions (left panel). Neither visual stimulation nor locomotion nor an interaction effect significantly increased the number of branch-specific events (Three-way ANOVA, p=0.29; 0.8 and 0.94, respectively; $p<10^{-15}$ for event amplitude; n = 70 branches from 14 neurons; 6 animals). *Inset*, frequency distribution of the calcium transients' amplitudes detected in the apical tuft branches. *Right panel*, pie chart showing that, on average, 3% of all calcium transients were detected as branch-specific (detected in one apical tuft dendritic branch and not detected in the other imaged branches).
The online version of this article includes the following figure supplement(s) for figure 1:

Figure supplement 1. Single spine calcium transients in the apical tuft dendrites of layer 5 neurons.
Figure supplement 2. Impact of different thresholds and coincident windows on the quantification of branch-specific and compartment-specific events.

We then assessed whether these widespread, highly correlated apical tuft calcium signals were modulated by visual stimulation and locomotion. We found that both visual stimulation and locomotion increased calcium signals in the apical tuft of layer 5 neurons (mean ΔF/F0; repeated measures Two-way ANOVA, p=0.005, 0.003 and 0.99 for visual stimulation, locomotion and interaction between both conditions, respectively; n = 14 neurons) (***Figure 1G and H***). However, the correlation of calcium signals between all imaged dendritic branches remained high ($r \geq 0.92$) during periods of darkness and visual stimulation as well as during stationary and locomotion periods, without a significant difference across conditions (Two-way ANOVA, p=0.43, 0.62 and 0.97 for visual stimulation, locomotion and interaction between both conditions, respectively) (***Figure 1I***).

In line with these findings, we found that branch-specific activity in the apical tuft was rare. We quantified the amount of branch-specific activity in all pairs of branches belonging to the same neuron as the proportion of calcium transients present in one branch and absent in the other. Among the 70 imaged branches across 14 neurons, branch-specific calcium transients represented less than 3% of the total number of transients. Among all imaged calcium transients, these local signals were dominated by calcium transients of the smallest amplitudes (***Figure 1J***). In addition, neither visual stimulation nor locomotion significantly affected this small proportion of branch-specific calcium signals (Three-way ANOVA, $p<10^{-15}$ for event amplitude and p=0.29; 0.8 and 0.94, for visual stimulation, locomotion and interaction between both conditions, respectively; no other interaction effect was statistically significant) (***Figure 1J***). We tested the robustness of our quantification by using different thresholds for the detection of individual calcium transients (***Figure 1—figure supplement 2A and B***). We found that lowering the threshold by 30% in one of the two pair branches reduced the proportion of branch-specific events from 3.8% to 0.8%, suggesting that most of these already rare events were near detection threshold (***Figure 1—figure supplement 2B***). We also confirmed that our results were not affected by the time window that we used to detect coincident events in pairs of dendritic branches (***Figure 1—figure supplement 2D and E***).

Altogether, our results show that apical dendritic calcium signals in V1 layer 5 neurons are almost exclusively dominated by highly correlated calcium transients in the whole apical tuft regardless of the dendritic branching order. Neither visual stimulation nor locomotion modulated this high correlation between apical tuft dendritic calcium signals.

Calcium signals are highly correlated throughout all compartments of individual layer 5 neurons

We then assessed how global, widespread apical tuft calcium signals were coupled across neuronal compartments. For this, we semi-simultaneously imaged GCaMP6s calcium signals at two focal planes, separated by 170 µm in depth, in four different pairs of neuronal compartments from the soma to the apical tuft: Soma-Trunk, proximal Trunk-distal Trunk, distal Trunk-apical Tuft, proximal Tuft-distal Tuft (***Figure 2A and B***). We used GCaMP6s which has higher signal amplitude and signal-to-noise ratio than GCaMP6f, in order to maximise our ability to detect somatic signals (***Chen et al.,***

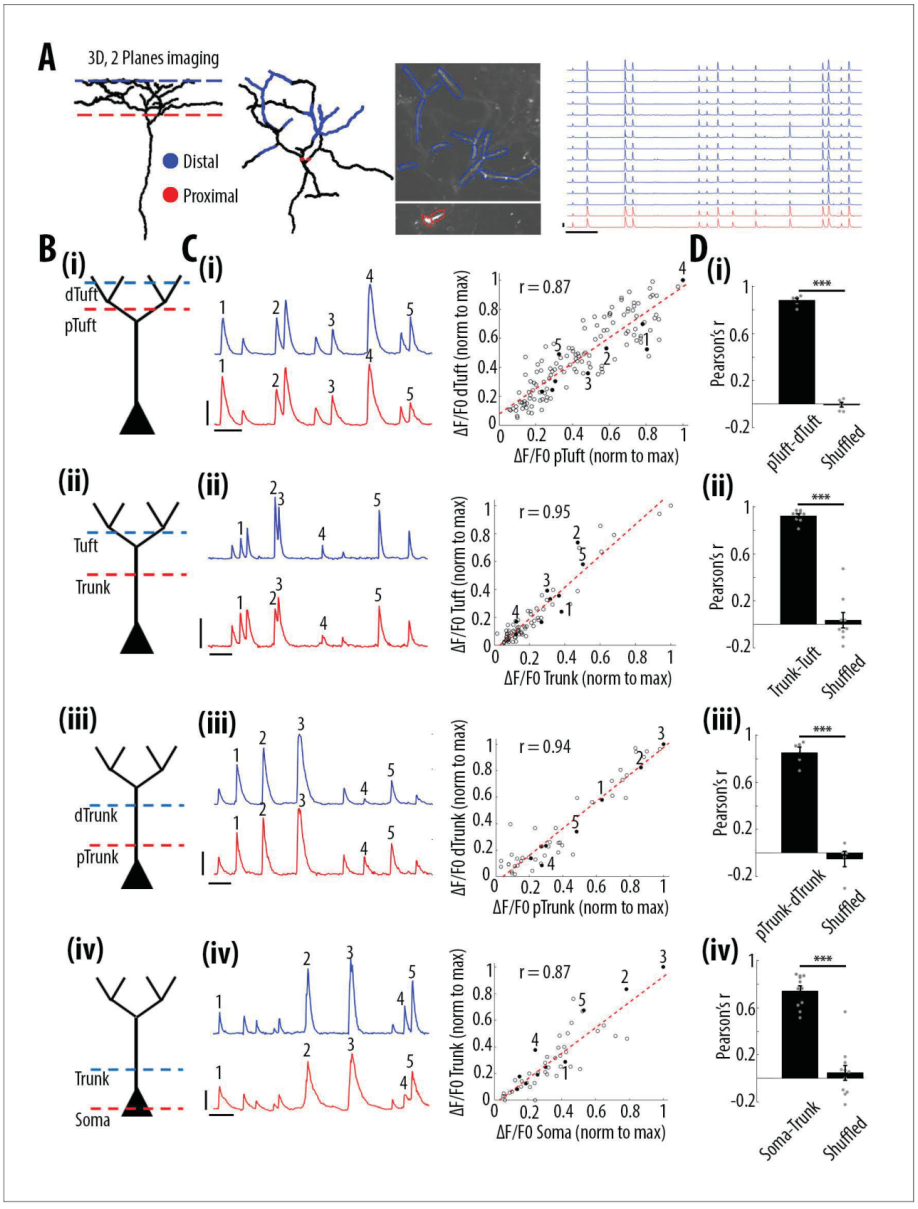

Figure 2. High correlation of calcium transients between neuronal compartments (soma, trunk, apical tuft) of individual layer 5 neurons. (**A**) Anatomical reconstruction of an individual GCaMP6s-labeled layer 5 pyramidal neuron imaged at two focal planes semi-simultaneously (red dotted lines, proximal; blue, distal). *Left panel*, coronal and horizontal views of the same imaged neuron. *Right panel*, two-photon image of dendritic branches highlighted in red and blue in the horizontal view of the anatomical reconstruction. Example ΔF/F0 traces of highly correlated calcium transients from dendritic

Figure 2 continued on next page

Figure 2 continued

branches indicated in red and blue. (**B**) Schemata of the compartments imaged semi-simultaneously, (**i**) proximal tuft-distal tuft, (ii) trunk-tuft, (iii), trunk-trunk, (iv) soma-trunk. pTrunk, dTrunk and pTuft, dTuft indicate proximal and distal portions of the trunk and the apical tuft, respectively. (**C**) *Left panel*, representative GCaMP6s transients imaged in two neuronal compartments semi-simultaneously as shown in B. *Right panel*, scatter plot of peak amplitudes of individual calcium transients in proximal and distal compartments imaged semi-simultaneously, in one example individual neuron. Each dot represents a calcium transient. Peak amplitudes were normalized to the maximum amplitude in each compartment. Filled dots correspond to the transients indicated by numbers in the left panel. Red dotted line indicates the best fit (least square). Pearson's correlation values (**r**) are indicated for each example pair of neuronal compartments. Scale bars 0.3 ΔF/F0 (normalised to max), 10 s. (**D**) Pearson's correlation values for each pair of compartments imaged semi-simultaneously and corresponding shuffled data (Paired t-test, (i)pTuft-dTuft, $p=1.6e^{-6}$, mean = 0.88; −0.01, sem = 0.02; 0.02, n = 6 pairs; (ii)Trunk-Tuft, $p=8e^{-7}$, mean = 0.92; 0.04, sem = 0.02; 0.07, n = 9; (iii) pTrunk-dTrunk, $p=4.4e^{-4}$, mean = 0.85; −0.05, sem = 0.05; 0.07, n = 5; (iv) Soma-Trunk, $p=4.4e^{-6}$, mean = 0.74; 0.05, sem = 0.04; 0.06, n = 11).
The online version of this article includes the following figure supplement(s) for figure 2:

Figure supplement 1. Scatter plots of peak amplitudes of individual calcium transients in all proximal and distal compartments imaged semi-simultaneously.
Figure supplement 2. Most dendritic events detected as branch-specific were also detected in the trunk.

2013). We found that calcium transients simultaneously imaged in each pair of proximal and distal compartments were highly correlated (***Figure 2A-D***). Since the rise and decay kinetics of calcium events were slower in the soma than in the dendrites, we performed our quantification on individual peaks of calcium transients (see Materials and methods). For each pair of compartments, we found that the average Pearson's correlation value between the peak amplitude of individual transients was 0.88 between the proximal and distal parts of the apical tuft, 0.92 between the trunk and the apical tuft and 0.85 between the proximal and distal trunk (***Figure 2D*** and ***Figure 2—figure supplement 1***). The lowest correlation value was found between the soma and the proximal trunk (0.74, ***Figure 2D***). These results also confirmed the high correlation of calcium transients throughout the apical tuft (***Figure 2A***, 2D(i)), that we found in our single-plane imaging experiments (***Figure 1D and F***). We checked whether the small proportion of events (3%) that were detected as branch-specific in apical tuft dendrites were also found in the apical trunk. On average, we found that 60% of the events detected as branch-specific were also found in the trunk (***Figure 2—figure supplement 2***).

Altogether, these results show that calcium transient amplitudes were highly correlated from the soma to the distal apical tuft of V1 layer 5 neurons.

Frequency of calcium transients decreases in a distance- and amplitude-dependent manner from soma to apical tuft

We then tested whether the high correlation of calcium transient amplitudes from the soma to the apical tuft was associated with distance-dependent changes in the frequency of these events. We quantified the frequency of GCaMP6s transients in each pair of proximal and distal compartments imaged semi-simultaneously (***Figure 3A***). We found that the frequency of calcium transients decreased from proximal to distal compartments (Paired t-test, $p=1.1e^{-6}$, n = 31 pairs of compartments from 19 neurons) by an average of 14% from soma to proximal trunk, 8% from proximal to distal trunk, 24% from distal trunk to apical tuft and 22% from proximal tuft to distal tuft (***Figure 3B***). From these proportions, we estimated a decrease of about 40% of calcium transients from soma to the distal part of the apical tuft (***Figure 3—figure supplement 1A and B***). This result was confirmed by a second data set, in which somatic and apical tuft calcium transients were imaged independently (at 120 Hz) in individual layer 5 neurons. We found that the mean frequency of calcium transients in the apical tuft corresponded to 62% of the frequency of events in the corresponding soma (n = 13 neurons ***Figure 3—figure supplement 1C***).

We then checked whether this decrease in frequency depended on the amplitude of the calcium transients. We calculated the percentage of compartment-specific calcium transients as a function of their amplitude (***Figure 3C***). Our results show that smaller amplitude calcium transients in the proximal compartment were more likely to attenuate below detection level in the distal compartment compared to larger amplitudes events (red trace in ***Figure 3C***). The vast majority of compartment-specific events were dominated by calcium transients in proximal compartments that were not detected in distal ones (red trace in ***Figure 3C***), while only few calcium transients were found in distal compartments and not in the corresponding proximal compartment (blue trace in ***Figure 3C***)

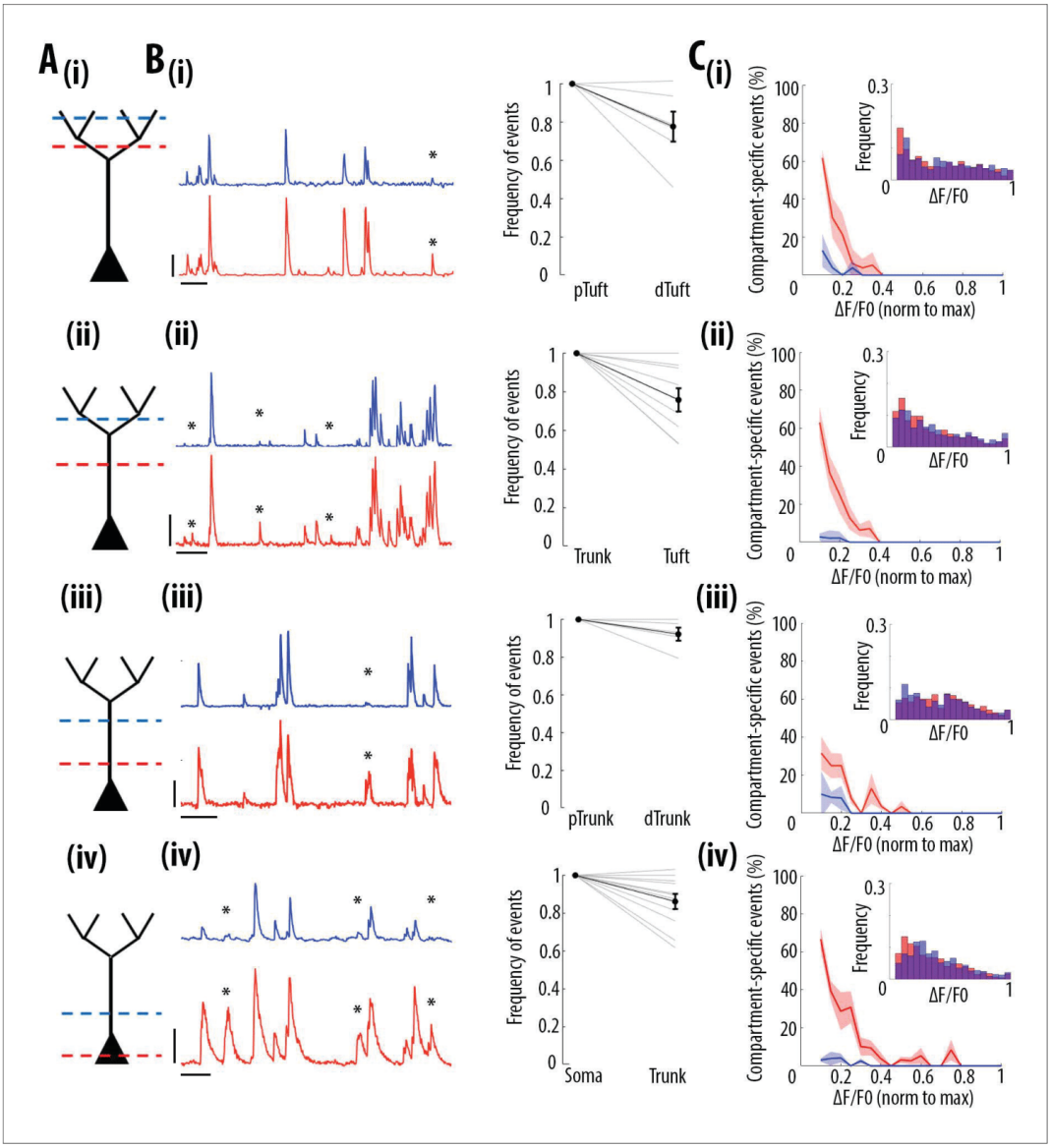

Figure 3. Frequency of calcium transients decreases in a distance and amplitude-dependent dependent manner from the soma to the apical tuft. (**A**) Schemata of the neuronal compartments imaged simultaneously in individual layer 5 neurons. (**B**) *Left panel*, representative ΔF/F0 traces of GCaMP6s calcium transients imaged semi-simultaneously in two different compartments as indicated in panel A. Asterisks indicate calcium transients detected in the proximal compartment (red trace) and not detected in the distal one (blue trace). Scale bars 0.25 ΔF/F0 (normalised to max), 20 s. *Right panel*, frequency of detected calcium transients, normalised to the proximal compartment. Individual lines represent individual neurons. Error bar: SEM. (**C**)

Figure 3 continued on next page

Figure 3 continued

Proportion of compartment-specific events as a function of calcium transients' amplitude. In red, proportion of events only detected in the proximal compartment. In blue, proportion of events only detected in the distal compartment. Thick line represents the weighted mean proportion. Shaded area represents the weighted sem for each bin (0.05). *Upper right panel*, frequency histogram of calcium transient peak amplitudes detected in the proximal (red) and distal (blue) compartments. Peak amplitudes were normalized to the maximum amplitude in each compartment. For all compartments, event amplitude, compartment (proximal vs distal) and an interaction between these two factors significantly affected the proportion of compartment-specific events (Two-way ANOVA, (i)pTuft-dTuft, $p<10^{-15}$, $p=7.8\times10^{-5}$, $p=6.2\times10^{-8}$, for event amplitude, proximal versus distal compartment and interaction between amplitude and compartment, respectively, n = 6 pairs; (ii)Trunk-Tuft, $p<10^{-15}$, $p=3.4\times10^{-9}$, $p<10^{-15}$, n = 9; (iii) pTrunk-dTrunk, $p=1.3\times10^{-13}$, $p=2.4\times10^{-4}$, $p=7\times10^{-3}$, n = 5; (iv) Soma-Trunk, $p<10^{-15}$, $p<10^{-15}$ and $p<10^{-15}$, n = 11).
The online version of this article includes the following figure supplement(s) for figure 3:

Figure supplement 1. Frequency decrease of calcium transients from soma to apical tuft.

(see also ***Video 1*** and ***Video 2***). As a result, compartment-specific events were dominated by small amplitude calcium transients that attenuated from proximal to distal compartments (Two-way ANOVA, $p<10^{-15}$, $p<10^{-15}$, $p<10^{-15}$, for compartment (proximal vs distal), amplitude, and interaction effect, respectively; Figure 5A). Our results were robust to the threshold (+/- 30%) that was used for detecting calcium transients (***Figure 1—figure supplement 2A and C***). Our results were also robust to the time window that was used to detect simultaneous events in different compartments (***Figure 1—figure supplement 2D and F***). Notably, we also observed relatively large calcium transients in soma and proximal trunk that were not detected in the distal compartment (see examples in ***Figure 3B (iii) and (iv)*** and percentage of compartment-specific event in ***Figure 3C (iii) and (iv)*** for ΔF/F0 >0.3), suggesting the presence of active mechanisms inhibiting calcium transients along the apical trunk.

These results indicate that almost all distal events were found in proximal compartments, while at least 40% of somatic transients attenuate in a distance-dependent manner along the apical trunk and distal dendrites. Thus, we found that somato-dendritic coupling in layer 5 neurons was strong, but asymmetric.

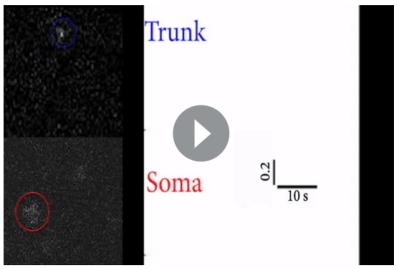

Video 1. Two-photon imaging movie showing calcium signals detected in the soma and not detected in the corresponding trunk of an individual layer 5 pyramidal neuron in V1. *Left panel*, two-photon calcium imaging (raw data) for a pair of neuronal compartments (Soma-Trunk) imaged semi-simultaneously. Both the soma (*lower quadrant*, circled in red) and the corresponding trunk (*upper quadrant*, circled in blue) of an individual layer 5 pyramidal neuron are shown. *Right panel*, GCaMP6s signals of the two compartments (red for Soma, blue for Trunk) shown in the video on the left panel. Data were acquired at 4.8 Hz per plane. The two fields of view were 170 µm apart in the coronal plane. Scale bars: 10 s and 0.2 ΔF/F0 (normalised to max).
https://elifesciences.org/articles/49145#video1

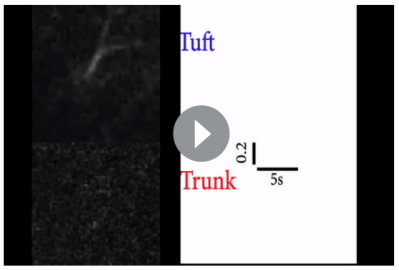

Video 2. Two-photon imaging movie showing calcium signals detected in the apical trunk and not detected in the corresponding tuft of an individual layer 5 pyramidal neuron in V1. *Left panel*, two-photon calcium imaging (raw data) for a pair of neuronal compartments (Trunk-Tuft) imaged semi-simultaneously. Both the apical trunk (*lower quadrant*, circled in red) and the corresponding tuft (*upper quadrant*, circled in blue, three branches) of an individual layer 5 pyramidal neuron are shown. *Right panel*, GCaMP6s signals of the two compartments (red for Trunk, blue for Tuft (upper right branch)) shown in the video on the left panel. Data were acquired at 4.8 Hz per plane. The two fields of view were 170 µm apart in the coronal plane. Scale bars: 5 s and 0.2 ΔF/F0 (normalised to max).
https://elifesciences.org/articles/49145#video2

Ex vivo calibration of GCaMP6s and GCaMP6f signals in layer 5 soma and apical tuft dendrites

We next sought to characterize the electrophysiological activity underlying our observations of strong, but asymmetric, somato-dendritic coupling in vivo. We reasoned that neuronal spiking driven by stimulation of either the soma or the apical tuft would differentially impact calcium event amplitudes in proximal and distal neuronal compartments. We examined this ex vivo by combining calcium imaging and whole-cell recordings in acute cortical slices from mouse V1. We imaged the soma and distal apical dendrite (nexus) of GCaMP6s- and GCaMP6f- expressing layer 5 neurons whilst driving neuronal spiking either by somatic current injections (somatic stimulation) or L1 electrical stimulation (dendritic stimulation) (***Figure 4A***). Somatic and dendritic stimulation consisted of a train of 10 suprathreshold stimuli delivered at 5–200 Hz; each stimulus reliably triggered single action potentials (***Figure 4B***). Action potentials evoked by dendritic stimulation were accompanied by an enhanced afterdepolarization in the soma, characteristic of distal dendritic electrogenesis (***Larkum et al., 1999a***; ***Shai et al., 2015***).

For somatic stimulation, we found that we could robustly detect somatic calcium signals with firing frequencies as low as 5 Hz with GCaMP6s (***Figure 4E, G***), and as low as 25 Hz with GCaMP6f (***Figure 4F, H***); we could not reliably detect calcium events associated with single action potentials with either indicator ($\Delta F/F0$ peak for GCaMP6s: mean = 0.02, sem = 0.01, t-test vs null, p=0.07, n = 10 neurons; $\Delta F/F0$ peak for GCaMP6f: mean = −0.02, sem = 0.03, t-test vs null, p=0.39, n = 9 neurons). Somatic signal amplitude increased monotonically with stimulation frequency for both indicators, with a plateau at 100–200 Hz. By contrast, in the distal dendrites, reliable signals for both indicators were only detected when somatically-driven spiking exceeded 50 Hz (***Figure 4E–H***), likely reflecting the critical frequency (50–100 Hz) of back-propagating action potentials required to trigger distal dendritic calcium spikes (***Larkum et al., 1999a***; ***Shai et al., 2015***). For dendritic stimulation, calcium signals were reliably detected in both the soma and distal dendrites. With GCaMP6s, this was true for all frequencies tested (***Figure 4C, E, G***). With GCaMP6f, somatic signals could not be observed at lower stimulation frequencies (5 Hz) (***Figure 4D, F, H***).

Our findings suggest that: 1) somatically-triggered back-propagating action potentials below the critical frequency (<50–100 Hz) may underlie the distant-dependent loss of dendritic calcium signals we observed in vivo; 2) spiking driven by strong apical tuft input or high-frequency spiking driven by somatic depolarization may underlie the strong somato-dendritic coupling detected in vivo.

Notably, compared to GCaMP6s, GCaMP6f had a reduced sensitivity for detecting calcium signals, specifically in the soma during low frequency spiking driven either by somatic or dendritic stimulation (***Figure 4E–H***). Consequently, as compared to GCaMP6s, attenuation of events from soma to dendrite was underestimated whereas attenuation of events from dendrite to soma was overestimated with GCaMP6f (***Figure 4G vs 4H***). With GCaMP6s, by contrast, attenuation of signals was asymmetric; we only found attenuation from soma to distal dendrites, as observed in vivo (***Figure 4G***).

We further examined GCaMP6s signals across a number of dendritic stimulation intensities (25–100% of somatic spike threshold) and frequencies (5–200 Hz) (***Figure 4—figure supplement 1C***) allowing for analysis of ex vivo somato-dendritic coupling across a range of stimulus-evoked depolarizations. We could not detect any global calcium signals in the apical tuft when L1 stimulation failed to evoke a somatic action potential, indicating a strong coupling between global calcium events and somatic spiking in our experimental conditions (***Figure 4—figure supplement 1D***). Thus, no calcium signal was detected in either compartment (soma and apical tuft) in trials with no action potential. When L1 stimulation only evoked a single action potential, apical tuft calcium signals were observed in 60% of the trials; however, these events were below the detection threshold of GCaMP6s in the soma (***Figure 4—figure supplement 1F***). Consequently, under these conditions, somato-dendritic coupling was low. Provided L1 stimulation evoked at least two action potentials, calcium signals in both apical tuft and soma were robustly detected (***Figure 4—figure supplement 1H***). Across stimulation parameters, both somatic and dendritic calcium transients increased with the number of action potentials evoked by L1 stimulation (***Figure 4—figure supplement 1D***). Collectively, our findings reveal that evoked apical tuft calcium events are strongly coupled to somatic spiking, and that this coupling can be detected by GCaMP6s imaging provided that somatic output is above the limits of detection ($\geq$2 action potentials ex vivo).

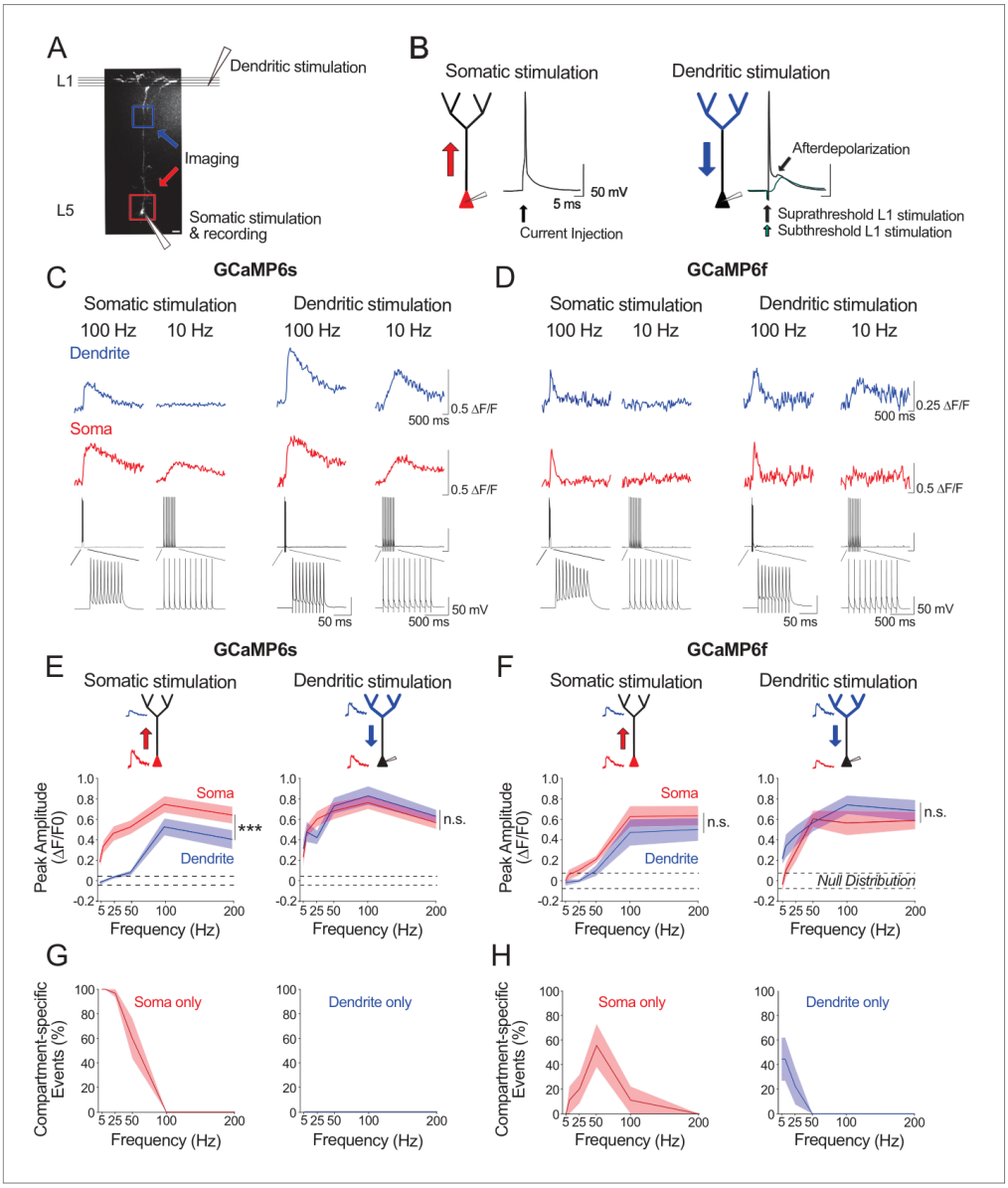

Figure 4. Ex vivo calibration of GCaMP6s and GCaMP6f signals in soma and apical tuft dendrites. (**A**) Experimental schemata. Layer 5 pyramidal neurons expressing GCaMP6s or GCaMP6f were recorded using whole-cell patch clamp in acute cortical slices of the primary visual cortex. An example neuron is shown (scale bar = 20 µm). The soma and distal apical dendrite (nexus) were imaged during neuronal spiking, driven either by suprathreshold somatic current injection (somatic stimulation) or layer 1 (**L1**) stimulation (dendritic stimulation), respectively. Somatic and dendritic stimulation consisted

Figure 4 continued on next page

Figure 4 continued

of a train of 10 pulses delivered at 5–200 Hz. (**B**) Examples of action potentials driven by somatic and dendritic stimulation. Action potentials triggered by dendritic stimulation were additionally accompanied by an enhanced afterdepolarization reminiscent of a dendritic spike, which had a faster rise time than subthreshold EPSPs and were absent from somatically-evoked action potentials. (**C, D**) Example calcium transients imaged in the soma and apical dendrite during somatic and dendritic stimulation in a L5 neuron expressing GCaMP6s (**C**) and GCaMP6f (**D**). Concurrent somatic electrophysiological recordings are shown below each transient. Negative deflections in electrophysiological traces are stimulation artefacts that have been cut for clarity. (**E, F**) Average peak amplitude of calcium transients recorded in the soma (red) and dendrites (blue) during somatic and dendritic stimulation for GCaMP6s (**E**) and GCaMP6f (**F**). Null distribution of peak amplitudes from sham stimulation trials are shown (dashed horizontal lines). (**G, H**) Proportion of compartment-specific events detected either in the soma or dendrite during somatic or dendritic stimulation for GCaMP6s (**G**) and GCaMP6f (**H**). Shaded areas represent S.E.M. Significance was assessed with two way (**E, F**) and one way (**G, H**) repeated measures ANOVA with post-hoc Sidak tests. Asterisks (***) in (**E,F**) denote factor (soma vs dendrite) significance of $p<0.0001$; n.s. denotes non-significance; significance is not shown for other comparisons but is listed below. For somatic stimulation in (**E**): soma vs. dendrite: $p<0.0001$ for all frequencies; soma vs. null: $p<0.0001$ for all frequencies; dendrite vs null; $p<0.0001$ for frequencies > 50 Hz, $p>0.44$ for frequencies $\leq$ 50 Hz. For dendritic stimulation in (**E**): soma vs. dendrite: $p>0.11$ for all frequencies; soma vs null: $p<0.0001$ for all frequencies; dendrite vs null: $p<0.0001$ for all frequencies. For somatic stimulation in (**F**): soma vs. dendrite: $p>0.49$ for>25 Hz, $p=0.074$ for 10 Hz, $p=0.054$ for 5 Hz; soma vs. null: $p<0.0001$ at>100 Hz, $p=0.09$ at 50 Hz, $p>0.7$ at<50 Hz; dendrite vs. null: $p<0.0001$ at>100 Hz; $p>0.52$ at<50 Hz. For dendritic stimulation in (**F**): soma vs. dendrite: $p>0.32$ for all frequencies; soma vs. null: $p<0.0001$ at>50 Hz, $p<0.01$ at 25 Hz, $p>0.47$ at<10 Hz; dendrite vs. null: $p<0.0001$ at>25 Hz, $p<0.002$ at 10 Hz, $p=0.11$ at 5 Hz. For somatic stimulation in (**G**): soma vs null: $p<0.0001$ for<50 Hz, $p>0.44$ for>100 Hz. For dendritic stimulation in (**G**): dendrite vs null: $p>0.11$ for all frequencies. For somatic stimulation in (**H**): soma vs null: $p<0.0001$ for 50 Hz; $p>0.12$ for all other frequencies. For dendritic stimulation in (**H**): dendrite vs null: $p<0.02$ for 5 Hz, $p=0.10$ for 10 Hz, $p>0.48$ for>25 Hz. GCaMP6s: n = 10 cells from 4 animals except for 5 Hz stimulation, where n = 5 cells from 3 animals; GCaMP6f: n = 9 cells from 3 animals.

The online version of this article includes the following figure supplement(s) for figure 4:

Figure supplement 1. Ex vivo calibration of GCaMP6s in soma and apical tuft dendrites across subthreshold and suprathreshold dendritic stimulation parameters.

Visual stimulation and locomotion do not alter the coupling of calcium signals between neuronal compartments from soma to apical tuft

We then tested whether visual stimulation and locomotion altered the coupling between the different compartments of individual layer 5 neurons. For each condition, we plotted the percentage of compartment-specific calcium transients as a function of their amplitude. We found that in all four conditions compartment-specific events were dominated by small amplitude calcium transients in proximal compartments: there was no significant difference between darkness and visual stimulation periods, both during stationary and locomotion periods (***Figure 5B***; Three-way ANOVA, p=0.69, p=0.21 and p=0.64 for visual stimulation, locomotion, and interaction respectively; $p<10^{-15}$ for event amplitude; no other interaction was found to be statistically significant). Similarly, we found no significant difference between behavioural states defined by stationary, locomotion and transition from still to running periods (see Materials and methods), either during visual stimulation or in darkness (***Figure 5—figure supplement 1A***). These results indicate that the relationship between calcium transient amplitude and percentage of attenuated events from soma to apical tuft remained unchanged by visual stimulation and behavioural-state changes. In addition, we found that, on average, the percentage of coincident calcium signals across compartments of individual neurons was not significantly modified either by visual stimulation or behavioural state changes (n = 19 neurons) (***Figure 5—figure supplement 1B*** and ***Figure 5—figure supplement 2***).

Even though smaller events were attenuated with similar probabilities across the four conditions, calcium transients that do propagate through different neuronal compartments, may be amplified or attenuated in a condition-dependent manner (***Figure 5C***). To capture these nonlinearities, we plotted the amplitude of each detected transient in each compartment and calculated a residual value as the distance from the linear robust regression fit (***Figure 5C***). We then plotted the cumulative distribution of the residual value for every calcium transient in all 4 pairs of imaged compartments from soma to apical tuft (***Figure 5D***). We found that the distribution of the residual values across neuronal compartments were neither significantly affected by locomotion nor by visual stimulation (Three-way ANOVA, p=0.96, p=0.23 and p=0.91 for visual stimulation, locomotion and interaction effect, respectively; p=0.86 for different compartments; no other interaction effect was found to be significant; n = 11 Soma–Trunk pairs; n = 5 pTrunk–dTrunk; n = 9 Trunk–Tuft; n = 6 pTuft-dTuft from 19 neurons). These results indicate that, while locomotion and visual stimulation increase the activity of layer 5 pyramidal neurons, the relationship between the amplitude of calcium transients and the

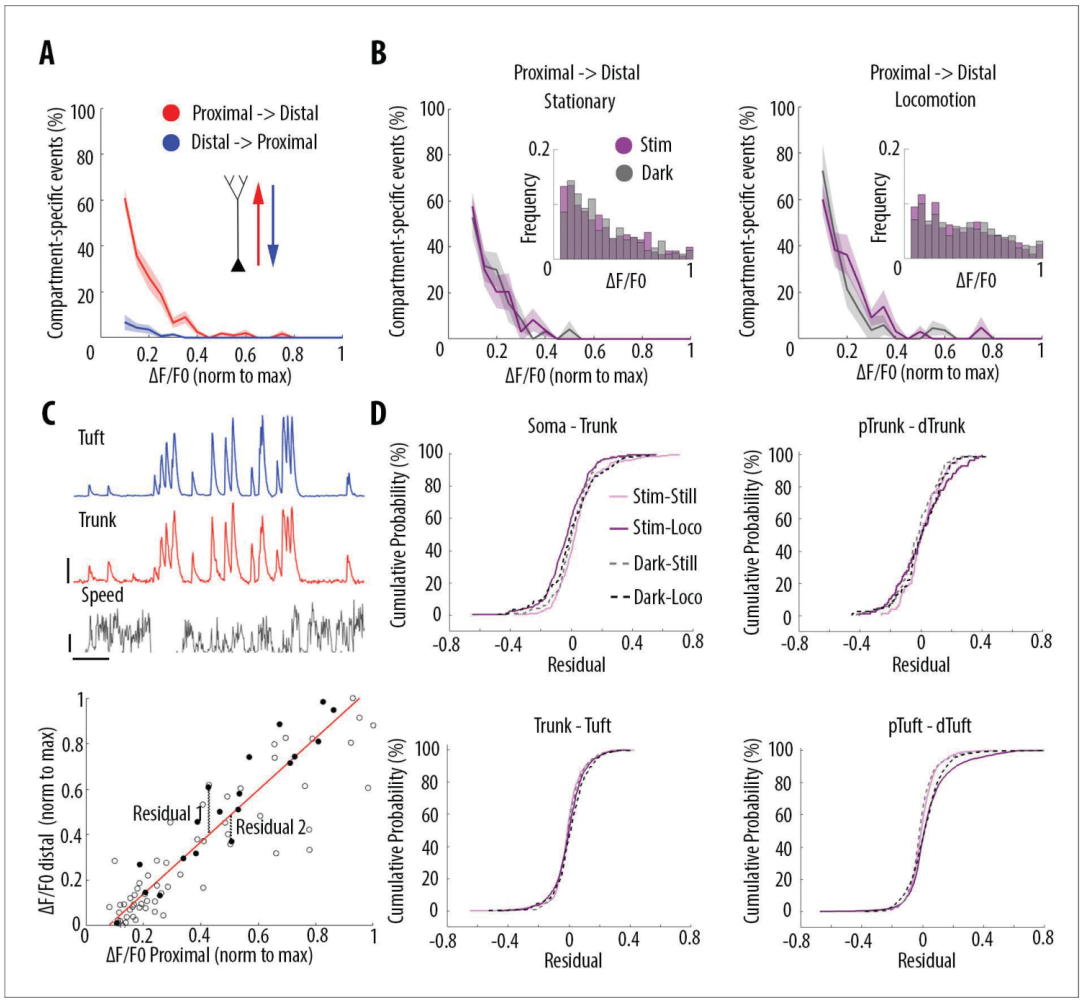

Figure 5. Locomotion and visual stimulation do not alter the relationship between somatic and dendritic calcium transients in layer 5 pyramidal neurons. (**A**) Mean proportion of compartment-specific calcium transients as a function of calcium transient amplitude (average of data points from ***Figure 3C*** (**i–iv**)). In red, proportion of events only detected in the proximal compartment. In blue, proportion of events only detected in the distal compartment. Thick line and shaded area: weighted mean and sem for each bin (0.05), respectively. Event amplitude, compartment (proximal vs distal) and an interaction between these two factors significantly affected the proportion of compartment-specific events (Two-way ANOVA, $p<10^{-15}$, $p<10^{-15}$, $p<10^{-15}$, n = 31 pairs of compartments from 19 neurons). (**B**) Proportion of compartment-specific events detected in the proximal compartment and not in the distal one, as a function of calcium transient amplitude, during periods of darkness (grey) and visual stimulation with drifting gratings (purple), while the animals were either stationary (left panel) or running (right panel). *Upper right panel*, frequency histogram of calcium transient peak amplitudes detected in proximal compartments during darkness (grey) and visual stimulation (purple). Peak amplitudes were normalized to the maximum amplitude in each compartment. Neither visual stimulation nor locomotion altered the function relating calcium transients amplitude with the proportion of compartment-specific events (Three-way ANOVA, p=0.69, p=0.21 and p=0.64 for visual stimulation, locomotion, and interaction respectively; $p<10^{-15}$ for event amplitude. No other interaction was found to be statistically significant). (**C**) *Upper panel*, example traces of a proximal (trunk, red) and distal (tuft, blue) compartment imaged semi-simultaneously, during stationary and locomotion periods (black trace, speed). Scale bars, 0.25 ΔF/F0 (normalised to max), 12 cm/s, 20 s. *Lower panel*, example of scatter plot of calcium transients' peak amplitudes imaged in a pair of neuronal

Figure 5 continued on next page

Figure 5 continued

compartments (trunk-tuft). Each dot represents an individual calcium transient. Filled dots correspond to the transients shown in the upper panel. The red line represents the robust linear regression fit. For each transient, a residual from the robust linear regression was calculated. (**D**) Cumulative distributions of the residuals calculated for each pair of compartments and for each condition: visual stimulation (pink, stim), darkness (grey, dark), stationary (still) and locomotion (loco) periods. No significant difference was found between any condition: Three-way ANOVA, p=0.96, p=0.23 and p=0.91 for visual stimulation, locomotion and interaction effect, respectively; p=0.86 for different neuronal compartments. No other interaction effect was found to be significant. n = 31 compartments (n = 11 Soma-Trunk; n = 5 pTrunk–dTrunk; n = 9 Trunk–Tuft; n = 6 pTuft-dTuft from 19 neurons).
The online version of this article includes the following figure supplement(s) for figure 5:

Figure supplement 1. Behavioural-state transitions between stationary and locomotion do not alter the relationship between somatic and dendritic calcium transients.

Figure supplement 2. Proportion of coincident calcium transients in proximal and distal compartments imaged semi-simultaneously during the different behavioural conditions: visual stimulation (stim), darkness (dark), stationary (still) and locomotion (loco) periods.

probability of coupled events across compartments remains unchanged. Independent of condition, single calcium transients of a given amplitude have the same probability of being compartment-specific.

Since layer 5 neurons in V1 respond selectively to drifting grating orientations and that dendritic spikes triggered by visual input were suggested to enhance somatic tuning to the preferred orientation (***Smith et al., 2013***), we quantified the impact of grating orientation on the correlation of calcium transients throughout neuronal compartments. In the apical tuft, we found that the selectivity of the responses to the drifting gratings orientation, quantified by an orientation selectivity index (OSI), did not affect the high correlation of calcium transients between tuft dendrites (***Figure 6A–D***). We then compared orientation selective responses during stationary and locomotion periods both in apical tufts and corresponding somata (n = 15 neurons) (***Figure 6E and F***). We found that locomotion similarly increased calcium transient amplitudes both in apical tuft and soma, without a significant difference between compartments (***Figure 6G***, Paired t-test, p=0.38), both during the presentation of preferred and non-preferred orientations (***Figure 6H***, Repeated measures Two-way ANOVA on log-transformed data, p=0.07, 0.71 and 0.28 for stimulus-type, compartment and interaction effects respectively). As a consequence, the OSI of somatic and apical tuft responses remained unchanged during both stationary and locomotion periods (***Figure 6I***, Repeated measures Two-way ANOVA, p=0.49, p=0.42 and p=0.45, for the effects of locomotion, neuronal compartment and interaction, respectively). In line with these results, we found that the preferred orientation was similar throughout tuft dendritic branches and neuronal compartments of individual neurons, both during stationary and locomotion periods (***Figure 6J and K***). Finally, the Pearson's correlation between apical tuft branches calcium signals and across neuronal compartments remained high and unchanged regardless of the gratings orientation (***Figure 6L and M***).

Altogether, these results indicate that calcium signals in individual layer 5 pyramidal neurons are highly correlated throughout apical tuft branches and neuronal compartments, and that this high somato-dendritic coupling remains unchanged by visual stimulation and locomotion.

Discussion

Our results show that GCamP6f and GCamP6s calcium transients are highly correlated in apical tuft dendrites of individual layer 5 neurons in the primary visual cortex of awake behaving mice; branch-specific calcium transients were rare and limited to small amplitude transients. GCaMP6s calcium transients were also found to be highly correlated throughout all compartments of individual neurons (soma, trunk, tuft). However, their frequency was found to decrease in a distance-dependent manner from soma to apical tuft. Whereas almost all transients observed in the tuft were present in proximal compartments, the frequency of calcium transients in apical tuft was about 60% of their frequency in the corresponding soma. Ex vivo experiments suggest that attenuated dendritic signals were likely associated with low frequency back-propagating action potentials, whereas highly correlated somato-dendritic signals were likely associated with high frequency somatic activity, or strong apical tuft inputs. Neither visual stimulation nor locomotion altered either the coupling between neuronal compartments from soma to apical tuft, nor the proportion of tuft branch-specific events.

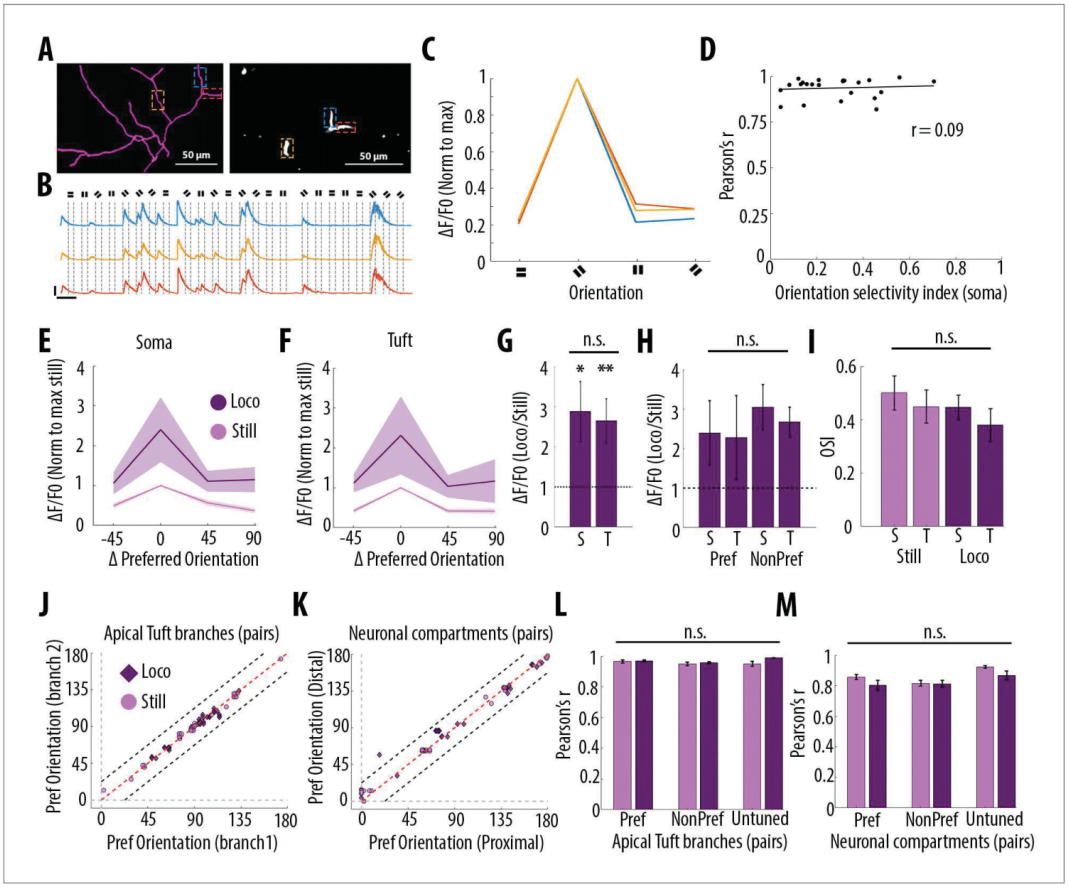

Figure 6. Orientation selectivity does not alter the relationship between somatic and dendritic calcium transients in layer 5 pyramidal neurons. (**A**) Morphological reconstruction (left) and two-photon image (right) of apical tuft branches of one individual neuron imaged during the presentation of drifting gratings. (**B**) Example GCaMP6s transients from the dendritic branches indicated by coloured dashed lines in panel A, during the presentation of drifting gratings of four different orientations. Dotted lines indicate the beginning and the end of drifting gratings stimulation. Scale bars 0.3 ΔF/F0 (normalised to max), 10 s. (**C**) Tuning curve showing calcium transients amplitudes (normalised to max) in response to the four grating orientations (average of 24 presentations of each grating,), from the three branches indicated by coloured dashed lines in panel A. (**D**) Mean Pearson's correlation value of all imaged tuft dendritic branches per neuron, as a function of the orientation selectivity of the corresponding soma (each dot corresponds to one neuron; $r^2 = 0.09$, p=0.67, n = 23 neurons). The straight black line represents the best fit line (least square). (**E**) Tuning curve of somatic calcium signals from orientation selective neurons (somatic OSI >0.3; n = 15 neurons) during stationary (still, pink) and locomotion (loco, purple) periods. Responses are normalised to the preferred orientation during stationary periods. Thick line and shaded area represent the mean and SEM, respectively. (**F**) Same as E, for the corresponding apical tuft branches of the same neurons. For each neuron, responses from all imaged apical tuft branches were averaged (n = 68 apical tuft branches from 15 neurons). (**G**) Relative increase in calcium transient amplitudes during locomotion compared to stationary periods both in soma (**S**) and in corresponding apical tuft dendrites (**T**), during drifting grating presentations. Locomotion significantly increased responses to drifting gratings both in soma and corresponding apical tuft dendrites (Repeated Measures Two-way ANOVA on log transformed data, p=0.02 and p=0.008 for the effect of locomotion on soma and tuft responses, respectively, n = 15 neurons) without a significant difference between compartments (Paired t-test, p=0.38; mean (normalised to stationary)=2.89 and 2.65, sem = 0.74 and 0.56; n = 15 soma and 15 apical tufts including 68 branches). (**H**) Same as G for responses to the preferred (Pref) and non-preferred (NonPref) orientations (Repeated measures Two-way ANOVA on log-transformed data, p=0.07, 0.71 and 0.28 for orientation, compartment and interaction effects respectively; mean = 2.4 and 2.28, sem = 0.81 and 1.06 for

Figure 6 continued on next page

Figure 6 continued

soma and apical tuft at the preferred orientation; mean = 3.05 and 2.67, sem = 0.57 and 0.38 for soma and apical tuft at the non-preferred orientation; n = 15 soma and 15 apical tufts). (**I**) Orientation selectivity index was not significantly different between somatic and corresponding tuft dendrites responses, both during stationary (still) and locomotion (loco) periods (Repeated measures Two-way ANOVA, p=0.49, p=0.42 and p=0.45, for the effects of locomotion, neuronal compartment (soma vs tuft) and interaction, respectively; mean = 0.5; 0.45, sem = 0.06, 0.06 for soma and apical tuft during stationary and mean = 0.45; 0.38, sem = 0.05, 0.06 for soma and apical tuft during locomotion, respectively; n = 15 soma and 15 apical tuft including 68 branches). (**J**) Scatter plot of the preferred orientation in pairs of apical tuft branches belonging to the same neuron and imaged simultaneously, during stationary (pink circles) and locomotion (purple diamonds) periods (n = 31 pairs). Dashed red line: identity line; Dashed black lines: identity +/- 22.5 degrees. (**K**) Same as J for pairs of neuronal compartments imaged simultaneously. n = 33 pairs. (**L**) Pearson's correlation of calcium transients between pairs of apical tuft branches belonging to the same orientation-selective neuron, during the presentation of the preferred (Pref) and non-preferred (NonPref) grating orientations, both during stationary (pink) and locomotion (purple) periods (n = 31 pairs). Correlation values from branches belonging to non-selective neurons (OSI <0.3, untuned), during the presentation of all oriented gratings, are shown on the right columns (n = 10 pairs). Neither gratings orientation nor locomotion significantly affected the correlation between pairs of branches (Two-way ANOVA, p=0.20, p=0.07 and 0.38 for orientation, locomotion and interaction effect, respectively). (**M**) Same as L, for different neuronal compartments (Two-way ANOVA, p=0.27, p=0.09 and 0.43 for orientation, locomotion and interaction effect, respectively; n = 33 pairs for Pref, NonPref and 36 pairs for untuned). Error bars: SEM.

Limitations of the use of calcium imaging to assess dendritic activity in awake behaving mice

Investigations of local dendritic activity in awake behaving mice have so far mainly relied on the use of genetically-encoded calcium indicators (***Xu et al., 2012***; ***Cichon and Gan, 2015***; ***Manita et al., 2015***; ***Takahashi et al., 2016***; ***Sheffield et al., 2017***; ***Ranganathan et al., 2018***; ***Kerlin et al., 2019***; ***Sheffield and Dombeck, 2019***). The analysis of our data set showed that several experimental constraints may bias results towards signals mistakenly interpreted as local dendritic activity. Dense labelling was already demonstrated to strongly affect correlation values (***Xu et al., 2012***); even in cases of relatively sparse labelling of individual neurons, contamination from axons or dendrites of other labelled neurons may lead to local signals detected in single dendrites. In our data set, we had a sparse labelling and we systematically reconstructed our imaged neurons and excluded regions of interest where overlapping dendrites from other neurons were observed. Movement artefacts may also lead to inaccurate detection of local dendrite signals; these artefacts are more likely to be found during specific behaviour, such as locomotion, and therefore can bias the interpretation of the results. In our data set we used the activity-independent marker tdTomato to correct for motion artefacts and excluded the recordings in which tdTomato marker was not detected. For most of our imaged neurons, baseline fluorescence of both GCaMP6s and GCaMP6f could also be used for the same purpose. Another parameter that may cause artefactual local dendritic signals, is the length of the imaged dendritic segments (and therefore the size of the regions of interest used to extract the changes of fluorescence over time). Small regions of interest could include spines not clearly distinguishable from the corresponding dendritic shaft, especially when the spine is located above the dendrite at the imaged focal plane. As a consequence, in small regions of interests, spine signals may be incorrectly interpreted as local dendritic signals.

Differences in calcium buffering properties of individual compartments also create detection biases as they lead to different decay times of fluorescent calcium indicators between somatic and dendritic compartments (***Beaulieu-Laroche et al., 2019***; ***Kerlin et al., 2019***). In order to account for this difference, we based our analysis on the detection of peak amplitudes of individual calcium transients. This detection depends on arbitrary thresholds; we thus showed the robustness of our results across different detection thresholds (***Figure 1—figure supplement 2***). An additional source of bias is linked to the affinities of calcium indicators. Previous studies have shown that dendritic calcium spikes can reliably be detected by calcium indicators with lower sensitivity than GCaMP6f and GCaMP6s (***Helmchen et al., 1999***; ***Xu et al., 2012***). However, while it was shown that GCaMP6s and GCaMP6f could detect individual somatic action potentials in layer 2/3 neurons in vivo (***Chen et al., 2013***), this is not the case in layer 5 neurons neither for GCaMP6f (***Beaulieu-Laroche et al., 2019***), nor for GCaMP6s based on our own ex vivo experiments. We did however find that GCaMP6s was superior in detecting somatic calcium events during low frequency spiking (<25 Hz) (***Figure 4***). Nonetheless, the detection of somatic action potentials in layer 5 neurons in

vivo with GCaMP sensors may be biased towards larger events, and as a consequence, the attenuation from soma to tuft may be underestimated.

The relatively low temporal resolution of genetically-encoded calcium signals presents another key limitation to the study of dendritic calcium signals in vivo. In our study, we found branch-specific events to be rare. Whereas ex vivo studies have demonstrated that branch-specific stimulation can trigger localized Ca^{2+} events detected by calcium indicators (*e.g.* ***Cai et al., 2004***; ***Sandler et al., 2016***; review: ***Major et al., 2013***), the detection of these events in vivo is more challenging, principally because they may be masked by ongoing global dendritic events (***Kerlin et al., 2019***). Given the relatively low temporal resolution of GCaMP6s, dissociating global dendritic calcium signals from potential underlying branch-specific events is challenging (***Kerlin et al., 2019***). The contribution of branch-specific calcium signalling to ongoing neuronal activity in vivo therefore requires further investigation.

Widespread, correlated calcium transients in apical tuft dendritic branches of layer 5 neurons

Our results show that in the apical tuft, calcium transients were highly correlated regardless of how distal the imaged branches were from the nexus. Branch-specific calcium transients were rare and limited to transients of the smallest amplitudes. Our results indicate that active dendritic integration associated with global calcium events in the apical tuft is widely recruited across different behavioural and sensory conditions. This widespread calcium activity throughout the layer 5 apical tuft may strongly influence plasticity and learning (***Magee, 1997***; ***Golding et al., 2002***; ***Kampa et al., 2006***; ***Sjöström and Häusser, 2006***; ***Remy and Spruston, 2007***; ***Bittner et al., 2017***; ***Bono and Clopath, 2017***; ***Guerguiev et al., 2017***).

High but asymmetric coupling of calcium signals from soma to apical tuft

Our results show an asymmetry in the coupling between somatic and apical dendritic calcium signals. Previous studies have shown that dendritic signals attenuate in a distance-dependent manner, suggesting that at least some of the calcium events generated in one compartment would attenuate as they reach the next compartment (***Stuart et al., 1997***; ***Svoboda et al., 1997***; ***Helmchen et al., 1999***; ***Vetter et al., 2001***; ***Larkum et al., 2009***; ***Waters et al., 2003***). To estimate the lower bound proportion of calcium events generated in the tuft and in the soma, we investigated the proportion of attenuated events in both somatofugal and somatopetal directions. Our results show that while around 40% of somatic calcium transients decay by the time they reach the apical tuft, only 1.4% of apical tuft calcium events were not associated with somatic events (***Figure 5A***). These results indicate that at least 40% of somatic calcium transients were not triggered by apical tuft calcium events, and that these transients attenuated from the soma to the apical tuft. Based on our ex vivo recordings, we suggest that attenuated calcium transients are associated with low-frequency back-propagating somatic action potentials, below the critical frequency required to trigger dendritic electrogenesis (***Larkum et al., 1999a***; ***Shai et al., 2015***). Attenuation may also involve active inhibitory mechanisms along the somato-dendritic axis (***Larkum et al., 1999a***; ***Naka and Adesnik, 2016***).

A recent study reported a high and symmetric somato-dendritic coupling in V1 layer 5 neurons concluding that GCaMP6f events occurred concurrently in soma and dendritic compartments (***Beaulieu-Laroche et al., 2019***). The authors reported that 83.9% (median) of dendritic calcium signal (rise events) were paired with events in the soma while 73.4% of somatic events were paired with dendritic ones. In our study, we found a stronger asymmetry with 98.6% of dendritic events paired with somatic ones and 60 % of somatic events paired with dendritic ones. This discrepancy may be explained by differences in imaging conditions including a denser labelling, which increases the amount of background signals, and the use of GCaMP6f, which has a lower signal amplitude and signal-to-noise ratio than the GCaMP6s indicator used in our study, leading to a lower probability of detecting small events in layer 5 somata, as shown by our ex vivo recordings (***Figure 4G-H***).

In our study, we estimated that 60% of somatic calcium signals were highly correlated with global apical tuft calcium signals. Based on our ex vivo experiments, high somato-dendritic coupling would occur during either 1) high frequency back propagating action potentials or 2) strong apical tuft activity capable of driving somatic spiking. Coupling could in principle also be observed with lower

frequency back propagating action potentials, provided they are paired with tuft inputs (**Larkum, 2013**; **Manita et al., 2015**). Further experiments are needed to resolve these potential mechanisms in vivo, for example using voltage-sensitive dyes (**Villette et al., 2019**; **Roome and Kuhn, 2018**; **Adam et al., 2019**) or dendritic electrophysiological recordings (**Moore et al., 2017**), that would provide the temporal resolution to resolve the different types of dendritic events.

Notably, both apical tuft signals and the somato-dendritic coupling may differ between different subtypes of layer 5 pyramidal neurons. It is known that at least two main types exist: intratelencephalic neurons which connect cortical areas, and pyramidal tract neurons which project to multiple subcortical areas (**Harris and Shepherd, 2015**; **Gerfen et al., 2018**). These two types display different morphologies (**Groh et al., 2010**) and receive different types of inputs (**Young, 2019**). The neurons included in this study had their soma located at various depths within layer 5 (median 528 µm, see **Figure 3—figure supplement 1**) and mainly displayed thick-tufted morphology, characteristic of pyramidal tract neurons. Since we selected the imaged neurons visually based on their GCaMP6 fluorescent signal, our sampled is likely biased towards layer 5 neurons with thick trunk and thick-tufted morphology.

Integration of visual and locomotion-related inputs in layer 5 neurons in awake behaving mice

Our results show that, in our passive viewing conditions, changes in visual inputs (darkness versus drifting gratings) and locomotion-related inputs do not affect the relationship between somatic, trunk and apical tuft calcium signals nor the prevalence of branch-specific dendritic events in the apical tuft. These results are in agreement with a previous study showing that somato-dendritic correlations of calcium transients remain unchanged by visual stimulation and locomotion (**Beaulieu-Laroche et al., 2019**). It is however possible that in both studies, untracked behavioural states (e.g. arousal, attention) during stationary and locomotion periods may differentially shape somato-dendritic activity.

It is known that the prevalence and the dynamics of synaptic inputs received by layer 5 pyramidal neurons strongly vary between passive sensory stimulation and active learning tasks (**Xu et al., 2012**; **Hong et al., 2018**). Apical tuft dendrites of layer 5 neurons receive a barrage of thousands of synaptic inputs in vivo (**Stuart and Spruston, 2015**) and it was shown that V1 neurons receive synaptic inputs conveying information not only about visual stimuli but also about non-visual variables (e.g. arousal/attention, motor activity, reward-related and spatial information) (**Pakan et al., 2016**; **Pakan et al., 2018a**; **Pakan et al., 2018b**). Finally, in addition to excitatory inputs, both inhibitory and neuromodulatory inputs were shown to modulate electrical interactions between soma and dendrites in layer 5 neurons (**Larkum et al., 1999a**; **Silberberg and Markram, 2007**; **Labarrera et al., 2018**; **Williams and Fletcher, 2019**). It is therefore possible that during the active learning of a behavioural task, the synaptic inputs associated with this learning process would lead to different mechanisms of dendritic integration than during passive viewing. For example, dendritic integration of multiplicative combinations of sensory and motor inputs in the tuft dendrites of layer 5 pyramidal neurons has been described during an active sensing task in mouse somatosensory cortex (**Ranganathan et al., 2018**). In addition, it was proposed that changes in neuronal representations during learning would rely on active dendritic signals generating calcium plateau potentials (**Bittner et al., 2015**; **Grienberger et al., 2017**). In that case, somato-dendritic coupling may change during the course of learning (**Sheffield et al., 2017**). This remains to be tested in the visual cortex. Similarly, somato-dendritic coupling may evolve during postnatal development when sensori-motor associations are formed. Recently, it was shown in the mouse primary visual cortex, that dendrites of layer 2/3 neurons increase their coupling during adulthood, as a consequence of decreased responsiveness of dendrite-targeting interneurons to locomotion-related inputs (**Yaeger et al., 2019**). Further investigations are needed to reveal these mechanisms in layer 5 visual cortical neurons.

Materials and methods

Animals

All experiments and procedures involving animals were approved by the University of Edinburgh Animal Welfare and the ethical review board (AWERB). Experiments were performed under the

appropriate personal and project licenses from the UK Home Office in accordance with the Animal (Scientific Procedures) act 1986 and the European Directive 86/609/EEC on the protection of animals used for experimental purposes. Adult male and female mice, aged between 8 to 10 weeks, were obtained from Jackson Laboratory, ME, USA (B6.Cg-Gt(ROSA)26Sor$^{tm14(CAG-tdTomato)Hze}$/J [RRID: IMSR_JAX:007914]). Mice were group caged in groups of 2–6 animals, with a running wheel and on a reverse 12:12 hr light/dark cycle, with ad libitum access to food and water.

Surgical procedures

Viral delivery of GCaMP6

To obtain sparse labelling of excitatory neurons we used a Cre-dependent approach, by co-injecting viral constructs AAV1.CamKII 0.4.Cre.SV40 (Penn Vector core catalogue No. 105558-AAV1) diluted at 1:10000 or 1:20000 with either AAV1.Syn.Flex.GCaMP6f.WPRE.SV40 (Penn Vector Core, catalogue No. 100833-AAV1) or AAV1.Syn.Flex.GCaMP6s.WPRE.SV40 (Penn Vector Core, catalogue No. 100845-AAV1) diluted 1:10 in the final solution. All dilutions were made in sterile artificial cerebrospinal fluid (ACSF). AAV1.Syn.Flex.GCaMP6f.WPRE.SV40 was used for single plane imaging of the apical tuft while AAV1.Syn.Flex.GCaMP6s.WPRE.SV40 was used for semi-simultaneous two-planes imaging. Animals were initially anesthetized with 4% Isoflurane and subsequently maintained on 1–2% isoflurane throughout the procedure. Body temperature was maintained at physiological levels using a closed-loop heating pad. Eye cream (Bepanthen, Bayer) was applied to protect the eyes from dryness and light exposure.

After induction of anaesthesia, mice were shaved and mounted onto a stereotaxic frame (David Kopf instruments, CA, USA). An analgesic was administered subcutaneously (Vetergesic, buprenorphine, 0.1 mg/kg of body weight). Viral injections were performed in the primary visual cortex of left hemispheres (centred around 2.5 mm lateral from midline and 0.5 mm anterior to lambda) at 650 and 500 µm from brain surface using a glass pipette (20 µm tip diameter, Nanoject, Drummond Scientific), coupled to a Nanoject II (Drummond Scientific). A total volume of 55.2 nl was injected across the two depths (6 × 4.6 nl at each location with 30 s intervals between each injection to allow sufficient time for diffusion). After each injection, pipettes were left in situ for an additional 5 min to prevent backflow. The scalp was then sutured (Ethicon, Ethilon polyamide size 6) and the animal monitored during recovery in a heated cage before returning to its home cage for 2–3 weeks.

Headplate and imaging window

Under anaesthesia (isoflurane), mice were shaved and mounted onto a stereotaxic frame (David Kopf instruments, CA, USA). Analgesic and anti-inflammatory drugs were administered subcutaneously (Vetergesic, buprenorphine, 0.1 mg/kg of body weight; Carpaphen, Carprieve, 5 mg/kg of body weight; Dexamethasone, Rapidexon, 2 mg/kg of body weight). For a cranial window over V1, a section of scalp was removed, the underlying bone was cleaned before a rectangular craniotomy of about 2 × 1.5 mm was made over the left primary visual cortex (centred around 2.5 mm lateral and 0.5 mm anterior to lambda). The dura was kept intact. The craniotomy was then sealed with a glass cover slip and fixed with cyanoacrylate glue. To stabilize the brain during imaging, we used a triple glass window by stacking three cover-slip glasses (Menzel-Glaser 24 × 32 mm # 0) on top of each other. These were glued together using an optically clear UV-cured glue (Norland Optical adhesive). Overall, the thickness of the glass window inserted through the cranial window, was comparable to the thickness of the skull at the time of imaging. A custom-built metal headplate was fixed on top of the skull with glue and cemented with dental acrylic (Paladur, Heraeus Kulzer). At the end of the procedure, a single dose of 25 mL/kg of Ringer's solution was injected subcutaneously to rehydrate the animal after the procedure. The animal was then released from the head fixation and returned to a heated recovery cage, until full motor capacity was recovered.

In vivo two-photon imaging data acquisition

Imaging was performed using a 25x Objective (Olympus). The excitation wavelength of the laser was set to 920 nm. Layer 5 pyramidal neurons were imaged between 500 and 650 µm below the brain surface and followed up to their distal tuft dendrites along the apical trunk. Neurons which had their nucleus filled with GCaMP6 or had blebbed dendrites were excluded. Imaging was performed using a 570 nm short-pass dichroic mirror and two single-band pass filters, a 525/50 and a 620/60

(Scientifica). At the end of each imaging session, a z-stack was acquired to allow offline morphological reconstruction of the imaged neuron. Reconstructions were done using the ImageJ plugin Simple Neurite Tracer.

Habituation and imaging started 2–3 weeks after AAV injection. Mice were habituated to head-fixation in the dark for 45 min and began to run freely on a polystyrene cylindrical treadmill (20 cm diameter, on a ball-bearing mounted axis). Running speed on the treadmill was continuously monitored using an optical encoder (E7P, 250cpr, Pewatron, Switzerland) that was connected to a data acquisition device (National Instrument, UK). Data were recorded with custom-written software in LabView (National Instrument, UK) and analysed in MATLAB (Mathworks, MA).

Single-plane two-photon imaging data were acquired using a custom-built galvo-resonant scanning system with a Ti:Sapphire pulsing laser (Chameleon Vision-S, Coherent, CA, USA;<70 fs pulse width, 80 MHz repetition rate) at 120 Hz, with a custom-programmed LabVIEW-based software (version 8.2; National Instruments, UK). Multi-plane data were acquired using an ultra-fast, solid-state, single 100 fs pulse width laser (InSight DeepSee, SpectraPhysiscs, CA, USA) and a FemtoSmart Dual two-photon microscope (Femtonics, Budapest, Hungary). Two focal planes (512 × 165 pixels), with an average distance of 170 µm in Z, were imaged at a frequency of 96 frames/s (48 frames/s per plane) using a Piezo objective positioner kit (P725.4CA, Physic Instruments, Germany), switching between planes at 9.6 Hz (4.8 Hz per plane).

Visual stimulation

Visual stimuli were generated using the Psychophysics Toolbox package (***Brainard, 1997***) for MATLAB (Mathworks, MA) and displayed on a custom-modified, backlit LED monitor (51 × 29 cm, Dell, UK), which was placed 20 cm from the right eye, covering 104°×72° of the visual field. Visual stimulation trials consisted of drifting full-field square-wave gratings for 3 s (spatial frequency of 0.05 cycles per degree, 1.5 Hz, eight equally spaced directions in randomized order, contrast 80%, mean luminance 37 cd/m^2). Drifting grating presentations were separated by 4 s periods of isoluminant grey stimuli. We acquired 8–12 trials in darkness and 12–20 trials during visual stimulation for each imaged field of view. Time stamps for the onset of every stimulus were recorded and aligned to imaging frames using custom-built Matlab scripts.

In vivo data analysis

Image analysis and signal extraction

To correct for brain motion after image acquisition, we used 2D plane translation-based image alignment (SIMA 1.2.0, sequential image analysis; ***Kaifosh et al., 2014***). We 3D reconstructed each imaged neuron and defined regions of interest (ROIs) corresponding to neuronal cell body and dendritic segments manually. Due to sparse labelling, signal contamination was negligible in most cases. ROIs that were contaminated by labelled structures from other neurons were excluded from further analysis.

The pixel intensity within each ROI was averaged to create a raw fluorescence time series F(t). Baseline fluorescence F0 was computed for each neuron by taking the fifth percentile of the smoothed F(t) (1 Hz lowpass, zero-phase, 60th-order FIR filter) over each trial (F0(t)), averaged across all trials. As a consequence, the same baseline F0 was used for computing the changes in fluorescence in darkness and during visual stimulation. The change in fluorescence relative to baseline, ΔF/F0 was computed by taking the difference between F and F0(t) and dividing by F0.

Single plane data was acquired at 120 Hz, and subsequently downsampled to 5 Hz for signal processing. Multi-plane data were analysed at 4.8 Hz.

Calcium transient analysis

We first estimated noise levels by filtering our ΔF/F0 signal using a 9th order, zero-phase, high-pass filter at 0.6 Hz (Matlab function *filter*). We then estimated the standard deviation of the filtered signal and used a threshold of 2.8 of this standard deviation to detect individual calcium transients, using the built-in Matlab function *findpeaks*. We tested the robustness of our results to different thresholds +/- 30% of the selected threshold (***Figure 1—figure supplement 2***).

For each peak found in any branch or compartment, we defined a calcium transient as coincident in another branch or compartment when it occurred in a time window of 3 s around the frame where

the first peak was originally detected (2 s before, one after). As a consequence, peaks detected as coincident could not be further apart than 2 s. ***Figure 1—figure supplement 2*** shows the distribution of time intervals between events detected as coincident. The mean time interval was close to 0 ($2.19xe^{-4}$ seconds) with standard deviation of 0.28 s, meaning that 95% of all coincident events were found within a time interval of 0.56 s. Each calcium transient could only be considered coincident with one transient. The peak amplitude of a calcium transient was determined by taking the difference between the ΔF/F0 amplitude at the frame in which the peak was detected and a local minimum in a 2 s, backward sliding window. Correlation values were calculated as the Pearson's correlation values between peak calcium transient amplitudes in pairs of branches or compartments. Whenever a peak was detected in only one compartment and not in the other (compartment-specific events), the correlation was made between the peak amplitude in one compartment and the difference between the maximum and minimum ΔF/F0 values in a 3 s window centred around the frame of the detected peak in the other compartment. Shuffling values were obtained by randomly shuffling the order of the events in one branch or compartment of each pair. Residuals were extracted by calculating the robust linear regression line between normalised event amplitudes in each compartment, and then extracting the distance, along the y-axis, of each individual point from this robust line.

Locomotion analysis

Changes in the position of the cylindrical treadmill (sampled at 12,000 Hz) were interpolated to match the rate of imaging. To define stationary and locomotion periods we used the following criteria: Stationary corresponded to periods where the instantaneous speed (as measured at the 40 Hz sampling rate) was less than 0.1 cm/s. Locomotion corresponded to periods meeting three criteria: instantaneous speed $\geq$0.1 cm/s, 0.25 Hz lowpass filtered speed $\geq$0.1 cm/s, and an average speed $\geq$0.1 cm/s over a 2 s window centered at this point in time (***Pakan et al., 2016***). Any inter-locomotion interval shorter than 500 ms was also labelled as locomotion. Stationary periods less than 3 s after or 0.2 s before a period of locomotion were removed from the analysis. For ***Figure 5—figure supplement 1***, behavioural transitions were defined as time windows including: (1) 2 s before the onset of locomotion as defined above and 1 s after the onset, as well as (2) 1 s before the offset of locomotion and 20 s after the offset (unless another locomotion period began before the 20 s) (***Vinck et al., 2015***). For this analysis, behavioural transitions were excluded from stationary and locomotion periods.

Orientation selectivity

To determine the specific stimulus response parameters of each neuron to the oriented gratings, the ΔF/F0 during each presented oriented stimulus was first averaged across all trials. The preferred orientation of each neuron was the orientation that elicited the maximal response when averaged across all trials. The orientation selectivity index (OSI) was calculated as $(O_{pref}-O_{orth})/(O_{pref}+O_{orth})$ where O_{pref} represents the mean ΔF/F0 value during the presentation of the preferred orientation across trials and O_{orth} represents the mean ΔF/F0 value during the presentation of the orientation orthogonal to the preferred one. For the detailed analysis of orientation preference in ***Figure 6J and K***, the preferred response angle was estimated by calculating the argument of the resultant vector (V) in the complex plane, which was given by:

$$V = \frac{\sum_k R(\theta_k) e^{2i\theta_k}}{\sum_k R(\theta_k)}$$

where $R(\theta_k)$ is the mean ΔF/F0 response to angle θ_k (***Mazurek et al., 2014***).

Ex vivo patch-clamp recordings and calcium imaging

C57BL/6 mice (8–10 week old) were injected with either flexed GCaMP6s (AAV1.Syn.Flex.GCaMP6s.WPRE.SV40; dilution 1:10; Penn Vector Core, catalogue 384 No. 100845-AAV1) or flexed GCaMP6f (AAV1.Syn.Flex.GCaMP6f.WPRE.SV40; dilution 1:10; Penn Vector Core, 383 catalogue No. 100833-AAV1) along with CaMKII-Cre (AAV1.CamKII 0.4.Cre.SV40; diluted 1:100 or 1:1000; Penn Vector core catalogue No. 105558-AAV1) targeted to Layer 5 in V1 (see Viral Delivery of GCaMP6 in Materials and methods for details on the injection parameters). 3–4 weeks following injection,

animals were decapitated under isoflurane anaesthesia. The brain was extracted and coronally sliced into 400 µm thick sections in ice cold, carbogenated (95% O_2, 5% CO_2) dissection media (in mM: 87 NaCl, 75 sucrose, 2.5 KCl, 25 NaHCO3, 1.25 NaH2PO4, 25 glucose, 0.5 CaCl2, 7 MgCl2,) using a vibratome (VT1200s, Leica, Germany). Slices containing V1 were isolated and allowed to recover for 30–60 min in heated (35˚C) carbogenated ACSF (in mM: 125 NaCl, 2.5 KCl, 25 NaHCO3, 1.25 NaH2PO4, 25 glucose, 2 CaCl2, 1 MgCl2) before being stored at room temperature.

During recordings, slices were perfused with heated (33˚C), carbogenated ACSF. Layer 5 GCaMP6-positive cells were patched with borosilicate glass electrodes (4–7 MΩ) filled with K-gluconate internal solution (in mM: 130 K-Gluconate, 10 KCl, 2 MgCl2, 10 EGTA, 10 HEPES, 2 Na2-ATP, 0.3 Na2-GTP; pH 7.2–74, 290–300 mOsm), containing 0.1 mM Alexa 594 (ThermoFisher, UK) to facilitate visualization of cells. Cellular electrophysiology was recorded using a Multiclamp 700B amplifier and associated pCLAMP software (Molecular Devices). Data were acquired at 10 kHz and filtered at 3 kHz. For somatic stimulation, 10 current pulses (2–5 ms, 1–1.5nA) were delivered at 5, 10, 25, 50, 100 and 200 Hz. Each pulse was of sufficient amplitude to trigger an action potential. For dendritic stimulation, a monopolar tungsten electrode was placed in L1. Using a constant current stimulator (Digitimer, UK) 10 stimulation pulses (100 µs) were delivered at 5, 10, 25, 50, 100 and 200 Hz at a stimulation intensity 25, 50, 75% and 100% of spiking threshold in the soma. Suprathreshold stimulation was often accompanied by an enhanced afterdepolarization reminiscent of a dendritic spike (***Larkum et al., 1999a***; ***Shai et al., 2015***). In sham stimulation trials, no stimulus was given.

Cells were imaged with a 25x Olympus Objective (1.05 NA; XLPlan N, Olympus) using a two-photon microscope (Femtonics) equipped with a Ti:sapphire pulsing laser (Chameleon Vision-S, Coherent, CA, USA) which was tuned at 920 nm for GCaMP6 imaging, and 800 nm for Alexa 594 imaging. During somatic and dendritic stimulation, xy scans of GCaMP6 signals at the soma and distal apical dendrite (nexus) were acquired at a rate >120 Hz. Each imaging trial was 6 s in duration, with stimulation commencing after a 1 s baseline recording.

Images were downsampled to 20 Hz and analysed using ImageJ software and custom MATLAB scripts. Electrophysiological traces were analysed using pCLAMP software and custom MATLAB scripts. $\Delta F/F0$ was calculated as: $(F - F0)/(F0 - F_{background})$ where F0 was the mean baseline fluorescent signal during the 1 s baseline recording, and $F_{background}$ was the background fluorescence. F0 in the distal dendrites was often very low ex vivo, leading to inflated $\Delta F/F0$ values. Consequently, $\Delta F/F0$ signals in the soma and dendrite were standardized to the maximum signal evoked in each compartment. This allowed for fairer comparisons between compartments, and across cells. Calcium transient amplitudes were measured as the peak $\Delta F/F0$ observed within 1 s after the cessation of stimulation. These values were then subtracted by the average peak $\Delta F/F0$ measured in sham stimulation trials. The procedure was repeated for each sham stimulation trial in order to derive a null distribution of peak amplitudes for statistical comparison. Calcium events were also classified as successfully detected if they exceeded 2.8 standard deviations from the expected null, similar to what was used to analyse our in vivo data. An event was considered compartment specific if it was detected in one compartment but not in the other.

Statistics

All analysis was performed either using MATLAB (Mathworks, MA), or GraphPad Prism 8. All error bars in the figures represent standard error of the mean (SEM). Statistical tests and independent samples are described in figure legends.

Acknowledgements

We thank the GENIE Program and the Janelia Research Campus, specifically V Jayaraman, R Kerr, D Kim, L Looger, and K Svoboda, for making GCaMP6 available. We would also like to thank Peter Kind, for allowing access to equipment and reagents required for ex vivo experiments. This work was funded by the Wellcome Trust and the Royal Society (Sir Henry Dale fellowship to NR), the Marie Curie Actions of the European Union's FP7 program (MC-CIG 631770 to NR), the Shirley Foundation, the Patrick Wild Center and the RS MacDonald Charitable Trust Seedcorn Grant (to NR), the Simons Initiative for the Developing Brain (to NR), the Royal Commission for the Exhibition 1851 (Research Fellowship to ZP) and the University of Edinburgh (PhD scholarship to VF).

Additional information

Funding

Funder	Grant reference number	Author
Wellcome	102857/Z/13/Z	Nathalie L Rochefort
Royal Society	102857/Z/13/Z	Nathalie L Rochefort
University Of Edinburgh	PhD fellowship	Valerio Francioni
Simons Initiative for the Developing Brain	Project grant	Nathalie L Rochefort
Seventh Framework Programme	CIG 631770	Nathalie L Rochefort
RS MacDonald Charitable Trust	Seedcorn Grant	Nathalie L Rochefort
Royal Society	Royal Commission for the Exhibition 1851	Zahid Padamsey

The funders had no role in study design, data collection and interpretation, or the decision to submit the work for publication.

Author contributions

Valerio Francioni, Data curation, Software, Formal analysis, Investigation, Visualization, Methodology; Zahid Padamsey, Formal analysis, Investigation, Methodology, Performed ex vivo experiments; Nathalie L Rochefort, Conceptualization, Resources, Data curation, Formal analysis, Supervision, Funding acquisition, Investigation, Methodology, Project administration

Author ORCIDs

Nathalie L Rochefort https://orcid.org/0000-0002-3498-6221

Ethics

Animal experimentation: All experiments and procedures involving animals were approved by the University of Edinburgh Animal Welfare and the ethical review board (AWERB) and performed under the appropriate PIL and PPL license from the UK Home Office in accordance with the Animal (Scientific Procedures) act 1986 and the European Directive 86/609/EEC on the protection of animals used for experimental purposes.

Decision letter and Author response

Decision letter https://doi.org/10.7554/eLife.49145.sa1
Author response https://doi.org/10.7554/eLife.49145.sa2

Additional files

Supplementary files

- Transparent reporting form

Data availability

Raw data (changes of fluorescence over time) are provided in all the main figures (figure 1-4) and in two supplementary figures. Additionally, we provide two data source videos (Video 1 and Video 2). Due to the large volume of imaging data sets, all raw data (videos) are on a dedicated server from Rochefort lab and are available upon request. The Center for Discovery Brain Sciences, University of Edinburgh, is setting up a repository for published data sets that will be used for the data included in this manuscript, as soon as it is available. All analyses were performed using custom-written scripts in MATLAB, which are freely available via GitHub repository (https://github.com/rochefort-lab/

Francioni-et-al.-eLife-2019; copy archived at https://github.com/elifesciences-publications/Francioni-et-al.-eLife-2019).

References

Adam Y, Kim JJ, Lou S, Zhao Y, Xie ME, Brinks D, Wu H, Mostajo-Radji MA, Kheifets S, Parot V, Chettih S, Williams KJ, Gmeiner B, Farhi SL, Madisen L, Buchanan EK, Kinsella I, Zhou D, Paninski L, Harvey CD, et al. 2019. Voltage imaging and optogenetics reveal behaviour-dependent changes in hippocampal dynamics. *Nature* **569**:413–417. DOI: https://doi.org/10.1038/s41586-019-1166-7, PMID: 31043747

Beaulieu-Laroche L, Toloza EHS, Brown NJ, Harnett MT. 2019. Widespread and highly correlated Somato-dendritic activity in cortical layer 5 neurons. *Neuron* **103**:235–241. DOI: https://doi.org/10.1016/j.neuron.2019.05.014, PMID: 31178115

Bittner KC, Grienberger C, Vaidya SP, Milstein AD, Macklin JJ, Suh J, Tonegawa S, Magee JC. 2015. Conjunctive input processing drives feature selectivity in hippocampal CA1 neurons. *Nature Neuroscience* **18**:1133–1142. DOI: https://doi.org/10.1038/nn.4062, PMID: 26167906

Bittner KC, Milstein AD, Grienberger C, Romani S, Magee JC. 2017. Behavioral time scale synaptic plasticity underlies CA1 place fields. *Science* **357**:1033–1036. DOI: https://doi.org/10.1126/science.aan3846, PMID: 28883072

Bono J, Clopath C. 2017. Modeling somatic and dendritic spike mediated plasticity at the single neuron and network level. *Nature Communications* **8**:706. DOI: https://doi.org/10.1038/s41467-017-00740-z, PMID: 28951585

Brainard DH. 1997. The psychophysics toolbox. *Spatial Vision* **10**:433–436. DOI: https://doi.org/10.1163/156856897X00357, PMID: 9176952

Cai X, Liang CW, Muralidharan S, Muralidharan S, Kao JP, Tang CM, Thompson SM. 2004. Unique roles of SK and Kv4.2 potassium channels in dendritic integration. *Neuron* **44**:351–364. DOI: https://doi.org/10.1016/j.neuron.2004.09.026, PMID: 15473972

Chen TW, Wardill TJ, Sun Y, Pulver SR, Renninger SL, Baohan A, Schreiter ER, Kerr RA, Orger MB, Jayaraman V, Looger LL, Svoboda K, Kim DS. 2013. Ultrasensitive fluorescent proteins for imaging neuronal activity. *Nature* **499**:295–300. DOI: https://doi.org/10.1038/nature12354, PMID: 23868258

Cichon J, Gan WB. 2015. Branch-specific dendritic ca(2+) spikes cause persistent synaptic plasticity. *Nature* **520**:180–185. DOI: https://doi.org/10.1038/nature14251, PMID: 25822789

Dadarlat MC, Stryker MP. 2017. Locomotion enhances neural encoding of visual stimuli in mouse V1. *The Journal of Neuroscience* **37**:3764–3775. DOI: https://doi.org/10.1523/JNEUROSCI.2728-16.2017, PMID: 28264980

Erisken S, Vaiceliunaite A, Jurjut O, Fiorini M, Katzner S, Busse L. 2014. Effects of locomotion extend throughout the mouse early visual system. *Current Biology* **24**:2899–2907. DOI: https://doi.org/10.1016/j.cub.2014.10.045, PMID: 25484299

Gerfen CR, Economo MN, Chandrashekar J. 2018. Long distance projections of cortical pyramidal neurons. *Journal of Neuroscience Research* **96**:1467–1475. DOI: https://doi.org/10.1002/jnr.23978, PMID: 27862192

Golding NL, Staff NP, Spruston N. 2002. Dendritic spikes as a mechanism for cooperative long-term potentiation. *Nature* **418**:326–331. DOI: https://doi.org/10.1038/nature00854, PMID: 12124625

Grienberger C, Chen X, Konnerth A. 2015. Dendritic function in vivo. *Trends in Neurosciences* **38**:45–54. DOI: https://doi.org/10.1016/j.tins.2014.11.002, PMID: 25432423

Grienberger C, Milstein AD, Bittner KC, Romani S, Magee JC. 2017. Inhibitory suppression of heterogeneously tuned excitation enhances spatial coding in CA1 place cells. *Nature Neuroscience* **20**:417–426. DOI: https://doi.org/10.1038/nn.4486

Groh A, Meyer HS, Schmidt EF, Heintz N, Sakmann B, Krieger P. 2010. Cell-type specific properties of pyramidal neurons in neocortex underlying a layout that is modifiable depending on the cortical area. *Cerebral Cortex* **20**:826–836. DOI: https://doi.org/10.1093/cercor/bhp152, PMID: 19643810

Guerguiev J, Lillicrap TP, Richards BA. 2017. Towards deep learning with segregated dendrites. *eLife* **6**:e22907. DOI: https://doi.org/10.7554/eLife.22901

Harris KD, Shepherd GMG. 2015. The neocortical circuit: themes and variations. *Nature Neuroscience* **18**:170–181. DOI: https://doi.org/10.1038/nn.3917

Helmchen F, Svoboda K, Denk W, Tank DW. 1999. In vivo dendritic calcium dynamics in deep-layer cortical pyramidal neurons. *Nature Neuroscience* **2**:989–996. DOI: https://doi.org/10.1038/14788, PMID: 10526338

Hill DN, Varga Z, Jia H, Sakmann B, Konnerth A. 2013. Multibranch activity in basal and tuft dendrites during firing of layer 5 cortical neurons in vivo. *PNAS* **110**:13618–13623. DOI: https://doi.org/10.1073/pnas.1312599110, PMID: 23904480

Hong YK, Lacefield CO, Rodgers CC, Bruno RM. 2018. Sensation, movement and learning in the absence of barrel cortex. *Nature* **561**:542–546. DOI: https://doi.org/10.1038/s41586-018-0527-y, PMID: 30224746

Kaifosh P, Zaremba JD, Danielson NB, Losonczy A. 2014. SIMA: python software for analysis of dynamic fluorescence imaging data. *Frontiers in Neuroinformatics* **8**:80. DOI: https://doi.org/10.3389/fninf.2014.00080, PMID: 25295002

Kampa BM, Letzkus JJ, Stuart GJ. 2006. Requirement of dendritic calcium spikes for induction of spike-timing-dependent synaptic plasticity. *The Journal of Physiology* **574**:283–290. DOI: https://doi.org/10.1113/jphysiol.2006.111062, PMID: 16675489

Kerlin A, Boaz M, Flickinger D, MacLennan BJ, Dean MB, Davis C, Spruston N, Svoboda K. 2019. Functional clustering of dendritic activity during decision-making. *eLife* **8**:e46966. DOI: https://doi.org/10.7554/eLife.46966, PMID: 31663507

Kim EJ, Juavinett AL, Kyubwa EM, Jacobs MW, Callaway EM. 2015. Three types of cortical layer 5 neurons that differ in Brain-wide connectivity and function. *Neuron* **88**:1253–1267. DOI: https://doi.org/10.1016/j.neuron.2015.11.002, PMID: 26671462

Labarrera C, Deitcher Y, Dudai A, Weiner B, Kaduri Amichai A, Zylbermann N, London M. 2018. Adrenergic modulation regulates the dendritic excitability of layer 5 pyramidal neurons in Vivo. *Cell Reports* **23**:1034–1044. DOI: https://doi.org/10.1016/j.celrep.2018.03.103

Larkum ME, Kaiser KM, Sakmann B. 1999a. Calcium electrogenesis in distal apical dendrites of layer 5 pyramidal cells at a critical frequency of back-propagating action potentials. *PNAS* **96**:14600–14604. DOI: https://doi.org/10.1073/pnas.96.25.14600, PMID: 10588751

Larkum ME, Zhu JJ, Sakmann B. 1999b. A new cellular mechanism for coupling inputs arriving at different cortical layers. *Nature* **398**:338–341. DOI: https://doi.org/10.1038/18686, PMID: 10192334

Larkum ME, Nevian T, Sandler M, Polsky A, Schiller J. 2009. Synaptic integration in tuft dendrites of layer 5 pyramidal neurons: a new unifying principle. *Science* **325**:756–760. DOI: https://doi.org/10.1126/science.1171958, PMID: 19661433

Larkum M. 2013. A cellular mechanism for cortical associations: an organizing principle for the cerebral cortex. *Trends in Neurosciences* **36**:141–151. DOI: https://doi.org/10.1016/j.tins.2012.11.006, PMID: 23273272

Magee JC. 1997. A synaptically controlled, associative signal for hebbian plasticity in hippocampal neurons. *Science* **275**:209–213. DOI: https://doi.org/10.1126/science.275.5297.209

Major G, Larkum ME, Schiller J. 2013. Active properties of neocortical pyramidal neuron dendrites. *Annual Review of Neuroscience* **36**:1–24. DOI: https://doi.org/10.1146/annurev-neuro-062111-150343, PMID: 23841837

Manita S, Suzuki T, Homma C, Matsumoto T, Odagawa M, Yamada K, Ota K, Matsubara C, Inutsuka A, Sato M, Ohkura M, Yamanaka A, Yanagawa Y, Nakai J, Hayashi Y, Larkum ME, Murayama M. 2015. A Top-Down cortical circuit for accurate sensory perception. *Neuron* **86**:1304–1316. DOI: https://doi.org/10.1016/j.neuron.2015.05.006, PMID: 26004915

Mazurek M, Kager M, Van Hooser SD. 2014. Robust quantification of orientation selectivity and direction selectivity. *Frontiers in Neural Circuits* **8**:92. DOI: https://doi.org/10.3389/fncir.2014.00092, PMID: 25147504

Moore JJ, Ravassard PM, Ho D, Acharya L, Kees AL, Vuong C, Mehta MR. 2017. Dynamics of cortical dendritic membrane potential and spikes in freely behaving rats. *Science* **355**:eaaj1497. DOI: https://doi.org/10.1126/science.aaj1497, PMID: 28280248

Naka A, Adesnik H. 2016. Inhibitory circuits in cortical layer 5. *Frontiers in Neural Circuits* **10**:35. DOI: https://doi.org/10.3389/fncir.2016.00035, PMID: 27199675

Niell CM, Stryker MP. 2008. Highly Selective Receptive Fields in Mouse Visual Cortex. *Journal of Neuroscience* **28**:7520–7536. DOI: https://doi.org/10.1523/JNEUROSCI.0623-08.2008

Pakan JM, Lowe SC, Dylda E, Keemink SW, Currie SP, Coutts CA, Rochefort NL. 2016. Behavioral-state modulation of inhibition is context-dependent and cell type specific in mouse visual cortex. *eLife* **5**:e14985. DOI: https://doi.org/10.7554/eLife.14985, PMID: 27552056

Pakan JMP, Currie SP, Fischer L, Rochefort NL. 2018a. The impact of visual cues, reward, and motor feedback on the representation of behaviorally relevant spatial locations in primary visual cortex. *Cell Reports* **24**:2521–2528. DOI: https://doi.org/10.1016/j.celrep.2018.08.010, PMID: 30184487

Pakan JM, Francioni V, Rochefort NL. 2018b. Action and learning shape the activity of neuronal circuits in the visual cortex. *Current Opinion in Neurobiology* **52**:88–97. DOI: https://doi.org/10.1016/j.conb.2018.04.020, PMID: 29727859

Palmer LM, Shai AS, Reeve JE, Anderson HL, Paulsen O, Larkum ME. 2014. NMDA spikes enhance action potential generation during sensory input. *Nature Neuroscience* **17**:383–390. DOI: https://doi.org/10.1038/nn.3646, PMID: 24487231

Peters AJ, Lee J, Hedrick NG, O'Neil K, Komiyama T. 2017. Reorganization of corticospinal output during motor learning. *Nature Neuroscience* **20**:1133–1141. DOI: https://doi.org/10.1038/nn.4596, PMID: 28671694

Ranganathan GN, Apostolides PF, Harnett MT, Xu NL, Druckmann S, Magee JC. 2018. Active dendritic integration and mixed neocortical network representations during an adaptive sensing behavior. *Nature Neuroscience* **21**:1583–1590. DOI: https://doi.org/10.1038/s41593-018-0254-6, PMID: 30349100

Remy S, Spruston N. 2007. Dendritic spikes induce single-burst long-term potentiation. *PNAS* **104**:17192–17197. DOI: https://doi.org/10.1073/pnas.0707919104, PMID: 17940015

Roome CJ, Kuhn B. 2018. Simultaneous dendritic voltage and calcium imaging and somatic recording from purkinje neurons in awake mice. *Nature Communications* **9**:3388. DOI: https://doi.org/10.1038/s41467-018-05900-3, PMID: 30139936

Sandler M, Shulman Y, Schiller J. 2016. A novel form of local plasticity in tuft dendrites of neocortical somatosensory layer 5 pyramidal neurons. *Neuron* **90**:1028–1042. DOI: https://doi.org/10.1016/j.neuron.2016.04.032, PMID: 27210551

Schiller J, Schiller Y, Stuart G, Sakmann B. 1997. Calcium action potentials restricted to distal apical dendrites of rat neocortical pyramidal neurons. *The Journal of Physiology* **505**:605–616. DOI: https://doi.org/10.1111/j.1469-7793.1997.605ba.x, PMID: 9457639

Shai AS, Anastassiou CA, Larkum ME, Koch C. 2015. Physiology of layer 5 pyramidal neurons in mouse primary visual cortex: coincidence detection through bursting. *PLOS Computational Biology* **11**:e1004090. DOI: https://doi.org/10.1371/journal.pcbi.1004090, PMID: 25768881

Sheffield MEJ, Adoff MD, Dombeck DA. 2017. Increased prevalence of calcium transients across the dendritic arbor during place field formation. *Neuron* **96**:490–504. DOI: https://doi.org/10.1016/j.neuron.2017.09.029, PMID: 29024668

Sheffield ME, Dombeck DA. 2019. Dendritic mechanisms of hippocampal place field formation. *Current Opinion in Neurobiology* **54**:1–11. DOI: https://doi.org/10.1016/j.conb.2018.07.004, PMID: 30036841

Silberberg G, Markram H. 2007. Disynaptic inhibition between neocortical pyramidal cells mediated by martinotti cells. *Neuron* **53**:735–746. DOI: https://doi.org/10.1016/j.neuron.2007.02.012, PMID: 17329212

Sjöström PJ, Häusser M. 2006. A cooperative switch determines the sign of synaptic plasticity in distal dendrites of neocortical pyramidal neurons. *Neuron* **51**:227–238. DOI: https://doi.org/10.1016/j.neuron.2006.06.017, PMID: 16846857

Smith SL, Smith IT, Branco T, Häusser M. 2013. Dendritic spikes enhance stimulus selectivity in cortical neurons in vivo. *Nature* **503**:115–120. DOI: https://doi.org/10.1038/nature12600, PMID: 24162850

Spruston N, Schiller Y, Stuart G, Sakmann B. 1995. Activity-dependent action potential invasion and calcium influx into hippocampal CA1 dendrites. *Science* **268**:297–300. DOI: https://doi.org/10.1126/science.7716524, PMID: 7716524

Stuart G, Schiller J, Sakmann B. 1997. Action potential initiation and propagation in rat neocortical pyramidal neurons. *The Journal of Physiology* **505**:617–632. DOI: https://doi.org/10.1111/j.1469-7793.1997.617ba.x, PMID: 9457640

Stuart GJ, Spruston N. 2015. Dendritic integration: 60 years of progress. *Nature Neuroscience* **18**:1713–1721. DOI: https://doi.org/10.1038/nn.4157, PMID: 26605882

Svoboda K, Denk W, Kleinfeld D, Tank DW. 1997. In vivo dendritic calcium dynamics in neocortical pyramidal neurons. *Nature* **385**:161–165. DOI: https://doi.org/10.1038/385161a0, PMID: 8990119

Takahashi N, Oertner TG, Hegemann P, Larkum ME. 2016. Active cortical dendrites modulate perception. *Science* **354**:1587–1590. DOI: https://doi.org/10.1126/science.aah6066, PMID: 28008068

Vetter P, Roth A, Häusser M. 2001. Propagation of action potentials in dendrites depends on dendritic morphology. *Journal of Neurophysiology* **85**:926–937. DOI: https://doi.org/10.1152/jn.2001.85.2.926, PMID: 11160523

Villette V, Chavarha M, Dimov IK, Bradley J, Pradhan L, Mathieu B, Evans SW, Chamberland S, Shi D, Yang R, Kim BB, Ayon A, Jalil A, St-Pierre F, Schnitzer MJ, Bi G, Toth K, Ding J, Dieudonné S, Lin MZ. 2019. Ultrafast Two-Photon imaging of a High-Gain voltage Indicator in awake behaving mice. *Cell* **179**:1590–1608. DOI: https://doi.org/10.1016/j.cell.2019.11.004, PMID: 31835034

Vinck M, Batista-Brito R, Knoblich U, Cardin JA. 2015. Arousal and locomotion make distinct contributions to cortical activity patterns and visual encoding. *Neuron* **86**:740–754. DOI: https://doi.org/10.1016/j.neuron.2015.03.028, PMID: 25892300

Waters J, Larkum M, Sakmann B, Helmchen F. 2003. Supralinear Ca2+ influx into dendritic tufts of layer 2/3 neocortical pyramidal neurons *in* vitro and *in* vivo. *The Journal of Neuroscience* **23**:8558–8567. DOI: https://doi.org/10.1523/JNEUROSCI.23-24-08558.2003, PMID: 13679425

Williams SR, Fletcher LN. 2019. A dendritic substrate for the cholinergic control of neocortical output neurons. *Neuron* **101**:486–499. DOI: https://doi.org/10.1016/j.neuron.2018.11.035, PMID: 30594427

Xu NL, Harnett MT, Williams SR, Huber D, O'Connor DH, Svoboda K, Magee JC. 2012. Nonlinear dendritic integration of sensory and motor input during an active sensing task. *Nature* **492**:247–251. DOI: https://doi.org/10.1038/nature11601, PMID: 23143335

Yaeger CE, Ringach DL, Trachtenberg JT. 2019. Neuromodulatory control of localized dendritic spiking in critical period cortex. *Nature* **567**:100–104. DOI: https://doi.org/10.1038/s41586-019-0963-3, PMID: 30787434

Young H. 2019. Laminar-specific cortico-cortical loops in mouse visual cortex. *bioRxiv*. DOI: https://doi.org/10.1101/773085

Appendix 2: Pakan J.M., Francioni V. and Rochefort N.L. (2018)

Available online at www.sciencedirect.com

ScienceDirect

Current Opinion in Neurobiology

Action and learning shape the activity of neuronal circuits in the visual cortex

Janelle MP Pakan[1,2], Valerio Francioni[3] and Nathalie L Rochefort[3,4]

Nonsensory variables strongly influence neuronal activity in the adult mouse primary visual cortex. Neuronal responses to visual stimuli are modulated by behavioural state, such as arousal and motor activity, and are shaped by experience. This dynamic process leads to neural representations in the visual cortex that reflect stimulus familiarity, expectations of reward and object location, and mismatch between self-motion and visual-flow. The recent development of genetic tools and recording techniques in awake behaving mice has enabled the investigation of the circuit mechanisms underlying state-dependent and experience-dependent neuronal representations in primary visual cortex. These neuronal circuits involve neuromodulatory, top-down cortico-cortical and thalamocortical pathways. The functions of nonsensory signals at this early stage of visual information processing are now beginning to be unravelled.

Addresses
[1] Center for Behavioral Brain Sciences, Institute of Cognitive Neurology and Dementia Research, Otto-von-Guericke University, Magdeburg, Germany
[2] German Center for Neurodegenerative Diseases, Magdeburg, Germany
[3] Centre for Discovery Brain Sciences, School of Biomedical Sciences, Edinburgh, United Kingdom
[4] Simons Initiative for the Developing Brain, Edinburgh, United Kingdom

Corresponding author: Rochefort, Nathalie L (n.rochefort@ed.ac.uk)

Current Opinion in Neurobiology 2018, **52**:88–97

This review comes from a themed issue on **Systems neuroscience**

Edited by **Michael Long and Rosa Cossart**

For a complete overview see the Issue and the Editorial

Available online 1st May 2018

https://doi.org.10.1016/j.conb.2018.04.020

Introduction

The brain integrates sensory information to generate sensations, thoughts and motor actions that are relevant for an animal's behaviour. This process involves the integration of sensory inputs with internal information about the animal's behavioural-state and its previous experience. For the same sensory stimulus, the outcome may be very different: for example, the vision of a dog can either trigger an affectionate or a fearful reaction depending on our past experience and physical condition.

Historically, primary sensory areas were thought to function as feature detectors. These areas create a representation of the external world that would be transmitted to higher cortical areas where this representation would be integrated with information related to past experience and behavioural state. This view was supported by *in vivo* electrophysiological recordings performed in anaesthetised and often paralysed animals, which have revealed fundamental principles of neuronal encoding of visual features in the visual cortex [1–3]. However, the use of anaesthetised animals prevented the investigation of the influence of nonsensory variables on V1 neuronal activity. In addition, anaesthesia itself modifies neuronal activity [4].

In this review, we present recent experimental approaches that were developed to investigate neuronal representations in the cortex of awake behaving mice. We also review current knowledge about the integration of nonsensory information in the adult rodent primary visual cortex, describing the impact of state-dependent changes (arousal and locomotion) as well as past experience on V1 neuronal activity. We review identified pathways that provide state-dependent and motor-related information to V1 neurons. We then discuss current challenges in the standardization of experimental conditions for awake-behaving animals as well as issues raised by big data analyses. Finally, we discuss potential functions of these nonsensory signals at this early stage of visual information processing.

Investigation of visual information processing in awake behaving mice

The development of recording methods in awake behaving animals has led to seminal discoveries about the impact of action and learning on the activity of visual neurons in cats and nonhuman primates [5–7]. However, the lack of genetic tools in these species limits the investigation of the neuronal circuits underlying these experience-dependent changes in V1 neuronal activity. Such mechanisms can be studied in the mouse visual system by combining genetic tools and recordings in awake behaving mice. Using either electrophysiological recordings or two-photon imaging in head-fixed awake mice, it is now possible to monitor the activity of hundreds to thousands of neurons, during several days and weeks (Figure 1a–c). Neuronal activity is then correlated with both visual stimuli presented during

Figure 1

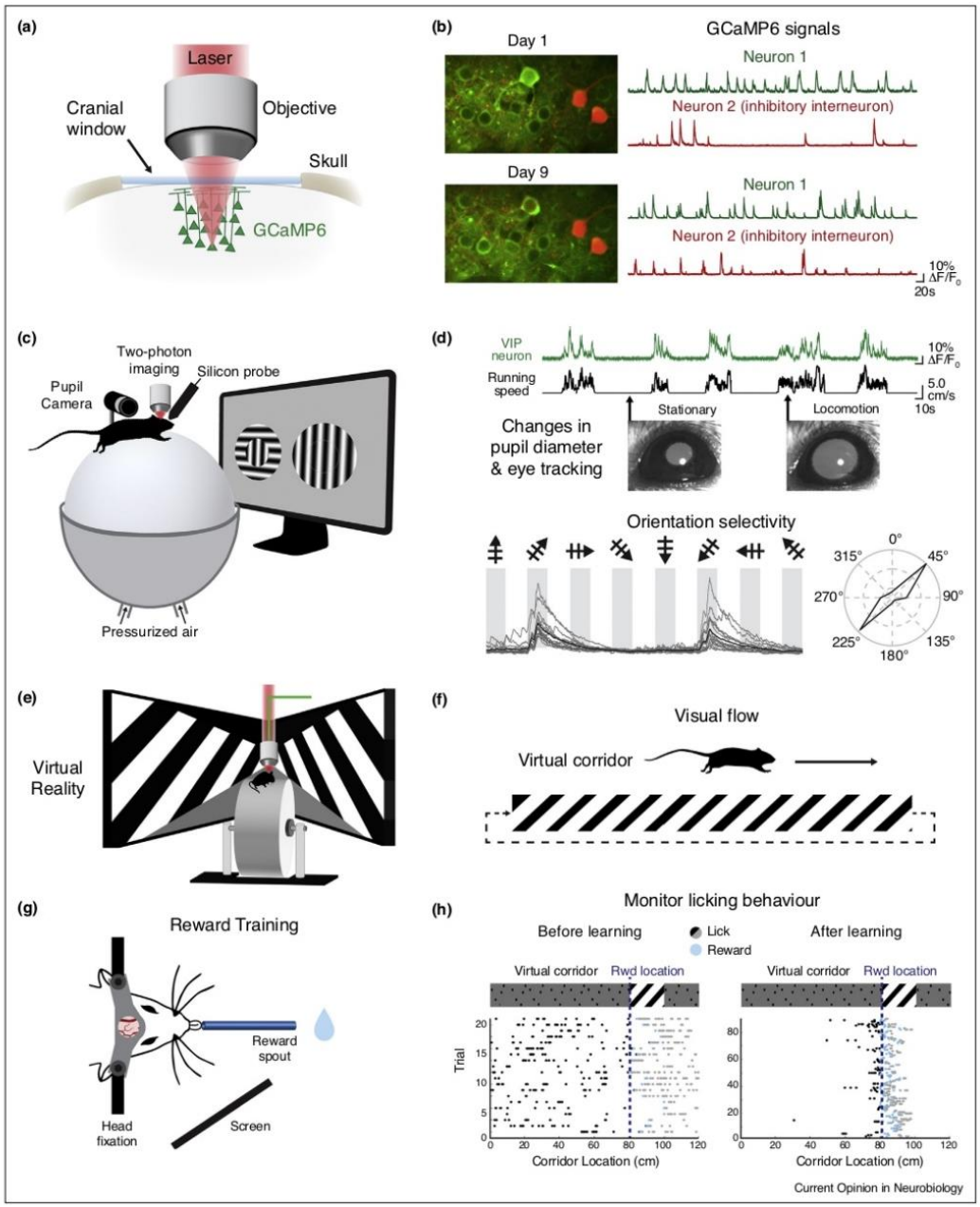

Experimental procedures for recording neuronal activity and correlated behavioural parameters in head-fixed awake behaving rodents. **(a)** Schematic of a cranial window preparation above primary visual cortex (V1) that allows chronic two-photon imaging of neurons labelled with a

the recordings as well as measured behavioural parameters such as task performance (Figure 1c,d). This approach not only reveals the impact of internal state and past experience on neuronal activity but also the dynamics of visual neuronal circuits during learning. Additionally, the availability of transgenic mice expressing Cre-recombinase in specific subtypes of inhibitory neurons has enabled the characterization of both excitatory and inhibitory activity in the visual cortex (Figure 1b).

Arousal and locomotion increase the gain and modulate selectivity of visual responses

The impact of arousal and locomotion on the activity of visual cortex neurons has been most commonly studied using recordings in head-fixed rodents that are freely running on a ball [8] or a disk (Figure 1c,e). The running speed of the animal, pupil dilation and local field potentials (LFP) are used to assess state-dependent changes in awake rodents [9] (Figure 1d). An increase in arousal measured by an increase in running speed, or pupil dilation, correlates with an increase in the visually evoked activity of neurons in V1 [10–13,14•,15,16,17••] and higher visual areas [18,19]. This gain in the visual responses during locomotion has been shown to preserve the orientation preference and spatial frequency of excitatory neurons [10,20•] (Figure 2a). During periods of high arousal while the animal is stationary, corresponding to periods of pupil dilation, responses at preferred orientations are enhanced, resulting in a sharpening of orientation selectivity [15]. During locomotion, neurons preferring high spatial frequencies display larger gain in visual responses than other neurons, suggesting an increased spatial resolution during locomotion [20•]. In addition, a shift towards higher temporal frequency preferences was observed in V1 and higher visual areas [18]. Finally, locomotion also increases spatial summation of V1 neurons by reducing surround suppression [11,21].

Altogether, these results suggest a more robust and accurate encoding of visual stimuli during high arousal and locomotion. Concordantly, decoders used to infer the identity of the presented visual stimulus from the activity of V1 neurons, perform better when using activity during locomotion than during still periods [20•,22•]. One potential mechanism underlying this increased stimulus discriminability is the decreased response variability both at the level of subthreshold membrane potentials [13,14•] and noise correlations in neuronal populations [11,16,22•] during periods of locomotion and high arousal. In addition, it has been suggested that different cortical layers may encode visuo-locomotor information in different ways [11,22•]. For instance, in layer 2/3, stimulus discriminability by decoders was improved mainly because of an increase in firing rate during locomotion. However, in layer 5, the increased stimulus discriminability was mainly the consequence of a decrease in noise correlations across the population [22•].

Experience shapes the neuronal representation of visual stimuli in V1

Integrating self-motion with visual inputs: visual flow predictions and spatial expectations in V1

A fundamental function of the visual system is to enable the detection of moving stimuli and to navigate through the environment. For this, it is necessary to assess the relation between self-motion and the position and speed of a visual stimulus. This process requires an estimate of the animal's self-motion and a comparison of this estimation with visual inputs. The use of virtual reality is well suited to investigate the circuit mechanisms underlying this process since it allows measuring the speed and manipulating the visual flow experienced by the animal [23,24] (Figure 1e,f).

(Figure 1 Legend Continued) genetically encoded calcium indicator (GCaMP6). **(b)** GCaMP6-labelled neurons (green) can be imaged over multiple days and even weeks (example field of view from imaging Day 1 and 9). Relative changes in fluorescence ($\Delta F/F_0$) over time are used as a proxy read-out of neuronal activity. Signals from genetically defined subpopulations of cells can be isolated via a second fluorescent marker (e.g. tdTomato expression in somatostatin expressing inhibitory interneurons, shown here in red). **(c)** Head-fixed rodents can freely move on an air-supported styrofoam ball that acts as a spherical treadmill while calcium imaging and/or electrophysiological recordings are performed. Optical computer mice are used to assess running speed. Pupil diameter and eye-tracking can be recorded with cameras. In this configuration, animals can navigate an open virtual reality environment or view a visual stimulus where left/right behavioural choices can be made with motor movements. **(d)** Neuronal activity can be correlated with running speed and changes in pupil diameter, used as a measure of arousal. GCaMP6 signal from a V1 VIP expressing interneuron is shown in green and animal's speed in black. As traditionally done in anaesthetised animals, neuronal activity in V1 can be correlated with visual stimulation in the form of passively viewed stimuli, such as drifting gratings displayed on a screen. Bottom panel shows single trials (grey) and average response (black) of a GCaMP6-labelled neuron to different oriented gratings. Polar plot shows the amplitude of calcium transients in response to each orientation, normalised to the maximum response. **(e)** Head-fixed rodents can be placed in a virtual environment: animals run as if on a linear treadmill and, with surrounding screens, can navigate virtual corridors with defined wall patterns. Note that the spherical treadmill can be replaced by a cylindrical wheel where an optical encoder attached to the central axle records speed. **(f)** Using a virtual reality environment, the visual flow experienced by the animal can be measured and manipulated. An animal navigating along a virtual corridor creates visual flow: the experimenter can manipulate this coupling to create a mismatch between the visual flow and the animal's movement. **(g)** Experience-dependent neuronal changes in V1 can be studied using head-fixed animals learning visually guided tasks. Water deprived animals learn to lick during key experimental cues and goal-directed behaviours in order to receive water rewards through a spout. **(h)** Licking behaviour is monitored by a lick sensor on the spout during task performance. Example of a task in which the animal must lick at a certain reward location demarcated by a visual cue (oriented grating) along a virtual track. Each dot represents a lick: prereward licking (black dots), rewarded-licking at the right visual cue (blue dots) and postreward licks (grey dots). With learning, licking behaviour becomes tightly coupled to the location of the rewarded visual cue along the track.

Figure 2

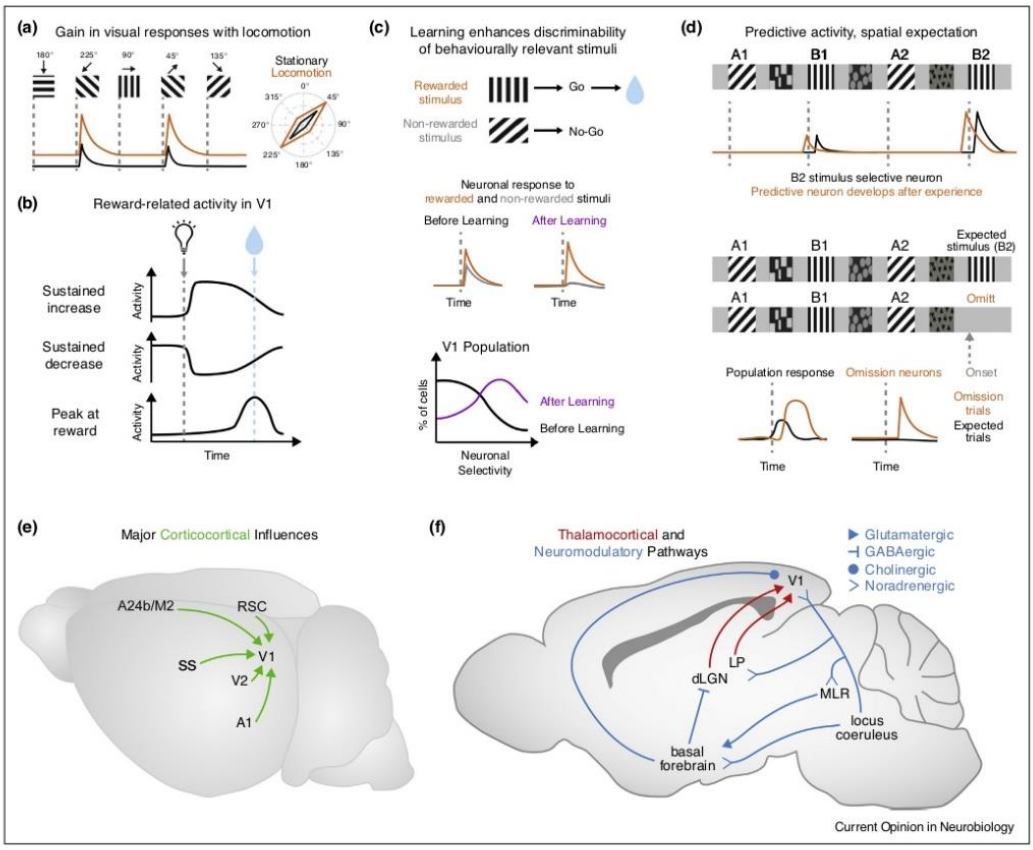

Neuronal activity in V1 is shaped by behavioural-state and experience-dependent processes, mediated through the integration of nonvisual inputs. **(a)** Schematic representing the increased gain in neuronal responses to oriented gratings during locomotion (orange trace) versus stationary periods (black trace). Both additive (as illustrated) and multiplicative gain modulations were reported in V1 excitatory neurons [22•]. Illustration is based on Ref. [10]. **(b)** Schematic of representations of reward timing in V1. After the learning of a task associating a visual cue (light bulb) and a reward (blue drop), neuronal responses in V1 predict the timing of reward events by sustaining either an increase or decrease in activity after a visual stimulus onset (grey dotted line) or peaking at the expected reward time (blue dotted line). Illustration is based on Refs. [37,38]. **(c)** Schematic of V1 responses during the learning of a visually guided task. Example of a go/no-go task with two oriented gratings and only one grating is rewarded (blue drop). A schematic of the responses of a single neuron to the two presented stimuli show that neuronal discriminability between the rewarded (orange) and nonrewarded (grey) stimuli increases with task learning. On the population level (bottom panel), a higher proportion of neurons in V1 show increased selectivity to task-relevant gratings after learning (purple). Illustrations are based on Ref. [43]. **(d)** Schematic of responses to spatial expectation of visual stimuli in V1. Top panel: schematic of a paradigm where animals are presented with a sequence of visual cues along a virtual track. Traces illustrate neuronal responses to visual cues, before (black) and after (orange) repeated exposure to the same sequence. A population of V1 neurons show specific responses to a given visual stimulus (e.g. vertical grating) but also specific responses for a given stimulus at a particular spatial location (response to vertical grating at B2 location larger than B1). With experience, a population of neurons develop predictive responses, shifting the onset of their response to before the appearance of their preferred stimulus (orange trace). Bottom panel illustrates the effect of omitting an expected stimulus in a trained sequence. On the population level, when the stimulus is present there is an evoked response to the stimulus (black trace), but when the stimulus is un-expectantly omitted (orange trace), there is a large and delayed increase in activity. A subpopulation of neurons respond selectively to these omission events, and not to the initially expected stimulus. Illustration is based on Ref. [28•]. **(e)** Schematic of the major cortico-cortical inputs to V1, including top-down influences from higher visual areas (V2), the retrosplenial cortex (RSC) and secondary motor regions (A24b/M2) as well as inputs from other sensory modalities such as the primary auditory cortex (A1) and the somatosensory cortex (SS). Inputs from higher visual areas (V2) include connections from lateral, medial and mediolateral secondary visual areas. **(f)** Schematic of neuromodulatory and thalamocortical inputs to V1 that have been shown to influence V1 activity in awake behaving mice. LP, Lateral posterior nucleus; dLGN, dorsal lateral geniculate nucleus; MLR, mesencephalic locomotor region.

As described above, in addition to feedforward visual inputs, motor-related signals modulate V1 activity. A subpopulation of neurons was found to detect mismatch between the animal's movement and the visual flow [12,25]. These neurons have restricted receptive fields and thus respond to local mismatch in a specific portion of visual space, as is the case when an object moves into the visual space of a behaving animal [25]. These mismatch responses are shaped by active visuomotor experience, that is, by the experience of a given relation between the animal's own movement and the motion of a visual stimulus, both during development and in adulthood [26,27••]. These results are consistent with a predictive coding interpretation of visual processing: since during normal development, the relation between visual-flow and self-movement is very consistent, this relation is thus predictable. This prediction could then be compared to feed-forward visual inputs in order to detect mismatches between the prediction and the visual stimuli: such mismatches would, for example, occur for objects moving independently of the animal.

Internal representations of the animal's self-movement are crucial for navigation and spatial expectations of visual stimuli. It was shown that a subset of V1 neurons respond specifically to a given stimulus placed in one location and less to the same stimulus at another location along a virtual track [28•] (Figure 2d). These responses were shaped by experience and became predictive: neurons responded before the expected encounter of the visual stimulus and to the absence of the expected stimulus (omission signal) [28•] (Figure 2d). These results are also consistent with predictive coding in the visual cortex: an internal representation of the visual scene is compared to feed-forward visual inputs, leading to experience-dependent representations of spatial expectations of visual stimuli.

Passive exposure either enhances or decreases responses to the exposed stimulus

Several studies have shown that the daily presentation of visual stimuli over consecutive days, without any associated reward or aversive stimuli, modifies the representation of these stimuli in V1. Electrophysiological recordings performed in awake head-fixed mice, placed in a tube, have revealed a long lasting (across weeks) stimulus-specific potentiation of visually evoked potentials in V1 layer 4 [29,30]. This stimulus-specific response potentiation correlated with the habituation of a behavioural response. Initially the mice would respond to novel gratings with fidget-like movements of the forepaws, but these movements habituated in a stimulus-specific manner and over the same time course as the potentiation of V1 responses [30]. Another study using intrinsic signal imaging and chronic two-photon calcium imaging in anaesthetised animals also showed a stimulus-specific increase in the responses of layer 2/3 neurons to a daily presented stimulus [31]. However, this effect was only observed in mice that had been running for a cumulative time of at least one hour during the stimulus presentations across days [31]. These results are contrasted by a third study using the same experimental approach in awake running mice but showing a stimulus-specific decrease in the number of layer 2/3 visually responsive neurons across days [32]. The discrepancies between these studies highlight the challenges of standardizing experimental conditions and data analysis for high-throughput recordings in awake behaving mice (see last section of this review).

A potential source of variability could be that different neuronal subnetworks may display either stable or plastic neuronal responses during passive viewing. A recent study showed that 2 weeks after the presentation of high-contrast gratings of different sizes, a systematic shift towards smaller size preferences and greater surround suppression was observed in a subpopulation of weakly responsive neurons, while the majority of excitatory neurons maintained stable responses [33].

Finally, another form of experience-dependent changes in V1 activity during passive exposure was demonstrated after repeated exposure to rapid sequences of stimuli [34] and fast-moving spots [35]. Such protocols triggered a recall of neuronal activity when some stimuli were omitted from the sequence. This effect was strongly dependent on the timing of the sequence [34] and was observed in anaesthetised animals and quiet, immobile awake animals. However, this effect was not observed in awake mice with facial/whisker movement and irregular, high-frequency LFP activity, which are characteristic of behaving animals [35].

Learning a behavioural task correlates with enhanced neuronal representations of relevant stimuli

By using either rewards or aversive stimuli, mice engage in performing and learning a task. Most commonly, animals are deprived of water or food and a given visual stimulus is paired with either reward [36] (Figure 1g,h).

Neurons in deep layers of rat V1 were shown to acquire responses specific to the timing interval preceding a reward [37] (Figure 2b). For this task, light flashes were delivered to either the left or the right eye; depending on which eye was stimulated, the animal had to perform a different number of licks (i.e. over time) to obtain a water-reward. The acquisition, but not the expression, of this reward-timing activity has since been shown to depend on cholinergic inputs from basal forebrain projections to V1 [38,39].

Rodents can also learn to discriminate a rewarded visual stimulus from a nonrewarded one [40–42] (Figure 1g,h). Combining chronic two-photon calcium imaging in V1 layer 2/3 neurons with a go/no-go discrimination task in a

virtual reality environment, a study has revealed that the V1 population becomes better at discriminating the rewarded from the nonrewarded stimulus [43] (Figure 2c). Task-specific changes in the activity of layer 2/3 neurons have also been observed in aversive conditioning tasks, in which, for example, mice had to detect a visual stimulus by initiating running on a treadmill; failure to run triggered a mild tail shock [32]. In this study, learning modulated the activity of both excitatory and somatostatin (SST)-expressing inhibitory neurons. Additionally, by imaging changes in fluorescence of GCaMP6-labelled axons from the retrosplenial cortex in V1, this study also showed an increase of calcium transients in these top-down inputs during learning [32].

The relationship between V1 encoding of relevant stimuli and behavioural performance was also recently investigated in a go/no-go visual stimulus detection task combined with *in vivo* two-photon imaging of OGB-labelled neurons [44]. The results showed that visual detection of a rewarded stimulus strongly correlates with the timing accuracy and sequence in which clusters of layer 2/3 neurons are active [44,45]. Using classical conditioning and electrophysiological recordings in adult mice, another study has shown that learning of orientation discrimination under classical conditioning correlated with increased neuronal discriminability between the rewarded and unrewarded stimulus, greater orientation tuning and improved contrast sensitivity. Notably, the improved representation of the relevant stimulus in V1 was fully developed before any improvement in the animal's behavioural performance [46•].

Finally, a direct test of the impact of stimulus behavioural relevance was performed by assessing contrast adaptation responses (reduced responses to sustained stimuli) of V1 neurons in a visually guided task in a virtual environment. While layer 2/3 neurons display an adaptation of their response for stimuli that were not relevant for the task, such adaptation was absent when stimuli became relevant to solve the same task [47••].

Altogether, these results support the view of a dynamic regulation of visual information processing in V1 based on the behavioural relevance of the stimulus. In this way, behaviourally salient visual representations are enhanced and stabilised while responses to nonrelevant stimuli are suppressed, for example, through mechanisms of adaptation. The long-term stability of these representations may also depend on their behavioural relevance [48].

Neuronal circuits underlying the integration of nonsensory inputs in the primary visual cortex

The precise origin of nonsensory inputs to V1 is still unclear. Recent advances in circuit mapping techniques (such as MAPseq technologies [49]) are bringing researchers closer to identifying these anatomical pathways on a whole brain scale. However, these large datasets now need to be integrated with functional recordings from neurons. So far, a number of studies have indicated that nonsensory signals can be conveyed through top-down cortico-cortical and thalamic inputs to V1, as well as via neuromodulatory pathways.

Neuromodulation has been shown to be a key mediator of brain state changes [9]. Both cholinergic [50] and noradrenergic [14•] inputs were shown to drive locomotion-related gain changes in V1. Results from stimulation of cholinergic neurons in basal forebrain [51] or stimulation of afferent projections to the basal forebrain [52], as well as calcium imaging of cholinergic projections in V1 [15], are all consistent with a role of cholinergic inputs in gain modulation of V1 activity [53]. It is also likely that other neuromodulators, including serotonin (5-HT), are involved in modulating V1 circuit activity during behaviour.

Changes in arousal or locomotion do not only modulate the activity of excitatory neurons but also the activity of inhibitory ones, including the three nonoverlapping classes of vasoactive intestinal peptide (VIP)-, SST- and parvalbumin-expressing neurons [14•,15,17••,26,50,54,55]. One proposed mechanism for gain modulation during locomotion has been an activation of VIP neurons through nicotinic acetylcholine receptors, leading to an inhibition of SST interneurons and a disinhibition of excitatory neurons [50]. Consistent with this mechanism, VIP neuronal activity reliably increases during periods of arousal and locomotion [17••,50,54] (Figure 1d) and activation of VIP neurons in V1 was found to elicit responses with similar properties as those elicited during locomotion [50,56].

However, SST interneurons were shown to be strongly responsive to visual stimuli and to further increase their activity during locomotion [17••,26,54,55], challenging the generality of the disinhibition model. In addition, the amplitude of this increased gain varies depending on the size of the stimulus and screen illumination [54] and SST neuronal activity is minimally, or slightly negatively, modulated by locomotion in darkness [17••,26,50,54]. This context-dependent change in SST responses was recently described in a computational model as an emerging property of circuits that include synaptic interactions between diverse neuronal populations and a nonlinear input–output relationship for each population [57•]. Considering that, in the rodent cortex, both excitatory and inhibitory neurons have different types of receptors (nicotinic and muscarinic) for different neuromodulators [14•,51,52,53,58–61], differential recruitment of interneuron subtypes may be triggered through a timely, coordinated release of different neuromodulators, depending on the behavioural context of the animal. Another hypothesis is that arousal and locomotion not only elicit the release of neuromodulators but also trigger direct excitatory inputs to V1.

Motor-related inputs to V1 are conveyed by axonal projections from a subdivision of anterior cingulate cortex (A24b) and an adjacent part of secondary motor cortex (M2) [27••]. These excitatory inputs were shown to drive motor and mismatch signals in V1 and adapt in an experience-dependent manner [27••]. Both layer 2/3 excitatory mismatch neurons and a subset of VIP interneurons were found to receive motor-related excitatory input, while a subset of SST interneurons was more strongly activated by visual flow [26]. A proposed mechanism is thus that mismatch excitatory neurons compute the difference between an inhibitory visual input provided by a subset of SST neurons, and an excitatory prediction of visual input based on motor output and provided by top-down connections [26,27••].

Finally, the integration of motor-related or experience-related information with visual inputs could occur in subcortical nuclei and then be transmitted to cortical areas. Locomotion-related activity was observed in thalamic nuclei processing visual information, the dorsal lateral geniculate nucleus (dLGN) [11] and the lateral posterior nucleus [62]. The contribution of feedback cortico-thalamic inputs to these activities remains unclear. Running speed also correlates with narrowband gamma power oscillations in V1 [52,63]. These oscillations were also found in the dLGN and silencing V1 optogenetically did not abolish them, suggesting that narrowband gamma power in V1 is mediated primarily by the rhythmic firing of LGN neurons [63].

Many aspects of the mechanisms underlying the impact of action and learning on V1 neuronal circuit activity remain unknown. These mechanisms involve diverse interconnected pathways: cortico-cortical, cortico-thalamo-cortical and neuromodulatory circuits (Figure 2e,f; see also Figure 1 of [27••]). In addition to the inputs described in this review, inputs from other sensory areas, in particular from the auditory cortex, also modulate V1 neuronal activity [64,65]. Each of these pathways can act independently or in synergy with each other, on different time and spatial scales and at different levels of neuronal activity, from membrane potential dynamics, to spike rates and neuronal population coding. Future challenges include the development of analysis tools that could encompass this high number of variables at different time scales. A comparison of neuronal activities across different sensory areas may reveal common circuit mechanisms; a recent study has combined large-scale imaging and voltage-sensitive dyes to demonstrate similar effects of arousal on neuronal responses to trains of sensory stimuli in visual, auditory and somatosensory areas [66].

Challenges: standardization of experimental conditions and analysis methods

In recent years, the number of neurons in which activity can be measured over long periods of time in awake behaving mice has increased exponentially. Such experiments provide extremely rich datasets including changes in neuronal population activity as well as different behavioural parameters measured over time. A current challenge is the development of standardised analysis tools for the reliable extraction of spiking activity [67] or calcium transients [68–71] of individual neurons from these large datasets. In addition, the criteria for the inclusion or exclusion of recorded neurons in the analysis strongly vary across studies making direct comparisons difficult. One example of such variability of results is the reported proportion of neurons in V1 whose activity is modulated by locomotion: this proportion ranges from 26% [11] to 55% [20•], 78% [22•] and 89% [33], in different studies. These challenges apply not only to studies of the visual system but also more broadly to *in vivo* calcium imaging datasets. Sharing custom-developed software that was used for data analysis in each calcium imaging publication would help increasing reproducibility for studies investigating visual processing, but also for a more accurate comparison of neuronal activity across cortical regions [72].

Another potential source of variability comes from the experimental conditions: housing conditions [73], noise and light levels in the imaging set-up, and circadian phase of the animals [74], were all found to affect the activity of visual neurons. A standardised quantification of arousal can be achieved by measuring LFP, pupil dilation and movement [9]. A detailed tracking and segmentation of the different components of a given behaviour [75] would also help to reduce variability across experiments and laboratories.

Finally, the development of methods to record neuronal activity and to track the behaviour of freely moving animals [76] would enable the study of more evolutionary relevant behaviours [77,78] than the ones tested in head-fixed mice. The influence of nonvisual inputs on visual processing may indeed vary between innate, natural behaviours that encompass multisensory and behaviourally relevant inputs and controlled behavioural tasks performed in front of a screen. Lastly, visual information processing may differ between the smaller but highly connected mouse brain and the highly hierarchical primate brain [5,79,80], with nonsensory influences in rodents being more prominent in primary sensory regions.

Conclusion

Recent studies in awake mice have revealed a previously unexpected diversity and plasticity of neuronal representations in the adult visual system. While the studies presented in this review show that action and learning shape neuronal representations, very little is known about the behavioural advantage or benefit of these activity-dependent and experience-dependent representations in the visual system. Potential functions include

improvements in the perception of stationary and moving objects, object recognition, movement control, spatial navigation, and acquisition of visually guided actions. The experimental challenge is to establish a causal link between specific neuronal representations and behavioural output.

One study has shown that locomotion does correlate with a significant improvement in the detection of low-contrast and medium-contrast gratings [13]: this decrease in perceptual threshold correlates with the increased signal-to-noise ratio of V1 visual responses during locomotion. Another study suggests a role for V1 activity in the acquisition of a visually guided task [46•]. Among other potential functions, prediction of visual flow based on self-movement could be used to detect mismatch between this prediction and moving objects, enhancing the detection of objects that move independently from the animal. Combined with the integration of running speed information [24], spatial expectations may help navigation by providing spatial landmarks. Lastly, since V1 neurons project to the superior colliculus and to brainstem nuclei via cortico-fugal projections, extravisual inputs to V1 neurons may directly be involved in the modulation of innate motor behaviours such as experience-dependent optokinetic reflex potentiation [81] or light-induced arrest behaviour [82].

Conflict of interest statement

Nothing declared.

Acknowledgements

This work was supported by the Wellcome Trust and the Royal Society (Sir Henry Dale fellowship, 102857/Z/13/Z) to N.R.; the European Commission (Marie Curie Actions (FP7), IEF 624461) and European Regional Development Fund (ERDF: Center for Behavioral Brain Sciences) to J.M. P. and MC-CIG 631770 to N.R.; University of Edinburgh (Graduate School of Life Sciences) to V.F.; Patrick Wild Centre, The Shirley Foundation, RS MacDonald Charitable Trust Seedcorn Grants to N.R.; The University of Edinburgh (Chancellor's fellow starting grant) to N.R.; Simons foundation (Simons Initiative for the Developing Brain) grant to N.R.

References and recommended reading

Papers of particular interest, published within the period of review, have been highlighted as:

- • of special interest
- •• of outstanding interest

1. Hubel DH, Wiesel TN: **Receptive fields of single neurones in the cat's striate cortex**. *J Physiol* 1959, **148**:574-591.
2. Priebe NJ: **Mechanisms of orientation selectivity in the primary visual cortex**. *Annu Rev Vis Sci* 2016, **2**:85-107.
3. Vidyasagar TR, Eysel UT: **Origins of feature selectivities and maps in the mammalian primary visual cortex**. *Trends Neurosci* 2015, **38**:475-485.
4. Haider B, Häusser M, Carandini M: **Inhibition dominates sensory responses in the awake cortex**. *Nature* 2013, **493**:97-100.
5. Gilbert CD, Li W: **Top-down influences on visual processing**. *Nat Rev Neurosci* 2013, **14**:350-363.
6. Maunsell JHR: **Neuronal mechanisms of visual attention**. *Annu Rev Vis Sci* 2015, **1**:373-391.
7. Stanisor L, van der Togt C, Pennartz CMA, Roelfsema PR: **A unified selection signal for attention and reward in primary visual cortex**. *Proc Natl Acad Sci U S A* 2013, **110**:9136-9141.
8. Dombeck DA, Khabbaz AN, Collman F, Adelman TL, Tank DW: **Imaging large-scale neural activity with cellular resolution in awake, mobile mice**. *Neuron* 2007, **56**:43-57.
9. McGinley MJ, Vinck M, Reimer J, Batista-Brito R, Zagha E, Cadwell CR, Tolias AS, Cardin JA, McCormick DA: **Waking state: rapid variations modulate neural and behavioral responses**. *Neuron* 2015, **87**:1143-1161.
10. Niell CM, Stryker MP: **Modulation of visual responses by behavioral state in mouse visual cortex**. *Neuron* 2010, **65**:472-479.
11. Erisken S, Vaiceliunaite A, Jurjut O, Fiorini M, Katzner S, Busse L: **Effects of locomotion extend throughout the mouse early visual system**. *Curr Biol* 2014, **24**:2899-2907.
12. Keller GB, Bonhoeffer T, Hübener M: **Sensorimotor mismatch signals in primary visual cortex of the behaving mouse**. *Neuron* 2012, **74**:809-815.
13. Bennett C, Arroyo S, Hestrin S: **Subthreshold mechanisms underlying state-dependent modulation of visual responses**. *Neuron* 2013, **80**:350-357.
14. • Polack PO, Friedman J, Golshani P: **Cellular mechanisms of brain state-dependent gain modulation in visual cortex**. *Nat Neurosci* 2013, **16**:1331-1339.
This study used whole-cell recordings in layer 2/3 and layer 4 of mouse V1 excitatory, PV-positive and SST-positive neurons to show that membrane potential of all cell types become more depolarised during locomotion. Noradrenergic receptors antagonists strongly reduced the tonic depolarization associated with locomotion. Cholinergic receptors antagonists were found to alter the unimodal distribution of the membrane potential of excitatory neurons during immobility, but did not affect the locomotion-related tonic depolarization.
15. Reimer J, Froudarakis E, Cadwell CR, Yatsenko D, Denfield GH, Tolias AS: **Pupil fluctuations track fast switching of cortical states during quiet wakefulness**. *Neuron* 2014, **84**:355-362.
16. Vinck M, Batista-Brito R, Knoblich U, Cardin JA: **Arousal and locomotion make distinct contributions to cortical activity patterns and visual encoding**. *Neuron* 2015, **86**:740-754.
17. •• Pakan JMP, Lowe SC, Dylda E, Keemink SW, Currie SP, Coutts CA, Rochefort NL: **Behavioral-state modulation of inhibition is context-dependent and cell type specific in mouse visual cortex**. *eLife* 2016, **5**:e14985.
This article shows that, in the presence of visual stimulation, the activities of excitatory neurons as well as VIP-positive, SST-positive, and PV-positive inhibitory neurons increase during locomotion, in mouse V1. In darkness, while most VIP and PV neurons remained locomotion responsive, SST were largely nonresponsive. Responses to locomotion thus differ depending on the visual context, with the highest difference found in SST neurons.
18. Andermann ML, Kerlin AM, Roumis DK, Glickfeld LL, Reid RC: **Functional specialization of mouse higher visual cortical areas**. *Neuron* 2011, **72**:1025-1039.
19. Huh CY, Peach JP, Bennett C, Vega RM, Hestrin S: **Specific organization of feedback pathways in mouse visual cortex feature-specific organization of feedback pathways in mouse visual cortex**. *Curr Biol* 2018, **28**:1-7.
20. • Mineault PJ, Tring E, Trachtenberg JT, Ringach DL: **Enhanced spatial resolution during locomotion and heightened attention in mouse primary visual cortex**. *J Neurosci* 2016, **36**:6382-6392.
This study shows that the relative gain (ratio between the gain of neurons during stationary and running periods) of mouse V1 neurons is higher in neurons with high spatial frequency selectivity compared to neurons with low spatial frequency selectivity. The authors conclude that the population activity in V1 can support better spatial acuity during locomotion and high arousal.
21. Ayaz A, Saleem AB, Schölvinck ML, Carandini M: **Locomotion controls spatial integration in mouse visual cortex**. *Curr Biol* 2013, **23**:890-894.

22. • Dadarlat MC, Stryker MP: **Locomotion enhances neural encoding of visual stimuli in mouse V1**. *J Neurosci* 2017, **37**:3764-3775.

This study proposes that locomotion improves the encoding of visual stimuli in mouse V1 by increasing firing rates and by decreasing noise correlations across neuronal population. Changes in firing rates were found to be more prominant in the upper layers while changes in noise correlations dominate in layer 5.

23. Leinweber M, Zmarz P, Buchmann P, Argast P, Hübener M, Bonhoeffer T, Keller GB: **Two-photon calcium imaging in mice navigating a virtual reality environment**. *J Vis Exp* 2014 http://dx.doi.org/10.3791/50885.

24. Saleem AB, Ayaz A, Jeffery KJ, Harris KD, Carandini M: **Integration of visual motion and locomotion in mouse visual cortex**. *Nat Neurosci* 2013, **16**:1864-1869.

25. Zmarz P, Keller GB: **Mismatch receptive fields in mouse visual cortex**. *Neuron* 2016, **92**:766-772.

26. Attinger A, Wang B, Keller GB: **Visuomotor coupling shapes the functional development of mouse visual cortex**. *Cell* 2017, **169**:1291-1302 e14.

27. •• Leinweber M, Ward DR, Sobczak JM, Attinger A, Keller GB: **A sensorimotor circuit in mouse cortex for visual flow predictions**. *Neuron* 2017, **95**:1420-1432 e5.

This study proposes that top-down projections, from the cortical area A24b and the adjacent secondary motor cortex (M2) provide to layer 2/3 neurons in V1 a signal prediction of visual flow based on the mouse's movement. Using a virtual reality environment, the authors created an artifical mismatch between motor movements and the associated visual flow to show that A24b/M2 axons in a given retinotopic location in V1 are activated most strongly by motor movements that maximize visual flow in the corresponding part of the visual space. The authors detail the experimental results that are consistent with an interpretation of the function of visual cortex in a predictive coding framework.

28. • Fiser A, Mahringer D, Oyibo HK, Petersen AV, Leinweber M, Keller GB: **Experience-dependent spatial expectations in mouse visual cortex**. *Nat Neurosci* 2016, **19**:1658-1664.

This study shows that following the repeated exposure to a specific virtual environment, a subset of V1 neurons and V1-projecting anterior cingulate cortex axons develop responses that are predictive of the upcoming visual stimulus in this environment. The omission of an expected stimulus elicit strong neuronal responses in V1. These result show that experience shapes the representation of an environment in mouse V1 and that this representation becomes increasingly more stable with experience.

29. Frenkel MY, Sawtell NB, Diogo ACM, Yoon B, Neve RL, Bear MF: **Instructive effect of visual experience in mouse visual cortex**. *Neuron* 2006, **51**:339-349.

30. Cooke SF, Bear MF: **Visual recognition memory: a view from V1**. *Curr Opin Neurobiol* 2015, **35**:57-65.

31. Kaneko M, Fu Y, Stryker MP: **Locomotion induces stimulus-specific response enhancement in adult visual cortex**. *J Neurosci* 2017, **37**:3532-3543.

32. Makino H, Komiyama T: **Learning enhances the relative impact of top-down processing in the visual cortex**. *Nat Neurosci* 2015, **2015**:173-180.

33. Ranson A: **Stability and plasticity of contextual modulation in the mouse visual cortex**. *Cell Rep* 2017, **18**:840-848.

34. Gavornik JP, Bear MF: **Learned spatiotemporal sequence recognition and prediction in primary visual cortex**. *Nat Neurosci* 2014, **17**:732-737.

35. Xu S, Jiang W, Poo MM, Dan Y: **Activity recall in a visual cortical ensemble**. *Nat Neurosci* 2012, **15**:449-455.

36. Guo ZV, Hires SA, Li N, O'Connor DH, Komiyama T, Ophir E, Huber D, Bonardi C, Morandell K, Gutnisky D *et al.*: **Procedures for behavioral experiments in head-fixed mice**. *PLOS ONE* 2014, **9**.

37. Shuler MG, Bear MF: **Reward timing in the primary visual cortex**. *Science* 2006, **311**:1606-1609.

38. Liu CH, Coleman JE, Davoudi H, Zhang K, Hussaina Shuler MG: **Selective activation of a putative reinforcement signal conditions cued interval timing in primary visual cortex**. *Curr Biol* 2015, **25**:1551-1561.

39. Gavornik JP, Bear MF: **Higher brain functions served by the lowly rodent primary visual cortex**. *Learn Mem* 2014, **21**:527-533.

40. Andermann ML, Kerlin AM, Reid RC: **Chronic cellular imaging of mouse visual cortex during operant behavior and passive viewing**. *Front Cell Neurosci* 2010, **4**:3.

41. Burgess CP, Lak A, Steinmetz NA, Zatka-Haas P, Bai Reddy C, Jacobs EAK, Linden JF, Paton JJ, Ranson A, Schröder S *et al.*: **High-yield methods for accurate two-alternative visual psychophysics in head-fixed mice**. *Cell Rep* 2017, **20**:2513-2524.

42. Aoki R, Tsubota T, Goya Y, Benucci A: **An automated platform for high-throughput mouse behavior and physiology with voluntary head-fixation**. *Nat Commun* 2017, **8**.

43. Poort J, Khan AG, Pachitariu M, Keller GB, Mrsic-flogel TD, Hofer SB, Poort J, Khan AG, Pachitariu M, Nemri A *et al.*: **Learning enhances sensory and multiple non-sensory representations in primary visual cortex**. *Neuron* 2015, **86**:1478-1490.

44. Montijn JS, Goltstein PM, Pennartz CMA: **Mouse V1 population correlates of visual detection rely on heterogeneity within neuronal response patterns**. *eLife* 2015, **4**.

45. Montijn JS, Olcese U, Pennartz CMA: **Visual stimulus detection correlates with the consistency of temporal sequences within stereotyped events of V1 neuronal population activity**. *J Neurosci* 2016, **36**:8624-8640.

46. • Jurjut O, Georgieva P, Busse L, Katzner S: **Learning enhances sensory processing in mouse V1 before improving behavior**. *J Neurosci* 2017, **37**:6460-6474.

This study compares the time course of changes in neuronal representations in V1 and behavioural performance, during the learning of a visual discrimination task. The learning-related improvements in V1 neuronal representation of relevant stimuli were fully expressed before the mice started to improve their success rate in the behavioural task. These findings suggest that V1 plays a role in the early phase of learning a visual discrimination task.

47. •• Keller AJ, Houlton R, Kampa BM, Lesica NA, Mrsic-Flogel TD, Keller GB, Helmchen F: **Stimulus relevance modulates contrast adaptation in visual cortex**. *eLife* 2017, **6**.

These results show that V1 neurons adapt their response to visual stimuli according to the acquired behavioural relevance of these stimuli. By using sustained high-contrast grating stimuli, the authors show that neurons adapted to these stimuli in anaesthetised mice but not in awake mice. When the mouse engaged in a visual task, neurons adapted their response when the stimulus was not relevant for the task while they maintained or increased activity when the same stimulus was relevant for the task.

48. Clopath C, Bonhoeffer T, Hübener M, Rose T: **Variance and invariance of neuronal long-term representations**. *Philos Trans R Soc B Biol Sci* 2017, **372**:20160161.

49. Han Y, Kebschull JM, Campbell RAA, Cowan D, Imhof F, Zador AM, Mrsic-Flogel TD: **The logic of single-cell projections from visual cortex**. *Nature* 2018 http://dx.doi.org/10.1038/nature26159.

50. Fu Y, Tucciarone JM, Espinosa JS, Sheng N, Darcy DP, Nicoll RA, Huang ZJ, Stryker MP: **A cortical circuit for gain control by behavioral state**. *Cell* 2014, **156**:1139-1152.

51. Pinto L, Goard MJ, Estandian D, Xu M, Kwan AC, Lee SH, Harrison TC, Feng G, Dan Y: **Fast modulation of visual perception by basal forebrain cholinergic neurons**. *Nat Neurosci* 2013, **16**:1857-1863.

52. Lee AM, Hoy JL, Bonci A, Wilbrecht L, Stryker MP, Niell CM: **Identification of a brainstem circuit regulating visual cortical state in parallel with locomotion**. *Neuron* 2014, **83**:455-466.

53. Chen N, Sugihara H, Sur M: **An acetylcholine-activated microcircuit drives temporal dynamics of cortical activity**. *Nat Neurosci* 2015, **18**:892-902.

54. Dipoppa M, Ranson A, Krumin M, Pachitariu M, Carandini M, Harris KD: **Vision and locomotion shape the interactions between neuron types in mouse visual cortex**. *bioRxiv* 2017 http://dx.doi.org/10.1101/058396.

55. Karnani MMM, Jackson J, Ayzenshtat I, Tucciarone J, Manoocheri K, Snider WGG, Yuste R: **Cooperative subnetworks of molecularly similar interneurons in mouse neocortex**. *Neuron* 2016, **90**:86-100.

56. Ayzenshtat I, Karnani MM, Jackson J, Yuste R: **Cortical control of spatial resolution by VIP+ interneurons**. *J Neurosci* 2016, **36**:11498-11509.

57. • Garcia Del Molino LC, Yang GR, Mejias JF, Wang XJ: **Paradoxical response reversal of top-down modulation in cortical circuits with three interneuron types**. *eLife* 2017, **6**.
This study presents a theoretical framework to explain how neurons within the same population can have responses with opposite sign to a particular variable. By taking the example of SST neuronal response to locomotion in mouse V1 they show that the context-dependent responses of these neurons can be explained by an emerging property of circuits including synaptic interactions between diverse neuronal populations and nonlinear neuronal input–output relationships.

58. Bennett C, Arroyo S, Hestrin S: **Controlling brain states**. *Neuron* 2014, **83**:260-261.

59. Kawaguchi Y: **Selective cholinergic modulation of cortical GABAergic cell subtypes**. *J Neurophysiol* 1997, **78**:1743-1747.

60. Arroyo S, Bennett C, Aziz D, Brown SP, Hestrin S: **Prolonged disynaptic inhibition in the cortex mediated by slow, non-α7 nicotinic excitation of a specific subset of cortical interneurons**. *J Neurosci* 2012, **32**:3859-3864.

61. Xiang Z: **Cholinergic switching within neocortical inhibitory networks**. *Science* 1998, **281**:985-988.

62. Roth MM, Dahmen JC, Muir DR, Imhof F, Martini FJ, Hofer SB: **Thalamic nuclei convey diverse contextual information to layer 1 of visual cortex**. *Nat Neurosci* 2016, **19**:299-307.

63. Saleem AB, Lien AD, Krumin M, Haider B, Rosón MR, Ayaz A, Reinhold K, Busse L, Carandini M, Harris KD *et al.*: **Subcortical source and modulation of the narrowband gamma oscillation in mouse visual cortex**. *Neuron* 2017, **93**:315-322.

64. Iurilli G, Ghezzi D, Olcese U, Lassi G, Nazzaro C, Tonini R, Tucci V, Benfenati F, Medini P: **Sound-driven synaptic inhibition in primary visual cortex**. *Neuron* 2012, **73**:814-828.

65. Meijer GT, Montijn JS, Pennartz CMA, Lansink CS: **Audio-visual modulation in mouse V1 depends on cross-modal stimulus configuration and congruency**. *J Neurosci* 2017 http://dx.doi.org/10.1523/JNEUROSCI.0468-17.2017.

66. Shimaoka D, Harris KD, Carandini M: **Effects of arousal on mouse sensory cortex depend on modality**. *Cell Rep* 2018, **22**:3160-3167.

67. Pachitariu M, Steinmetz N, Kadir S, Carandini M, Harris KD: **Kilosort: realtime spike-sorting for extracellular electrophysiology with hundreds of channels**. *bioRxiv* 2016 http://dx.doi.org/10.1101/061481.

68. Keemink SW, Lowe SC, Pakan JMP, Dylda E, van Rossum MCW, Rochefort NL: **FISSA: a neuropil decontamination toolbox for calcium imaging signals**. *Sci Rep* 2018, **8**:3493.

69. Pnevmatikakis EA, Soudry D, Gao Y, Machado TA, Merel J, Pfau D, Reardon T, Mu Y, Lacefield C, Yang W *et al.*: **Simultaneous denoising, deconvolution, and demixing of calcium imaging data**. *Neuron* 2016, **89**:299.

70. Deneux T, Kaszas A, Szalay G, Katona G, Lakner T, Grinvald A, Rózsa B, Vanzetta I: **Accurate spike estimation from noisy calcium signals for ultrafast three-dimensional imaging of large neuronal populations *in vivo***. *Nat Commun* 2016, **7**:12190.

71. Pachitariu M, Stringer C, Dipoppa M, Schröder S, Rossi LF, Dalgleish H, Carandini M, Harris KD: **Suite2p: beyond 10,000 neurons with standard two-photon microscopy**. *bioRxiv* 2017 http://dx.doi.org/10.1101/061507.

72. Gleeson P, Davison AP, Silver RA, Ascoli GA: **A commitment to open source in neuroscience**. *Neuron* 2017, **96**:964-965.

73. Greifzu F, Pielecka-Fortuna J, Kalogeraki E, Krempler K, Favaro PD, Schluter OM, Lowel S: **Environmental enrichment extends ocular dominance plasticity into adulthood and protects from stroke-induced impairments of plasticity**. *Proc Natl Acad Sci U S A* 2014, **111**:1150-1155.

74. Tsanov M, Manahan-Vaughan D: **Intrinsic, light-independent and visual activity-dependent mechanisms cooperate in the shaping of the field response in rat visual cortex**. *J Neurosci* 2007, **27**:8422-8429.

75. Krakauer JW, Ghazanfar AA, Gomez-Marin A, MacIver MA, Poeppel D: **Neuroscience needs behavior: correcting a reductionist bias**. *Neuron* 2017, **93**:480-490.

76. Stowers JR, Hofbauer M, Bastien R, Griessner J, Higgins P, Farooqui S, Fischer RM, Nowikovsky K, Haubensak W, Couzin ID *et al.*: **Virtual reality for freely moving animals**. *Nat Methods* 2017, **14**:995-1002.

77. De Franceschi G, Vivattanasarn T, Saleem AB, Solomon SG: **Vision guides selection of freeze or flight defense strategies in mice**. *Curr Biol* 2016, **26**:2150-2154.

78. Hoy JL, Yavorska I, Wehr M, Niell CM: **Vision drives accurate approach behavior during prey capture in laboratory mice**. *Curr Biol* 2016, **26**:3046-3052.

79. Busse L, Cardin JA, Chiappe ME, Halassa MM, Mcginley MJ, Yamashita T, Saleem XAB: **Sensation during active behaviors**. *J Neurosci* 2017, **37**:10826-10834.

80. Gămănuț R, Kennedy H, Toroczkai Z, Essen D Van, Knoblauch K, Burkhalter A: **The mouse cortical connectome characterized by an ultra dense cortical graph maintains specificity by distinct connectivity profiles**. *bioRxiv* 2017 http://dx.doi.org/10.1101/156976.

81. Liu BH, Huberman AD, Scanziani M: **Cortico-fugal output from visual cortex promotes plasticity of innate motor behaviour**. *Nature* 2016, **538**:383-387.

82. Liang F, Xiong XR, Zingg B, Ji XY, Zhang LI, Tao HW: **Sensory cortical control of a visually induced arrest behavior via corticotectal projections**. *Neuron* 2015, **86**:755-767.